ISSN: 2408-2384 (Online)
ISSN: 1686-5456 (Print)

Environment and Natural Resources Journal

Volume 20, Number 1, January - February 2022

Environment and Natural Resources Journal (EnNRJ)

Volume 20, Number 1, January - February 2022 ISSN: 1686-5456 (Print)
ISSN: 2408-2384 (Online)

AIMS AND SCOPE

The Environment and Natural Resources Journal is a peer-reviewed journal, which provides insight scientific knowledge into the diverse dimensions of integrated environmental and natural resource management. The journal aims to provide a platform for exchange and distribution of the knowledge and cutting-edge research in the fields of environmental science and natural resource management to academicians, scientists and researchers. The journal accepts a varied array of manuscripts on all aspects of environmental science and natural resource management. The journal scope covers the integration of multidisciplinary sciences for prevention, control, treatment, environmental clean-up and restoration. The study of the existing or emerging problems of environment and natural resources in the region of Southeast Asia and the creation of novel knowledge and/or recommendations of mitigation measures for sustainable development policies are emphasized.

The subject areas are diverse, but specific topics of interest include:

- Biodiversity
- Climate change
- Detection and monitoring of polluted sources e.g., industry, mining
- Disaster e.g., forest fire, flooding, earthquake, tsunami, or tidal wave
- Ecological/Environmental modelling
- Emerging contaminants/hazardous wastes investigation and remediation
- Environmental dynamics e.g., coastal erosion, sea level rise
- Environmental assessment tools, policy and management e.g., GIS, remote sensing, Environmental Management System (EMS)
- Environmental pollution and other novel solutions to pollution
- Remediation technology of contaminated environments
- Transboundary pollution
- Waste and wastewater treatments and disposal technology

Schedule

Environment and Natural Resources Journal (EnNRJ) is published 6 issues per year in January-February, March-April, May-June, July-August, September-October, and November-December.

Publication Fees

There is no cost of the article-processing and publication.

Ethics in publishing

EnNRJ follows closely a set of guidelines and recommendations published by Committee on Publication Ethics (COPE).

Environment and Natural Resources Journal (EnNRJ)

Volume 20, Number 1, January - February 2022 ISSN: 1686-5456 (Print)
ISSN: 2408-2384 (Online)

Editorial Office Address
Research Management and Administration Section,
Faculty of Environment and Resource Studies, Mahidol University
999, Phutthamonthon Sai 4 Road, Salaya, Phutthamonthon, Nakhon Pathom, Thailand, 73170
Phone +662 441 5000 ext. 2108 Fax. +662 441 9509-10
Website: https://ph02.tci-thaijo.org/index.php/ennrj/index
E-mail: ennrjournal@gmail.com

Environment and Natural Resources Journal (EnNRJ)

Volume 20, Number 1, January - February 2022 ISSN: 1686-5456 (Print)
ISSN: 2408-2384 (Online)

CONTENT

Recovery of Lignocellulolytic Enzymes and Valorization of Spent Mushroom Substrate

Anumeha Vats[1], Anuj Sangam Kurade[2], and Srikanth Mutnuri[1*]

[1]Applied Environmental Biotechnology Laboratory, Birla Institute of Technology and Science, Pilani, K.K. Birla Goa campus, India
[2]Zycon Renew Energy Private Limited, Caranzalem North Goa GA 403002, India

ARTICLE INFO

Received: 27 May 2021
Received in revised: 26 Jul 2021
Accepted: 2 Aug 2021
Published online: 21 Sep 2021
DOI: 10.32526/ennrj/20/202100099

Keywords:
Spent mushroom substrate/ Lignocellulolytic enzymes/ Laccase/ Cellulase/ Dye decolorization/ Briquette

*** Corresponding author:**
E-mail: srikanth@goa.bits-pilani.ac.in

ABSTRACT

Spent Mushroom Substrate (SMS) comprises sugarcane bagasse, coconut coir, chicken manure, and paddy straw; inoculated with and farmed for *Agaricus bisporus*. At present, the waste generation at a mushroom cultivation plant in Goa is 40 tons/day (15,000 tons annually). Valorization of this waste has been explored in terms of extracting lignocellulolytic enzymes and briquette production. SMS was screened for the presence of lignocellulolytic enzymes and then was used to make briquettes. The enzymes found in SMS were cellulase and laccase, which were further concentrated via tangential flow filtration (TFF). Enzyme activity for Cellulase increased by four-fold (from 255.34±1.30 U/mL increased to 1022.21±4.84 U/mL) and Laccase increased by three-fold (from 4.83±0.02 U/mL to 13.21±0.05 U/mL). The concentrated enzyme cocktail was used to decolorize congo red dye. After only eight hours of enzymatic treatment at pH 4.8 on congo red, approx. 40-49% decolorization was accomplished. The color removal was due to the presence of the laccase enzyme. After enzyme extraction, all the residual SMS was utilized to generate briquettes with an initial reduction in its moisture content from 50% to 10%. The resulting briquette gave a Gross Calorific Value of 4,143 Kcal/kg with 12.60% ash content. Thus, SMS proves to be a valuable source for recovering enzymes and a cost-effective material for briquette production rather than going into landfills.

1. INTRODUCTION

The common button mushroom, *Agaricus bisporus*, is cultivated for commercial purposes in a controlled environment. *Agaricus bisporus* is grown on a biomass substrate consisting of clay, sugarcane bagasse, coconut coir, chicken feed, and paddy straw mixed in a predetermined proportion. At Tropical Mushrooms Pvt. Ltd. (Goa) India, approximately 15,000 tons of Spent Mushroom Substrate (SMS) is generated annually. Currently, after the mushroom is harvested at the farm, the biomass substrate is disposed of in the landfill. Three significant environmental impacts that occur due to the landfill are: (a) Landfill construction-can damage the ecology; (b) Landfill gas-gaseous emission consists mainly of CO_2 and CH_4, which contributes to global warming; (c) Leachate-can invade to groundwater causing water pollution and also, metals (from groundwater) retained by the soil absorb by plants and then enters in the food chain (Danthurebandara et al., 2013). Therefore, landfill is not a feasible way of waste management, which originates the need to explore a sustainable waste management solution.

SMS is rich in lignocellulosic content. The fungal mycelium inherently present in the SMS consumes these lignocellulosic content and flourish (Fen et al., 2014). The microorganisms utilize these contents (by degradation) for their growth with the help of extracellularly secreted lignocellulolytic enzymes (Singh et al., 2003). Therefore, SMS will be a rich source for extracting these enzymes, which are of commercial interest.

The extensive industrial application of lignocellulolytic enzymes makes them valuable, mainly for the food and textile industries. In particular, cellulase and xylanase are used for biofuel production, as they possess the ability to saccharify biomass. The lignin-degrading laccase is a versatile enzyme as it also

Citation: Vats A, Kurade AS, Mutnuri S. Recovery of lignocellulolytic enzymes and valorization of spent mushroom substrate. Environ. Nat. Resour. J. 2022;20(1):1-9. (https://doi.org/10.32526/ennrj/20/202100099)

has a vital role in the treatment of dye wastewater/textile industry effluent (Thurston, 1994; Abadulla et al., 2000; Lim et al., 2013). Laccase possesses the ability to decolorize dyes by oxidizing the aromatic rings; also, it is much less specific because it can work on a vast range of synthetic dyes such as Remazol brilliant blue R, Congo red, Indigo, etc. which are extensively used in industries these days (Thurston, 1994; Abadulla et al., 2000; Lim et al., 2013).

Residues generated from the agricultural industry have a very high potential for resource recovery and reuse as the substrate for fermentation, biogas, biofuel, briquette, etc. (Demirbas, 1999; Sadh et al., 2018). Agro-wastes, which can be used for briquettes production are corn straw, leaves of various species, coconut husk, bagasse, sawdust, etc. (Tamilvanan, 2013; Garrido et al., 2017). The SMS biomass generated after mushroom harvesting and recovery of enzymes can be converted into high-quality biofuel products by compacting into a high-density product called briquettes - a source of green energy (Garrido et al., 2017). Briquetting is a densification process that produces a compact material with higher energy per unit volume (Garrido et al., 2017). Low-cost production and with increased access to consumers, briquettes can be chosen over coal and other non-renewable burning fuel for domestic and agro-industries usage. The advantages of briquetting - higher heat intensity, uniform clean and stable fuel, convenience in use, and relatively smaller space requirements for storage, and reduced transportation costs (Garrido et al., 2017). Briquetting without the binder makes the process convenient but increases cost and sophistication in drying equipment and briquette press, thus making the process less attractive for a developing country like India. Briquetting with a binder like paper, wood chips, etc., is suitable for developing countries, as it decreases the production cost and requirement of more skilled labor. Preliminary research showed that the briquettes produced with binders like cassava starch and palm oil sludge result in smoky briquettes. Generally, briquettes are made from locally available materials, which include sawdust, cowpea chaffs, corncobs, and water hyacinth (Olorunnisola, 2007). The waste used as raw materials for briquette production is oil palm residue, paper waste, plastic waste, coconut husk and wheat straw (Demirbas, 1999; Olorunnisola, 2007; Sing and Aris, 2013; Garrido et al., 2017). The key significant factors for making briquetting are low production cost, waste material management, and conversion of waste to revenue.

It is proposed here to utilize the SMS for enzyme recovery and manufacturing of fuel briquettes. The study is focused on waste management at the mushroom farm by enzyme recovery followed by briquette production. Enzymes such as cellulase and laccase were recovered. Tangential Flow Filtration (TFF) technique was applied to crude enzyme extract (CEE) to increase the enzyme concentration. The recovered lignocellulolytic enzymes were tested for their dye decolorization ability. Briquetting from reusing the SMS material post mushroom production and enzyme recovery with and without a binding agent (wood chips) was also demonstrated.

2. METHODOLOGY

2.1 Chemicals

Carboxymethylcellulose (CMC) and Congo red (CR) were procured from HiMedia, India. 2,2'-azino-bis (3-ethylbenzothiazoline-6-sulphonic acid) (ABTS) was purchased from Roche Diagnostic, Germany. Mira cloth of 22-25 µm pore size was bought from Merck Millipore.

2.2 Crude enzyme extraction

A mushroom bed has two distinct layers; the top layer is the casing layer (3.8 cm height, 2.0 kg weight) and at the bottom is the compost layer (16.5 cm height, 8.5 kg weight). The extraction of the enzyme from SMS was carried out by removing the casing layer from the mushroom bed. SMS (300 g) was added in 500 mL of sterile distilled water and agitated at 300 rpm for 60 min at 4°C. Antunes (2020) found that, using a solvent like water, recovery of enzymes (with notable activity) from SMS is possible. The mixture was filtered through Mira cloth (Lim et al., 2013), the filtrate was then centrifuged at 7,000 rpm for 10 min at 4°C to obtain a clear supernatant. The supernatant containing crude enzymes was retained and stored at 4°C until enzyme activity analysis was carried out (Lim et al., 2013). Crude enzyme extract (CEE) was concentrated by passing the CEE through the Krosflo® KR2i TFF system from Spectrum Labs, using the NMCW-30kDa column at operating conditions of 2.5 psi feed pressure and feed flow rate was 140 mL/min, these conditions were maintained throughout the process. All the extraction procedures were performed in triplicate.

2.3 Screening of enzyme

The CEE samples were analyzed for the presence of various enzymes, namely cellulase, laccase, xylanase, amylase, and invertase, by agar plate diffusion assay. The assay was performed in duplicate. Substrates used for cellulase, laccase, xylanase, amylase, and invertase were CMC, ABTS, xylan, starch, and sucrose, respectively. Agar plates (1%) containing 0.5% CMC, 0.2 mM of ABTS, 0.5% xylan, 0.5% starch, and 0.5% sucrose were poured. The media for all the enzymes were prepared with one substrate only to get the specific activity. In each agar plate, a well of approximately 5 mm diameter was made. CEE was then added into the wells, following which the plates were incubated at 37°C (for cellulase, xylanase, amylase, and invertase activity) and 25°C (for laccase activity) (More et al., 2011). Cellulase activity on the plates was obtained by staining with CR dye (1 g/L, 1% ethanol) followed by destaining with 1 M NaCl.

2.4 Enzyme activity

The CEE, TFF-retentate, and TFF-permeate samples were analyzed for cellulase and laccase activity. The cellulase and laccase activity was determined in duplicates by the DNS method (using CMC solution) and ABTS oxidation, respectively. CMCase activity was estimated (employing 0.5% CMC as substrate) by the assay described by Isikhuemhen and Mikiashvili (2009). The reaction mixture, composed of enzyme sample (0.5 mL), CMC (0.5 mL), and 0.05 M sodium citrate buffer (pH 4.8), was held at 50°C (Isikhuemhen et al., 2009) for 60 min. Following the reaction, the amount of reducing sugar was determined by the DNS method (Miller, 1959). One unit of enzyme activity is defined as 1 µmol of glucose equivalent molecules released per minute under the given conditions.

Laccase activity was determined by measuring oxidized ABTS at 420 nm, as described earlier (Shin and Lee, 2000; Suwannawong et al., 2010; Lim et al., 2013). The reaction mixture, consisting of enzyme sample (0.3 mL), 0.2 mM ABTS (0.7 mL) and 0.1 M sodium acetate buffer (pH 4.5), was incubated at 25°C for 15 min. One unit of enzyme activity is defined as the amount of enzyme required to oxidizing 1 µmol of ABTS per minute under the given conditions.

2.5 Dye decolorization

CR dye was the substrate employed to determine the decolorization ability of CEE at the lab scale. The stock solution of CR (1.0%) was prepared in sterile distilled water with 1.0% ethanol. The working solution concentration was 0.01%. Enzyme concentration, ranging from 0.25% to 5.0% (0.25%, 0.50%, 0.75%, 1.0%, 2.5% and 5.0%) was mixed with 0.01% CR in 0.1 M sodium citrate buffer (pH 4.8) and 0.1 M sodium acetate buffer (pH 6.0). The experiment was carried out at 28±2°C. Decolorization was determined spectrophotometrically at 592 nm using Spectroquant® Prove 100 from Merck. The effect of agitation on decolorization rate was also tested with an experimental set up with 0.01% CR, and 1% enzyme concentration at pH 4.8 kept at 28±2°C for 24 h, one set was shaken, and the other was in a stationary state. All experiments were carried out in triplicate.

2.6 Briquetting process

The SMS left after the enzyme extraction, along with the rest of the mushroom bed, were used to produce briquette, a clean and green energy source. SMS consists mainly of bagasse, wheat husk, coconut husk, etc. The material was in bags of ~20 kg each, contained 40-60% moisture, and existed as lumps. The moisture content of the raw materials for briquette manufacturing should be in the range of 10-15%. Therefore, the SMS was dried in a rotary drum drier to decrease the moisture down to 10%, making it suitable for the briquetting process. The input temperature of the drier was kept at 250°C, and the output temperature was monitored to be 125°C. The rotation cycle of the drum drier was set at 15-20 rpm to give SMS enough exposure to the heat.

For the briquetting process, the material was fed into the briquetting press, which has a 75HP motor to drive its ram and two 1,200 kg flywheels. Since the ram has a diameter of 90 mm, this translates into a pressure of 8.79 MPa. Alternatively, SMS was mixed with wood chips (WC, size 8 mm with moisture level 15-20%) as binding material. Thus, three different types of briquettes were prepared: (a) only SMS; (b) 65% SMS and 35% WC; (c) 50% SMS, and 50% WC. All final products were tested for calorific value, moisture content, ash content, volatile matter, carbon content, bulk density, size, ignition test, and flow ability test.

3. RESULTS AND DISCUSSION

3.1 Lignocellulolytic enzyme profile in SMS

Bioactive compounds like lignocellulolytic enzymes have been previously extracted and characterized from mycelium, fruiting body, SMS,

and fermentation broth (Antunes et al., 2020). The lignocellulolytic enzymes involved in breaking down lignin and cellulosic material are cellulases, laccases, xylanases proteases, and amylases (Antunes et al., 2020). The lignocellulolytic enzymes, namely cellulase, laccase, xylanase, amylase, and invertase, were screened qualitatively for their presence in CEE from SMS by plate diffusion assay. The predominant presence of cellulase and laccase was observed, while amylase activity was below the limit of detection. No xylanase and invertase activity were seen. Cellulase activity was confirmed by the formation of a yellow halo zone (4.50±0.25 mm diameter of zone of activity) around the well. The yellow halo zone formation confirms the cellulose degradation by cellulase enzyme to monosaccharides. CR is unable to stain monosaccharides which causes yellow halo zones to form (Figure 1(a)). Laccase activity was due to ABTS oxidation, which turns into a green color. This green color formed around the well confirmed the presence of laccase; the diameter of the activity zone was 9.0±0.5 mm (Figure 1(b)). The enzymatic unit of cellulase and laccase was found to be 255.34±1.30 U/mL and 4.83±0.02 U/mL, respectively (Figure 2(a) and 2(b)). Based on several reports, the range of cellulase and laccase activity achieved in the extract from was 0.4-133.0 U/mL (Ryu and Mandels, 1980; Mtui, 2012; Saravanan et al., 2013; Saroj et al., 2018) and 0.14-0.89 U/mL (Sahay et al., 2008; Mtui, 2012; Haripriya et al., 2014), respectively. Comparison of enzymes activity in our study with the reported literature revealed higher cellulase and laccase activity recovered from lignocellulosic waste. To enhance the laccase activity, concentration of the enzyme is essential for rendering recovered enzymes from SMC for potential industrial application. After the enzyme was extracted from SMS, various value-added products also have been reported to be obtained from SMS, such as biogas, organic fertilizer, animal feed supplements, fertilizer, cosmeceuticals, bio-remediation, bio-based materials, and energy (Sadh et al., 2018; Antunes et al., 2020).

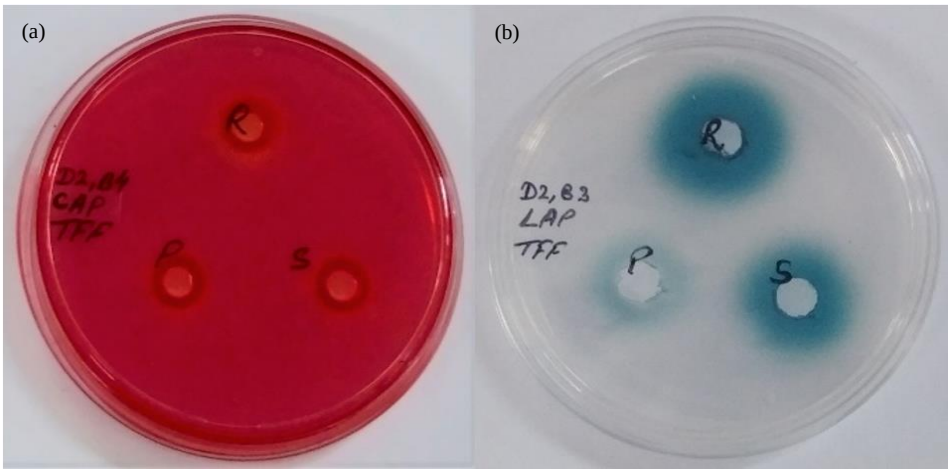

Figure 1. Agar plate diffusion assay: (a) cellulase assay; (b) laccase activity. (R=retentate, P=permeate, S=initial sample)

3.2 Lignocellulolytic enzyme concentration

TFF was employed to concentrate the crude enzyme extract. The filtration of CEE via the TFF process resulted in two streams, permeate and the retentate. The enzymatic activity determination of both the streams showed that the retentate stream had a highly considerable amount of enzyme activity. During qualitative analysis, the diameter of activity noted in the retentate was 14.50±0.25 mm and 22.75±0.89 mm; and in permeate 2.00±0.50 mm and 1.00±0.50 mm, for cellulase and laccase, respectively (Table 1). The cellulase and laccase activity increased by 3.2 times and 2.25 times, respectively. The activities recorded in the quantitative analysis were 1022.21±4.84 U/mL (Figure 2(a)) for cellulase and 13.21±0.05 U/mL for laccase (Figure 2(b)). Cellulase and laccase in permeate were nearly the same as in non-concentrated CEE were 251.30±1.56 U/mL and 2.95±0.08 U/mL, respectively. The increase in activity observed was 300.34% for cellulase and 173.56% for laccase. As expected, the cellulase and laccase activity in the permeate stream decreased by 1.58% and 38.84%, respectively, compared to the feed enzyme activity. In comparison to other techniques like ultra-centrifugation etc., TFF is a robust, scalable, time-efficient, and reproducible method, especially for large volume samples as experienced during our study (Busatto et al., 2018). Narra et al. (2016) and Rajeeva

and Lele (2010) found the recovery of cellulase and laccase via TFF to be 79-84% and 97%, respectively. Recovery rate of CEE from the optimized process during the present study was found to be 98%, with a processing time of 10 min/L. Hence, concentrating enzyme by TFF is an efficient method in terms of efficiency, consistency, reliability, and stability. The concentrated enzyme cocktail post TFF has the potential to be used for various industrial applications like anaerobic digestion, textile industry, food industry, etc. However, economic feasibility is the study that should be focused on in the future.

Table 1. Qualitative analysis: Measured diameter of the enzyme activity of the samples before and after TFF concentration

Sample	Activity diameter (mm)	
	Cellulase	Laccase
Initial	1.2	2
Retentate	14	25
Permeate	0	0

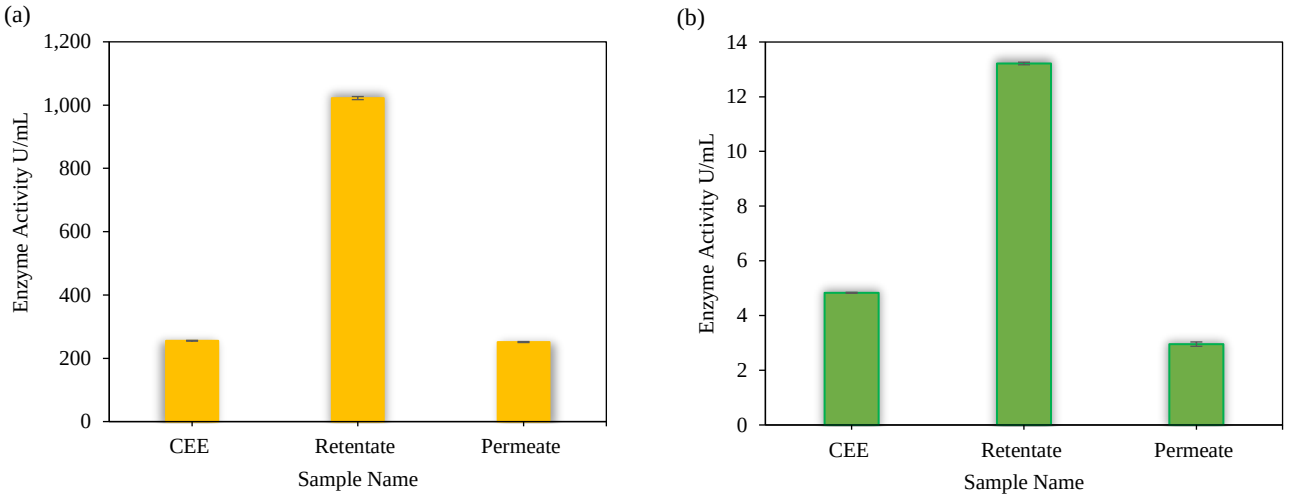

Figure 2. Quantification of enzyme activity using, (a) CMCase-DNS method, (b) by oxidation ABTS; comparing activity between CEE, retentate, and permeate

3.3 Dye decolourization

Laccase is a versatile enzyme as its applications range from lignin degradation to bioremediation. In this study, the ability of CEE to decolorize CR was explored. It is the most extensively used dye in the textile industry, making it the major constituent of the effluent. Hence, the removal of CR dye is a crucial step in treating textile industry wastewater. Laccase proves to be the most efficient in dye decolorization, where the pH of the reaction mixture plays a vital role during the CR decolorization process.

From the graph shown in Figure 3(a), it can be seen that there was an exponential increase in the dye removal rate at pH 4.8 as compared to that achieved at pH 6.0. On the contrary, Suwannawong et al. (2010) found the optimum pH for decolorization was 6.0-7.0 (Suwannawong et al., 2010). The percentage of dye removal achieved at pH 4.8 with enzyme solution concentration being 1% was around 50% after 8 h incubation, while the removal reached 25% after 40 h incubation at pH 6.0. The possible reason is that the optimum pH at which activity is maximum for laccase is acidic pH ranging pH 3.0 to 5.0 (Heinzkill et al., 1998; Madhavi and Lele, 2009), and pH >6.5 inhibits decolorization rate (Asses et al., 2018). From the graph shown in Figure 3(b), it can be seen that with the increase in the enzyme concentration from 0.25% to 0.5%, the maximum dye removal percentage after 70 h incubation increases (i.e., from 24% to 35%) at pH 6.0. However, a further increase in the enzyme concentration to 0.75% and 1% does not cause any further increase in the maximum dye removal percentage. Therefore, from Figures 3(a) and 3(b), it can be concluded that pH 4.8 is the optimal pH for achieving better removal rates. Figure 3(c) and Figure 4 shows the results of dye removal experiments carried out at pH 4.8 at different CEE concentrations. From the graph, it can be seen that the removal trend with respect to time for all the enzyme solution concentrations is the same. The maximum removal is achieved after 24 h. However, in comparison, there is no significant difference in the removal achieved after 16 h. Further, increase in the enzyme concentration (0.25-2.5%) increases the enzyme removal rate up to a concentration of 5%. Further increase in the enzyme concentration does not have any effect on the dye

removal percentage. Also, the faster removal rate is achieved after 8 h at 2.5% enzyme concentration. Figure 3(d) illustrates that with agitation decolorization rate of 49% attained in eight hours, which is approximately double compared to the set kept without agitation, which showed only 23% of decolorization in eight hours. The dye removal percentage achieved in our study was significant and higher than that reported by Das et al. (2016) which was 36.84% decolorization after 20 h incubation at 35±2°C (Das et al., 2016). Thus, from the obtained results, it can be inferred that pH 4.8 is the ideal pH for decolorization of congo red. Also, the optimum pH for laccase enzymatic activity is 5.0 (Kumar et al., 2016). Therefore 4.8 pH is ideal for the enzymatic mediated decolorization process.

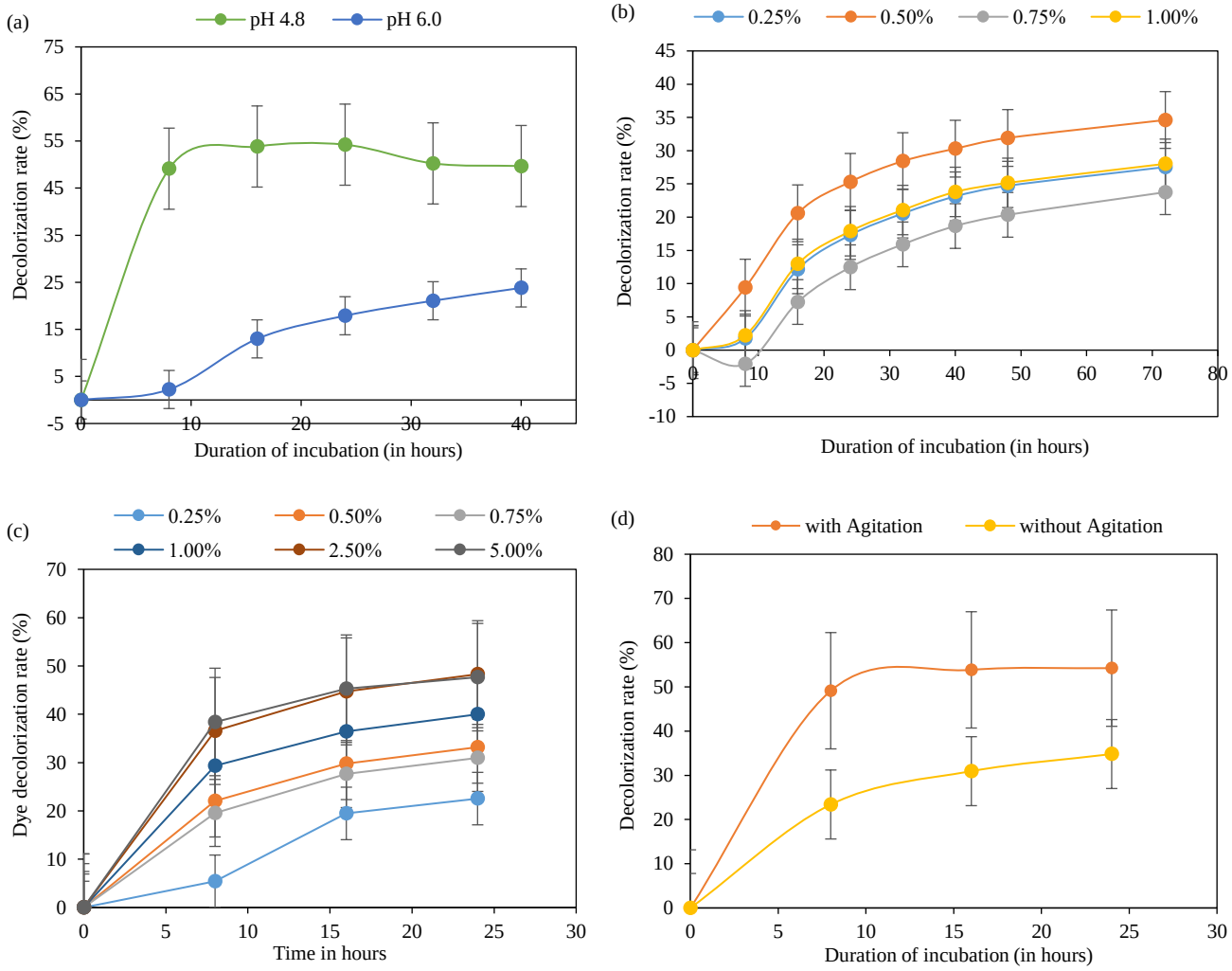

Figure 3. (a) 1% concentrated enzyme (TFF retentate) used for dye decolorization of 0.01% congo red at pH 4.8 and pH 6.0; (b) Dye decolorization rate (%) of 0.01% congo red at pH 6.0. Concentrated or TFF retentate enzyme sample was added at 0.25%, 0.50%, 0.75% and 1.00% different concentration; (c) Dye decolorization rate (%) of 0.01% congo red at pH 4.8. SMC CEE TFF-R is the concentrated or TFF retentate enzyme sample. A range of 0.25% to 5.00% - different concentrations of enzyme used; (d) Effect of agitation on decolorization rate of 0.01% congo red using 1.0% SMC CEE TFF-R enzyme in both cases

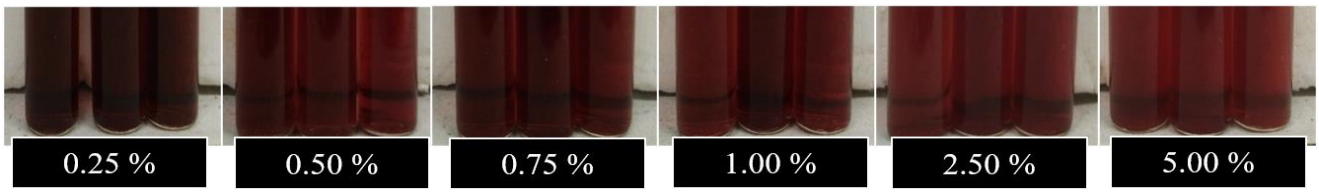

Figure 4. Different concentrations of SMC CEE TFF-R enzyme showing congo red decolorization at pH 4.8 after 8 h of incubation at room temperature

As congo red is a diazo dye, the degradation or decolorization is a complex process. Chakravarthi et al. (2021), demonstrated that the CR is attacked by laccase enzyme by asymmetric cleavage of azo bonds which is then followed by oxidative cleavage, desulfonation, deamination, and demethylation, yielding the end product of benzene dicarboxylic acid and CO_2.

3.4 Briquettes from mushroom bed

The characterization of SMS is summarized in Table 2. As mentioned, SMS consist of 47% moisture, which needs to be decreased to a minimum of 10% before using it as a raw material for briquette production.

Table 2. SMS characterization

Parameter	Value
Moisture on a wet basis (%)	47
Ash (dry) (%)	14
Volatile (dry) (%)	66
Fixed carbon (dry) (%)	21
Ash fusion (°C)	1,100
Bulk density (kg/m^3)	140
Size (mm)	>3 mm 66%
	<3 mm 34%
Ignition test	Burns easily
Flow ability test	Flows easily
Calorific value on dry basis (kcal/kg)	4,000

The presence of high moisture content makes SMS less suitable for briquette production until now. A drying step has been added here before starting briquette production. For moisture reduction, two parameters that play essential roles are the temperature and rotation speed of the drum.

The lignin within the material (SMS) gets activated at a high temperature. The material temperature rises due to the friction caused by the material with the carbon steel die on the application of the pressure by the ram. This raises the temperature inside the die, and the lignin binds the material from outside. The die has to be cooled with circulating water in its shell to keep the material from charring. With proper moisture levels, the briquetting happens, and the ultimate output was little on the harder side.

WC was mixed with SMS to decrease ash and volatile matter content, which increases the calorific value and lignin content of the final product, i.e., briquette. The briquettes with 65% SMS and 35% WC are the finest among others, as it showed the highest calorific value of 4,143 Kcal/kg and the lowest ash content of 12.60% compared to briquettes prepared with only SMS, and 50% SMS and 50% WC (Table 3). Increasing the percentage of WC for making briquette showed an increment in moisture content and production cost. Briquette from SMS and WC prove to be superior in terms of calorific value compared to routinely used raw materials like sawdust, paper, wood, plastic, coal, rice husk, and others (Table 4). Some of the different briquettes, along with their calorific value in comparison with the SMS briquette, are listed in Table 4 (Demirbas, 1999; Yaman and Kuc, 2001; Olorunnisola, 2007; Kers et al., 2010; Sing and Aris, 2013; Garrido et al., 2017).

Apart from the competent physical attributes of SMS briquettes, they are cheap and cost-effective also. The cost of briquette production with SMS is 3,500 INR per ton, which is lesser than 50% of the cost of briquettes made of rice husk, wheat straw, cocopeat, wood dust sawdust that comes to 8,000 INR per ton (Source: Kushi Bio Fuel Briquettes, Goa (India)-commercial company).

Table 3. Comparison between different types of briquettes produced from SMS

Parameter	Only SMS	65% SMS and 35% WC	50% SMS and 50% WC
Moisture (%)	5	10.81	12.32
Ash content (%)	17	12.60	15.59
Volatile matter (%)	66	72.04	70.81
Gross calorific value (Kcal/kg)	3,600	4,143.46	4,244.47

Table 4. Calorific value comparison between different types of briquettes

Raw material for briquetting	Calorific value (MJ/kg)	References
Palm kernel shells	19.38	Sing and Aris (2013)
Palm fiber	18.08	Sing and Aris (2013)
Coal/lignite	16.28	Sing and Aris (2013)

Table 4. Calorific value comparison between different types of briquettes (cont.)

Raw material for briquetting	Calorific value (MJ/kg)	References
Coconut husk	18.80-20.80	Olorunnisola (2007)
Straw	17.30	Demirbas (1999)
Waste paper	16.40	Demirbas (1999)
Rice husk (biocoal)	17.58-18.13	Demirbas (1999)
Lignite	19.80	Yaman and Kuc (2001)
Wood, carton, paper, plastic and textile	26.14	Kers et al. (2010)
Automotive shredder residues	18.75	Garrido et al. (2017)
Print circuit board	11.08	Garrido et al. (2017)
Sawdust	18.90	Garrido et al. (2017)
Palm trunk	21.00	Garrido et al. (2017)
Cover (wire)	13.15	Garrido et al. (2017)
Insulation (wire)	10.40	Garrido et al. (2017)
Molasses	17.50	Yaman and Kuc (2001)
Olive refuse	21.40	Yaman and Kuc (2001)
Pine cone	18.10	Yaman and Kuc (2001)
Paper mill waste	13.00	Yaman and Kuc (2001)
Cotton refuse	17.50	Yaman and Kuc (2001)
Sawdust	16.70	Yaman and Kuc (2001)
Rice husk, wood dust and saw dust	10.46	Kushi Bio Fuel Briquettes, Goa (India)
Spent mushroom substrate (SMS)	15.06	Zycon ReNew Energy, Goa (India)
SMS and wood chips	17.33	Zycon ReNew Energy, Goa (India)

3.4 Mushroom farm waste management

Annual waste production of 15,000 tons at the mushroom farm can be utilized for enzyme recovery and produce 2,034 L/day of enzyme solution possessing 1,022 U/mL of cellulase and 13.21 U/mL of laccase. The remaining biomass can be used to generate 24,000 kg of briquettes per day.

4. CONCLUSION

The study presents the potential direct and indirect use of SMS, which would otherwise be disposed of in a landfill. The extraction of lignocellulolytic enzymes was achieved and application of the extracted enzymes were demonstrated in terms of decolorization of CR dye. The crude extract consisting mainly of cellulase and laccase enzymes showed lower activities and hence was concentrated by TFF. TFF enhanced the cellulase and laccase enzyme activity by 4.0 fold and 2.74 fold, respectively. The concentrated CEE achieved decolorization of congo red dye exhibiting its potential application. The removal percentage achieved by 2.5% enzyme solution after 8 h incubation was 40%. Agitation enhanced the removal to 49% even at lower concentration enzyme solution (1%). The direct use of the SMS after enzyme extraction was also demonstrated. The briquette obtained from SMS post enzyme recovery with wood chips as binding material was found to have a calorific value of 4,143 Kcal/kg, making it a potential green energy fuel. The low production cost of 3,500 INR per ton to the briquette economic option of fuel too. In the future, the CEE can be studied for its ability to treat textile industry wastewater. Overall, the study proposes a process to obtain value-added products from the SMS.

ACKNOWLEDGEMENTS

The authors would like to thank Tropical Mushrooms Pvt. Ltd. (Goa) India for supplying and delivering Spent Mushroom Substrate as per the requirement and BITS-Pilani K.K. Birla Goa Campus for providing equipped laboratory facilities to carry out the research.

REFERENCES

Abadulla E, Tzanov T, Costa S, Robra K, Cavaco-paulo A, Gubitz GM. Decolorization and detoxification of textile dyes with a laccase from *Trametes hirsuta*. Applied and Environmental Microbiology 2000;66(8):3357-62.

Antunes F, Marçal S, Taofiq O, Morais AMMB, Freitas AC, Ferreira ICFR, et al. Valorization of mushroom by-products as a source of value-added compounds and potential applications. Molecules 2020;25:1-40.

Asses N, Ayed L, Hkiri N, Hamdi M. Congo red decolorization and detoxification by *Aspergillus niger*: Removal mechanisms

and dye degradation pathway. BioMed Research International 2018;2018:Article No. 9.

Busatto S, Vilanilam G, Ticer T, Lin WL, Dickson D, Shapiro S, et al. Tangential flow filtration for highly efficient concentration of extracellular vesicles from large volumes of fluid. Cells 2018;7(12):Article No. 273.

Chakravarthi B, Mathkala V, Palempalli UMD. Degradation and detoxification of congo red azo dye by immobilized laccase of *Streptomyces sviceus*. Journal of Pure and Applied Microbiology 2021;15(2):864-76.

Danthurebandara M, Passel S Van, Nelen D, Tielemans Y, Acker K Van. Environmental and socio-economic impacts of landfills. Proceedings of Linnaeus Eco-Tech; 2010 Nov 26-28; Kalmar, Sweden; 2012.

Das A, Bhattacharya S, Panchanan G, Navya BS, Nambiar P. Production, characterization, and congo red dye decolourizing efficiency of a laccase from *Pleurotus ostreatus* MTCC 142 cultivated on co-substrates of paddy straw and corn husk. Journal of Genetic Engineering and Biotechnology 2016; 14:281-8.

Demirbas A. Physical properties of briquettes from waste paper and wheat straw mixtures. Energy Conversion and Management 1999;40:437-45.

Fen L, Xuwei Z, Nanyi L, Puyu Z, Shuang Z, Xue Z, et al. Screening of lignocellulose-degrading superior mushroom strains and determination of their CMCase and laccase activity. The Scientific World Journal 2014;6:Article No. 763108.

Garrido MA, Conesa JA, Garcia MD. Characterization and production of fuel briquettes made from biomass and plastic wastes. Energies 2017;10(7):Article No. 850.

Haripriya R, Parkavi V, Jothi D, Delphin DV, Thirumalaivasan P. Industrially important enzymes from spent oyster mushroom bed wastes. World Journal of Pharmaceutical Research 2014;3(5):483-92.

Heinzkill M, Bech L, Halkier T, Schneider P, Anke T. Characterization of laccases and peroxidases from wood-rotting fungi (family Coprinaceae). Applied and Environmental Microbiology 1998;64(5):1601-6.

Isikhuemhen OS, Mikiashvili NA, Kelkar V. Application of solid waste from anaerobic digestion of poultry litter in *Agrocybe aegerita* cultivation: Mushroom production, lignocellulolytic enzymes activity and substrate utilization. Biodegradation 2009;20:351-61.

Kers J, Kulu P, Aruniit A, Laurmaa V, Križan P, Soos L, et al. Determination of physical, mechanical, and burning characteristics of polymeric waste material briquettes. Estonian Journal of Engineering 2010;16(4):307-16.

Kumar R, Kaur J, Jain S, Kumar A. Optimization of laccase production from *Aspergillus flavus* by design of experiment technique: Partial purification and characterization. Journal of Genetic Engineering and Biotechnology 2016;14:125-31.

Lim SH, Lee YH, Kang HW. Efficient recovery of lignocellulolytic enzymes of spent mushroom compost from oyster mushrooms, *Pleurotus* spp., and potential use in dye decolorization. Mycobiology 2013;41(4):214-20.

Madhavi V, Lele SS. Laccase: Properties and applications. BioResources 2009;4(4):1694-717.

Miller GL. Use of dinitrosalicylic acid reagent for determination of reducing sugar. Analytical Chemistry 1959;31(3):426-8.

More SS, Renuka PS, Pruthvi K, Swetha M, Malini S, Veena SM. Isolation, purification, and characterization of fungal laccase from *Pleurotus* sp. Enzyme Research 2011:Article No. 248735.

Mtui GYS. Lignocellulolytic enzymes from tropical fungi: Types, substrates, and applications. Scientific Research and Essays 2012;7(15):1544-55.

Narra M, Balasubramanian V, James JP. Enhanced enzymatic hydrolysis of mild alkali pre-treated rice straw at high-solid loadings using in-house cellulases in a bench scale system. Bioprocess and Biosystems Engineering 2016;39:993-1003.

Olorunnisola A. Production of fuel briquettes from waste paper and coconut husk admixtures. Agricultural Engineering International: CIGR Journal 2007;9:1-11.

Rajeeva S, Lele SS. Bioprocessing of laccase produced by submerged culture of *Ganoderma* sp. WR-1. Separation and Purification Technology 2010;76:110-9.

Ryu DDY, Mandels M. Cellulases: Biosynthesis and applications. Enzyme and Microbial Technology 1980;2(2):91-102.

Sadh PK, Duhan S, Duhan JS. Agro-industrial wastes and their utilization using solid state fermentation: A review. Bioresources and Bioprocessing 2018;5(1):1-15.

Sahay R, Yadav RSS, Yadav KDS. Purification and characterization of extracellular laccase secreted by *Pleurotus sajor-caju* MTCC 141. Chinese Journal of Biotechnology 2008;24(12):2068-73.

Saravanan P, Muthuvelayudham R, Viruthagiri T. Enhanced production of cellulase from pineapple waste by response surface methodology. Journal of Engineering 2013;8:Article No. 979547.

Saroj P, Manasa P, Narasimhulu K. Characterization of thermophilic fungi producing extracellular lignocellulolytic enzymes for lignocellulosic hydrolysis under solid-state fermentation. Bioresources and Bioprocessing 2018;5(13):Article No. 31.

Shin K, Lee Y. Purification and characterization of a new member of the laccase family from the white-rot basidiomycete *Coriolus hirsutus*. Archives of Biochemistry and Biophysics 2000;384(1):109-15.

Sing CY, Aris SS. A study of biomass fuel briquettes from oil palm mill residues. Asian Journal of Scientific Research 2013; 6(3):537-45.

Singh AD, Abdullah N, Vikineswary S. Optimization of extraction of bulk enzymes from spent mushroom compost. Journal of Chemical Technology and Biotechnology 2003;78:743-52.

Suwannawong P, Khammuang S, Sarnthima R. Decolorization of rhodamine B and congo red by partial purified laccase from *Lentinus polychrous* Lév. Journal of Biochemical Technology 2010;3(2):182-6.

Tamilvanan A. Preparation of biomass briquettes using various agro-residues and waste papers. Journal of Biofuels 2013; 4(2):47-55.

Thurston CF. The structure and function of fungal laccases. Microbiology 1994;140:19-26.

Yaman S, Sahan M, Haykiri-Acma H, Sesen K, Kucukbayrak S. Fuel briquettes from biomass-lignite blends. Fuel Processing Technology 2001;72:1-8.

Enhancement of Methane Production in Anaerobic Digestion of Food Waste using Thermal Pretreatment

T.U. Habarakada Liyanage and Sandhya Babel*

School of Bio-chemical Engineering and Technology, Sirindhorn International Institute of Technology, Thammasat University, Pathum Thani, Thailand

ARTICLE INFO

Received: 16 Apr 2021
Received in revised: 3 Aug 2021
Accepted: 4 Aug 2021
Published online: 21 Sep 2021
DOI: 10.32526/ennrj/20/202100063

Keywords:
Food waste/ Anaerobic Digestion/ Bio-methane/ Pretreatment/ Buffer/ Bioreactor

*** Corresponding author:**
E-mail: sandhya@siit.tu.ac.th

ABSTRACT

Anaerobic digestion (AD) is an energy production process and food waste is a potential feedstock. The main biochemical reactions are Hydrolysis, Acidogenesis, Acetogenesis, and Methanogenesis. The hydrolysis step acts as the rate-limiting reaction and the pretreatment of the feedstocks can be used to support this step. In this research, thermal pretreatment was used as a potential method for food waste pretreatment. Six different pretreatment conditions were used: two different temperatures (80°C and 100°C) and three different pretreatment times (30, 60, and 90 min). The Bio-Methane Potential (BMP) test was conducted using 120 mL serum bottles for 20 days to determine the most suitable pretreatment conditions. An experiment was also conducted at the selected optimal conditions (80°C for 90 min) using a small-scale bioreactor against the control with a $NaHCO_3$ buffer solution. The highest Soluble Chemical Oxygen Demand (SCOD) was observed at 100°C for 90 min. The optimal pretreatment was selected as 80°C for 90 min, which produced 14.75 mL/g VS of methane while the control produced 8.64 mL/g VS in BMP test. After a few days, the methane production started to slow down due to a decrease in pH. When a buffer was added, a specific methane yield of 120.13 mL/g VS was observed in the small-scale bioreactor. This was an 11.24% increase compared to the buffered control without thermal pretreatment. In conclusion, thermal pretreatment has a potential to enhance the AD but it is economical to use with less biodegradable waste than food waste.

1. INTRODUCTION

At present, the world generates about 2.01 billion tonnes of solid waste per year (known as Municipal Solid Waste (MSW)), and it is projected to increase to 3.40 billion tonnes by 2050. The average personal waste generation is about 0.74 kg/day (Kaza et al., 2018). Food waste accounts for the largest faction of MSW, and one-third of the food produced goes to waste. Several methods are used to manage organic waste such as landfilling, incineration, composting, and AD. According to the World Bank, the most practiced method of dealing with MSW is landfilling. Landfilling causes many environmental effects such as groundwater contamination, the release of Greenhouse gases (GHGs), odors, and acts as a breeding ground for rats, insects, and other scavenging animals (Hoornweg and Bhada-Tata, 2012). Current food waste generation is estimated at 1.3 billion tonnes per year, and the GHGs emission is estimated at 3.3 billion tonnes of CO_2/year (FAO, 2021). About 18% of global warming occurs due to these processes that can be easily avoided by diverting landfilling to AD or composting (Ward et al., 2008). Therefore, it is important to divert organic waste, especially food waste from landfills to AD processes.

AD is a complex biological reaction with four distinguishable steps: Hydrolysis, Acidogenesis or Fermentation, Acetogenesis, and Methanogenesis. The hydrolysis step slows down the AD because (in hydrolysis) complex molecules are broken down into simpler molecules (such as carbohydrates into glucose, proteins into amino acids, and lipids into fatty acids). Therefore, hydrolysis requires much more time than the other steps (Zhang et al., 2014; Merlin et al., 2014). Slow processes require larger reactors, and higher initial and operating costs. These issues can be

Citation: Liyanage TUH, Babel S. Enhancement of methane production in anaerobic digestion of food waste using thermal pretreatment. Environ. Nat. Resour. J. 2022;20(1):10-18. (https://doi.org/10.32526/ennrj/20/202100063)

addressed by employing pretreatment methods (Merlin et al., 2014). There are several methods to improve AD, and pretreatment can assist in the hydrolysis step. Many researchers have reported different pretreatment methods such as biological, mechanical, chemical, and thermal methods on different substrates such as organic-portion of MSW, activated sludge, lignocellulose biomass, and manure (Carrere et al., 2016). Only a few researchers have focused on food waste using thermal pretreatment as a potential method. Moreover, these researchers focused on high temperatures for short duration or low temperatures for long duration (Ariunbaatar et al., 2014; Krishna and Kalamdhad, 2014; Naran et al., 2016). In this research, high and low temperatures were examined for short pretreatment times using food waste as the substrate.

Thus, the objective of this study is to determine the optimal thermal pretreatment conditions that are suitable for food waste, to enhance methane production. A bio-methane potential test was conducted to measure the effects of pretreatment temperature and time. The scope of this study was limited to food waste and two thermal pretreatments with three short time pretreatment durations. The potential use of thermal pretreatment was further investigated using small-scale anaerobic reactors.

2. METHODOLOGY

2.1 Substrate and inoculum

Food waste was used as the feedstock and granular sludge was used as the inoculum. The feedstock was collected from the engineering faculty canteen at Thammasat University, Thailand, and indigestible materials such as bones and seashells were sorted out. The waste samples were then ground and stored at 4°C until use. Granular sludge was collected from an upflow anaerobic sludge blanket anaerobic digester (UASB) at Pathum Thani Brewery Co., Ltd (Pathum Thani, Thailand). The TS content was maintained at 5% by diluting to maintain a lower VS content so that the digestion can be carried out easily in a small-scale reactor.

2.2 Characterization

The C, H, N, and S elemental contents of the food waste and inoculum were determined using an elemental analyzer (THERMO FLASH 2000), and the C:N ratio was calculated following USDA (2015). The Total Solid Content (TS) and Volatile Solid content (VS) were measured according to the Environmental Protection Agency (United State) method 1684 (USEPA, 2001).

2.3 Thermal pretreatment

Two different pretreatment temperatures were used with three different durations, which were 80°C and 100°C for 30 min, 60 min, and 90 min. These conditions were selected to determine the suitable thermal pretreatment condition at low temperatures and short treatment time. Lower pretreatment thermal conditions are economically viable compared to higher temperature or longer pretreatment time (Zhang et al., 2015). Furthermore, these conditions are selected so that it also can be used as conditioning process which agrees to the EU Regulation EC1774/2002 (Ariunbaatar et al., 2014). Treatments were conducted in glass bottles and 200 mL of sample were used for each pretreatment. The thermal pretreatment was conducted in a preheated forced air oven. The samples were stored at 4°C after pretreatments until used further.

2.4 Solubilization

SCOD was measured to determine the effects of pretreatment on solubilization. The pretreated samples were filtered using GF/C filter papers. The chemical oxygen demand (COD) of the filtrate was measured according to the closed reflux titrimetric method, following the standard methods for water and wastewater treatment (APHA, 2017).

2.5 Bio-methane potential test

BMP tests were conducted to determine the effectiveness of pretreatments on enhancing methane generation. BMP tests were conducted in 120 mL serum bottles. Substrate and inoculum were mixed in a 1:1 ratio (g VS to g VS). After mixing, the pH was adjusted to 7 by adding 1 M NaOH or 1 M HCl. The sample size was 75 mL, leaving 45 mL of headspace. The serum bottles were sealed with rubber stoppers and aluminum (Al) crimpers. The headspace was replaced by N_2 gas to facilitate AD. Then, the serum bottles were covered with Al foil and placed in a shaking incubator at 37°C. Two replicates were performed for each sample. The BMP tests were conducted for 20 days. Biogas production in each day was measured by the displacement method using a disposable syringe. The methane content was measured by a gas chromatograph (GC) (PerkinElmer, USA), equipped with a thermal conductivity detector (TCD) with a Porapak Q, 50/80 mesh column. The

operating temperatures of the column, detector, and injector were 45, 100, and 100ºC, respectively. Helium gas was used as the mobile phase with a flow rate of 25 mL/min. The produced methane amount was calculated accordingly (Naran et al., 2016; Ta and Babel, 2019). The conditions with the highest cumulative methane yield were selected as the optimal pretreatment.

2.6 Small-scale bioreactor

After selecting the optimal thermal pretreatment conditions, small-scale bioreactors (2 L) were used to determine the effects of the thermal pretreatment on food waste. In this experiment, the pH was controlled in both control and the reactor with thermally pretreated substrate by adding $NaHCO_3$ buffer (300 mg/g VS) (Habarakada and Babel, 2020). As described in the BMP tests, 1:1 was used for the inoculum to feedstock ratio. A final working volume of 1 L was used for the AD. The headspace was purged with N_2 gas. The experiment was conducted at room temperature (28-30ºC). The experimental setup is shown in Figure 1. For comparison, a control reactor was also run in a similar way where the substrate was not thermally pretreated.

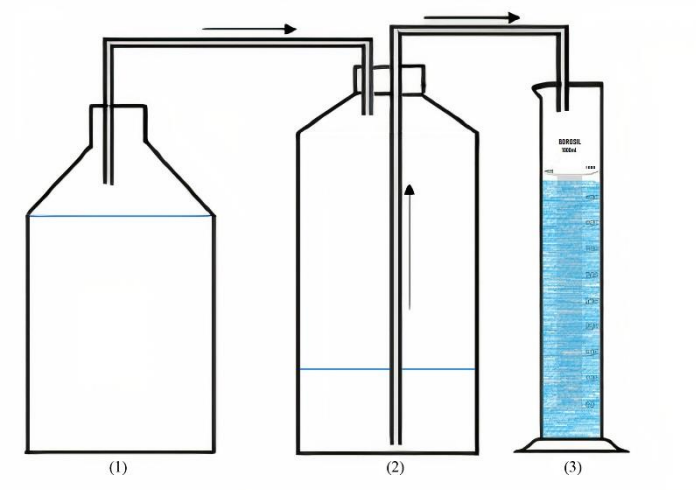

Figure 1. Schematic diagram of the bioreactor and the gas collecting apparatus. (1) 2 L glass reactor; (2) gas collecting bottle; (3) volumetric flask

3. RESULTS AND DISCUSSION

3.1 Characterization of food waste and inoculum

The characteristics of the substrate and inoculum are shown in Table 1. The food waste mainly consisted of cooked rice, noodles, pasta, meats, eggs, seafood, and vegetables. Occasionally raw vegetables and green leaves were also found. The composition of food waste varies as food preferences are fluctuating. The VS and TS of the substrate and feedstock were 90.94±0.89% and 21.91±0.8%, respectively, while the VS and TS of the inoculum were 89.01±3.8% and 4.54±0.5%, respectively. The TS of the feedstock was decreased to 5±0.5% by diluting with distilled water. The pH of the feedstock and inoculum were 5.2±0.4 and 7.83±0.10, respectively. The sample pH was measured between 4.5 and 6, after mixing with the inoculum. The final pH was adjusted to 7 by adding 1 M NaOH. The C/N ratio of the feedstock and inoculum was calculated as 18.03:1 and 4.76:1, respectively. The C/N ratio of the mixture was determined as 10.95:1. According to Divya et al. (2015), a suitable C/N ratio for AD is from 10 to 35.

Table 1. Characteristics of substrate and inoculum

Parameter	Substrate	Inoculum
C	53.57±0.23%	47.02±0.52%
H	8.06±0.03%	6.62±0.08%
N	2.97±0.42%	9.87±0.14%
S	0	1.11±0.26%
pH	5.2±0.4	7.83±0.10
C:N	18.03:1	4.76:1
TS	21.91±0.8%	4.54±0.5%
VS	90.94±0.89%	89.01±3.8%

3.2 Effects of pretreatment on solubilization

The solubilization of organic compounds was measured after pretreatment. Pretreatment aids AD, either by increasing the SCOD through solubilization or breaking down the larger molecules into smaller

molecules or both (Kim et al., 2003). Figure 2 shows the measured SCOD values after each pretreatment. The highest SCOD was observed in the 100°C for 90 min pretreatment which was a 5% increase, compared to the control. The SCOD values increased with an increase in the pretreatment time and temperature. According to the T-test, there is no significant difference ($p>0.05$) between the SCOD values at 100°C for 90 min pretreatment and the control (Table S1). Previous researchers also have observed the same pattern where higher temperatures had higher SCOD values in food waste (Kumar et al., 2020). Menon et al (2016) has obtained the highest SCOD increase for the 130°C pretreatment. The increase of SCOD level was due to the solubilization of extracellular matter and extracellular polymeric substances which leads to the increase of SCOD in the waste (Elbeshbishy and Nakhla, 2011). The increase of SCOD increases the nutrient content in the soluble state, which means that bacteria can utilize these nutrients much easier and quicker.

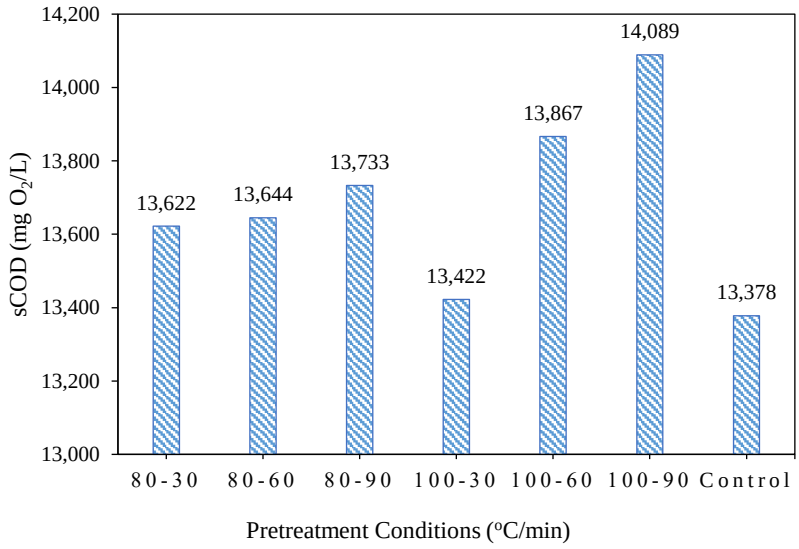

Figure 2. Changes in SCOD after thermal pretreatment

El Gnaoui et al. (2020) observed the highest solubilization in food waste at the 100°C pretreatment. The solubilization increased with the increase of temperature. Their study observed higher solubilizations in shorter pretreatment durations compare to this research where the highest solubilization was observed at 30 min pretreatment. The composition of waste plays a major role as optimum solubilization can be achieved with different pretreatment conditions. However, higher temperature pretreatments give higher SCOD levels and depending on the type, composition, and digestibility of the waste, the treatment duration can vary. A recent research study reported higher SCOD levels at pretreatment conditions of 170°C for 60 min with an initial TS of 150 g/L. This indicates that the substrate TS level is also a major factor when determining the most suitable thermal pretreatment conditions for food waste AD (Zhang et al., 2021).

3.3 Bio-methane potential

The results of methane generation after thermal pretreatment are shown in Figure 3. Figure 3(a) shows the cumulative methane production measured for 20 days, Figure 3(b) shows the cumulative methane production at the end of the 20-day BMP test, and Figure 3(c) compares the daily methane generation between the best pretreatment and the control.

As shown in Figures 3(a) and 3(b), the highest methane yield was observed in the 80°C for 90 min pretreated samples, followed by 80°C for 60 min. This increase can be explained by the deflocculation of macromolecules. Due to the deflocculation of macromolecules by the thermal pretreatment, the surface area is increased for the reactions, causing an increase in methane production (Ariunbaatar et al., 2014). Pretreated samples at 100°C for 60 min and 90 min did not show any (substantial) improvement compared to the control. No visible lag phase was observed in all pretreated samples and the control.

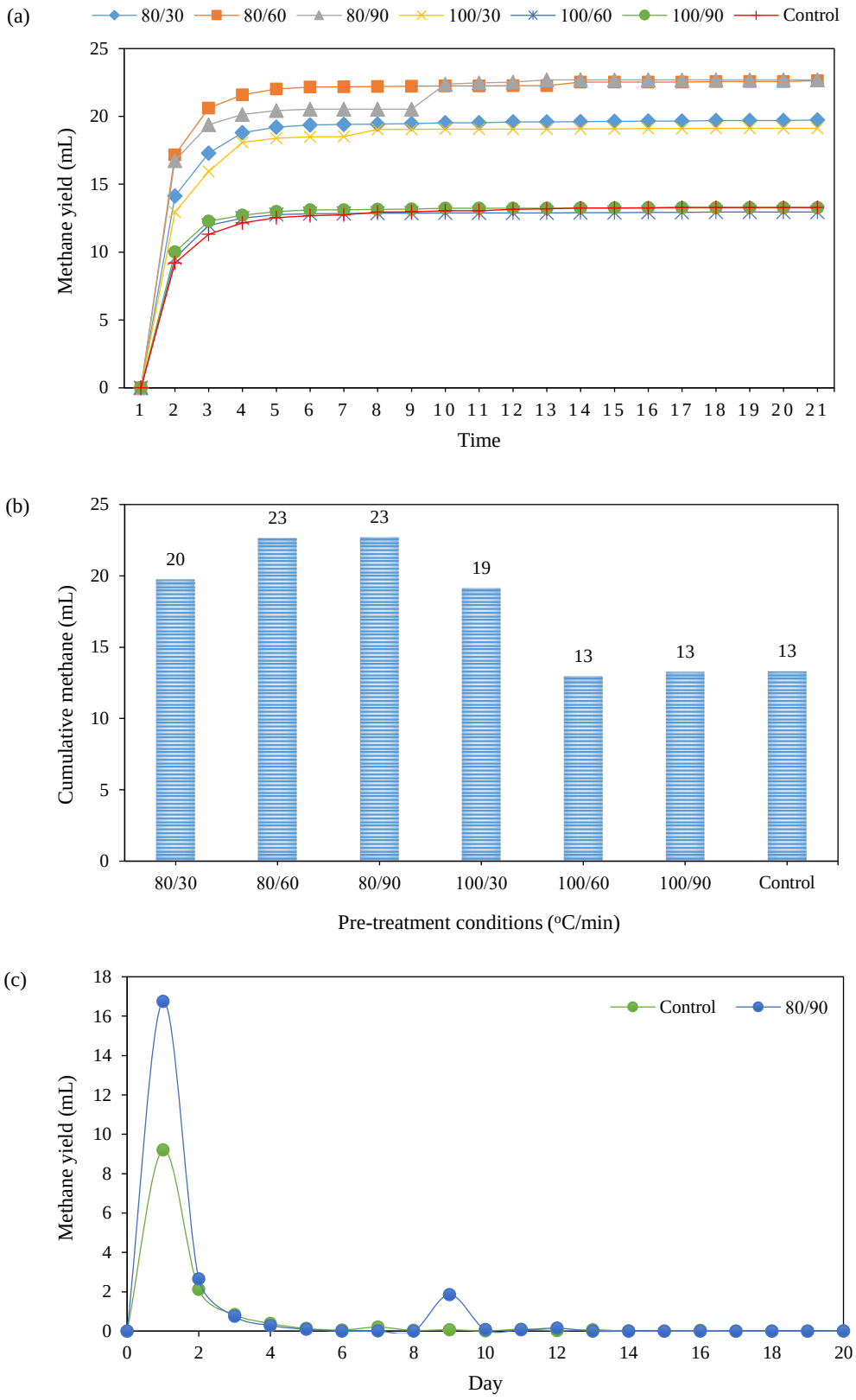

Figure 3. (a) Cumulative methane production with time at different pretreatment conditions, (b) Cumulative methane production after 20 days, (c) Daily methane production comparison between the 80°C/90 min and control

Several BMP tests were performed to verify the data. In all the BMP tests, the same pattern was observed. The high biodegradability of food waste may be the reason for no visible lag phase. More than 65% of the cumulative methane yield was observed within the first 24 h. In all cases, more than 90% of methane was observed within the first 4 days. The methane production drastically decreased after a few

days (Figure 3(c)), due to a decrease in pH as methanogenic bacteria are susceptible to changes in media pH. The average pH at the end of the BMP test of the control and the 80ºC for 90 min pretreated sample was 4.07 and 4.04, respectively. A pH decrease was observed in all the pretreated samples at the end of the BMP tests. This may be due to the initial high VS content of the feedstock. Although the initial TS content was decreased to 5%, the available VS content was high enough for the reactor to produce a high amount of Volatile Fatty Acids (VFA). The accumulation of VFA in anaerobic media can result in a pH decrease (Cho et al.,1995). The pH was adjusted to pH 7 at the beginning of the BMP test. However, this was not enough to maintain the AD process, as the production of VFA caused a decrease in the media pH. In AD, different reactions prefer different pH levels, as pH is a governing factor in microbial growth. Hydrolytic bacteria prefer a pH level of 5.5-6.0, while acidogenic and acetogenic bacteria prefer a pH level of 6.0-7.0. Methanogenic bacteria prefer a pH level of 6.5-7.5 (Leung and Wang, 2016). Therefore, it is clear that the methane generation was affected by the pH variation after a few days of the BMP test. This can also be observed in Figure 3(a) and 3(c) where there is no substantial amount of methane produced after few days.

Figure 4 shows the cumulative biogas production after 20 days of BMP tests. The highest cumulative biogas production was observed in the 80ºC for 30 min pretreatment. The 80ºC for 30 min pretreatment and 80ºC for 90 min pretreatment had a 12% and 3% increase in cumulative biogas yield respectively, compared to control.

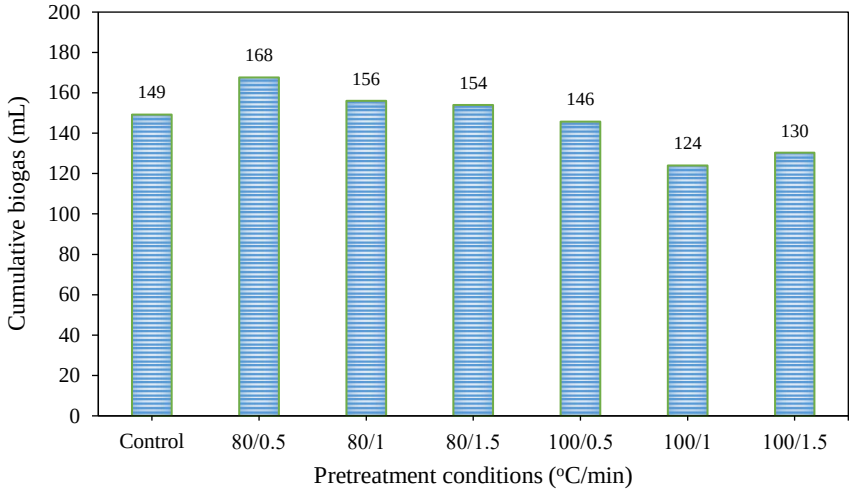

Figure 4. Cumulative biogas production at different pretreatment conditions after 20 days

Although the increase of biogas production was less in the 80ºC for 90 min pretreatment compared to the 80ºC for 30 min pre-treatment, the cumulative methane yield was higher. In the 100ºC pretreatments, the cumulative biogas yield was less than the control. This biogas decrease may be due to the occurrence of the Maillard reaction. Researchers have reported that the Maillard reaction can occur between amino acids and reducing sugars at temperatures above 80ºC (Menon et al., 2016). The end products of this reaction are not easily biodegradable. Hence, this can decrease methane production. The possibility of the Maillard reaction increases with an increase in the pretreatment temperature and time. This could be the reason for low biogas generation in the 100ºC treatments (Ariunbaatar et al., 2014; Eskicioglu et al., 2007). The daily methane yield (Figure 3(a)) in this study also showed no improvement compared to control at higher temperatures. Some researchers have reported a slower methane generation after pretreatments using higher temperatures compared to the control. Also, they have observed higher Maillard reaction products when feedstock concentrations are high (Ortega-Martínez et al., 2021).

In the 80ºC for 90 min pretreatment, the volume of methane produced per one gram of VS is 14.75 mL, and the control produced 8.64 mL. These results are lower than those reported by Cho et al. (1995). They observed more than 300 mL/g VS of methane during the AD of food waste. According to Cho et al. (1995), the initial VS content should be less than 10 g/L to obtain a higher methane yield from food waste when using a 1:4 inoculum to feedstock ratio. The authors have observed rapid production of VFAs in high initial

VS samples, causing a pH decrease, with inhibition of methane production. In this research, the initial VS content was estimated to be 35 to 45 g/L.

As the next step, $NaHCO_3$ buffer solution was used to control the pH changes. Although more dilution can also be used to decrease the initial VS, this was not used as a higher dilution factor requires a large reactor and a larger storage area to manage the same amount of waste.

3.4 Small-scale bioreactor

The BMP assay is a commonly used method to predict the theoretical methane yield of a substrate and for dimensioning anaerobic reactors. A small-scale anaerobic reactor was used to determine the behavior of AD of food waste after thermal pretreatment.

The selected optimal thermal pretreatment was used along with a control experiment. The AD was conducted for 20 days, as in the BMP tests. The pH in the reactor was regulated by adding $NaHCO_3$ 300 mg/g VS. The optimal $NaHCO_3$ concentration was determined by a separate set of experiments (Habarakada and Babel, 2020). Figure 5 shows the cumulative methane generation for the 20-day experiment.

The highest cumulative methane yield was observed in the thermally pretreated (80°C 90 min) food waste, which was 120.13 mL/g VS, while the control produced 107.99 mL/g VS. The thermal pretreatment had an increased cumulative methane yield of 11.24% compared to the control. Unlike in the previous BMP test, the methane production did not decrease, as the added $NaHCO_3$ acted as a buffer and maintained the pH. The reactors continued to produce methane after 20 days of AD. The cumulative biogas yield of the thermal pretreatment was not significantly different from the control ($p>0.05$) after 20 days (Table S2). However, the cumulative methane yield increased after 20 days. Therefore, a pretreated sample may have better performance (long-term), compared to the control.

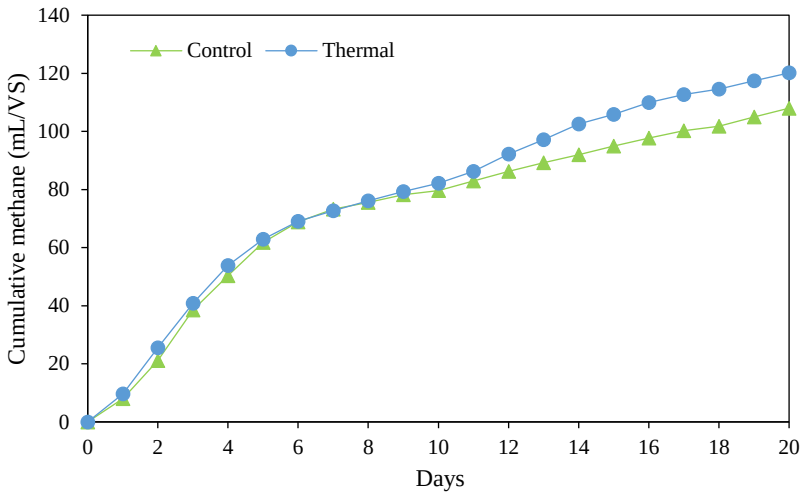

Figure 5. Cumulative methane production by food waste, with and without thermal pretreatment in a small-scale anaerobic reactor

As in Figure 6(a), methane was produced from the 1st day, and it continued to increase until day 3 in both conditions. After day 3, the daily methane production decreased and by days 7-8 of the digestion, the daily methane production became stable for the control and the reactors with a pretreated substrate. This can be described as the stationary phase. As these experiments were conducted in ambient conditions, small fluctuations can be observed (Figure 6(b)) in the daily methane yield. After 20 days of AD, the average biogas yield for the control bioreactor was 35.34% while the thermal pretreatment had an average methane yield of 39%. In the thermal pretreatment, the maximum daily methane yield was 50.97% (on day 13) while the control had a maximum daily methane yield of 48.47% (on day 5). The overall reaction has improved in the thermal pretreatment compared to the control but it was not much different. This might be due to several reasons such as the relatively easy digestibility of food waste and the initial bacterial activity in the food waste before adding it to the bioreactor.

In the initial BMP tests, the 80°C for 90 min pretreated food waste produced only 14.75 mL/g VS of methane while the bioreactor with the same conditions produced 120.13 mL/g VS of methane.

Therefore, the added buffer played a major role in controlling and stabilizing the pH of the anaerobic media for better digestion. Also, a larger reactor better shows the AD process compared to the BMP test. Increased cumulative methane generation can be observed even after 20 days (Figure 6). Fadzil et al. (2020) has observed higher methane production at 80ºC for 90 min pretreatment compared to control. The increase of methane production was due to the improved biodegradability of food waste due to the thermal pretreatment.

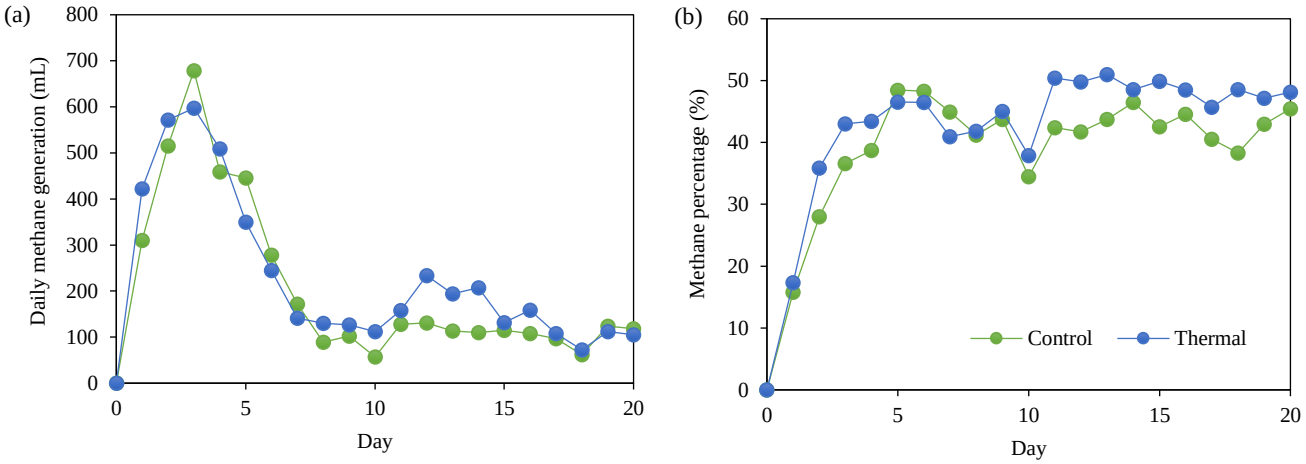

Figure 6. Small scale bioreactor (a) Daily methane generation, (b) Daily percentage of methane in biogas

4. CONCLUSION

The use of thermal pretreatment to increase methane production was examined in this research. The SCOD of sludge increased after thermal treatment and the highest SCOD was observed at 100ºC for 90 min pretreatment. The BMP test results showed an initial methane generation in each sample but after a few days the methane production was drastically decreased due to the accumulation of VFA that causes a reduction in pH. These pH reductions are not suitable for methanogenesis. The highest methane yield was observed in the 80ºC for 90 min thermal pretreated sample. The methane production increased by 11.24% compared to the control in small-scale bioreactor where $NaHCO_3$ buffer solution was used to control the pH level. Therefore, thermal pretreatment can be used as a method to increase the methane yield. From an economical standpoint, it is more suitable for less digestible feedstock such as garden waste or agricultural waste than food waste as it requires energy.

The potential use of thermal pretreatment has two main benefits. One is the increase of methane production and the other benefit is that the thermal pretreatment can act as a conditioning process for the substrate (Ariunbaatar et al., 2014). Conditioning is vital for substrates that contain pathogenic bacteria, and in some countries, they require sterilization before or after AD. Furthermore, $NaHCO_3$ can be used as a buffer in AD to stabilize pH variations without decreasing the initial VS level.

ACKNOWLEDGEMENTS

The authors would like to thank the Excellent Foreign Student (EFS) Master's Scholarship Program in Sirindhorn International Institute, Thammasat University for financial support.

REFERENCES

American Public Health Association (APHA), American Water Works Association (AWWA), and Water Environment Federation (WEF). Standard Methods for the Examination of Water and Wastewater. Washington, DC, USA: American Public Health Association; 2017.

Ariunbaatar J, Panico A, Frunzo L, Esposito G, Lens PNL, Pirozzi F. Enhanced anaerobic digestion of food waste by thermal and ozonation pretreatment methods. Journal of Environmental Management 2014;146:142-9.

Carrere H, Antonopoulou G, Affes R, Passos F, Battimelli A, Lyberatos G, et al. Review of feedstock pretreatment strategies for improved anaerobic digestion: From lab-scale research to full-scale application. Bioresource Technology 2016;199: 386-97.

Cho JK, Park SC, Chang HN. Biochemical methane potential and solid state anaerobic digestion of Korean food wastes. Bioresource Technology 1995;52:245-53.

Divya D, Gopinath LR, Merlin CP. A review on current aspects and diverse prospects for enhancing biogas production in sustainable means. Renewable and Sustainable Energy Reviews 2015;42:690-9.

Elbeshbishy E, Nakhla G. Comparative study of the effect of

ultrasonication on the anaerobic biodegradability of food waste in single and two-stage systems. Bioresource Technology 2011;102:6449-57.

El Gnaoui Y, Karouach F, Bakraoui M, Barz M, El Bari H. Mesophilic anaerobic digestion of food waste: Effect of thermal pretreatment on improvement of anaerobic digestion process. Energy Reports 2020;6:417-22.

Eskicioglu C, Terzian N, Kennedy KJ, Droste RL, Hamoda M. Athermal microwave effects for enhancing digestibility of waste activated sludge. Water Research 2007;41:2457-66.

Fadzil F, Fadzil F, Sulaiman SM, Shaharoshaha AM, Seswoya R. Methane production from the digestion of thermally treated food waste at 80°C. Journal of Environmental Treatment Techniques 2020;8:1017-22.

Food and Agriculture Organization of the United Nations (FAO). Food wastage: Key facts and figures [Internet]. 2021 [cited 2021 July 30]. Available from: http://www.fao.org/news/story/en/item/196402/icode/.

Habarakada LTU, Babel S. Thermal, ultrasonic and electrochemical pretreatment methods to enhance the solubilization of organic substance and methane generation in food waste. Journal of Material Cycles and Waste Management 2020;22:1418-26.

Hoornweg D, Bhada-Tata P. What a Waste: A Global Review of Solid Waste Management. Washington, DC, USA: World Bank; 2012.

Kaza S, Yao LC, Bhada-Tata P, Van Woerden F. What a Waste 2.0: A Global Snapshot of Solid Waste Management to 2050. Vol. 139. Washington, DC, USA: World Bank; 2018.

Kim J, Park C, Kim TH, Lee M, Kim S, Kim SW, et al. Effects of various pretreatments for enhanced anaerobic digestion with waste activated sludge. Journal of Bioscience and Bioengineering 2003;95:271-5.

Krishna D, Kalamdhad AS. Pre-treatment and anaerobic digestion of food waste for high rate methane production: A review. Journal of Environmental Chemical Engineering 2014;2: 1821-30.

Kumar BB, Huang H, Dai J, Chen GH, Wu D. Impact of low-thermal pretreatment on physicochemical properties of saline waste activated sludge, hydrolysis of organics and methane yield in anaerobic digestion. Bioresource Technology 2020;297:ID 122423.

Leung DYC, Wang J. An overview on biogas generation from anaerobic digestion of food waste. International Journal of Green Energy 2016;13:119-31.

Menon A, Ren F, Wang JY, Giannis A. Effect of pretreatment techniques on food waste solubilization and biogas production during thermophilic batch anaerobic digestion. Journal of Material Cycles and Waste Management 2016;18:222-30.

Merlin CP, Gopinath LR, Divya D. A review on anaerobic decomposition and enhancement of biogas production through enzymes and microorganisms. Renewable and Sustainable Energy Reviews 2014;34:167-73.

Naran E, Toor UA, Kim DJ. Effect of pretreatment and anaerobic co-digestion of food waste and waste activated sludge on stabilization and methane production. International Biodeterioration and Biodegradation 2016;113:17-21.

Ortega-Martínez E, Chamy R, Jeison D. Thermal pre-treatment: Getting some insights on the formation of recalcitrant compounds and their effects on anaerobic digestion. Journal of Environmental Management 2021;282:ID 111940.

Ta AT, Babel S. Utilization of green waste from vegetable market for biomethane production: Influences of feedstock to inoculum ratios and alkalinity. Journal of Material Cycles and Waste Management 2019;21:1391-401.

United States Department of Agriculture (USDA). Soil Survey Laboratory Information Manual: Soil Survey Investigations Report No. 45. Nebraska, USA: Lulu.com; 2015.

United States Environmental Protection Agency (USEPA). Method 1684: Total, Fixed, and Volatile Solids in Water, Solids, and Biosolids. Washington, DC, USA: United States Environmental Protection Agency, Office of Water, Office of Science and Technology, Engineering and Analysis Division; 2001.

Ward AJ, Hobbs PJ, Holliman PJ, Jones DL. Optimisation of the anaerobic digestion of agricultural resources. Bioresource Technology 2008;99:7928-40.

Zhang C, Su H, Baeyens J, Tan T. Reviewing the anaerobic digestion of food waste for biogas production. Renewable and Sustainable Energy Reviews 2014;38:383-92.

Zhang J, Lv C, Tong J, Liu J, Liu J, Yu D, et al. Optimization and microbial community analysis of anaerobic co-digestion of food waste and sewage sludge based on microwave pretreatment. Bioresource Technology 2015; 200:253-61.

Zhang W, Cao H, Liang Y. Optimization of Thermal Pretreatment of Food Waste for Maximal Solubilization. Journal of Environmental Engineering 2021;147(4):ID 04021010.

Enzymatic Degradation of Azo Bonds and Other Functional Groups on Commercial Silk Dyes by *Streptomyces coelicoflavus* CS-29

Wai Phyo Mon[1], Phongphan Jantaharn[2], Sophon Boonlue[1], Sirirath McCloskey[3], Somdej Kanokmedhakul[2], and Wiyada Mongkolthanaruk[1*]

[1]*Department of Microbiology, Faculty of Science, Khon Kaen University, Khon Kaen 40002, Thailand*
[2]*Department of Chemistry, Faculty of Science, Khon Kaen University, Khon Kaen 40002, Thailand*
[3]*Natural Products Research Unit, Centre of Excellence for Innovation in Chemistry (PERCH-CIC), Department of Chemistry, Faculty of Science, Khon Kaen University, Khon Kaen 40002, Thailand*

ARTICLE INFO

Received: 4 Jun 2021
Received in revised: 4 Aug 2021
Accepted: 8 Aug 2021
Published online: 21 Sep 2021
DOI: 10.32526/ennrj/20/202100104

Keywords:
Azo silk dyes/ Biosorption/ Decolorization/ Degradation

*** Corresponding author:**
E-mail: wiymon@kku.ac.th

ABSTRACT

Azo dyes are used for silk textile manufacture, where their decolorization and detoxication are necessary after initial dying in the craft industry. The bio-decolorization efficiency of *Streptomyces coelicoflavus* CS-29 toward commercial azo blue and red dyes was investigated, analyzing the degradation and adsorption of dye molecules. *S. coelicoflavus* CS-29 showed reductions of 70% and 51% in red and blue dyes, respectively, after seven days. Morphological observation by light microscopy showed that dye molecules were adsorbed onto *S. coelicoflavus* CS-29 cell surface to form a dense cell pellet. Moreover, peroxidase and laccase activity were detected as extracellular enzymes, but no azo-reductase was detected. From the enzymatic activity, changes of dye profiles in HPLC showed differences between control dyes (untreated dyes) and metabolized products of dyes treated with *S. coelicoflavus* CS-29. The presence of main functional azo groups (-N=N-) in both blue and red silk dyes was indicated by FTIR analysis, in the untreated azo dyes. The azo bonds seemed to disappear in metabolites after *S. coelicoflavus* CS-29 treatment and other functional groups were changed compared to the control dyes. The treated dyes showed no significant effect on seed germination, root length, and shoot length of mung beans during phytotoxicity analysis. The red dyes showed a more negative effect on shoot lengths than the blue dyes. The overall results showed that *S. coelicoflavus* CS-29 is an effective and promising tool for the treatment of dye contaminated wastewater and the permanent elimination of recalcitrant commercial azo dye pollutants.

1. INTRODUCTION

Dyes play a very important role all over the world as an essential material for multiple manufacturing purposes ranging from small to industrial scale usage. Dyes are used in the textile, pulp and paper, dye and dye intermediate industries, in pharmaceutical, tannery and kraft bleaching capacities. Among these industries, the textile sector utilizes many classes of dyes such as azo dyes, nitro dyes, indigo dyes, anthraquinone dyes, phthalein dyes, triphenyl methyl dyes, and nitrated dyes, with choice based on the dye's chemical structure and chromophore, the dyeing process used, the color index and application (Benkhaya et al., 2020). Azo dyes are one of the largest families of textile dyes used. These dyes are xenobiotic compounds containing electron withdrawing groups, generating electron deficiency in the dye molecule, making them resistant to degradation (Singh et al., 2014). Azo dyes are recalcitrant compounds due to a structure of (-N=N-) heterocyclic and aromatic amine which can cause both toxicity (carcinogenic and mutagenic) and a non-biodegradable nature (Sinha and Osborne, 2016).

Silk cottage in Chonnabot istrict, Chaiyaphum, Thailand, is a successful craft industry producing silk products; as such, dyes, particular from Phua Kiam Seen Company, are utilized for the silk dying process in high levels. Disposal of contaminated dyeing

Citation: Mon WP, Jantaharn P, Boonlue S, McCloskey S, Kanokmedhakul S, Mongkolthanaruk W. Enzymatic degradation of azo bonds and other functional groups on commercial silk dyes by *Streptomyces coelicoflavus* CS-29. Environ. Nat. Resour. J. 2022;20(1): 19-28. (https://doi.org/10.32526/ennrj/20/202100104)

effluents in natural water has the potential to severely affect environments and create health hazards, including to freshwater organisms. When this water is in turn used for agriculture, it can affect germination rates and biomass of several ecological crops, with consequences also for wildlife habitats and soil fertility (Saratale et al., 2013). Effective effluent treatment is an important step towards reducing pollutants in natural water and conserving water resources. Bioremediation is considered one possible way to decontaminate wastewater, based on natural technologies using microorganisms, plants and enzymatic system. Many organisms are able to decolorize and metabolize dyes, such as bacteria, fungi, yeasts, actinomycetes and algae (Garg and Tripathi, 2017). This occurs through an enzymatic transformation reaction in which reductive cleavage of azo bond leads to the formation of colourless aromatic amines or adsorption of dye onto the biomass of cells. Toxic amines in dyes can further oxidize to simpler non-toxic forms only under aerobic conditions. The end products of azo dye degradation are dependent on enzymatic system and growth condition of microorganisms; therefore, toxicity of metabolites should be detected using phytotoxicity which is a common tool for monitoring whether compounds are toxic on seed germination and growth of monocotyls or dicotyls, particularly compounds contaminated in environments, such as, metal compounds contaminated in soil, secondary metabolites produced by organisms. The phytotoxicity test is a criteria to detect toxic compounds (end products/by-products) before releasing into environments for safety.

Streptomyces is one of the most plenteous genera of Gram-positive bacteria, which have a superior sorption capacity from mycelia structure consisting of carboxyl, phosphonate, amine and hydroxyl groups for dye interaction. *Actinomyces* used as an adsorbent was able to adsorb and decolorize anthroquinone, phalocyanine and azo dyes effluents without dye degradation (Zhou and Zimmermann, 1993). Meanwhile, the role of peroxidase, laccase, veratryl alcohol oxidase, tyrosinase and azo reductase has been reported for degradation and detoxification of textile dyes (Kurade et al., 2016), particularly laccase likely in *Streptomyces ipomoeae* CECT 3341 (Blánquez et al., 2019). This study focused on the decolorization and detoxification of silk azo dyes using *S. coelicoflavus* CS-29 by observing bacterial morphology changes and dye chemical changes. Biosorption and detoxification are criteria for wastewater treatment systems including dyes and metals. The mycelial bacteria, *Streptomyces*, are good candidates as adsorbents in this system as following removal of biomass after treatment, they can perhaps be re-used.

2. METHODOLOGY

2.1 A bacterium strain and cultivation

The bacterium, *Streptomyces coelicoflavus* CS-29 was a candidate as it had the potential for removal of azo textile dyes from wastewater in previous study (Mon et al., 2020). This strain was isolated from dye-contaminated soil in Chonnabot District, Khon Kaen Province, Northeastern Thailand. The cells grew in minimal broth medium [containing (g/L) Na_2HPO_4 (5.3), KH_2PO_4 (1.98), $MgSO_4 \cdot 7H_2O$ (0.2), NaCl (0.2), yeast extract (2.5) and 1 mL of trace metal solution (g/L) which contained $CaCl_2 \cdot 2H_2O$ (0.05), $CuSO_4 \cdot 5H_2O$ (6.4), $FeSO_4 \cdot 7H_2O$ (1.1), $MnCl_2 \cdot 4H_2O$ (7.9), $ZnSO_4 \cdot 7H_2O$ (1.5)]; the medium was incubated with shaking at 37°C for 2 days and then was used as an inoculum.

2.2 Determination of dye removal

The bacterium grew in the minimal broth medium containing 300 mg/L of commercial textile dyes, blue dye (No. 21) and red dye (No. 34) from Phua Kiam Seen, Co., Ltd, and incubated at 37°C under shaking speed of 150 rpm. The bacterial culture was collected at three, five, seven and 10 days to separate cells and supernatant by centrifugation; the experiment was performed in triplicate. Color residue was measured from the supernatant by UV-VIS spectrophotometer at 554 and 506 nm for blue and red dyes, respectively. The cells were washed with methanol (98%) until no color remained in the cell pellets; the dyes dissolved in methanol solution were measured at 554 and 506 nm for blue and red dyes, respectively; and then the dye concentration (mg/L) was calculated from standard curves with equations of each dye below.

$$\text{Blue dye concentration (y)} = 0.3149X - 0.0029$$

$$\text{Red dye concentration (y)} = 0.2777X + 0.4303$$

Where; X is absorbance values at 554 and 506 nm for blue and red dyes, respectively.

2.3 Enzyme assay for biodegradation

The cell free supernatant of *S. coelicoflavus* CS-29 was collected by centrifugation at 12,000 rpm for 5 min after culturing by inoculating into nutrient broth [(g/L) beef extract (3), peptone (5), sodium chloride (5)] and incubated at 37°C for 3, 5, and 7 days. The supernatant was used as the crude extracellular enzyme for determination of enzyme activity. Each enzyme activity was calculated using the equation below based on the definition of each enzyme.

$$\text{Enzyme activity} = \frac{\text{absorption x test volume x dilution factor}}{\text{absorption coefficient x enzyme volume x time}}$$

2.3.1 Peroxidase activity

The crude enzyme (500 µL) and 1 mL of pyrogallol (0.013 M) in 0.1 M potassium-phosphate buffer (pH 7.0) were mixed into a cuvette. The potassium-phosphate buffer was used as a blank and 1 mL of pyrogallol substrate in 500 µL of potassium phosphate buffer was used as the control sample. 50 µL of hydrogen peroxide (3% v/v) was added into the control and enzyme sample to start the reaction. Color change (the yellow to dark brown) was measured by using UV-Vis spectrophotometer at 420 nm. This showed the change of the pyrogallol to purpurogallin (Buntić et al., 2017). One unit of enzyme was defined as the amount of enzyme that expressed 1 µmol of purpurogallin/min. The molar extinction coefficient of purpurogallin is 12 M/cm^{-1}.

2.3.2 Laccase activity

The bacterium was cultivated in nutrient broth containing 0.1% guaiacol; the activity of laccase in supernatants was determined by observing the oxidation of ABTS (2,2′-Azino-bis (3-ethylbenzothiazoline-6-sulfonic acid)). The aliquots of the crude enzyme (200 µL) and 0.2 mM ABTS in 0.1 M sodium acetate buffer (pH 4.5) were mixed into a final volume of 1 mL. The reaction was held at 32°C for 10 min; and then was stopped by adding 0.5 mL of 80% trichloroacetic acid. The green formation of oxidized ABTS was examined at A_{420} nm. The substrate blank (200 µL of nutrient broth instead of crude enzyme) and enzyme blank (without ABTS) were performed. The absorbance of samples was calculated by subtracting from the absorbance of both blanks. One unit of enzyme was defined as the amount of enzyme oxidizing 1 µmol of ABTS/min. The molar extinction coefficient is 36,000 M/cm^{-1} (Mongkolthanaruk et al., 2012).

2.3.3 Manganese peroxidase activity

Enzyme assay is based on the oxidation of phenol red with or without peroxidase. For manganese dependent peroxidase, the mixture was prepared with 1 mL of sodium succinate buffer (0.25 M, pH 4.5), 700 µL of phenol red (0.71 mM), 400 µL of $MnSO_4$ (1.25 mM), 1 mL of sodium lactate buffer (0.25 M, pH 4.5), 1 mL of gelatin (0.5%), and 500 µL of the crude enzyme. In parallel, the mixture of manganese independent peroxidase was prepared without addition of $MnSO_4$. Distilled water was used instead of enzyme for control sample. The reaction was started by adding 400 µL of hydrogen peroxide (0.62 mM) with the incubation temperature at 30°C for 20 min; 1 mL of the assay mixture was added into 40 µL of NaOH (5 M) to stop the reaction. All samples were measured at A_{610} nm. Manganese dependent peroxidase activity was calculated by subtracting the extinction value of phenol red-oxidizing activity in the absence of $MnSO_4$ from the extinction value of the activity obtained in the presence of manganese. One unit of manganese dependent peroxidase activity was expressed as an absorbance increase of 0.1 units/min/mL of the enzyme sample (Buntić et al., 2017). The molar extinction coefficient of phenol red is 22 mM/cm^{-1}.

2.3.4 Azo-reductase activity

The mixture of 400 µL of crude enzyme, 100 µL of methyl red (500 mg/L) and 50 mM of sodium phosphate buffer in a final volume of 1 mL was prepared, resulting in a final concentration of methyl red at 50 mg/L. The addition of 8 µL of NADH (50 mM) was added to start reaction. Control was all reaction mixture, except the crude enzyme. The reaction was held at 37°C for 20 min. Enzymatic activity was determined by following the disappearance of methyl red (ε = 8.5 mM/cm^{-1}) at its maximum absorbance wavelength (430 nm). One unit of enzyme activity was defined as the amount of enzyme required to reduce 1 µmol of methyl red per min under the assay condition (Leelakriangsak and Borisut, 2012).

2.4 Chemical analysis of commercial synthesis textile dyes and degraded dyes from bacterial treatment

The bacterium grew in the minimal broth medium with the dyes (300 mg/L) at 37°C for seven days and the medium containing dyes without bacteria was prepared as controls. The supernatants were

collected and the dye metabolites were extracted with ethyl acetate, dried with anhydrous Na_2SO_4, and evaporated using rotary evaporator. The pellets were dissolved in methanol. The crude extracts of the treated dyes (medium with dyes and bacteria) and the crude extract of the untreated dyes (medium with dyes) were analyzed by High Performance Liquid Chromatography (HPLC) and Fourier Transform Infrared Spectroscopic (FTIR). Both commercial textile dyes (blue and red dyes) were prepared in methanol and also determined by HPLC and FTIR as original dyes. The HPLC (Shimadzu) unit was equipped with UV-vis detector and was used to study the degradation of dye. The samples were injected into a C8 column; the mobile phase used was 80% methanol, 20% deionized water with 0.05% acetic acid at a flow rate of 1.0 mL/min with 100 µL of injection volume. The samples were detected at respective wavelengths of 554 nm for the blue dye and 254 nm for the red dye. FTIR analysis of all samples was carried out using a spectrophotometer in the mid-infrared region of 600-4,000 cm^{-1} with 16-scan speed for examination of main functional groups (Bankole et al., 2018).

2.5 Phytotoxicity assay

Phytotoxicity of the treated dyes and the untreated dyes was studied using *Vignabean radiata* (Mung bean) seeds. Healthy seeds of uniform size were selected. Seeds were surface sterilized with 1.5% sodium hypochlorite solution and then washed five times with sterilized distilled water before transferring to the petri plates layered with two sheets of tissue paper (Sarayu and Sandhya, 2010). The crude extracts of the treated and untreated samples were dissolved in 1 mL of methanol first to dissolve well and added distilled water to final concentration of 200 mg/L. All of samples were performed in 30 individual seeds including control without dyes (distilled water) and with commercial dye solution at concentration of 50, 100, and 200 mg/L. Germination of mung bean was performed at 30°C in dark and tissue paper was damped with 5 mL of respective dye solution for all replications. The assay was carried out triplicate. The results were recorded after four days by determination of shoot and root length. The percentage of germination index (GI) and percentage of phytotoxicity were expressed by the following equations (Rahman et al., 2018).

$$\text{Germination Index (\%)} = \frac{(\text{\% Relative seed germination}) \times (\text{\% Relative root growth})}{100}$$

$$\text{Phytotoxicity (\%)} = \frac{\text{Radical root length of control} - \text{Radical root length of sample}}{\text{Radical root length of control}} \times 100$$

2.6 Statistical analysis

All experiments were performed in triplicate. The phytotoxicity test was designed in a completely randomized design (CRD). Data were analyzed using analysis of variance and Tukey HSD all-pairwise comparisons test at $p<0.05$ to compare the means of each experiment. All statistical analyses were conducted using Statistix 10.0.

3. RESULTS AND DISCUSSION

3.1 Dye removal and observation of cell aggregation with dye molecules

The dye concentration was determined from the supernatant (residual dyes) and the adsorbed dyes (washed out from cells by methanol) to confirm the mechanism of decolorization by *S. coelicoflavus* CS-29. The results showed clearly that the dyes were aggregated with the cell, with higher dye concentrations detected in the cell pellets (Table 1); the residual dyes in the supernatant were at low concentrations, indicating a percentage of decolorization of 70% for red dye and 51% for blue dye. This result was the opposite of that from previous study (Mon et al., 2020), which reported that the blue dye gave higher percentage of dye removal than the red dye. These results could be explained by Figure 1 in the previous study (Mon et al., 2020). The graph showed that the red dye absorbance was higher than the blue dye absorbance at the same concentration. It is possible that the red dye type is more color-rich at low concentrations as many dyes are visible in water at a concentration of 1 mg/L (Pandey et al., 2007). Thus, if more of the red dye was adsorbed to cell, the residual dye in the supernatant should be at low concentration. However, the dye was still visible, suggesting high absorbance.

Table 1. Concentration of dyes that were adsorbed to cell and remained in medium for decolorization of bacteria

Day	Blue dye concentration (mg/L)				
	3	5	7	10	Average
Control	249.00±0.03	239.00±0.06	241.00±0.04	214.00±0.05	236.00±0.09
Supernatant	128.00±0.13	132.00±0.08	96.00±0.02	105.00±0.02	115.00±0.10
Cell pellet	199.00±0.09	167.00±0.15	318.00±0.05	261.00±0.06	236.00±0.39
Day	Red dye concentration (mg/L)				
	3	5	7	10	Average
Control	261.00±0.02	231.00±0.06	151.00±0.15	204.00±0.05	212.00±0.24
Supernatant	64.00±0.01	59.00±0.03	63.00±0.01	67.00±0.01	63.00±0.02
Cell pellet	378.00±0.06	326.00±0.06	280.00±0.24	316.00±0.14	325.00±0.21

The blue dye particles aggregated with mycelia of the bacterium to form dense cell pellets (Figure 1). The bacterial filaments grew and protruded from the outer edge of older pellets. Interestingly, the red dye was more attracted to mycelia for the adsorption process and aggregated with the cells, resulting in opaque dense pellets with red color. The new mycelial fragments could establish new pellets in minimal broth medium, increasing the number of dye pellets. However, pellet size was not significantly different over long incubation; this might be caused by a limitation of nutrients (minimal broth medium with/without dyes). In *Streptomyces*, mycelia adhere to one-another in a process called germling aggregation which requires adhesive glycan. With an absence of new nutrients, hyphae protrude from the periphery of aging pellets. This event may be due to weak adhesive forces between hyphae prone to fragmentation as a result of mechanical stress (Zacchetti et al., 2018). Similarly, the dyes were adhered to extracellular glycan of *S. coelicoflavus* CS-29 that associated with cell surface, showing adsorption mechanism on the surface of cell pellet. This result matched that found in *Streptomyces* (Zacchetti et al., 2018). Likely, lactic acid bacteria adsorbed Dorasyn Red azo dye showed smoother cell surfaces from dye coating pores of biomass (Sofu, 2019); also in fungi, the surface of *Aspergillus niger* filaments was coated with small particles (0.1-1.0 µm) after adsorbing acid dyes (Li et al., 2019). According to the results, the decolorization mechanism of *S. coelicoflavus* CS-29 may occur by adsorption of dyes in the cell pellets. The enzyme system may be necessary for next step mechanism.

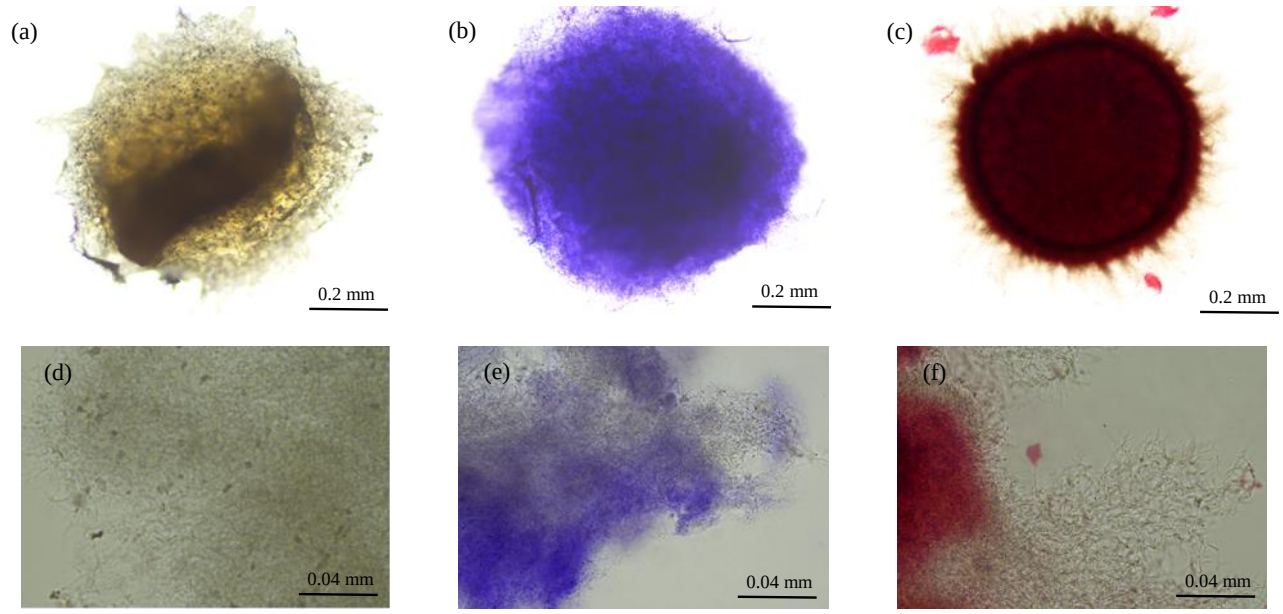

Figure 1. Pellets consistency of *Streptomyces coelicoflavus* CS-29 during growth in minimal broth medium with 300 mg/L dyes for five days observed under light microscope; dense pellets of filamentous bacteria that grew in the medium without dye (a, d), with blue dye (b, e), and with red dye (c, f)

3.2 Mechanism of commercial textile dyes biodegradation by bacterial enzyme

The active enzymatic system of biodegradation in commercial dye (Azo dyes) is peroxidases and azo-reductases which were determined in *S. coelicoflavus* CS-29. The bacterium produced peroxidases of high significance in seven days, as opposed to laccase which produced the highest activity after three days (Table 2). Mn-peroxidase was produced consistently during seven days of incubation. The azo-reductases could not be detected in cell free culture as an extracellular enzyme. The presence of peroxidase, Mn peroxidase and laccase enzyme could be confirmation that *S. coelicoflavus* CS-29 secreted enzymes to oxidize structurally different organic compounds, including polymeric dyes of both silk dyes in this study. Similarly, to *Streptomyces chromofuscus* A11 oxidized azo dyes by extracellular peroxidase (Pasti-Grigsby et al., 1996). The functions of Mn-dependent peroxidase and laccase are the oxidation of phenolic compounds with a requirement of Mn^{3+} and oxygen, respectively (Stolz, 2001). The possible degradation mechanism of the silk dyes were oxidation of phenolic structures and conversion of azo bond by additional methyl or methoxy substituents or by breaking down into two components. In the case of azo-reductase, no activity was detected in the cell free culture of *S. coelicoflavus* CS-29; it may be produced as an intracellular enzyme. This enzyme is involved in the reductive cleavage of the azo bond as the initial stage in degradation of azo dyes and transforms the parent dye molecule into compounds with reduced toxicity (Buntić et al., 2017).

Table 2. Enzyme activities related to dye reduction by *Streptomyces coelicoflavus* CS-29 in various time interval

Incubation time (day)	Peroxidase (U/mL)	Manganese peroxidase (U/mL)	Laccase (U/mL)
3	0.022±0.030^{b}	0.093±0.060^{a}	0.045±0.030^{a}
5	0.022±0.010^{b}	0.077±0.020^{b}	0.034±0.020^{b}
7	0.032±0.050^{a}	0.097±0.020^{a}	0.026±0.010^{c}

Values are mean for triplicate readings using Analysis of variance and Tukey HSD All-Pairwise Comparisons Test. Different letters in each column show significant values of enzyme activity.

3.3 Analysis of commercial textile dyes and degraded dye products by FTIR

The FTIR analysis of commercial blue dye exposed the presence of the main functional group, azo bond (–N=N–) between 1,576-1,597 cm^{-1} corresponding to N-H bending, peaks at 1,716-1,737cm^{-1} possible alkenes conjugation with C=O, C-N bond at 1,033.19 cm^{-1}, and nitro group (NH_2) at 1,500-1,660 cm^{-1} (Figure 2(a)). The blue dye treated with bacteria (bacterial metabolites) showed a clear absence of peak at 1,580 cm^{-1} of azo bond and showed the change of peaks around C-N stretching and C-O stretching. The thioethers group, CH_3-S- (C-S stretch), in the region of 660-630 cm^{-1} disappeared in the bacterial metabolite of the blue dye after treatment.

Interpretation of commercial red dye found the existence of aromatic amine at 1,551 cm^{-1}, N-H bond at 1,598 cm^{-1} corresponding to azo bond (-N=N-), C=C bond at 1,619 cm^{-1}, C-N bond between 1,042-1,200 cm^{-1}, C=C-H bending between 701-868 cm^{-1} (Figure 2(b)). The absence of peak at 1,598 cm^{-1} for azo bond indicated the cleavage of red dye in bacterial metabolite; the changes at 1,327 cm^{-1} and 893 cm^{-1} of untreated dye corresponded to C-N stretch of aromatic amines (1,290-1,310 cm^{-1} in bacterial metabolite) and C-H deformation (780-910 cm^{-1}), respectively.

The dyes were prepared in the minimal broth medium without bacterial cell designed as untreated controls which showed a different pattern from commercial dyes. This may be due to the high temperature and pressure of the sterilization process (Autoclave); the C-H, O-H bonds (2,800-3,300 cm^{-1}) were changed and aromatic compounds obtained C=O at 1,723 cm^{-1} differed from those in the untreated control dye. Another possibility, is that the commercial dyes were not extracted with ethyl acetate, but they were impurities containing various compounds with a complex structure. According to the results, the main functional groups (–N=N–) in both of blue and red dyes indicated a type of azo dye. The general structure of azo dyes is R_1–N=N–R_2; where R_1 brings electron withdrawing substituents and R_2 bears electron releasing substituents, mostly sulfonic (SO_3^-) substituent. It can be assumed that bacteria could break some compounds in dyes by oxidation and cause reduction via enzymatic activity.

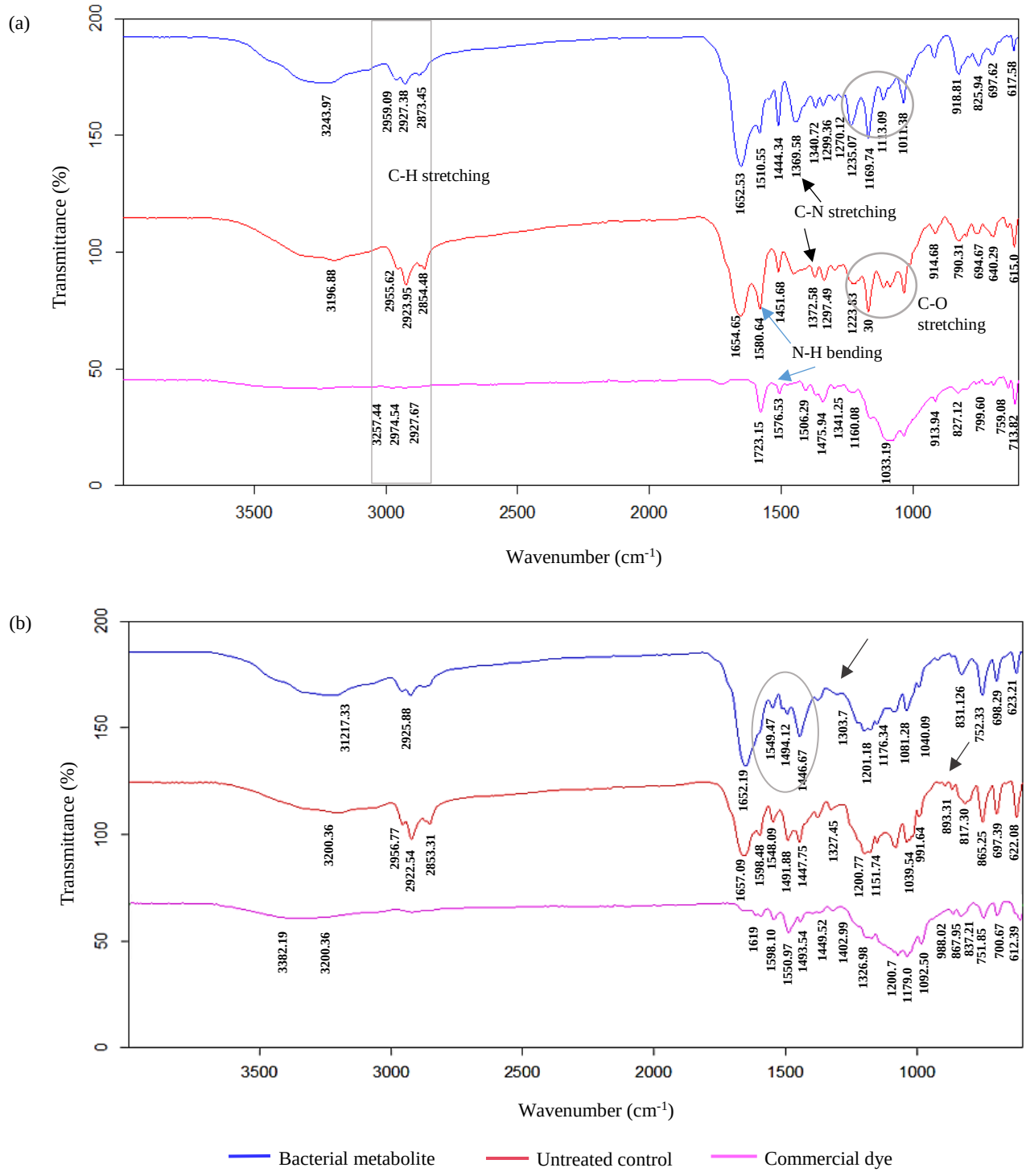

Figure 2. Main functional groups of commercial dyes, untreated dyes, bacterial metabolites for blue dye (a) and red dye (b) by FTIR

3.4 Analysis of bacterial metabolites by HPLC

HPLC analysis of commercial dyes, untreated control dyes, and bacterial metabolites of *S. coelicoflavus* CS-29 is presented in Figure 3. The main peak for commercial blue dye was at 4.171 min of retention time (Figure 3(a)). The profile of the control blue dye was 4.222, 3.198, 2.707 min, and this changed in the treated dye shown at 4.314, 3.281, 2.425 min (Figure 3(b) and (c)). In parallel, the main peak of commercial red dye was at 3.881, 2.701, 2.081 and 1.982 min of retention time (Figure 3(d)); these peaks disappeared from the control dye, which showed a main peak at 1.807 min (Figure 3(e)). This result confirmed that the dye components were treated by autoclave process, particularly in the red dye. The different peaks at the retention times of 1.807, 2.374,

3.354, 3.820 min indicated the degradation of red dye into different metabolites (Figure 3(f)). The HPLC profiles implied that dye adsorption to the cell imparts an approximate decrease of all peaks in proportion to each other, whereas dye removal by biodegradation indicates a complete reduction of the major peaks and the formation of new peaks at the same time.

To summarize for both blue and red dyes, peaks that appeared in the control dyes differed from the bacterial metabolites; there might be two degradation mechanisms such as the degradation of main compounds into intermediate products or the mineralization of parent compounds. According to enzyme activity, *S. coelicoflavus* CS-29 released the peroxidase and laccase enzymes to oxidize dyes molecules, mineralizing dye compounds which showed in HPLC profiles. The small dye compounds interacted with the filamentous surface of *S. coelicoflavus* CS-29 obtaining negative charges and then aggregating into the cells as shown in SEM. The results showed that *S. coelicoflavus* CS-29 plays the role of bio-adsorption in decolorization of textile dyes and degrade dye molecules. Similarly, *Streptomyces* sp., removed triphenylmethane dyes via biosorption and biodegradation (Adenan et al., 2021).

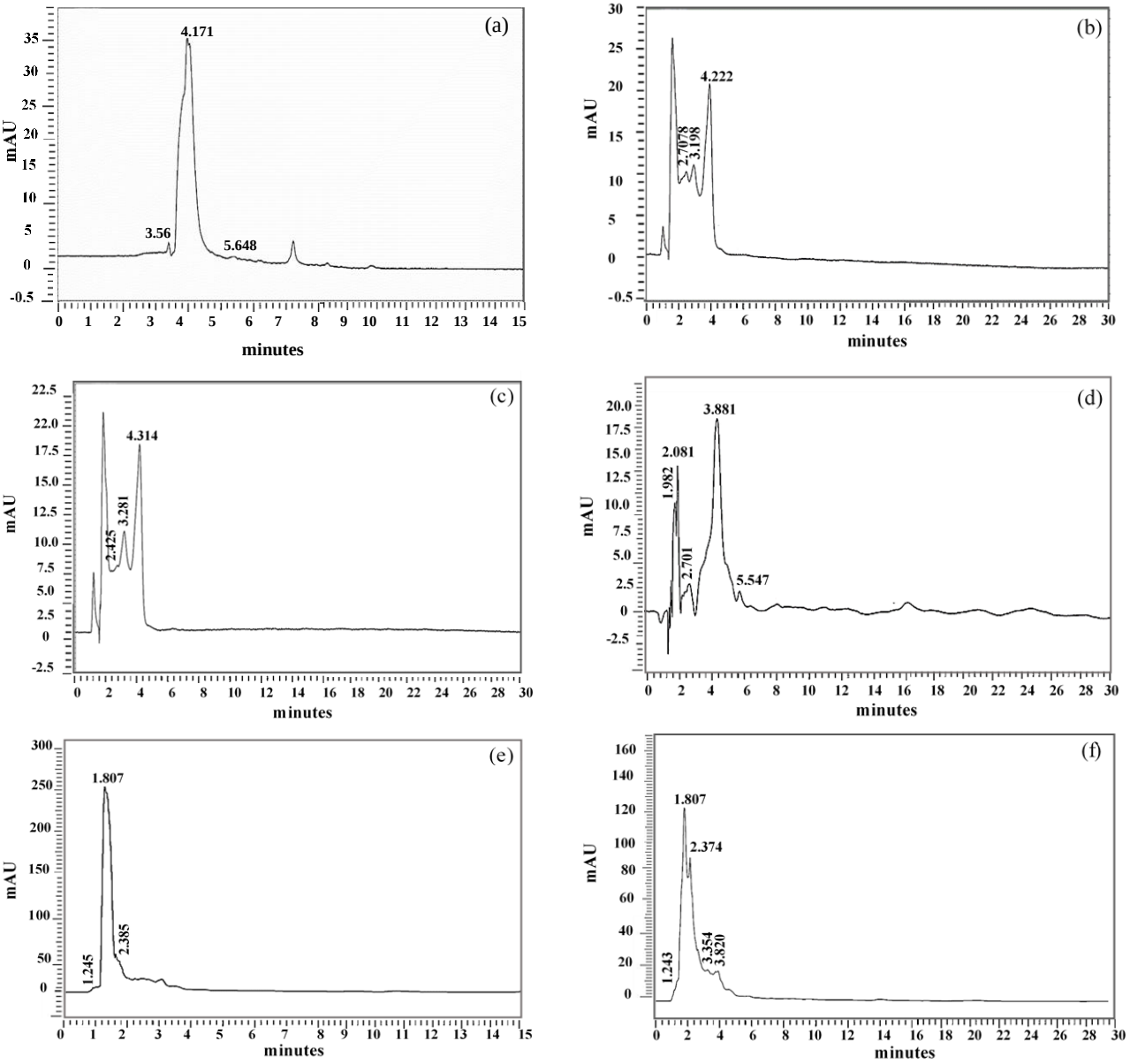

Figure 3. HPLC Chromatogram of commercial dyes, blue dye (a), red dye (d); untreated control dyes, blue dye (b), red dye (e); bacterial treated dyes, blue dye (c), red dye (f). The dyes were treated by *Streptomyces coelicoflavus* CS-29 for seven days.

3.5 Phytotoxicity study of degraded dye products by bacteria

This study focused on the actual consequences of significant wastewater discharge from Chonnabot District, Khon Kaen Province, Northeastern Thailand which causes harm to the living environment. Thus, a phytotoxicity test was carried out on the degraded silk dye products after treatment with *S. coelicoflavus* CS-29. This test confirmed that there was no significant difference in root length between control, untreated dyes and treated dyes extracts at 50 and 100 mg/L (Table 3). Of note, the treated blue dye showed greater shoot length than control, but in the treated red dye shoot length was less than control. In the case of the extracted metabolites might perform some nutritive role in seed germination and plant growth. Meanwhile, the red dye was evidently more toxic than the blue dye; it can be inferred that the red dye contains toxic components. The germination index (GI) was low in all dye treatments, showing lower GI percentage in higher dye concentrations according to the percentage of phytotoxicity. Comparison of phytotoxicity between untreated dyes and treated dyes revealed no difference in all parameters; this might be caused by an extraction method which recovered specific compounds. Moreover, the phytotoxicity effect of degraded dye products depended on the types and chemical structure of the dyes and types and tolerances of the seed cultivars (EPPO, 2007). The tolerance of untreated methyl red to seed germination and plant growth showed different levels in *Vigna radiata*>*Arachis hypogaea*>*Vigna unguiculata* (Sari and Simarani, 2019). The results implied that the bacterial metabolites still had low levels of toxicity after dyes biosorption with *S. coelicoflavus* CS-29. Similarly, the degraded metabolites of methyl red by *Lysinibacillus fusiformis* strain W1B6 were less toxic to the plants (Sari and Simarani, 2019). To conclude, *S. coelicoflavus* CS-29 has potential for the decolorization of silk dyes via enzymatic activity and adsorption as a biomass.

Table 3. Phytotoxicity analysis of the azo blue dye from control and bacterial degraded products tested in mung bean for four days after inoculation

Sample/parameters	Germination index (%)	Root (cm)	Shoot (cm)	Phytotoxicity (%)
Control (distilled water)	100.00±0.00^{a}	3.40±0.77^{a}	1.40±0.44^{b}	0.00±0.00^{e}
Blue dye				
Untreated dye extract				
• 50 mg/L	62.00±0.21^{c}	2.20±0.95^{ab}	2.20±0.38^{a}	33.00±0.25^{c}
• 100 mg/L	62.00±0.05^{c}	2.10±0.77^{ab}	2.10±0.12^{ab}	38.00±0.05^{bc}
• 200 mg/L	50.00±0.09^{d}	1.90±0.81^{ab}	1.90±0.20^{ab}	43.00±0.09^{b}
Treated dye extract				
• 50 mg/L	76.00±0.34^{b}	2.10±0.89^{ab}	2.10±0.24^{ab}	33.00±0.32^{c}
• 100 mg/L	62.00±0.08^{c}	1.90±0.63^{ab}	1.90±0.28^{ab}	43.00±0.05^{b}
• 200 mg/L	45.00±0.05^{d}	1.90±0.42^{ab}	1.90±0.12^{ab}	44.00±0.05^{b}
Red dye				
Untreated dye extract				
• 50 mg/L	72.00±0.21^{b}	2.40±0.66^{ab}	0.60±0.41^{c}	26.00±0.19^{d}
• 100 mg/L	66.00±0.23^{c}	2.10±0.62^{ab}	0.50±0.32^{cd}	34.00±0.23^{c}
• 200 mg/L	50.00±0.20^{d}	1.60±0.61^{b}	0.50±0.25^{cd}	50.00±0.20^{ab}
Treated dye extract				
• 50 mg/L	76.00±0.22^{b}	2.50±0.76^{ab}	0.50±0.24^{cd}	24.00±0.22^{d}
• 100 mg/L	62.00±0.07^{c}	2.10±0.72^{ab}	0.70±0.32^{c}	38.00±0.07^{bc}
• 200 mg/L	45.00±0.22^{d}	1.50±0.80^{b}	0.40±0.24^{d}	54.00±0.21^{a}

Values are mean of triplicate readings using analysis of variance and Tukey HSD All-Pairwise Comparisons Test at $p<0.05$. Different letters in each column show significant value of germination index, root length, shoot length and phytotoxicity.

4. CONCLUSION

Synthetic silk dyes are azo dyes with main functional groups, such as aromatic amine with double bonds of nitrogen. These dyes do not easily degrade and present a hazard to the natural environment. Biosorption is an effective system to treat contaminated dye molecules, leading to a reduction in both dye color and toxicity. *S. coelicoflavus* CS-29 was selected for

cell absorbent as it produces mycelium, giving it a high biomass. This strain was able to aggregate dye molecules with mycelium or adsorbed dye on the cell surface, showing dense cell under light microscope. Moreover, it produced laccase and peroxidase enzymes to mineralize dye structures. FTIR and HPLC were used to confirm the changes of functional groups and structure in the treated dyes. Finally, the metabolites of treated dyes were found to be non-toxic for seed germination, and not deleterious to root and shoot length of mung bean.

ACKNOWLEDGEMENTS

This study was financially supported by KKU Scholarship for ASEAN and GMS Countries's Personnel of Academic Year 2017 and partially supported by Salt-tolerant Rice Research Group, Khon Kaen University, Thailand.

REFERENCES

Adenan NH, Lim Y, Ting AS. Identification and optimization of triphenylmethane dyes removal by *Streptomyces* sp. from forest soil. Sustainable Environment Research 2021;31: Article No. 8.

Bankole PO, Adekunle AA, Govindwar SP. Enhanced decolorization and biodegradation of acid red 88 dye by newly isolated fungus, *Achaetomium strumarium*. Journal of Environmental Chemical Engineering 2018;6:1589-600.

Benkhaya S, Rabetb SM, Harf A. A review on classifications, recent synthesis and applications of textile dyes. Inorganic Chemistry Communications 2020;115:Article No. 107891.

Blánquez A, Rodríguez J, Brissos V, Mendes S, Martins L, Ball A, et al. Decolorization and detoxification of textile dyes using a versatile *Streptomyces* laccase-natural mediator system. Saudi Journal of Biology Science 2019;26(5):913-20.

Buntić AV, Pavlović MD, Antonović DG, Šiler-Marinković SS, Dimitrijević-Branković SI. A treatment of wastewater containing basic dyes by the use of new strain *Streptomyces microflavus* CKS6. Journal of Cleaner Production 2017; 148:347-54.

European and Mediterranean Plant Protection Organization (EPPO). Efficacy evaluation of plant protection products: Phytotoxicity assessment. OEPP/EPPO Bulletin 2007;37:4-10.

Garg SK, Tripathi M. Microbial strategies for discoloration and detoxification of azo dyes from textile effluents. Research Journal of Microbiology 2017;12(1):1-19.

Kurade MB, Waghmode TR, Khandare RV, Jeon BH, Govindwar SP. Biodegradation and detoxification of textile dye disperse red 54 by *Brevibacillus laterosporus* and determination of its metabolic fate. Journal of Bioscience and Bioengineering 2016;121(4):442-9.

Leelakriangsak M, Borisut S. Characterization of the decolorizing activity of azo dyes by *Bacillus subtilis* azoreductase AzoR1. Songklanakarin Journal Science Technology 2012;34(5): 509-16.

Li S, Huang J, Mao J, Zhang L, He C, Chen G, et al. *In vivo* and *in vitro* efficient textile wastewater remediation by *Aspergillus niger* biosorbent. Nanoscale Advances 2019;1:168-76.

Mon WP, Boonlue S, Mongkolthanaruk W. Investigation of *Streptomyces* for reduction of commercial silk dyes. Korean Journal of Microbiology 2020;56(3):206-13.

Mongkolthanaruk W, Tongbopit S, Bhoonobtong A. Independent behavior of bacterial laccases to inducers and metal ions during production and activity. African Journal of Biotechnology 2012;11(39):9391-8.

Pandey A, Singh P, Iyengar L. Bacterial decolorization and degradation of azo dyes. International Biodeterioration and Biodegradation 2007;59:73-84.

Pasti-Grigsby MB, Burke NS, Goszczynski S, Crawford DL. Transformation of azo dye isomers by *Streptomyces chromofuscus* A11. Applied and Environmental Microbiology 1996;62:1814-7.

Rahman A, Rayhan YH, Chowdhury AH, Mohiuddin KM. Phytotoxic effect of synthetic dye effluents on seed germination and early growth of red amaranth. Fundamental and Applied Agriculture 2018;3(2):480-90.

Saratale RG, Gandhi SS, Purankar MV, Kurade MB, Govindwar SP, Oh SE, et al. Decolorization and detoxification of sulfonated azo dye C.I. remazol red and textile effluent by isolated *Lysinibacillus* sp. RGS. Journal of Bioscience and Bioengineering 2013;115(6):658-67.

Sarayu K, Sandhya S. Aerobic biodegradation pathway for remazol orange by *Pseudomonas aeruginosa*. Applied Biochemistry and Biotechnology 2010;160:1241-53.

Sari IP, Simarani K. Comparative static and shaking culture of metabolite derived from methyl red degradation by *Lysinibacillus fusiformis* strain W1B6. Royal Society Open Science 2019;6:Article No. 190152.

Singh RL, Singh PK, Singh RP. Enzymatic decolorization and degradation of azo dyes: A review. International Biodeterioration and Biodegradation 2015;104:21-31.

Sinha A, Osborne WJ. Biodegradation of reactive green dye (RGD) by indigenous fungal strain VITAF-1. International Biodeterioration and Biodegradation 2016;114:176-83.

Sofu A. Investigation of dye removal with isolated biomasses from whey wastewater. International Journal of Environmental Science and Technology 2019;16:71-8.

Stolz A. Basic and applied aspects in the microbial degradation of azo dyes. Applied Microbiology and Biotechnology 2001; 56:69-80.

Zacchetti B, Smits P, Claessen D. Dynamics of pellet fragmentation and aggregation in liquid-grown cultures of *Streptomyces lividans*. Frontiers in Microbiology 2018;9: Article No. 943.

Zhou W, Zimmermann W. Decolorization of industrial effluents containing reactive dyes by actinomycetes. FEMS Microbiology Letters 1993;107:157-62.

Natural Phosphates Characterization and Evaluation of their Removal Efficiency of Methylene Blue and Methyl Orange from Aqueous Media

Meryem Assimeddine, Mohamed Abdennouri, Noureddine Barka, Rachid Elmoubarki, and M'hamed Sadiq*

Sultan Moulay Slimane University of Beni Mellal, Research Group in Environmental Sciences and Applied Materials (SEMA), FP Khouribga, B.P. 145, 25000, Morocco

ARTICLE INFO

Received: 5 Aug 2021
Received in revised: 30 Sep 2021
Accepted: 3 Oct 2021
Published online: 8 Oct 2021
DOI: 10.32526/ennrj/20/202100147

Keywords:
Natural phosphate/ Adsorption/ Methyl orange/ Methylene blue

*** Corresponding author:**
E-mail: m.sadiq@usms.ma

ABSTRACT

This study evaluated the capacity of a rock phosphate for the adsorption of organic dyes methylene blue MB and methyl orange MO in aqueous solution, in order to minimize the impact of these dyes on the environment. The physicochemical characterization of natural phosphates (NP) shows that its mineralogy is carbonate-fluorapatite, calcite and quartz, as demonstrated by X-ray diffraction. An infrared (IR) analysis completed the structural study by confirming the characteristic bands of a carbonated fluorapatite type B. The influence of adsorbent dose, pH, initial concentration and temperature of the dye solution on adsorption onto NP was studied. The experimental results show that MB is adsorbed almost entirely at an adsorbent dose of 1 g/L and at a more basic pH and that the Langmuir model describes its isotherm well. For MO, adsorption is performed at acidic pH, such that discoloration reaches 60% at pH 4 and NP adsorbent dose of 10 g/L. The maximum adsorbed amounts of MB (pH=9) and MO (pH=4) were found to be 9.54 and 1.09 mg/g, respectively. The kinetic data were analyzed to show that the pseudo-second-order model seems to be the most appropriate to describe the adsorption dynamics of both dyes on the naturel phosphate. The thermodynamic results show that the adsorption is endothermic for MB and exothermic for MO. So, rock phosphate shows a good potential as a sorbent for cationic dyes removal from wastewater.

1. INTRODUCTION

Currently, drinking water resources are greatly reduced due to an increase in population accompanied by intensive development of agriculture and strong industrialization. In addition, the discharge of wastewater into the natural environment from urban, rural, and industrial centers, without preliminary treatment, negatively impacts the quality of water resources. The garment and the textile industry are among the most demanding industries in the world in terms of water consumption and, therefore, discharge large amounts of wastewater charged in dyes. This industry uses chemicals, including dyes, which are generally responsible for many harmful environmental and health effects (Combes and Haveland-Smith, 1982; Chen, 2006; Tsuda et al., 2000; Heiss et al., 1992; Daneshvar et al., 2003) due to their complex synthetic nature, which makes them more stable and therefore not easily biodegradable (Damodar et al., 2007; Gupta and Khatri, 2019; Elmoubarki et al., 2015). The elimination of these effluents is one of the main problems in the treatment process of liquid waste. Several techniques such as chemical, physical, physicochemical and biological have been used to remove organic dyes. Their objective is to find a treatment process that is technically accessible and economically suitable for the industry. The adsorption technique is the most favorable method for removing organic dyes and has become an analytical method of choice, highly effective and simple to use (Sabar et al., 2020; Bedin et al., 2017). In addition, the use of a natural and abundant adsorbent for wastewater treatment is a legitimate way to preserve water capital (Bensalah et al., 2017; Assimeddine et al., 2020). Moroccan natural phosphates are mainly constituted by fluoroapatite $Ca_{10}(PO_4)_6F_2$ and partially substituted by carbonate. Due to their surface properties and multiple chemical components, they are widely used

Citation: Assimeddine M, Abdennouri M, Barka N, Elmoubarki R, Sadiq M. Natural phosphates characterization and evaluation of their removal efficiency of methylene blue and methyl orange from aqueous media. Environ. Nat. Resour. J. 2022;20(1):29-41. (https://doi.org/10.32526/ennrj/20/202100147)

as adsorbent for many physico-chemical processes. Among them, removal of methylene blue (MB), basic yellow 28 and reactive yellow 125 (Barka et al., 2009), elimination of cationic dye rhodamine 6G (Rh6G) as well as anionic dye congo red (CR) from wastewater (Bensalah et al., 2017) and removal of lead ions from aqueous solution (Mouflih et al., 2006). In order to broaden the scope and improve the previous research, the present work is based on the physico-chemical characterization of Moroccan naturel phosphate and the study of its capacity to decolorize wastewater. Methylene blue (MB) and methyl orange (MO) were chosen as dyes because they are among the most widely used in dyeing. They are also two model dyes for the evaluation of the adsorption capacity of adsorbents and have two different characters where MB is cationic dye and OM is anionic dye. In addition, these dyes have harmful effects on the environment and health, so it is preferable to treat them before they are discarded.

The choice of natural phosphate comes from the fact that phosphate ores are known for their ability to establish bonds with organic molecules of different sizes due to their physicochemical properties and diversity of chemical composition, its low cost and their use without any pre-treatment. In addition, this study examined the effects of different parameters such as adsorbent dose, dye solution pH, initial concentration, and temperature on the removal efficiency of MO and MB dyes by adsorption. The thermodynamics of adsorption were also evaluated.

2. METHODOLOGY

2.1 Samples and techniques

The phosphate used in this study was extracted from the Khouribga-Morocco region. It was used in crude form, and without prior purification; only particles of size between 180-125 µm were used. Particle size was measured using a set of vertically stacked sieves (Retsch) with mesh sizes between 90 and 500 µm. A mass of material was shaken and vibrated to pass through the sieves for 5 min and the retained quantity on each sieve was weighed. A phosphate portion was further calcined in a porcelain boat at 500°C in a tubular furnace. The interest of the calcination of phosphate sample was essentially the elimination of a part of the organic matter in gaseous form (CO_2) to study its effect on the adsorption, and the choice of this temperature, which is not high, was to preserve the basic amorphous morphology of this material. The obtained products were denoted as non-calcined NP and calcined NP, and then characterized using the following techniques:

X-ray fluorescence (XRF) was used to analysis the chemical composition of both samples. The elemental composition was determined by a Axios wavelength dispersive XRF spectrometer (Epsilon 3X, Manufacturer PANalytical, Netherlands). Samples were prepared in the form as compacted powder into pellets (PROT-ELE03-v01).

X-ray diffraction (XRD) measurements were recorded on a D2 Phaser powder diffractometer (Manufacturer Bruker, Germany) equipped with a copper anticathode (CuK_α line, λ=1.5406 Å) operating at 30 kV and 10 mA. The samples were irradiated in an angular range of 2θ of 10° to 80° with a 0.01° measurement pitch and a 0.5 sec/step count time.

Infrared spectroscopy measurements were obtained using a Perkin Elmer FTIR-2000 spectrophotometer (Netherlands). The results are presented in transmittance for wavenumbers between 4,000 and 400 cm^{-1}. The samples are packaged as pellets, consisting of 1 mg of the solid, diluted in 100 mg of KBr.

The specific surface area of non-calcined and calcined NP was determined from N_2 adsorption at -196°C using the BET method on a Quantasorb junior apparatus which provides only the specific surface. Samples were degassed for half an hour at 150°C before measurements.

2.2 Adsorption studies

The required initial dye concentrations were prepared by dissolving the desired weight of each dye in distilled water. The sorption processes were carried out in graded beakers containing the desired adsorbent dose and 200 mL of the colouring solution at a given concentration. These experiments were carried out with constant agitation and varying the pH of the solution, the phosphate solids dose 0-14 g/L, the contact time from 0 to 180 min and the starting dye concentration of 10 to 40 mg/L at five temperatures from 10 to 50°C which was controlled using a Cryothermostat. The pH was adjusted by adding sodium hydroxide or nitric acid solution. At the given time intervals, about 3 mL of the sample mixtures were collected and then filtered to separate the solid from solution using a syringe attached to a Sartorius filter (Porosity 0.2 µm). The maximum absorption wavelengths are 665 and 465 nm for methylene blue and methyl orange, respectively. The adsorption capacity was calculated using Equation 7 in Table 1.

Table 1. Mathematical equations and models using in this adsorption study

Eq. No.	Formula	Functionality	Parameters and/or assumptions	References
1	$\frac{dq}{dt} = k_1(q_e - q_t)$	Speed law equation: pseudo-first-order model	- q_t and q_e are the adsorbed quantity at time t and equilibrium respectively, in (mg/g), k_1 is the pseudo-first order velocity constant (min^{-1}), and t is the contact time (min). - Adsorption is considered reversible	Lagergren (1898)
2	$q = q_e(1 - e^{-k_1 t})$	Integration of speed law equation		
3	$\frac{dq}{dt} = k_2(q_e - q_t)^2$	Pseudo-second-order model	q_t and q_e in (mg/g), are the adsorbed quantity at time t and equilibrium respectively, k_2 (g/mg·min) is the rate constant of pseudo-second order adsorption and t is the contact time (min).	Ho and Mckay (1998)
4	$q_t = \frac{k_2 q_e^2 t}{1 + k_2 q_e t}$	Integration of differential equation		
5	$q_e = \frac{q_m K_L C_e}{1 + K_L C_e}$	Langmuir isotherm model	- K_L: direct measure of the intensity of the adsorption process; q_m: maximum adsorption capacity - Uniform energetic adsorption sites, single-ply coverage, and no lateral interaction between adsorbed molecules.	Langmuir (1916) Pignatello (1999)
6	$q_e = K_f C_e^{1/n}$	Freundlich isotherm model	K_F: adsorption maximum capacity; n: adsorption behavior; q_e: amount adsorbed per gram of solid, C_e: concentration of adsorbent at adsorption equilibrium	Freundlich and Heller (1939); Tóth (1994)
7	$q = \frac{(C_0 - C)}{R}$	Adsorption capacity	q is the adsorbed quantity (mg/g), C_0 (mg/L) is the initial dye concentration, C (mg/L) is the dye concentration at t and R (g/L) is the mass adsorbents per liter of solution.	Assimeddine et al. (2020)
8	$R_L = \frac{1}{1 + K_L C_0}$	Adsorption feasibility	C_0 is the initial concentration of the dye (mg/L), and K_L is the Langmuir constant (L/mg).	Yous et al. (2018)
9	$\Delta G^\circ = -RT\ln(K_D)$	Gibbs free energy	- $\Delta G°$: Gibbs free energy change; K_D: an equilibrium distribution constant (dimensionless) $K_D = \frac{q_e}{C_e}$; R the universal gas constant (8,314 J/mol K), and T is the solution's temperature (K). - $\Delta S°$: entropy variation; $\Delta H°$: enthalpy variation	Machrouhi et al. (2020)
10	$\ln K_D = -\frac{\Delta H^\circ}{RT} + \frac{\Delta S^\circ}{R}$	Van't Hoff		

2.3 Adsorption kinetics and isotherms models

Diverse theoretical adsorption kinetic (pseudo-first-order and pseudo-second-order) and Freundlich and Langmuir isotherm models are applied to experimental data in order to determine the best-fitting model as shown in Table 1. The Langmuir model considers that the adsorption sites are uniformly energetic, that they are covered by a single layer and that there is no lateral interaction between the adsorbed molecules. Graphically, a saturation point is reached at equilibrium (Langmuir, 1916). The Freundlich isotherm model considers that the number of sites likely to adsorb the compound is unlimited. Thus, the Freundlich isotherm has no maximum unlike that of Langmuir. This empirical model is widely used for the practical representation of adsorption equilibrium (Freundlich and Heller, 1939).

3. RESULTS AND DISCUSSION

3.1 Characterization

3.1.1 X-ray fluorescence

X-ray fluorescence chemical analysis is a non-destructive technique used to quantify the elemental composition of a sample. The percentages by mass of the oxides found in the uncalcined and calcined at 500°C natural phosphates are presented in Table 2.

It can be seen that the lower levels of P_2O_5 and higher amounts of CaO indicate the presence of other mineral phrases containing calcium such as calcite ($CaCO_3$) and gypsum ($CaO+SO_3$) in addition to apatite. Indeed, the percentage ratio of CaO/P_2O_5 obtained by XRF (equal to 3.04 for non-calcined NP and 3.18 for calcined NP) is greater than that calculated from fluorapatite (equal to 1.31). There is also silica (SiO_2) and lower contents of Al_2O_3, Fe_2O_3, MgO, and SO_3. The increase in the percentages of oxides that form phosphate after calcination at 500°C is due to the calcination eliminating part of the organic matter in gaseous form (CO_2) and water (Mgaidi et al., 2004), subsequently increasing the contents of the remaining elements. It should also be noted that other metals (Pb, Cu, Cd, Cr, Zn, Ti,…) were detected in the ppm range.

3.1.2 X-ray diffraction

X-ray diffraction analysis of non-calcined and calcined natural phosphates at 500°C, as shown in Figure 1, shows that these materials are well crystallized and they are mainly composed of a fluorapatite carbonated mineral (also known as francolite), which is derived from an ore fluorapatite $Ca_{10}(PO_4)_6F_2$ (Kenzour et al., 2019; Gallala et al., 2016; Fahami and Nasiri-Tabrizi, 2014). Carbonate-fluorapatite have an essential substitution in the crystal lattice of carbonate apatite, Ca^{2+} cations by Na^+, K^+, Mg^{2+}..., and also by the partial substitution of phosphate and/or fluoride ions by carbonate ions, which leads to the formation of B- and/or A-type carbonate-fluorapatite (Madupalli et al., 2017; Fleet and Liu, 2008), respectively. Phosphate ores also contain secondary minerals, or gangue impurities including contents of quartz (SiO_2), calcite ($CaCO_3$), and carbonates, which are in the form of dolomite $CaMg(CO_3)_2$ (Kenzour et al., 2019). XRD also reveals the presence of weak amounts of fluorapatite evident by the 2θ=11° peak. The diffractograms show that with calcination at 500°C, the diffraction lines become more resolute and intense (2θ=20.8°, 23.0°, 26.6°, 29.4°, 39.3°, 47.5°, 57.5°); which reflects an improvement in the crystalline quality of the phosphate studied. On the other hand, there was a decrease in the intensity of the lines corresponding to carbonate-fluorapatite due to calcination, which acts on the elimination of some carbonates.

Table 2. Mineralogical composition of natural phosphate (non-calcined and calcined).

Compounds	wt% of non-calcined NP	wt% of NP calcined at 500°C
CaO	34.337	49.086
P_2O_5	11.281	15.407
SiO_2	1.479	6.959
Al_2O_3	0.584	2.007
Fe_2O_3	0.262	0.693
MgO	0.231	0.692
SO_3	0.541	0.630
K_2O	**	0.177
TiO_2	**	0.161
Cr_2O_3	**	0.105

3.1.3 Infrared spectroscopy

To determine the carbonates type of the fluorapatite indexed by the XRD analysis, we recorded the IR absorbance spectra of the phosphate solids. Figure 2 corresponds to the infrared absorption spectra of non-calcined and calcined natural phosphates at 500°C. The strong band observed around 1,040 cm^{-1} is attributed to asymmetric stretching vibration ν_3 of PO_4 phosphate anions, which broadened by shoulder band at 1,080 cm^{-1} can be assigned also to ν_3 PO_4^{3-} (Furuzono et al., 2001). The bands centered at 576 cm^{-1} (it becomes shoulder after

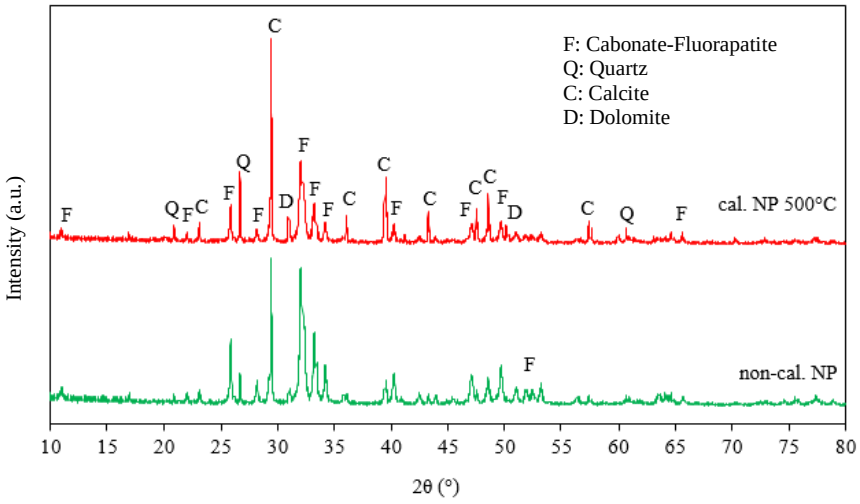

Figure 1. XRD patterns of the non-calcined and calcined natural phosphate

calcination) and 606 cm^{-1} can be assigned to out-of-plane bending vibration ν_4 of phosphate group (PO_4^{3-}) (Dakkach et al., 2012; Sadiq et al., 2015). The band located at 480 cm^{-1} is attributed to the symmetrical strain mode ν_2 (PO_4^{3-}) (Drouet, 2013). The spectra of solids exhibit the shoulder for orthophosphates (PO_4^{3-}) ions, at 966 cm^{-1}. It is attributed to symmetric stretching vibration ν_1 of phosphate PO_4^{3-} (Drouet, 2013). The doublet located around 1,428 and 1,454 cm^{-1}, is associated to ν_3 (CO_3^{2-}), while the absorption band observed at 872 cm^{-1} is assigned to the ν_2 bending vibrations of the carbonate group (CO_3^{2-}) (Zahrani and Fathi, 2009; Nikcevic et al., 2004), consistent with the carbonate fluorapatite spectra previously reported by Fleet (2009) and Wang et al. (2018). It corresponds to the out-of-plane oscillating motion of C atoms. The wavenumbers of carbonate vibrations illustrated in Figure 2 show the characteristic bands of type B carbonate- fluorapatite (CO_3^{2-} substitute PO_4^{3-} ions). Therefore, the intensities of all bands corresponding to CO_3 and PO_4 vibrational modes in the calcined phosphate were lower relative to non-calcined phosphate, possibly indicating the transfer of a carbonate amount from carbonated-fluorapatite into calcite and dolomite (Figure 2). This confirms the results obtained by XRD (Figure 1).

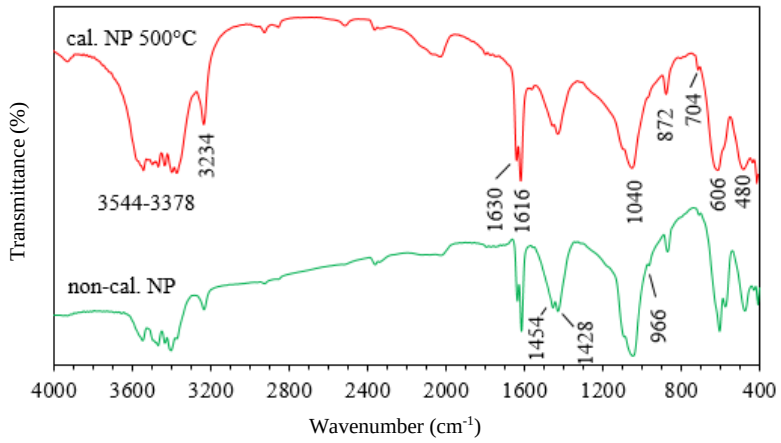

Figure 2. FT-IR spectra of non-calcined and calcined natural phosphate

Both bands at 1,616 and 1,630 cm^{-1} are due to the bending vibration of the hydroxyl (OH^-) (H-O-H) (Nikcevic et al., 2004; Yous et al., 2018; Aines and Rossman, 1984; Boughzala and Bouzouita, 2015). A series of vibrations was observed in the 3,200-3,550 cm^{-1} region which could be assigned to OH group vibrations bound by hydrogen bonds (O-H asymmetrical and symmetrical stretching vibrations). The additional shoulder at 704 cm^{-1} can be assigned to free vibration of OH (ν_L(O-H) (Nikcevic et al., 2004; Wang et al., 2018). No band was observed at 880 cm^{-1}, which is assigned to the A-type carbonate and

can be found in the spectra of natural phosphate, as reported previously by Madupalli et al. (2017).

3.1.4 Specific surface area

The specific surface area of non-calcined and calcined NP was 27 and 32 m^2/g, respectively. These BET surface area values remained low compared to other adsorbents such as activated carbon (Wang et al., 2017). A slight increase after calcination of sample may be due to the creation of new sites by the release of volatile molecules.

3.1.5 pH zero charge point (pH_{pzc})

The pHpzc (zero charge point pH) is the pH value at which the net adsorbent surface charge is zero. This is a key parameter in adsorption processes, especially when electrostatic forces are implied in the mechanisms. The pHpzc is determined by the pH drift method, which consists in adjusting the pH of NaCl solutions with a concentration of 0.01 M and a volume of 50 mL (pH values between 2 and 12) by adding a solution of NaOH or HCl (0.1 M). Then, a mass of 0.05 g of the phosphate sample added to each volume. The suspensions must be kept stirring at room temperature for 6 h, and the final pH is then measured. Furthermore, the natural phosphate used is insoluble in water at different pH studied (acidic and basic).

We have plotted the evolution of the final pH as a function of the adjusted initial pH (Figure 3). The point of intersection between the curve obtained and that of the bisector corresponds to the pHpzc, which equals 8. As well as for pH higher than pHpzc, the adsorbent surface would be negatively charged so that the cations can be adsorbed, while for pH lower than pHpzc, the surface would be positively charged so that the anions can be adsorbed.

3.2 Adsorption studies

3.2.1 Adsorbent dose

Figure 4 shows the percentage of removal of methyl orange (MO) and methylene blue (MB) dyes as a function of the crude phosphate dose, with a contact time of 3 h. It can be seen that the degree of discoloration rises as the mass of natural phosphate adsorbent increases. For MB, the total staining of solution is extinguished at around 1 g/L, while for MO, the solution remains colored even at 14 g/L, the percentage of elimination stabilizes almost at 20% for a mass ratio of 10 g/L. This is can be explained by the anionic (MO) and cationic (MB) nature of adsorbate and surface charge of adsorbent without any modification of solution initial pH (pH_i=9).

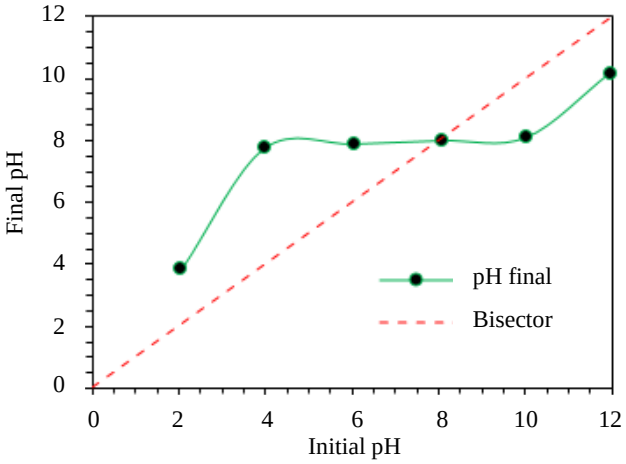

Figure 3. pH zero charge point of natural phosphate (NP)

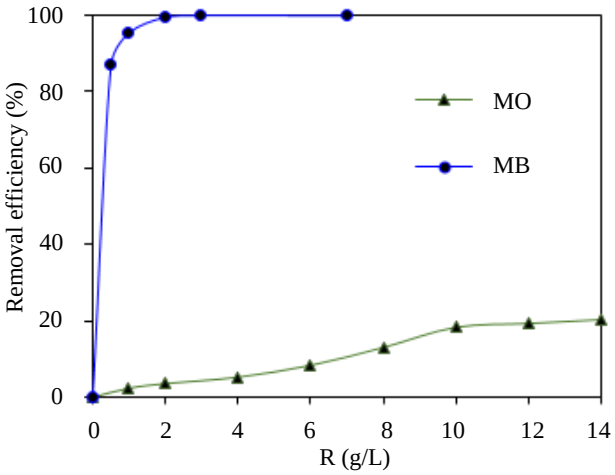

Figure 4. Effect of adsorbent dose on MB (C_0=10 mg/L) and MO (C_0=20 mg/L) adsorption

3.2.2 Removal efficiency by non-calcined and calcined phosphate

Figure 5 shows the comparison of dye removal efficiency of the solutions prepared by adsorption on uncalcined and calcined phosphate at 500°C. The curves show that the adsorption mechanism is almost the same for both MB and MO dyes. This can be explained by the fact that both samples have similar structural properties and compositions, according to the results obtained from their characterization. It can be concluded that a calcination temperature of 500°C does not result in a significant difference in the texture of the phosphate studied. So, in the rest of the work, we limited ourselves to the examination of the adsorption capacity of the non-calcined crude phosphate.

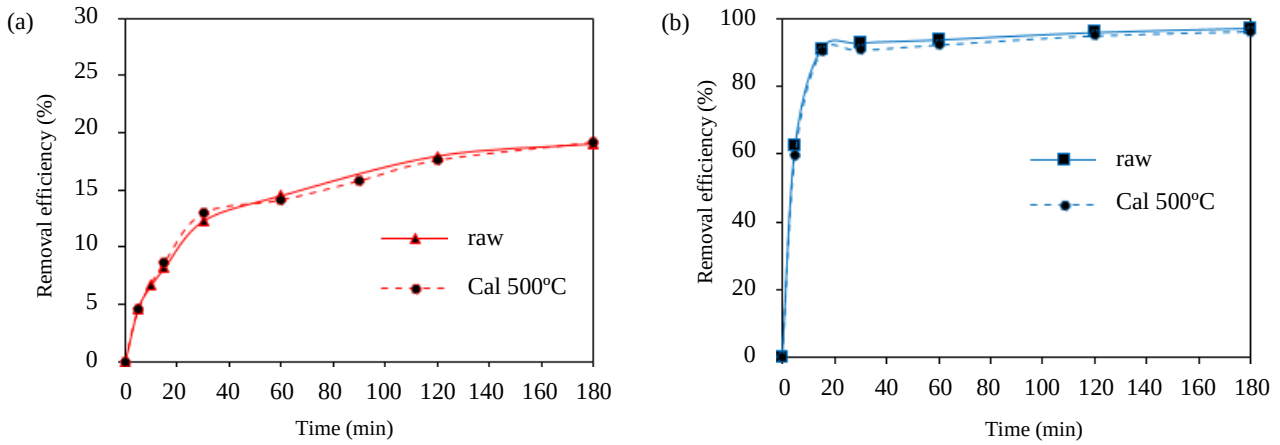

Figure 5. Adsorption kinetics by non-calcined and calcined phosphate at pHi=9 of MO (a): C_0=20 mg/L, R=10 g/L; and of MB (b): C_0=10 mg/L, R=1 g/L

3.2.3 Effect of pH on dyes removal

The pH is a more important parameter in the adsorption process, as it can influence both the adsorbent surface and adsorbate structure as well as the mechanism of adsorption (Elmoubarki et al., 2017). For this, we carried out several adsorption tests in different pH values. The experimental results presented in Figure 6 clearly show that the pH has a strong influence on the adsorption of the anionic dye MO, in which the percentage of discoloration is canceled out in the most basic pH, while the elimination is more favorable in the acidic medias, it reaches 60% for a pH value of 4. For MB, the rate of elimination increases with increasing pH value. It went from 75% for a more acidic pH (pH=2) and arrived at 99% for a basic pH equal 12. These results can be explained that when the pH of the solution is lower (pH<pHpzc), the richer the solution is in hydrogen ions. The number of positively charged sites increases and the surface of the phosphate solid become positively charged, and therefore likely to attract the negative charges of the anionic dye (MO) (Guo et al., 2013). On the other hand, at pH superior to pHpzc, the surface is negatively charged, which promotes adsorption of the cationic dye. The initial adsorption of dyes was higher compared to the equilibrium point, due to the high activity (strength and numbers) of the initial sites available on the material surface. Equilibrium was reached at 30 min and 60 min for BM and MO, respectively, followed by plateaus signifying equilibrium, and this is valid for all pH values. In the sequel of this work, we kept the pH of the solution for the MO dye at 4, by adjustment with nitric acid solution, because the pH of the colored solution reached a value of 9, once the NP is added, and we have found that the adsorption of MO almost canceled out at basic pH.

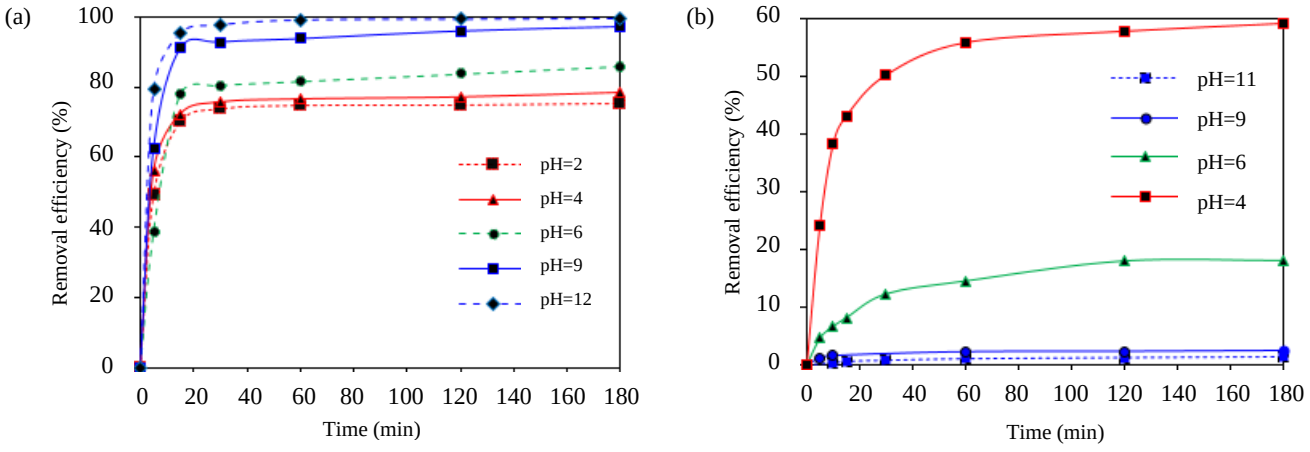

Figure 6. pH effect on adsorption of MB (a): C_0=10 mg/L, R=1 g/L and of MO (b): C_0=20 mg/L, R=10 g/L

3.2.4 Effect of initial dye concentration

The initial dye concentration affects its kinetics and the adsorption capacity; for this, the initial concentration of dye was varied from 10 to 50 mg/L. The results obtained are presented in Figure 7, which show that the adsorption process starts with a short transient regime and ends with a steady state. The curves show that the adsorbed quantity rises rapidly during the first 30 min for MB and 60 min for MO until reaching a plateau whatever the concentration. This may be due to the saturation of all active sites on the surface of the phosphate material. The adsorbed amount increases from 3.2 to 10.2 mg/g in the case of MB and from 0.3 to 2.8 mg/g in the case of MO for concentrations ranging from 10 to 50 mg/L. According to the curves, the concentration threshold has not been reached since the plateaus are far from each other and are approaching each other for MB at higher concentrations. Increasing the initial concentration enhances the interaction between the adsorbate molecules and the adsorbent particles, thus increasing the adsorption capacity. More, increasing the initial dye concentration induces an increase in the driving force of the concentration gradient, hence increasing the diffusion of the dye molecules in solution through the adsorbent surface (Deniz and Saygideger, 2010). A similar trend has been described for the adsorption of methyl orange dye onto mesoporous carbon by Mohammadi et al. (2011) and methylene blue onto activated carbon by Kuang et al. (2020).

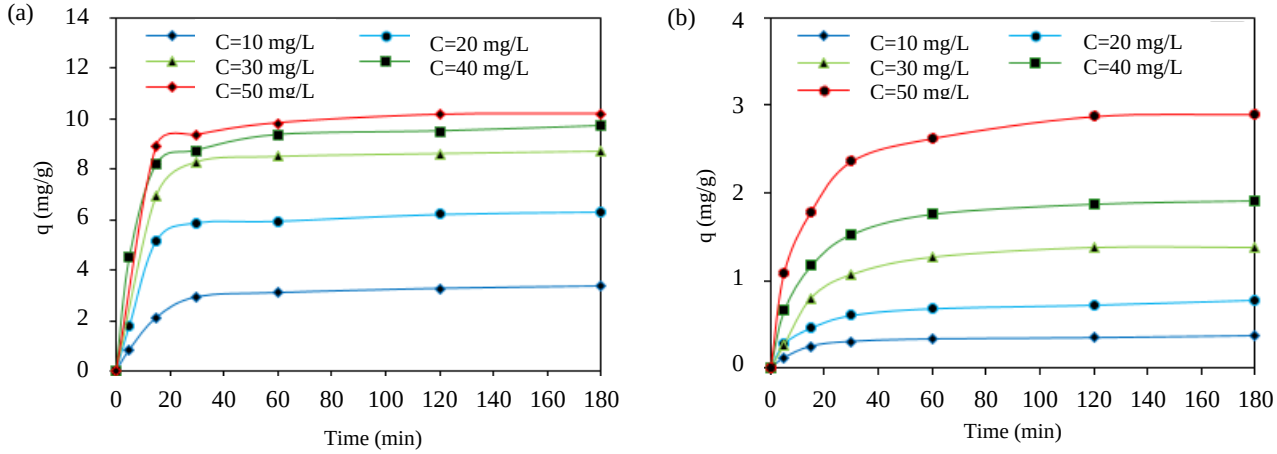

Figure 7. Effect of initial concentration: MB (a): dye at R=1 g/L, pH=9 and MO (b): dye at R=10 g/L, pH=6

3.2.5 Adsorption isotherms

The adsorbed quantities at equilibrium (qe), as a function of the equilibrium concentration of each dye, are shown in Figure 8. The experimental results obtained were compared with adsorption isotherm models of Langmuir (Langmuir, 1918) and Freundlich (1906). All constants involved in the expression of each model were calculated by non-linear regression analysis and presented in Table 3. From Figure 8 we can notice that the adsorption of dyes at equilibrium increases with increasing concentration at equilibrium, this was due to a high driving force for the mass transfer of the dye at high concentration in solution.

Table 3. Constants for isothermal models of dyes adsorption on natural phosphate

Dyes	q_m (mg/g)	Langmuir		K_F ($mg^{1-1/n}/L^{1/n}/g$)	Freundlich	
		K_L (L/mg)	r^2		n	r^2
MB	10.3321	1.7811	0.98921	5.93569	4.92987	0.89382
MO	25.9014	0.0050	0.84625	0.02011	0.60961	0.99554

It can be seen from the values of the correlation coefficients r^2, the Langmuir model best describes the adsorption isotherm of MB. This result indicates that the adsorption process takes place in a monolayer, where all adsorption sites on adsorbent surface are energetically uniform, and there are no lateral interactions between the adsorbed molecules. It can be seen graphically that a saturation point is reached where no further adsorption can occur afterwards, this is a plateau which characterizes the Langmuir

isotherm at equilibrium. The constant called the separation factor whose Langmuir isotherm characteristic can be expressed in the form established by Equation 8 in Table 1.

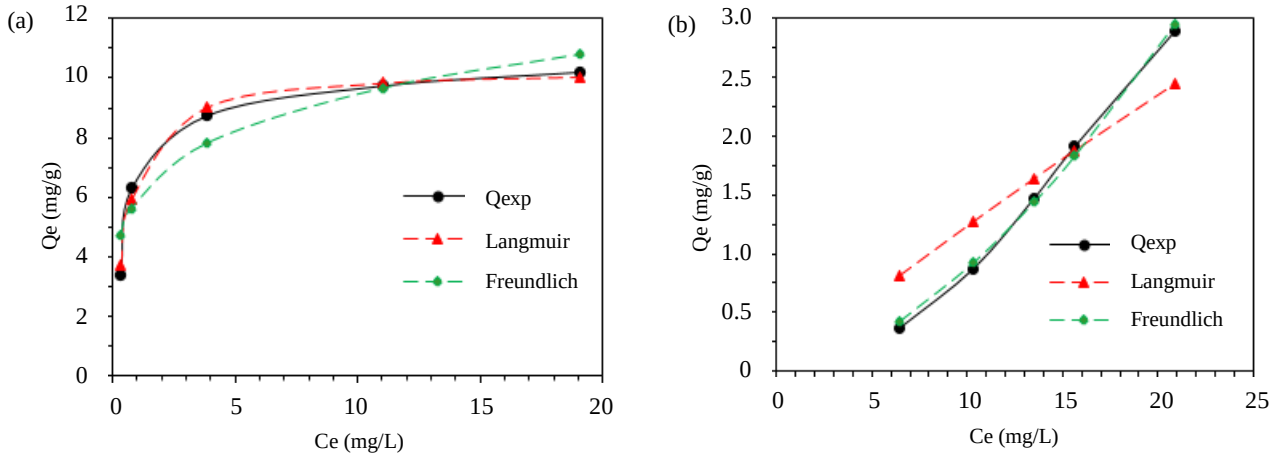

Figure 8. Adsorption isotherms for MB (a): dye at R=1 g/L, pH=9 and MO (b): dye at R=10 g/L, pH=6

Three cases of adsorption can be distinguished according to the value of R_L, the adsorption is unfavorable when the separation factor value is strictly superior to one, if the R_L=1 the adsorption is said to be linear, when $0<R_L<1$ the adsorption is said to be favorable (Yous et al., 2018). The measured values for the studied dyes are less than one and more than 0 (R_L=0.053 for MB and 0.909 for MO). This reveals favorable adsorption of MB and MO over adsorbent surface.

Linearity also shows that the adsorption isotherm of MO follows the Freundlich model, based on the heterogeneous sorption surface where the number of sites that can adsorb the compound is unlimited. Thus, this isotherm does not present a maximum. The shape of the isotherm will depend on the value of 1/n, which represents the absorption intensity; in this case, we have 1/n>1, representing the S-type convex isotherm according to Giles classification (Giles et al., 1960), in which the adsorbate- adsorbent interactions take place due to electrostatic attractions, but also adsorbate-adsorbate, due to intermolecular interactions.

3.2.6 Adsorption kinetics

The two kinetic models, pseudo-first order and pseudo-second order, have been examined to characterize the kinetics involved in the adsorption process of both MB and MO dyes. The kinetic data were evaluated by the values of the correlation coefficient (r^2) and the quantity adsorbed at equilibrium of dye. The parameters were estimated using non-linear regression.

The kinetics results of the adsorption of methylene blue and methyl orange by non-calcined NP are presented in Table 4 and Figure 9. The figure indicates that the removal of cationic MB and anionic MO were very rapid in the first 30 min of contact time; the adsorption capacity of the dyes reached 0.91 mg/g and 8.35 mg/g for MO and MB, respectively. After this period, the rate of removal was slower and stagnated with the increase in contact time. Around 90% of the quantity of dye adsorbed at the end of equilibrium was carried out in the period 0-30 min. At 180 min, adsorption capacity stabilizes at 1.09 mg/g for the MO and 9.54 mg/g for the MB dyes.

According to the results obtained, the two models give a reasonably good fit to the experimental data, but the pseudo-second order model is found to be the most suitable to describe the adsorption dynamics of the two dyes on the phosphate due to the excellent correlation of the parameters calculated by the model with the experimental data. Our results are in accordance with that reported by others works (Assimeddine et al., 2020; Elmoubarki et al., 2015; Mahjoubi et al., 2016). They showed that the adsorption process of the same dyes on clays and layered double hydroxides (LDH) absorbents obeys the pseudo-second-order model. This model allows the characterization of adsorption kinetics by taking into account both the rapid uptake of solutes at the most reactive sites and the slow uptake at low energy sites.

Table 4. Kinetic parameters of adsorption of MB and MO on natural phosphate

Dyes	Pseudo-first-order				Pseudo-second-order		
	qe (exp) (mg/g)	qe (mg/g)	k_1 (L/min)	r^2	qe (mg/g)	k_2 (g/mg·min)	r^2
MB	9.540906	9.15594	0.08868	0.9836	10.00316	0.01308	0.99472
MO	1.091152	1.04556	0.09365	0.99073	1.140725	0.11214	0.99579

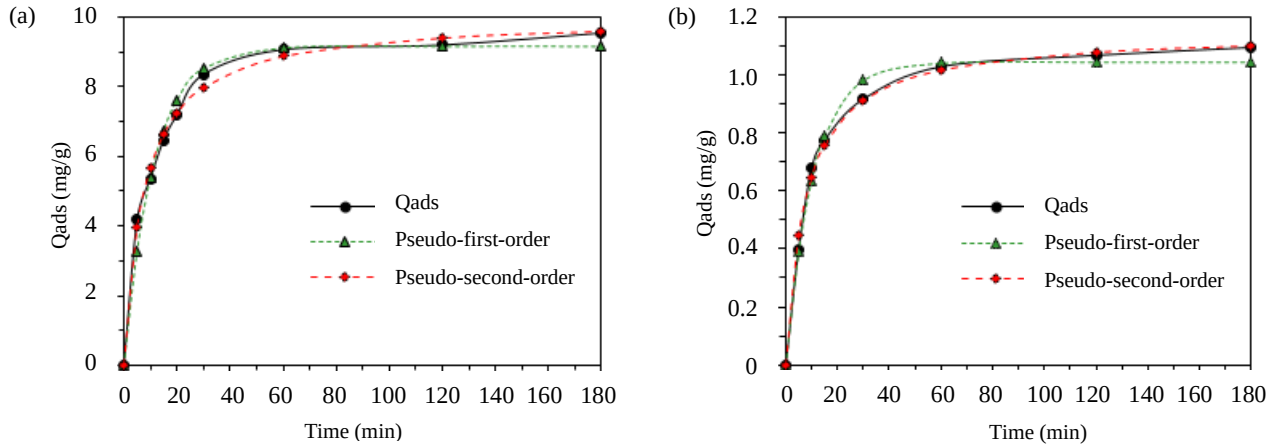

Figure 9. Adsorption kinetics, pseudo-first-order and pseudo-second-order of MB (a) and MO (b)

3.2.7 Effect of temperature and thermodynamic study

Depending on the type of adsorbent material and the nature of the adsorbed molecules, adsorption is a process that can be endothermic or exothermic (Rytwo and Ruiz-Hitzky, 2003). To make a thermodynamic study of the phenomenon of adsorption of dyes such as methylene blue and methyl orange by crude phosphate, we carried out discoloration tests by varying the temperature of colored solutions from 10 to 50°C, because the effect of temperature on the dye adsorption is very important in the adsorption mechanism. Figure 10 represents the percent removal of BM and OM on crude phosphate as a function of solution temperature. The curves in the figure indicate that increasing the solution temperature leads to an increase in removal efficiency (%), which promotes MB adsorption, suggesting an endothermic process. This probably results from an increase in the number of active adsorption sites, via the release of new sites, with increasing temperature. Moreover, an increase in temperature promotes the diffusion of molecules through the outer boundary layer to the inner pores of the adsorbent particles, this may be due to the decrease in the viscosity of the solution and the increase in the concentration of monomers in the solution. These results are in agreement with those found by Al-Ghouti et al. (2005) on a study of MB adsorption by manganese-oxides-modified diatomite. In contrast, other studies show that temperature change has almost no or little influence on the efficiency of MB adsorption by raw maize corncob (Farnane et al., 2018) or by clays (Elmoubarki et al., 2015), respectively. Thus, it is noticed that the effect of temperature could be related to the nature of the adsorbent particles. On the other hand, the removal of MO decreases significantly with increasing temperature, is due to the presence of desorption steps in the adsorption mechanism, in agreement with Arrhenius'law, suggesting that the surface reaction is exothermic.

From the results obtained, we determined the thermodynamic parameters of adsorption such as enthalpy (ΔH°) and entropy (ΔS°), which were estimated respectively from the slope and intercept of the ln(K_D) vs. 1/T plot, and free energy (ΔG°), using the Equations 9 and 10 in Table 1. From the calculated constants which are shown in Table 5, we can confirm that the adsorption process is endothermic for MB (positive ΔH°), then, the negative values of ΔG° are accompanied by a decrease with the rise in temperature indicates that the adsorption is spontaneous and more feasible at higher temperatures (Machrouhi et al., 2020). The value of the standard enthalpy, higher than 40 kJ/mol, can tell us that adsorption is chemical nature. In the case of MO,

according to the value of ΔH° the adsorption is exothermic, and this is physisorption type. It is also noted that ΔG° increases with increasing temperature, indicating a decrease in adsorption feasibility of MO dye onto phosphate materials.

Furthermore, it can be seen from the values of ΔS° that the randomness increases for MB (ΔS°>0) and decreases for MO (ΔS°<0) at the solid/ solution interface in the course of the dyes adsorption onto the surface of natural phosphate.

Table 5. Thermodynamic parameters calculated for adsorption

T (°C)	BM				OM			
	K_D	ΔG° (kJ/mol)	ΔH° (kJ/mol)	ΔS° (J/K mol)	K_D	ΔG° (kJ/mol)	ΔH° (kJ/mol)	ΔS° (J/K mol)
10	6.818	-4.519			0.134	4.734		
20	12.301	-6.117			0.107	5.435		
30	29.472	-8.528	56.421	214.43	0.090	6.066	-16.042	-73.181
40	64.714	-10.857			0.076	6.695		
50	121.666	-12.899			0.055	7.782		

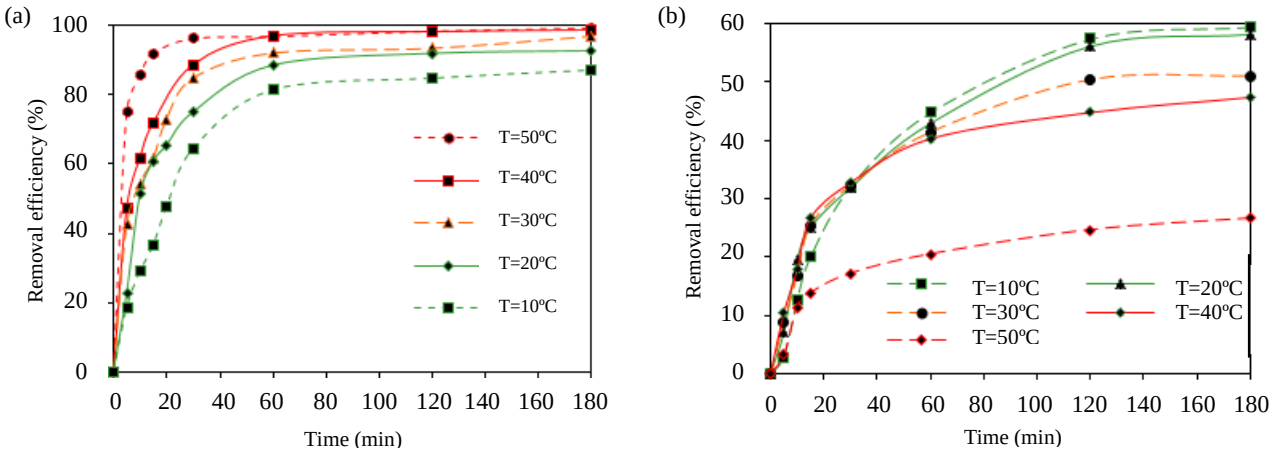

Figure 10. Effect of temperature on adsorption over crude phosphate of MB (a): R=1 g/L, pH=9 and MO (b): R=10 g/L, pH=6

4. CONCLUSION

This modest work examined the potential of a local natural phosphate, from the Khouribga-Morocco region, in the removal of cationic and anionic dyes from an aqueous solution. Different adsorption parameters such as contact time, initial dye concentration, adsorbent dose, pH of the initial solution and temperature were optimized. Experimental results of the adsorption tests showed that the phosphate material follows a pseudo-second-order adsorption kinetics for MO and MB dyes. This material exhibited high adsorption capacity at a more basic pH for the cationic dye MB (9.54 mg/g) and at a more acidic pH for the anionic dye MO (1.09 mg/g). The adsorption capacity of natural phosphate increases with the increase in the initial concentration of dyes, and the complete saturation of all surfactant sites on the material is reached at 30 min for MB and 60 min for MO, then the appearance of an equilibrium plateau. Increasing the temperature of the solution increases the removal efficiency (%) of methylene blue and decreases that of methyl orange. The adsorption process is spontaneous (ΔG° negative) and endothermic (ΔH° positive) for MB and exothermic for MO. Finally, the present study has shown that the local natural phosphate appears to be a good adsorbent candidate for the decoloration of dye-containing effluents.

ACKNOWLEDGEMENTS

The authors thank all who assisted in conducting this work.

REFERENCES

Al-Ghouti M, Khraisheh MAM, Ahmad MNM, Allen S. Thermodynamic behaviour and the effect of temperature on the removal of dyes from aqueous solution using modified diatomite: A kinetic study. Journal of Colloid and Interface Science 2005;287:6-13.

Aines RD, Rossman GR. Water in minerals? A peak in the infrared. Journal of Geophysical Research: Solid Earth 1984;89:4059-71.

Assimeddine M, Abdennouri M, Barka N, Rifi EH, Sadiq M. Physicochemical characterization of Moroccan natural clays and the study of their adsorption capacity for the methyl orange and methylene blue removal from aqueous solution. Journal of Environmental Treatment Techniques 2020; 8(4):1258-67.

Barka N, Assabbane A, Nounah A, Laanab L, Aît- Ichou Y. Removal of textile dyes from aqueous solutions by natural phosphate as a new adsorbent. Desalination 2009;235:264-75.

Bedin KC, de Azevedo SP, Leandro PKT, Cazetta AL, Almeida VC. Bone char prepared by CO_2 atmosphere: Preparation optimization and adsorption studies of Remazol Brilliant Blue R. Journal of Cleaner Production 2017;161:288-98.

Bensalah H, Bekheet MF, Younssi SA, Ouammou M, Gurlo A. Removal of cationic and anionic textile dyes with Moroccan natural phosphate. Journal of Environmental Chemical Engineering 2017;5(3):2189-99.

Boughzala K, Bouzouita K. Synthesis and characterization of strontium-calcium-lanthanum apatites $Sr_{7-x}Ca_xLa_3(PO_4)_3(SiO_4)_3F_2$ $0\leq x\leq 2$. Comptes Rendus Chimie 2015;18(8):858-66.

Chen BY. Toxicity assessment of aromatic amines to *Pseudomonas luteola*: Chemostat pulse technique and dose-response analysis. Process Biochemistry 2006;41(7):1529-38.

Combes RD, Haveland-Smith RB. A review of the genotoxicity of food, drug and cosmetic colors and other azo, triphenylmethane and xanthene dyes. Mutation Research/Reviews in Genetic Toxicology 1982;98(2):101-248.

Dakkach M, Atlamsani A, Sebti S. Natural phosphate modified by vanadium: A new catalyst for oxidation of cycloalkanones and α- ketols with oxygen molecular. Comptes Rendus Chimie 2012;15(6):482-92.

Damodar RA, Jagannathan K, Swaminathan T. Decolourization of reactive dyes by thin film immobilized surface photoreactor using solar irradiation. Solar Energy 2007;81(1):1-7.

Daneshvar N, Salari D, Khataee AR. Photocatalytic degradation of azo dye acid red 14 in water: Investigation of the effect of operational parameters. Journal of Photochemistry and Photobiology A: Chemistry 2003;157(1):111-6.

Deniz F, Saygideger SD. Investigation of adsorption characteristics of Basic Red 46 onto gypsum: Equilibrium, kinetic and thermodynamic studies. Desalination 2010;262 (1-3):161-5.

Drouet C. Apatite formation: Why it may not work as planned, and how to conclusively identify apatite compounds. BioMed Research International 2013;2013(4):1-12.

Elmoubarki R, Mahjoubi FZ, Elhalil A, Tounsadi H, Abdennouri M, Sadiq M, et al. Ni/Fe and Mg/Fe layered double hydroxides and their calcined derivatives: Preparation, characterization and application on textile dyes removal. Journal of Materials Research and Technology 2017;6(3):271-83.

Elmoubarki R, Mahjoubi FZ, Tounsadi H, Moustadraf J, Abdennouri M, Zouhri A, et al. Adsorption of textile dyes on raw and decanted Moroccan clays: Kinetics, equilibrium and thermodynamics. Water Resources and Industry 2015;9:16-29.

Fahami A, Nasiri-Tabrizi B. Mechanochemical behavior of $CaCO_3$-P_2O_5-CaF_2 system to produce carbonated fluorapatite nanopowder. Ceramics International 2014;40(9):14939-46.

Farnane M, Tounsadi H, Machrouhi A, Elhalil E, Mahjoubi FZ, Sadiq M, et al. Dye removal from aqueous solution by raw maize corncob and H_3PO_4 activated maize corncob. Journal of Water Reuse and Desalination 2018;8(2):214-24.

Fleet ME. Infrared spectra of carbonate apatites: ν_2-region bands. Biomaterials 2009;30(8):1473-81.

Fleet ME, Liu X. Accommodation of the carbonate ion in fluorapatite synthesized at high pressure. American Mineralogist 2008;93:1460-9.

Freundlich H, Heller W. The adsorption of cis- and trans-azobenzene. Journal of the American Chemical Society 1939;61:2228-30.

Freundlich HMF. Over the adsorption in solution. The Journal of Physical Chemistry 1906;57:385-471.

Furuzono T, Walsh D, Sato K, Sonoda K, Tanaka J. Effect of reaction temperature on the morphology and size of hydroxyapatite nanoparticles in an emulsion system. Journal of Materials Science Letters 2001;20(2):111-4.

Gallala W, Herchi F, Ben Ali I, Abbassi L, Gaied ME, Montacer M. Beneficiation of phosphate solid coarse waste from redayef (Gafsa Mining Basin) by grinding and flotation techniques. Procedia Engineering 2016;138:85-94.

Giles CH, MacEwan TH, Nakhwa SN, Smith D. Studies in adsorption**.** Part XI. A system of classification of solution adsorption isotherms, and its use in diagnosis of adsorption mechanisms and in measurement of specific surface areas of solids. Journal of the Chemical Society 1960;846:3973-93.

Guo Y, Zhu Z, Qiu Y, Zhao J. Enhanced adsorption of acid brown 14 dye on calcined Mg/Fe layered double hydroxide with memory effect. Chemical Engineering Journal 2013;219:69-77.

Gupta K, Khatri OP. Fast and efficient adsorptive removal of organic dyes and active pharmaceutical ingredient by microporous carbon: Effect of molecular size and charge. Chemical Engineering Journal 2019;378:Article No.122218.

Heiss GS, Gowan B, Dabbs ER. Cloning of DNA from a *Rhodococcus* strain conferring the ability to decolorize sulfonated azo dyes. FEMS Microbiology Letters 1992; 99:221-6.

Ho YS, Mckay FG. Kinetic models for the sorption of dye from aqueous solution by wood. Process Safety and Environmental Protection 1998;76:183-91.

Kenzour A, Belhouchet H, Kolli M, Djouallah S, Kherifi D, Ramesh S. Sintering behavior of anorthite- based composite ceramics produced from natural phosphate and kaolin. Ceramics International 2019;45:20258-65.

Kuang Y, Zhang X, Zhou S. Adsorption of methylene blue in water onto activated carbon by surfactant modification. Water 2020;12(2):587-605.

Lagergren S. About the theory of so-called adsorption of soluble substance. Kungliga Svenska Ventenskapsakademiens Handlingar 1898;24:1-39.

Langmuir I. The constitution and fundamental properties of solids and liquids. Part I. Solids. Journal of the American Chemical Society 1916;38:2221-95.

Langmuir I. The adsorption of gases on plane surfaces of glass, mica and platinum. Journal of the American Chemical Society 1918;40:1361-403.

Machrouhi A, Boumya W, Khnifira M, Sadiq M, Abdennouri M, Elhalil A, et al. Synthetic dyes adsorption and discoloration of a textile wastewater effluent by H_3PO_4 and H_3BO_3 activated *Thapsia transtagana* biomass. Desalination and Water Treatment 2020;202:435-49.

Madupalli H, Pavan B, Tecklenburg MMJ. Carbonate substitution in the mineral component of bone: Discriminating the

structural changes, simultaneously imposed by carbonate in A and B sites of apatite. Journal of Solid-State Chemistry 2017;255:27-35.

Mahjoubi FZ, Khalidi A, Abdennouri M, Barka N. M-Al-SO_4 layered double hydroxides (M=Zn, Mg, or Ni): Synthesis, characterization and textile dyes removal efficiency. Desalination and Water Treatment 2016;57:21564-76.

Mgaidi A, Ben Brahim F, Oulahna D, Nzihou A, El Maaoui M. Chemical and structural changes of raw phosphate during heat treatment. High Temperature Materials and Processes 2004;23(3):185-94.

Mohammadi N, Khani H, Gupta VK, Amereh E, Agarwal S. Adsorption process of methyl orange dye onto mesoporous carbon material-kinetic and thermodynamic studies. Journal of Colloid and Interface Science 2011;362:457-62.

Mouflih M, Aklil A, Jahroud N, Gourai M, Sebti S. Removal of lead from aqueous solutions by natural phosphate. Hydrometallurgy 2006;81:219-25.

Nikcevic I, Jokanovic V, Mitric M, Nedic Z, Makovec D, Uskokovic D. Mechanochemical synthesis of nanostructured fluorapatite/fluorhydroxyapatite and carbonated fluorapatite/ fluorhydroxyapatite. Journal of Solid State Chemistry 2004; 177:2565-74.

Pignatello JJ. The measurement and interpretation of sorption and desorption rates for organic compounds in soil media. Advances in Agronomy 1999;69:1-73.

Rytwo G, Ruiz‐Hitzky E. Enthalpies of adsorption of methylene blue and crystal violet to montmorillonite: Enthalpies of adsorption of dyes to montmorillonite. Journal of Thermal Analysis and Calorimetry 2003;71:751-9.

Sabar S, Abdul-Aziz H, Yusof NH, Subramaniam S, Foo KY, Wilson LD, et al. Preparation of sulfonated chitosan for enhanced adsorption of methylene blue from aqueous solution. Reactive and Functional Polymers 2020;151:Article No.104584.

Sadiq M, Abdennouri M, Barka N, Baalala M, Lamonier C, Bensitel M. Influence of the crystal phase of magnesium phosphates catalysts on the skeletal isomerization of 3,3-dimethylbut-1-ene. Canadian Chemical Transactions 2015; 3(2):225-33.

Tóth J. Thermodynamical correctness of gas/solid adsorption isotherm equations. Journal of Colloid and Interface Science 1994;163:299-302.

Tsuda S, Matsusaka N, Madarame H, Ueno S, Susa N, Ishida K, et al. The comet assay in eight mouse organs: Results with 24 azo compounds. Mutation Research/Genetic Toxicology and Environmental Mutagenesis 2000;465(1-2):11-26.

Wang M, Li G, Huang L, Xue J, Liu Q, Bao N, et al. Study of ciprofloxacin adsorption and regeneration of activated carbon prepared from *Enteromorpha prolifera* impregnated with H_3PO_4 and sodium benzenesulfonate. Ecotoxicology and Environmental Safety 2017;139:36-42.

Wang M, Qian R, Bao M, Gu C, Zhu P. Raman, FT-IR and XRD study of bovine bone mineral and carbonated apatites with different carbonate levels. Materials Letters 2018;210:203-6.

Yous R, Mohellebi F, Cherifi H, Amrane A. Competitive biosorption of heavy metals from aqueous solutions onto *Streptomyces rimosus*. Korean Journal of Chemical Engineering 2018;35:890-9.

Zahrani EM, Fathi MH. The effect of high-energy ball milling parameters on the preparation and characterization of fluorapatite nanocrystalline powder. Ceramics International 2009;35:2311-23.

The Effect of Change in Function from Paddy Field to Dry Land on Soil Fertility Index

Mujiyo Mujiyo*, Galih Joko Puspito, Suntoro Suntoro, Rahayu Rahayu, and Purwanto Purwanto

Universitas Sebelas Maret, Faculty of Agriculture, Department of Soil Science, Surakarta, Indonesia

ARTICLE INFO

Received: 6 Jul 2021
Received in revised: 6 Sep 2021
Accepted: 24 Sep 2021
Published online: 18 Oct 2021
DOI: 10.32526/ennrj/20/202100127

Keywords:
Change in function/ Dry land/ Minimum soil fertility index (MSFI)/ Paddy field/ Soil fertility index

*** Corresponding author:**
E-mail: mujiyo@staff.uns.ac.id

ABSTRACT

This research studied the effect of the change in function from paddy field to dry land on the soil fertility index. The research was conducted in Girimarto Sub-district, Wonogiri District, in the Province of Central Java. The five stages of the research were: determination of Land Mapping Units in areas with a change in land use; field survey; laboratory analysis; determination of Minimum Data Sets (MDSs) or Minimum Soil Fertility Index (MSFI); analysis of Soil Fertility Index (SFI). The research results show that the change in function of 231 ha of land in Girimarto Sub-district is due to the topographical factor of the mountain region and the shortage of water. This change in land function has caused an increase in the soil fertility index. Soil fertility in paddy fields is classed as moderate but after undergoing a change in function to dry land, its classification increases to moderate-high. The increase in soil fertility index of dry land is due to the fact that farming patterns on dry land use more animal manure, which has a long-term residual effect on organic matter content. In order to maintain and improve the fertility of paddy field soil, it is necessary to add organic fertilizer as well as inorganic fertilizer.

1. INTRODUCTION

The increase in population density reflects an increase in the need for housing and food. Population growth suppresses agricultural land, in this case related to the increase in built-up land for housing and also intensification of land management to meet food needs. The increase in population indirectly causes changes in land use and also decreases land quality and productivity. Girimarto Sub-district is located in Wonogiri District, Central Java, Indonesia, including one of the Sub-districts facing the problem of land conversion due to population pressure. According to Wuryanta and Susanti (2015), there has been population pressure on agricultural land in the moderate category. The increase in population also causes a water deficit, where the availability of water is not sufficient for both household and agricultural activities. According to the research of Kumalajati et al. (2015), water demand will increase by 3.38% per year, while water availability will decrease by 0.09% per year, and it is predicted that in 2023 there will be a water deficit.

Change in land function refers to the change in use of an area of land (Janah et al., 2017). A change in land function is often associated with changes in soil parameters (Don et al., 2011). Change in land function is also one of the main factors that has a strong impact on climate change (Maharjan et al., 2017). As well as influencing climate, the change of land use or land function also has an effect on soil fertility (Hartemink, 2010; Rolando et al., 2018). Analysis of soil fertility is the key to sustainable planning in a particular area (Khadka et al., 2018). The evaluation of change in land function and land management on soil fertility can use potential indicators such as macro and micro nutrient availability, cation exchange capacity, and soil organic carbon (Cardoso et al., 2013).

Girimarto Sub-district is an area that has more dry land than paddy field. Most of the agricultural land in Girimarto Sub-district is dry land (Murni et al., 2016). The total area of paddy field is 1,691 ha, while dry land covers an area of 2,275.45 ha. The definition of dry land is land used for plant cultivation, which is never flooded or waterlogged, most of the time of the

Citation: Mujiyo M, Puspito GJ, Suntoro S, Rahayu R, Purwanto P. The effect of change in function from paddy field to dry land on soil fertility index. Environ. Nat. Resour. J. 2022;20(1):42-50. (https://doi.org/10.32526/ennrj/20/202100127)

year (Wahyunto and Shofiyanti, 2012). The use of dry land for agriculture in Indonesia is generally grouped for yards, moor/fields/gardens, pastures, plantations, timber plants, and uncultivated land. In reality, the activity of change in land function from paddy field to dry land leads to a change in the nutrient content of the soil. Changes in land use are related to changes in soil properties (Willy et al., 2019), both physical, chemical and biological properties. Given that land use changes can lead to a decrease in soil fertility, it is important to understand which specific soil parameters are affected by changes in agricultural land use (Willy et al., 2019).

The evaluation of soil fertility status can provide information to improve strategies and techniques that are effective for achieving sustainable farming in the future (Khaki et al., 2017). Soil Fertility Index (SFI) is the indicator most commonly used to evaluate soil fertility (Yang et al., 2020). Most of the indicators that are used to evaluate the soil fertility index are related to the physical, chemical, and biological properties of the soil (Recena et al., 2019). The determination of indicators of soil fertility is carried out based on the chemical parameters of the soil, including Cation Exchange Capacity (CEC) and Organic Matter (OM) as indicators of soil quality, and macro nutrients including Nitrogen (N), Phosphorus (P), Potassium (K), and Magnesium (Mg), soil pH, and texture (Bagherzadeh et al., 2018; Panwar et al., 2011). In the system of evaluation of soil fertility, the determination of weight values of each index is the main factor that can influence the accuracy of the evaluation (Chen et al., 2020).

This study focused on dry land, namely moor, which is the result of the conversion of rice fields. The moor in Girimarto Sub-district are usually planted with secondary crops such as maize, peanuts and cassava. This is mainly due to the topography of Girimarto Sub-district which is located on a highland plateau, leading to farmers to change the function of paddy field to dry land. Land management efforts are needed in order to maintain and increase soil fertility. The goal of this research is to evaluate soil fertility in areas where there has been a change in land function from paddy field to dry land, and to compare the levels of soil fertility in the two different land types, followed by recommendations for land management in the future.

2. METHODOLOGY

The research was conducted in Girimarto Sub-district, Wonogiri District, in the Province of Central Java, Indonesia, located at 7°42′51.32″-7°49′19.46″ SL and 111°9′49.59″-111°2′29.91″ EL, with Karanganyar Sub-district to the north, Sidoharjo Sub-district to the south, Ngadirojo Sub-district to the west, and Jatipurno Sub-district to the east. Girimarto Sub-district is located at an altitude of 40-1,000 m.a.s.l., on undulating terrain with an incline of 14°-45°. The research location covers an area of 6,236.68 ha, of which most of the land is used for agricultural cultivation, including paddy fields and dry land. Approximately 63.6% of the land in Girimarto Sub-district is agricultural land (Wonogiri District Statistic Center, 2020). The research consists of 6 stages: (1) identification of land use change; (2) determination of Land Mapping Units (LMU); (3) field survey; (4) laboratory analysis; (5) determination of Minimum Data Sets (MDS) or Minimum Soil Fertility Index (MSFI); (6) analysis of Soil Fertility Index (SFI).

Changes in land use were identified by observing land use maps in 2012 and 2020 obtained from Google Earth images. Then the mapping of changes in the use of paddy fields to dry land was carried out. The land use change map is used as the basis for determining the Land Mapping Unit (LMU). The LMU were obtained by overlaying several different maps, including a land use change map, a slope map, a map of rainfall, and a map of soil type. The area in the survey consisted of 6 LMU (Figure 1). The sampling points were determined in accordance with the goal of the research. The locations for collecting samples were determined using a method of purposive sampling, by selecting areas with conditions that were representative of the entire research area (Sofiana et al., 2016). Each LMU consists of six sampling points where three points are dry land (conversion from paddy fields) and three points are paddy fields. A total of 36 samples of soil were collected at a depth of 0-30 cm. The collection of soil samples at the location points used the Global Positioning System to find the location points.

A laboratory analysis was carried out to determine the soil fertility index by observing soil physical and chemical properties (Wicaksono et al., 2018). Soil physical properties was texture (pipette method). Soil chemical properties included pH (pH meter with a soil to water ratio of 1.0:2.5), total N (Tot-N) (Kjeldahl method), available P (Av-P) (Olsen method), organic C (Org-C) (Walkley and Black method), exchangeable K (Exch-K) (NH_4OAc 1 N pH 7 extractant, analyzed using Flame Photometer), exchangeable Ca, Mg, and Na (Exch-Ca; Exch-Mg; Exch-Na) (NH_4OAc 1 N pH 7 extractant, analyzed

using Atomic Absorption Spectrophotometer with different wavelengths for each element), cation exchange capacity (CEC) (extract all cations with NH_4OAc 1 N pH 7), Base Saturation (BS) (NH_4OAc 1 N pH 7 extractant, number of exchangeable base cations (K; Ca; Mg; Na) divided by CEC and multiplied by 100%).

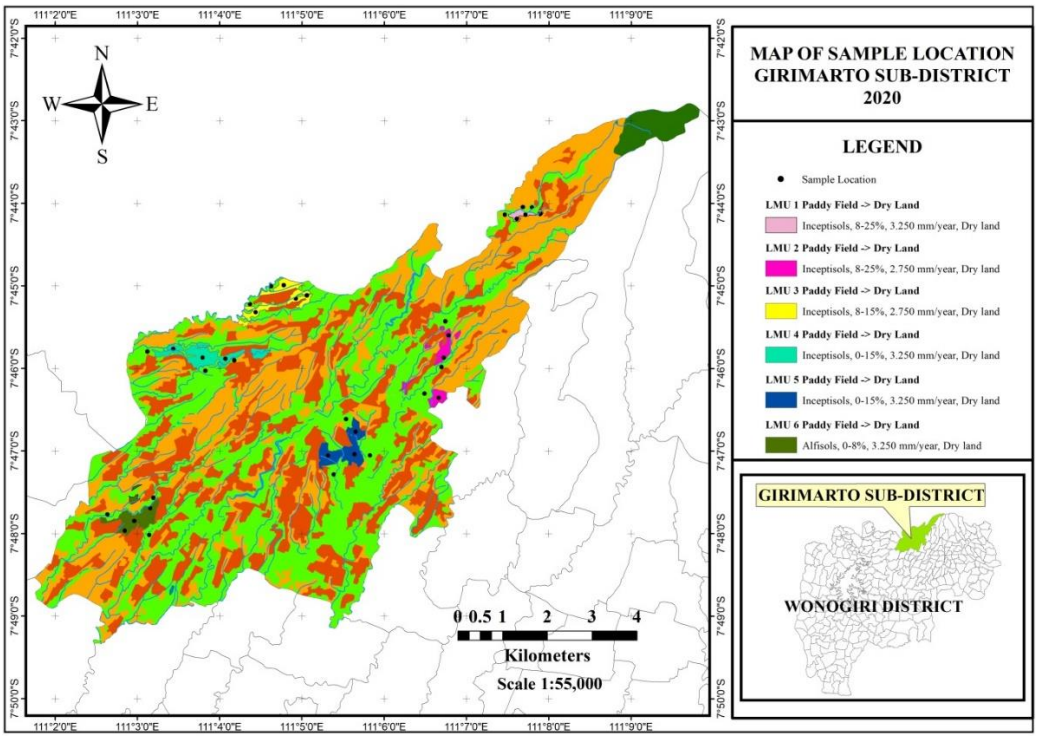

Figure 1. Map of sampling location

The soil fertility index was determined using the data selected from the Minimum Data Sets (MDSs) (Wang et al., 2018). The selection of a MDS that was representative of the soil properties was made based on the results of a Principal Component Analysis (PCA) (Romadhona and Arifandi, 2020). The Minimum Data Set (MDS) is the smallest data obtained through a Principal Component Analysis (PCA), and continues with the Principal Components (PC). The MDS was obtained with a PCA test using a statistical application.

Soil Fertility Index (SFI) is commonly used as a quantitative evaluation of soil fertility (Wang et al., 2018). The calculation of the soil fertility index is the result of the division of the number of weights with the number of Minimum Soil Fertility Index (MSFI) indicators (Mukashema, 2007), using the formula below:

$$SFI = \left(\frac{Sci}{N}\right) \times 10$$

Where; $Sc_i = c_j \times p_c$ [$c_j = w_i \times s_i$ and $p_c = \frac{1}{n_c}$]

Description: SFI=soil fertility index (Table 1); c_j=total score weight; Sc_i=total MSFI weights; p_c=appreciation value; N=total MSFI (MDS); n_c=the amount of value used; wi=weight index; s_i=scoring index (Table 2).

Table 1. Soil fertility index classification

SFI value	SFI class
0.00-0.25	Very low
0.25-0.50	Low
0.50-0.75	Moderate
0.75-0.90	High
0.90-1.00	Very high

Source: Bagherzadeh et al. (2018)

The SFI scores were used to compare the fertility index of paddy field with that of dry land, so that recommendations can be made about future land management. Paired t-test was used to determine the effect of land use on SFI, as well as correlation analysis to determine the relationship between SFI and soil fertility indicators.

Table 2. Scoring index for each indicator

Indicator	Unit	Scoring index (Soil Research Institute, 2009)				
		1	2	3	4	5
Tot-N	(%)	<0.1	0.1-0.2	0.21-0.50	0.51-0.75	>0.75
Av-P	(ppm)	<5	5-10	11-15	16-20	>20
Exc-K	(me/100g)	<0.1	0.1-0.3	0.4-0.5	0.6-1.0	>1.0
Exc-Ca	(me/100g)	<2	2-5	6-10	11-20	>20
Exc-Mg	(me/100g)	<0.3	0.4-1	1.0-2.0	2.1-8.0	>8.0
pH	-	4.5-5.5	5.5-6.5	6.6.7.5	7.6-8.5	>8.5
Org-C	(%)	<1	1-2	2-3	3-5	>5
CEC	(me/100g)	<5	5-16	17-24	25-40	>40
BS	(%)	<20	20-40	41-60	61-80	>80

3. RESULTS AND DISCUSSION

3.1 Change in land function

Change in land function cannot be separated from human activity (Li et al., 2017), nor can it be separated from various natural factors such as topography and climate, and especially drought (Rahman et al., 2017) (Table 3). The results of research by Rahmawati et al. (2019) show that Wonogiri District has low rainfall, which has the potential to cause drought and a continuous decline in water supply. Girimarto Sub-district is located at an incline of 14°-45° which makes it difficult to access the water needed to irrigate paddy field in this mountain area.

Table 3. Distribution of change in land function from paddy field to dry land

LMU	Location (Village)	Area (ha)	Land use change
1	Bubakan	8.7	Paddy field to dry land
2	Semagarduwur	33.3	Paddy field to dry land
3	Giriwarno	41.4	Paddy field to dry land
4	Giriwarno and Jatirejo	54.1	Paddy field to dry land
5	Tambakmerang	50.7	Paddy field to dry land
6	Waleng and Doho	42.8	Paddy field to dry land
Total Area		231.0	

Shortage of water is the primary reasons why paddy fields relying solely on rainfall have been forced to be transformed into dry land, which is ultimately used for growing other crops. The change in land function from paddy field to dry land in Girimarto Sub-district has led to the cultivation of peanuts, cassava, and corn, using a multi cropping system in which more than one type of crop is grown on the same area of land, while in other places banana trees are also grown at the edge of the land. Rice requires an average rainfall of 200 mm/month or more, with a distribution of four months to grow well (Paski et al., 2017). Meanwhile, the rainfall in Girimarto Sub-district is less than 200 mm/month, and this condition lasts for six months (Figure 2).

The reduced availability of water affects agricultural activities. Girimarto Sub-district is included in the Keduang watershed, where the results of research by Kumalajati et al. (2015) stated that the availability of water in 2018 decreased by 0.32% from 2013. The reduced availability of water can lead to a water deficit. The research results of Sanjaya (2020) in the villages of Bubakan, Semagarduwur, and Tambakmerang show a water deficit, where the amount of water available is less than the amount needed. This shortage of water in the Girimarto Sub-district has led to a change in function from paddy field to dry land. This change in function has occurred in six villages in the Girimarto Sub-district, namely the villages of Bubakan, Semagarduwur, Giriwarno, Jatirejo, Tambakmerang, and in an area between the villages of Welang and Doho.

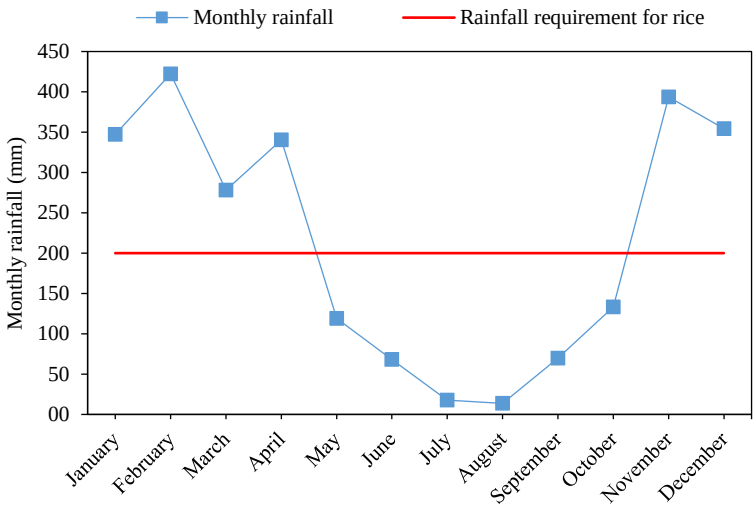

Figure 2. Average monthly rainfall in Girimarto Sub-district year 2012-2017 (Source: Wonogiri District Statistics Center, 2021)

3.2 Soil parameters

According to the results of the laboratory analysis of the parameters total N, available P, exchanged K, organic C, pH, Ca, Mg, CEC, and BS, the data for paddy field and dry land in every LMU showed a change in the content of these elements in the soil, as presented in Table 4. From the various parameters, organic C shows quite a sizeable change, with organic C in dry land being higher than in paddy field. This is due to the continuous use of animal manure on dry land, which can increase the organic matter content, and this is the main key to success in dry land cultivation. Organic C is closely related to soil fertility level (Lal, 2013). The organic C content can be seen from the amount of organic matter in an area of land (Ringgih et al., 2018).

Table 4. Soil chemical properties on paddy fields and dry land for each LMU

Land use	Tot-N (%)	Av-P (ppm)	Exch-K (me/100g)	Exch-Ca (me/100g)	Exch-Mg (me/100g)	pH	Org-C (%)	CEC (me/100g)	BS (%)
Paddy field 1	0.30	3.49	0.30	2.34	0.63	6.14	1.13	25.15	19.06
Paddy field 2	0.32	3.42	0.41	1.87	0.90	6.26	0.90	28.04	18.38
Paddy field 3	0.30	4.39	0.41	4.47	1.06	6.11	1.33	34.92	26.36
Paddy field 4	0.23	2.91	0.28	1.72	0.52	6.24	0.52	23.99	15.62
Paddy field 5	0.23	3.72	0.44	2.19	0.83	5.90	1.04	26.63	18.58
Paddy field 6	0.29	3.66	0.40	3.45	0.61	6.37	1.01	27.46	24.19
Dry land 1	0.25	3.08	0.38	2.19	0.97	6.18	2.99	34.26	18.81
Dry land 2	0.26	3.80	0.31	4.38	0.64	6.13	2.84	37.31	19.02
Dry land 3	0.36	3.88	0.55	3.98	1.18	6.17	3.41	41.66	20.55
Dry land 4	0.18	3.37	0.36	1.57	0.80	5.84	2.36	28.51	14.31
Dry land 5	0.28	3.39	0.36	4.20	1.01	6.16	3.05	41.91	18.17
Dry land 6	0.25	3.72	0.34	2.21	1.03	6.11	3.32	33.54	14.34

In the parameter CEC, a higher value is seen in dry land than paddy field. The CEC value is influenced by organic C content and the types of clay forming minerals in the soil. The higher the organic C content, the higher the CEC. As stated by Ringgih et al. (2018), the difference between CEC values in dry land and paddy field is largely influenced by the amount of organic matter present in the soil, which explains why a higher organic C value will be accompanied by a higher CEC value.

3.3 Soil fertility index

The results of the PCA analysis produced four PCs with an eigenvalue >1, which were selected as the main components, and six indicators as the MDS with the highest weight value for each PC, which were

used to determine the soil fertility score. The PCA analysis generated the Minimum Soil Fertility Index (MSFI) which represents all the soil fertility indicator values used (Prastiwi et al., 2021). For PC 1 there were two indicators that represented the highest weight values for soil fertility, namely Ca and CEC. For PC 2, a single indicator was chosen to represent the soil fertility value, namely base saturation (BS). For PC3, 2 indicators were selected that represented the fertility value with with highest weight, namely pH and total N which showed mutual correlation, while for PC4, a single indicator was chosen that displayed a high weight value, namely organic C (Table 5).

Table 5. Results of PCA

Eigenvalue	2.7491	1.7430	1.3294	1.0988
Proportion	0.3050	0.1940	0.1480	0.1220
Cumulative	0.3050	0.4990	0.6470	0.7690
Variable	PC1	PC2	PC3	PC4
pH	-0.017	-0.116	**0.684***	0.471
Tot-N	0.289	-0.314	**0.411***	-0.196
Av-P	0.357	0.220	-0.145	-0.222
Exch-K	0.318	-0.072	0.235	-0.632
Org-C	0.352	-0.186	-0.487	**0.366***
Exch-Ca	**0.422***	0.325	0.132	0.325
Exch-Mg	0.403	0.207	-0.044	-0.057
CEC	**0.466***	-0.382	-0.022	0.207
BS	0.079	**0.711***	0.175	0.069

Note: CEC=cation exchange capacity, BS=base saturation *=MDS

The analysis of soil fertility index (Table 6) shows a SFI for paddy field classed as moderate, while for dry land the SFI classed as moderate to high. A decrease in soil fertility in paddy field can occur due to a loss of nutrients from the soil. It is the culture of rice farmers to use a lot of inorganic fertilizer which is easily absorbed by crops and is lost through washing and denitrification. The disproportionate use of man-made fertilizer with a high concentration also creates an imbalance of nutrients in the soil, which can lead to the deficiency of other nutrients.

According to Adi et al. (2017), the use of chemical fertilizer with a high nutrient content is not always beneficial. The use of this synthetic fertilizer encourages nutrient loss, environmental pollution, and causes damage to nature. The research results of Nabavi-Pelesaraei et al. (2018) show that the use of chemical fertilizer also has an impact on the environment. Kai et al. (2020) also state that the excessive use of chemical fertilizer has the potential to affect the environment, causing a decrease in microorganisms and water pollution. One of the consequences of using inorganic fertilizer is a decline in nutrient content in the soil, which in turn leads to a decrease in soil fertility. In rice cultivation, this can cause very high drainage of nutrients through the transportation in crops.

The results of the Paired t-test analysis showed that changes in land use from paddy fields to dry land had a significant effect on increasing SFI (t-value=6.53; p-value=0.000; n=36). Changes in the use of paddy fields to dry land significantly increase C-Organic (t-value=13.77; p-value=0.000; n=36), exchangeable Ca (t-value=2.94; p-value=0.009; n=36) and CEC (t-value=6.87; p-value=0.000; n=36). C-Organic, exchangeable Ca and CEC were also significantly positively correlated with SFI (p-value<0.05; n=36).

The increase in soil fertility index of dry land is due to the fact that farming patterns on dry land use more animal manure, which has a long-term residual effect on organic matter content. The key to successful cultivation on dry land is the use of animal manure. The application of animal manure to corn crops has a highly significant effect on the residual product and effect in the following season (Suntoro et al., 2018). Farmers are often unaware of the important role of organic matter in connection with soil fertility. Therefore, efforts can be made to maintain soil fertility by adding sufficient organic matter. According to Suntoro et al. (2020), the use of organic fertilizer from livestock can be implemented to preserve and improve soil fertility. The research of Cruz-Paredes et al. (2017) shows that animal manure can increase soil pH and CEC, which is beneficial for increasing soil fertility. Ahmad et al. (2015) also state that organic matter is an important source of nutrition for increasing soil fertility. The research of Yu et al. (2020) finds that the result of continuous application of organic matter to paddy field over a period of 10 years can significantly increase the content of organic C, biomass microbes, and active organic C. The addition of animal manure to dry land has a long term residual effect that lasts until the following season. According to Arisana et al. (2017), the use of animal manure as organic fertilizer on dry land is more effective for increasing soil fertility because of its micro and macro nutrient content.

Table 6. SFI of paddy field and dry land for each LMU

Paddy field																			
MSFI	Proportion	Cumulative	Wi	Si each sampling point															
				1.1	1.2	1.3	2.1	2.2	2.3	3.1	3.2	3.3	4.1	4.2	4.3	5.1	5.2	5.3	6.1	6.2	6.3
Exch-Ca	0.305	0.769	0.1983	1	1	1	1	1	1	1	1	1	1	1	1	1	1	1	1	1	1
CEC	0.305	0.769	0.1983	3	3	4	3	3	5	4	4	4	3	3	4	4	3	4	4	4	4
BS	0.194	0.769	0.2523	1	1	1	1	2	1	2	2	1	1	1	1	1	1	1	2	2	1
pH	0.148	0.769	0.0962	2	2	2	3	2	2	2	2	2	2	2	2	2	2	2	2	2	3
Tot-N	0.148	0.769	0.0962	3	2	3	3	3	3	3	3	3	3	2	3	3	1	3	3	3	3
Org-C	0.122	0.769	0.1586	2	1	2	1	2	1	2	1	2	1	1	1	2	1	2	1	2	1
Cj				1.84	1.59	2.04	1.78	2.10	2.08	2.29	2.14	2.04	1.69	1.59	1.88	2.04	1.49	2.04	2.14	2.29	1.98
nc				5.00	5.00	5.00	5.00	5.00	5.00	5.00	5.00	5.00	5.00	5.00	5.00	5.00	5.00	5.00	5.00	5.00	5.00
Pc (1/nc)				0.20	0.20	0.20	0.20	0.20	0.20	0.20	0.20	0.20	0.20	0.20	0.20	0.20	0.20	0.20	0.20	0.20	0.20
Sci (Cj × Pc)				0.37	0.32	0.41	0.36	0.42	0.42	0.46	0.43	0.41	0.34	0.32	0.38	0.41	0.30	0.41	0.43	0.46	0.40
N				6.00	6.00	6.00	6.00	6.00	6.00	6.00	6.00	6.00	6.00	6.00	6.00	6.00	6.00	6.00	6.00	6.00	6.00
SFI (Sci/N) ×10				0.61	0.53	0.68	0.59	0.70	0.69	0.76	0.71	0.68	0.56	0.53	0.63	0.68	0.50	0.68	0.71	0.76	0.66
SFI each LMU				0.61			0.66			0.72			0.57			0.62			0.71		
SFI Class				Moderate			Moderate			Moderate			Moderate			Moderate			Moderate		

Dry land																			
MSFI	Proportion	Cumulative	Wi	Si each sampling point															
				1.1	1.2	1.3	2.1	2.2	2.3	3.1	3.2	3.3	4.1	4.2	4.3	5.1	5.2	5.3	6.1	6.2	6.3
Exch-Ca	0.305	0.769	0.1983	1	1	1	1	1	1	1	1	1	1	1	1	1	1	1	1	1	1
CEC	0.305	0.769	0.1983	4	4	5	4	4	5	4	4	5	4	4	4	5	5	5	4	4	4
BS	0.194	0.769	0.2523	1	2	1	1	2	1	2	2	1	1	1	1	1	2	1	1	1	1
pH	0.148	0.769	0.0962	2	2	2	2	2	3	2	2	2	2	2	2	2	2	2	2	2	2
Tot-N	0.148	0.769	0.0962	3	2	3	3	2	3	3	3	3	2	2	3	3	2	3	3	2	3
Org-C	0.122	0.769	0.1586	4	3	3	3	4	3	4	3	4	3	2	3	3	4	3	4	3	4
Cj				2.36	2.36	2.40	2.20	2.52	2.50	2.61	2.45	2.56	2.10	1.95	2.20	2.40	2.71	2.40	2.36	2.10	2.36
nc				5.00	5.00	5.00	5.00	5.00	5.00	5.00	5.00	5.00	5.00	5.00	5.00	5.00	5.00	5.00	5.00	5.00	5.00
Pc (1/nc)				0.20	0.20	0.20	0.20	0.20	0.20	0.20	0.20	0.20	0.20	0.20	0.20	0.20	0.20	0.20	0.20	0.20	0.20
Sci (Cj × Pc)				0.47	0.47	0.48	0.44	0.50	0.50	0.52	0.49	0.51	0.42	0.39	0.44	0.48	0.54	0.48	0.47	0.42	0.47
N				6.00	6.00	6.00	6.00	6.00	6.00	6.00	6.00	6.00	6.00	6.00	6.00	6.00	6.00	6.00	6.00	6.00	6.00
SFI (Sci/N)×10				0.79	0.79	0.80	0.73	0.84	0.83	0.87	0.82	0.85	0.70	0.65	0.73	0.80	0.90	0.80	0.79	0.70	0.79
SFI each LMU				0.79			0.80			0.85			0.69			0.83			0.76		
SFI Class				High			High			High			Moderate			High			High		

4. CONCLUSION

The change in land function that has taken place in Girimarto Sub-district on an area of 231 ha is due to the topographical factor of the mountain region and the shortage of water, which has led to a change in land function from paddy field to dry land. The soil fertility of paddy field in Girimarto Sub-district is classed as moderate while that of dry land is classed as moderate to high. The factor that has the greatest influence on soil fertility is the difference in soil nutrient content, especially organic matter, Ca and cation exchange capacity. Increased efforts need to be made to maintain and improve soil fertility, and especially the organic matter content in paddy field soil. The use of man-made fertilizer or chemical fertilizer needs to be balanced with the use of animal manure, which can provide an alternative solution for increasing the amount of organic matter contained in the soil. Changes in the use of paddy fields to dry land with good land management can increase soil fertility, increase land productivity and maintain the sustainability of agricultural production.

ACKNOWLEDGEMENTS

This research study was supported by Universitas Sebelas Maret under the research grant PNBP 2020-2021. We would like to thank Tiara Hardian and Novi Rahmawati Sutopo for their participation in the paper elaboration.

REFERENCES

Adi IA, Barunawati N, Wardiyati T. The effects of chemicals fertilizer combination with the type of manure on the growth and yield of potato (*Solanum tuberosum* L.) in medium plains. Produksi Tanaman 2017;5(4):531-7.

Ahmad I, Akhtar MJ, Zahir ZA, Mitter B. Organic amendments: effects on cereals growth and cadmium remediation. International Journal of Environmental Science and Technology 2015;12(9):2919-28.

Arisana PJ, Armaini, Ariani E. Effect of cow manure and spacing to baby corn and mungbean (*Vigna radiata* L.) growth and yield on intercropping system. Jurnal Online Mahasiswa Fakultas Pertanian Universitas Riau 2017;4(1):1-16.

Bagherzadeh A, Gholizadeh A, Keshavarzi A. Assessment of soil fertility index for potato production using integrated Fuzzy and AHP approaches, Northeast of Iran. Eurasian Journal of Soil Science 2018;7(3):203-12.

Cardoso EJBN, Vasconcellos RLF, Bini D, Miyauchi MYH, dos Santos CA, Alves PRL, et al. Soil health: Looking for suitable indicators. What should be considered to assess the effects of use and management on soil health? Scientia Agricola 2013;70(4):274-89.

Chen S, Lin B, Li Y, Zhou S. Spatial and temporal changes of soil properties and soil fertility evaluation in a large grain-production area of subtropical plain, China. Geoderma 2020;357:Article No. 113937.

Cruz-Paredes C, López-García Á, Rubæk GH, Hovmand MF, Sørensen P, Kjøller R. Risk assessment of replacing conventional P fertilizers with biomass ash: Residual effects on plant yield, nutrition, cadmium accumulation and mycorrhizal status. Science of the Total Environment 2017;575:1168-76.

Don A, Schumacher J, Freibauer A. Impact of tropical land-use change on soil organic carbon stocks: A meta-analysis. Global Change Biology 2011;17:1658-70.

Hartemink AE. Land use change in the tropics and its effect on soil fertility. World Soil Information 2010;1990:55-8.

Janah R, Eddy BT, Dalmiyatun T. Changes in agricultural land use and Its impacts on the lives of farmers at Sayung Subdistrict, Demak Regency. Agrisocionomics 2017;1(1):1-10.

Kai T, Kumano M, Tamaki M. A study on rice growth and soil environments in paddy fields using different organic and chemical fertilizers. Journal of Agricultural Chemistry and Environment 2020;09(04):331-42.

Khadka D, Lamichhane S, Bhurer KP, Chaudhary JN, Ali MF, Lakhe L. Soil fertility assessment and mapping of regional agricultural research station, Parwanipur, Bara, Nepal. Journal of Nepal Agricultural Research Council 2018;4:33-47.

Khaki BD, Honarjoo N, Davatgar N, Jalalian A, Golsefidi HT. Assessment of two soil fertility indexes to evaluate paddy fields for rice cultivation. Sustainability (Switzerland) 2017; 9(8):1-13.

Kumalajati E, Sabarnudi S, Budiadi B, Sudira P. Analysis of water needs and availability in the Duang Watershed, Central Java. Jurnal Teknosains 2015;5(1):Article No. 9.

Lal R. Soil carbon management and climate change. Carbon Management 2013;4(4):439-62.

Li J, Zhang Y, Qin Q, Yan Y. Investigating the impact of human activity on land use/cover change in China's Lijiang River Basin from the perspective of flow and type of population. Sustainability (Switzerland) 2017;9(3):Article No. 383.

Maharjan M, Sanaullah M, Razavi BS, Kuzyakov Y. Effect of land use and management practices on microbial biomass and enzyme activities in subtropical top-and sub-soils. Applied Soil Ecology 2017;113:22-8.

Mukashema A. Mapping and Modelling Landscape-based Soil Fertility Change in Relation to Human Induction [dissertation]. Enschede, Netherlands: International Institute for Geo-Information Science and Earth Observation; 2007. p.10-9.

Murni S, Seventi IS, Octoria D, Rahmawati. Increasing profit and industrial marketing through empowering financial insights and website design. Jurnal Economia 2016;12(1):54-66.

Nabavi-Pelesaraei A, Rafiee S, Mohtasebi SS, Hosseinzadeh-Bandbafha H, Wing CK. Integration of artificial intelligence methods and life cycle assessment to predict energy output and environmental impacts of paddy production. Science of the Total Environment 2018;(631-632):1279-94.

Panwar P, Pal S, Reza SK, Sharma B. Soil fertility index, soil evaluation factor, and microbial indices under different land uses in acidic soil of humid subtropical India. Communications in Soil Science and Plant Analysis 2011; 42(22):2724-37.

Paski JAI, Faski GISL, Handoyo MF, Pertiwi DS. Analysis of land water balance for rice and corn plants in Bengkulu City. Jurnal Ilmu Lingkungan 2017;15(2):83-9.

Prastiwi P, Sumani S, Slamet M, Suntoro S, Supriyadi S. The assessment of soil fertility index for evaluation of rice production in Karanganyar Regency. Modern Applied Science 2021;15(2):63-72.

Rahman F, Sukmono A, Yuwono B. Analysis of drought on agricultural land using the NDDI method and Perka BNPB Number 02 of 2012 (Case Study: Kendal Regency 2015). Jurnal Geodesi Undip 2017;6(4):274-84.

Rahmawati E, Hadiani RRR, Solichin S. Hydrological drought analysis based on the moisture adequacy index (MAI) method in the Temon River Basin, Wonogiri Regency. Matriks Teknik Sipil 2019;7(3):189-96.

Recena R, Fernández-Cabanás VM, Delgado A. Soil fertility assessment by Vis-NIR spectroscopy: Predicting soil functioning rather than availability indices. Geoderma 2019; 337:368-74.

Ringgih D, Rayes ML, Utami SR. Study of changes in physical and chemical properties due to paddy in Andisol Sukabumi, West Java. Agrovigor: Jurnal Agroekoteknologi 2018; 11(1):21-7.

Rolando JL, Dubeux JCB, Ramirez DA, Ruiz-Moreno M, Turin C, Mares V, et al. Land use effects on soil fertility and nutrient cycling in the peruvian high-andean puna grasslands. Soil Science Society of America Journal 2018;82(2):463-74.

Romadhona S, Arifandi JA. Index of soil quality and land use in the Suco River Basin, Jember Regency. Geography: Jurnal Kajian, Penelitian Dan Pengembangan Pendidikan 2020;8(1):37-45.

Sanjaya IR. Analisis Daya Dukung Sumber Daya Air [dissertation]. Surakarta; Universitas Muhammadiyah; 2020.

Sofiana UR, Sulardiono B, Nitisupardjo M. Relationship between organic of sediment matter with infauna abundance in different seagrass density, Bandengan Beach Jepara. Management of Aquatic Resources 2016;5(3):135-41.

Soil Research Institute. Technical Guide Edition 2: Chemical Analysis of Soil, Plants, Water, and Fertilizer. Bogor, Indonesia: Soil Research Institute; 2009.

Suntoro S, Mujiyo M, Widijanto H, Herdiansyah G. Cultivation of rice (*Oryza sativa*), corn (*zea mays*) and soybean (*glycine max*) based on land suitability. Journal of Settlements and Spatial Planning 2020;11(1):9-16.

Suntoro S, Widijanto H, Suryono, Syamsiyah J, Afinda DW, Dimasyuri NR, et al. Effect of cow manure and dolomite on nutrient uptake and growth of corn (*Zea mays* L.). Bulgarian Journal of Agricultural Science 2018;24(6):1020-6.

Wahyunto, Shofiyanti R. Potential dry land to support fulfillment of food needs in Indonesia. In: Dariah A, Kartiwa B, Sutrisno N, Suradisastra K, Sarwani M, Soeparno H, et al, editors. The Prospect of Dry Land Agriculture in Supporting Food Security. Jakarta, Indonesia: IAARD Press; 2012. p. 297-315.

Wang D, Bai J, Wang W, Zhang G, Cui B, Liu X, et al. Comprehensive assessment of soil quality for different wetlands in a Chinese delta. Land Degradation and Development 2018;29(10):3783-94.

Wicaksono AS, Herlambang S, Saidi D. Analysis of dryland soil quality index in various land uses in Ngalang Village, Gedangsari Subdistrict, Gunungkidul District. Jurnal Tanah dan Air (Soil and Water Journal) 2018;15(2):61-72.

Willy DK, Muyanga M, Mbuvi J, Jayne T. The effect of land use change on soil fertility parameters in densely populated areas of Kenya. Geoderma 2019;343:254-62.

Wonogiri District Statistic Center. Kecamatan Girimarto dalam angka tahun 2020 [Internet]. 2020 [cited 2021 Jun 25]. Available from: https://wonogirikab.bps.go.id/publication/2020/09/28/b673c6573c806c59db4b2d26/kecamatan-girimarto-dalam-angka-2020.html.

Wonogiri District Statistic Center. Rainfall [Internet]. 2021 [cited 2021 Aug 28]. Available from: https://wonogirikab.bps.go.id/subject/151/iklim.html#subjekViewTab3.

Wuryanta A, Susanti PD. Spatial analysis of population pressure on agricultural land in the Keduang Watershed, Wonogiri Regency, Central Java. Jurnal Penelitian Sosial Dan Ekonomi Kehutanan 2015;12(3):149-62.

Yang M, Mouazen A, Zhan X, Guo X. Assessment of a soil fertility index using visible and near- infrared spectroscopy in the rice paddy region of southern China. European Journal of Soil Science 2020;71:615-26.

Yu Q, Hu X, Ma J, Ye J, Sun W, Wang Q, et al. Effects of long-term organic material applications on soil carbon and nitrogen fractions in paddy fields. Soil and Tillage Research 2020;196;Article No. 104483.

The Alternating Growth of Bacteria within a Consortium During Desulfurization of Coal

Megga Ratnasari Pikoli[1*], Pingkan Aditiawati[2], Dea Indriani Astuti[2], and Akhmaloka[3]

[1]*Department of Biology, Faculty of Science and Technology, Universitas Islam Negeri Syarif Hidayatullah Jakarta, Indonesia*
[2]*School of Life Sciences and Technology, Institut Teknologi Bandung, Indonesia*
[3]*Faculty of Mathematics and Natural Sciences, Institut Teknologi Bandung, Indonesia*

ARTICLE INFO

Received: 30 Jul 2021
Received in revised: 17 Sep 2021
Accepted: 28 Sep 2021
Published online: 27 Oct 2021
DOI: 10.32526/ennrj/20/202100145

Keywords:
Biodesulfurization/ Bacterial consortium/ Coal/ Dibenzothiophene/ *Moraxella osloensis*/ *Pseudomonas*

*** Corresponding author:**
E-mail: meggapikoli@uinjkt.ac.id

ABSTRACT

Efforts to reduce organic sulfur in coal are taken through biodesulfurization by using desulfurization bacteria to release covalently-bound sulfur from the coal matrix. Coal is a complex hydrocarbon material that requires collaboration from more than one type of bacteria in a consortium for desulfurization. The current study shows how the individual members of a bacterial consortium obtained directly from coal samples grew on the coal. Mineral medium containing sub-bituminous coal with a concentration of 10%, 15%, and 20% served as a carbon source and the only sulfur to support the consortium's growth. The examination included growth patterns, concentrations of dibenzothiophene as an organic sulfur representative, pH, and sulfate concentration as the sulfur product released into the medium. The growth of individual members of the consortium was observed for 336 h. The consortium grew in all three coal concentrations with slightly different cell growth patterns and the release of dibenzothiophene. Members of the consortium grew alternately and overlapped, which showed possible linkages or dependence on products and existence from the growth of other members. The existence of the primary strain *Moraxella osloensis* COK1 indicated that they played a role in the activities and growth of other members. The alternating growth is discussed to produce a hypothetical illustration of how several other members play in using sulfur in a well-known desulfurization pathway. In conclusion, this study provides a deeper insight into the value of consortium members individually but growing together while swarming coal as a complex resource to become low-sulfur coal.

1. INTRODUCTION

Coal is a complex natural material mainly composed of carbon interspersed with minerals. These minerals include sulfur-forming compounds such as; dibenzothiophene, thiophenol alkyl, aryl sulfide, and dialkyl sulfides. When coal is used as a fuel, sulfur compounds are emitted and lower the surrounding air quality. Therefore, various attempts should be made to address the sulfur content in coal. Biodesulfurization is an alternative to minimize the tightly associated sulfur content associated with coal which works at medium temperature, hence lower operational cost. Most studies on coal biodesulfurization employ bacteria as the sulfur releasing agent, which is considered an economical and environmentally friendly technique (Jatoi et al., 2021; Kotelnikov et al., 2020).

As with any other natural materials, coal can be attacked and thus a harboring habitat for bacteria. Coal originally comes from plant material and is a target of carbon source for heterotrophic bacteria. Some studies have proved the presence of bacteria: the role of bacteria in coal formation (Burke and Wiley, 1937) and the isolation of bacteria from acid drainage of coal mines (Colmer et al., 1949). Other studies include recent publications about the presence of

Citation: Pikoli MR, Aditiawati P, Astuti DI, Akhmaloka. The alternating growth of bacteria within a consortium during desulfurization of coal. Environ. Nat. Resour. J. 2022;20(1):51-60. (https://doi.org/10.32526/ennrj/20/202100145)

methanogenic bacterial communities on coal and water formations (Strąpoć et al., 2008), the microscopic appearance of bacterial cells on coal particles (Yossifova et al., 2011), the dominance of hydrogen-producing bacteria and methanogens in coal seams (Su et al., 2018), and different taxa in the microbial community are responsible for the degradation of different coal components (Vick et al., 2019). A most recent study showed that the adherent microbial community preferred to form dense biofilms around cracks in the mineral-rich coal surface, which may provide shelter for the bacteria (McLeish et al., 2021). All the proof about the presence of bacteria that come from coal show the ability of the bacteria to adapt to the coal matrix environment. Accordingly, coal could be used as an object to explore desulfurization bacteria.

Apart from coal as a living space and its abiotic environment, the bacteria in coal cannot be separated from its biotic environment and other bacteria. The interactions have been established for a long time until coal formed, which caused the bacteria to coexist with the coal maturation. Although it is suspected that their growth occurs very slowly, or even quiescent or dormant in the coal (Burke and Wiley, 1937), due to limited growth factors, their coexistence in coal over millions of years of maturation has resulted in a consortium of bacteria that even helps restructure coal carbon. Some studies demonstrating the effectiveness of microbial consortia in reducing sulfur content in coal were oriented to the final results (Kotelnikov et al., 2020). Biodesulfurization of a mixed culture bacteria worked more efficiently than physico-chemical methods, lowering SO_2 emissions by 72.4% and reducing ash content by 33% (Makgato and Chirwa, 2020). Therefore, in the current study, we examined the activity of a consortium of bacteria from coal in batch culture with a medium containing minerals and coal as a sole source of sulfur. The consortium members were not isolated singly beforehand nor reconstructed, but mixed inoculum cultures were obtained directly from coal and enriched in stages. The results of this study provide an overview of how consortium members took turns in using coal as a sulfur source so that they overall worked to reduce sulfur in coal or carried out sequential biodesulfurization.

Examination of the bacterial consortium activity from coal samples was carried out in coal media of 10%, 15%, and 20% to determine the effect of growth support, i.e., carbon and sulfur sources, on desulfurization activity and bacterial community. The concentration of dibenzothiophene is a parameter measured for desulfurization because it is the most significant organic sulfur in coal (Constanti et al., 1994; Jatoi et al., 2021) and has become an internal standard for assessing coal maturation (Li et al., 2012). In addition, the desulfurization of dibenzothiophene also means the attack of other organic compounds because the microorganisms that desulfurize the compound can use a wide range of sulfur compounds as substrates (Chen et al., 2019; Nassar et al., 2021).

2. METHODOLOGY

2.1 Materials and chemicals

The coal samples used are sub-bituminous coal from South Sumatra, Indonesia. The media used were mineral salts medium and nutrient agar. The mineral salt medium was sulfur-free and contained NaCl 0.075 g/L, NH_4Cl 2.0 g/L, Na_2HPO_4 5.77 g/L, K_2HPO_4 2.44 g/L, trace mineral solution 10 mL/L, and glucose 10.0 g/L (Gunam et al., 2006). All media was sterilized by autoclaving at 121°C for 15 min. Molecular identification of isolate used PeqGold Bacterial DNA kit (Peqlab, UK), DreamTaq polymerase PCR kit (Thermo Fisher Scientific), primers 27F/1492R, agarose, and buffer Tris-acetate EDTA pH 9.0.

2.2 Isolation of consortium inoculum

Isolation was carried out by using the stratified enrichment method in three stages. In the first stage, five grams of 100 mesh coal samples were used as a source of isolation and inserted into a 95 mL sterile mineral salts medium containing 10% (w/v) coal in a 250 mL Erlenmeyer flask. The coal concentration of 10% in the medium did not include coal added as a source of isolation. The cultures were incubated at room temperature for 24 h while being shaken at 120 rpm. In the second stage, following the duration of 24 h, 10 mL of culture solution from the first stage was transferred into 90 mL of new mineral salts medium and incubated under the same conditions for 24 h or achieved a minimum cell concentration of 10^6 cells/mL. In the final stage, 15 mL of the second stage culture was transferred into 135 mL of new mineral salts medium and incubated under the same conditions for 24 h. This culture was used as an inoculum for examination. Bacteria in this culture were also isolated on a nutrient agar medium to obtain single colonies, and pure cultures were identified.

2.3 Examination of bacterial growth

The medium used for growth examination was a mineral salts medium treated with coal powder with concentrations (w/v) of 10%, 15%, and 20%. The examination was carried out by inoculating 10% (w/v) of the inoculum culture into the sterile mineral salts medium containing coal, i.e., 10%, 15%, or 20%. The cultures were incubated while shaking at 120 rpm at room temperature for 48 h. Sampling on culture solution was carried out at specific intervals to check the cell concentration, dibenzothiophene concentration, and culture pH. The cell concentration was measured using dilution and plating on a nutrient agar medium by the total plate count method. At the time of colony counting, colony morphology was observed to differentiate between bacteria in the consortium. Their morphology was compared to colony morphology in single isolates. Isolates were distinguished from their colony morphological characteristics: whole shape, margin, elevation, and color. Thus, each colony can be identified as a single species, and the individual species concentration can be calculated. For pH and dibenzothiophene measurements, the sample was filtered first to reduce the undissolved coal flakes. The concentration of dibenzothiophene was determined by spectrophotometric analysis using absorbance at a wavelength of 323.8 nm (Etemadifar et al., 2008). Sulfate measurements were carried out by the turbidimetric method at a wavelength of 420 nm after the addition of $BaCl_2$.

2.4 Identification of isolates

The pure bacteria were identified individually based on the 16S rRNA gene. The isolated DNA was PCR-amplified by using universal primers 27F/1492R according to the well-known general protocol. The following PCR conditions were carried out: initial denaturation at 95°C for 5 min, 30 cycles of denaturation at 95°C for 1 min, annealing at 51°C for 1 min, extension at 72°C for 1 min, and a final extension step at 72°C for 10 min. The consensus sequences of forward and reverse PCR products were aligned with GenBank (NCBI) reference sequences retrieved by using BLAST (Altschul et al., 1990), and the phylogenetic tree was reconstructed with MEGA6 (Tamura et al., 2013) using the neighbor-joining method with bootstrap 1000. The identified sequences COK1 to COK5 were deposited in GenBank with accession numbers AB931117 to AB931121, respectively.

3. RESULTS AND DISCUSSION

Organic sulfur represented by dibenzothiophene has been detected in all coal media of 10%, 15%, and 20% since the beginning of incubation. The organic sulfur was released from the coal by previous autoclaving. It resulted in a low initial pH of the medium, with an average of 5.82, 5.42, and 4.78, respectively, in 10%, 15%, and 20% coal medium. The pH decreased because it was influenced by the sulfate content that increased simultaneously with the coal concentration, an average of 0.18, 0.61, and 1.19 mg/L, respectively, in 10%, 15%, and 20% coal medium. Sulfate is inorganic sulfur in coal and is easily leached from coal and is easily dissolved into the medium. Unlike sulfate, the initial concentration of dibenzothiophene decreased with an increase in coal concentration, i.e., an average of 0.56, 0.51, and 0.27 mM, respectively, in 10%, 15%, and 20% coal medium. Organic sulfur such as dibenzothiophene is covalently bound to form large complex structures in coal (Kotelnikov et al., 2020). If the coal is more concentrated, the heating effect using autoclaving-sterilization on coal degradation will decrease, resulting in less organic sulfur released into the medium.

The molecular identification results indicated COK1 to COK5 belong to *Moraxella osloens*is, *Micrococcus endophyticus*, *Pseudomonas aeruginosa*, *Pseudomonas psychrotolerans*, and *Enhydrobacter aerosaccus*, respectively. However, COK6 was not identified because its viability could not be maintained during storage. Each isolate showed distinct morphological characteristics on the nutrient agar plate. Isolate 1 was circular, entire (smooth), raised, and translucent. Isolates 2, 3, and 6 were similar in shape, margin, and elevation but were light yellow, pink, and yellowish transparent, respectively. Isolate 4 was circular with a wrinkled surface, undulate margin, umbonate elevation, and yellow. Isolate 5 was circular, entire, flat, and was milky white or opaque in color. They are all heterotrophic bacteria that correspond to the predominant organic sulfur in the coal sample. The organic sulfur content in the coal sample was 57% of the total sulfur, meaning that the high organic sulfur environment selected the organic sulfur users. The species name followed by the isolate codes are used in the following discussions.

In the 10% coal medium, *Moraxella osloensis* COK1 was the only bacteria detected at the beginning of incubation; cell concentration decreased until hour 6, accompanied by an increase in dibenzothiophene

and a slow increase in sulfate concentration (Figures 1 and 2). The decrease in the concentration of *M. osloensis* COK1 indicates the adaptation of bacteria once they enter the coal medium. Growth of *M. osloensis* COK1 continued to be detected until the end of incubation, indicating that its growth dominates the consortium.

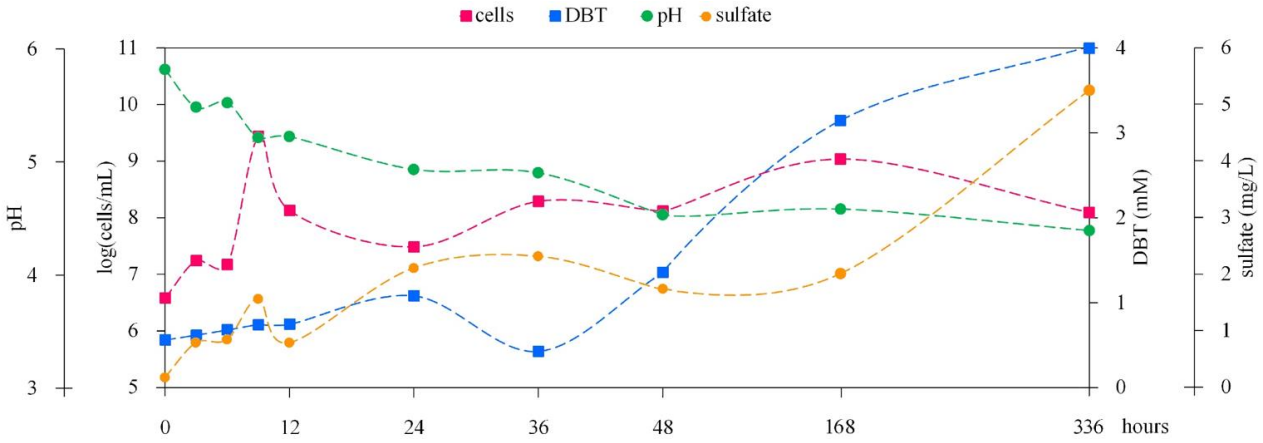

Figure 1. The activity of coal-origin bacteria consortium in 10% coal medium

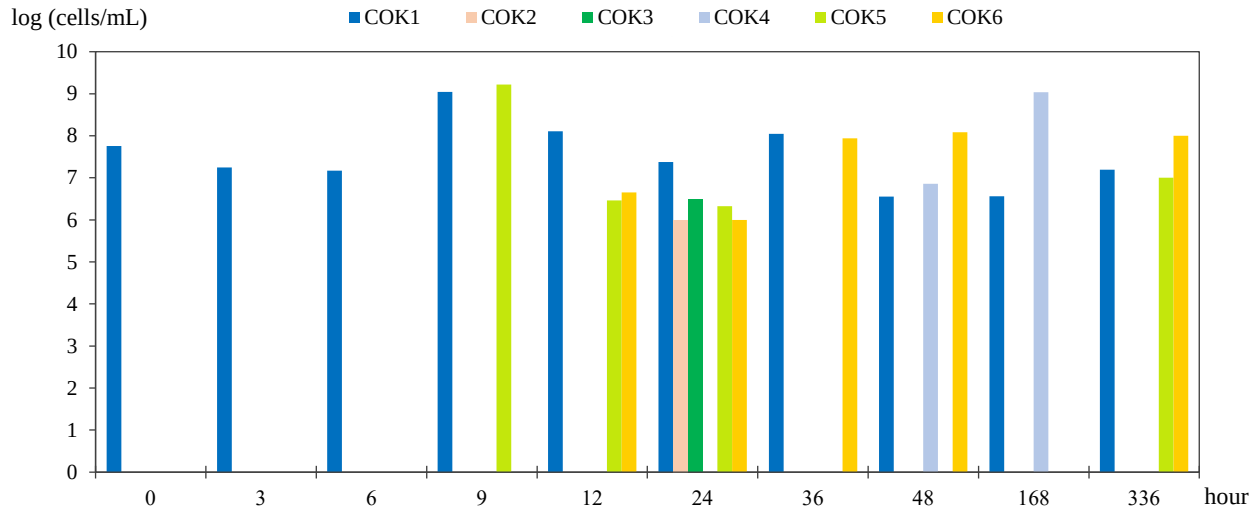

Figure 2. The concentrations of individual consortium members in 10% coal medium

At the beginning of its growth in a coal medium containing glucose, *M. osloensis* COK1 got carbon from glucose and sulfur released from coal due to autoclaving-sterilization to be assimilated into cells. Due to this action, the cells obtained energy to produce enzymes used to remove organic sulfur from coal which was further used and can be seen from an increase in the concentration of dibenzothiophene and sulfate. Degradation of black carbon in nature, including coal, is through the mechanism of cometabolism, which increases with the addition of glucose, namely through increased growth of biomass and the enzymes it produces (Hamer et al., 2004; Jatoi et al., 2021). Meanwhile, culture pH tended to decrease from the beginning to the end of incubation, although it appears that there was a fluctuation. pH changes were affected by sulfates and the release of organic acids resulting from coal degradation, such as fulvic acid and humic acid found in coal. These acids are products from extracellular laccase activities while using coal as a carbon source (Taiwo et al., 2020).

During hours 6-9, the cell concentration increased rapidly, accompanied by decreased pH, and increased sulfate and dibenzothiophene concentrations. The growth of *M. osloensis* COK1 cells, which is heterotrophic bacteria (use organic matter), and an increase in sulfate concentrations, indicated that degradation of organic compounds, including the organic sulfur, was taking place. The concentration of dibenzothiophene that also increased revealed that not

all of the released organic sulfur was used by bacteria. This is possible because other organic sulfur compounds can be released when coal degradation occurs and become an alternative sulfur source. Degradation of dibenzothiophene released sulfur in the sulfate form, allowing some sulfur to be assimilated for cell growth. At this stage, the desulfurization by *M. osloensis* COK1 was assisted by *E. aerosaccus* COK5. The emergence of *E. aerosaccus* COK5 led to an assumption that they were the user of degradation products by *M. osloensis* COK1. This assumption was supported by the fact that *E. aerosaccus* COK5 could not grow well as a single culture (data not shown).

During hours 9-24, the cell concentration decreased significantly, the dibenzothiophene concentration increased, and the sulfate concentration decreased then increased. At this stage, desulfurization was not only played by *M. osloensis* COK1 and *E. aerosaccus* COK5 because *Micrococcus endophyticus* COK2, *Pseudomonas aeruginosa* COK3, and COK6 also appeared. *Micrococcus endophyticus* is a gram-positive bacterium relatively recently discovered and characterized from the roots of *Aquilaria sinensis* (Hamer et al., 2004). Meanwhile, *Pseudomonas aeruginosa* has been widely known for its ability to degrade hydrocarbon compounds, including dibenzothiophene. *P. aeruginosa* isolated from oil sludge was able to degrade a mixture of carbazole, dibenzothiophene, and fluorene in petroleum refinery wastewater (Ghosh and Mukherji, 2020). In the current stage, the cell concentrations were lower than before. However, the consortium members were more diverse, so the release of organic sulfur compounds and their desulfurization continued. Desulfurization can be triggered by a decrease in sulfate during hours 9-12. Under limited sulfate conditions, some bacteria synthesize an extra set of proteins required to metabolize an alternative sulfur source, called sulfate-starvation-induced proteins, which are synthesized only in the absence of a sulfur source, including sulfate. The proteins can be enzymes and transport systems involved in the metabolism of alternative sulfur sources from the environment, including Dsz desulfurization enzymes in the 4S pathway (Mohebali and Ball, 2016). The sulfate-starvation reactions include restricting sulfur assimilation, enforcing sulfur-sparing, and maintaining redox homeostasis. However, it is currently unknown how desulfurizing bacteria respond to this stressor (Hirschler et al., 2021).

At hour 24, five strains of bacteria were detected, and *M. osloensis* COK1 still predominated. However, at hour 36, only *M. osloensis* COK1 and COK6 dominated, approximately in the same proportion. COK6 was challenging to grow as a single culture, either in general bacterial media (nutrient agar) or minimal media containing dibenzothiophene. The decrease in dibenzothiophene concentration accompanied by an increase in sulfate concentration at this stage indicated that COK6 was the user of organic sulfur released by *M. osloensis* COK1 from coal.

During hours 36-48, the cell concentration decreased until it was relatively constant, the dibenzothiophene concentration increased again, and the sulfate concentration decreased, but the pH continued to decrease. *Pseudomonas psychrotolerans* COK4 appeared, in addition to *M. osloensis* COK1 and COK6, which remained the members who played a role. The increase in dibenzothiophene concentration indicated that *P. psychrotolerans* COK4 enhanced the release of organic sulfur from coal. The growth of *P. psychrotolerans* COK4 was still detected at hour 168, causing high cell concentrations and dibenzothiophene concentrations. The genus *Pseudomonas* is known to degrade various aromatic hydrocarbons. They were widely used as a bioremediation agent of environmental pollutants (Wasi et al., 2013) and a member of consortia in coal desulfurization (Kotelnikov et al., 2020; Makgato and Chirwa, 2020).

The decrease in sulfate concentration and the increase in the concentration of dibenzothiophene indicated that the release of organic sulfur compounds from coal did not increase their use. This result could be due to the high concentration of sulfate from the previous step (before hour 36), resulting in repression of the desulfurization activity. The byproduct of desulfurization, including sulfate in a particular concentration, has an inhibitory effect on the activity of desulfurization enzymes and repression on the expression of *dsz* genes, although not on microbial growth (Martín-Cabello et al., 2020; Sousa et al., 2020).

At hour 336, bacterial growth still occurred; the concentrations of dibenzothiophene and sulfate showed the highest values compared to previous times. The detected bacteria were *M. osloensis* COK1, *E. aerosaccus* COK5, and COK6, so it is assumed that these bacteria are the most adapted in the coal environment than other bacteria in this coal consortium. In another study, the activity of a bacterial consortium on coal continued for up to 18 days

(432 h), which significantly reduced almost 70% of the sulfur (Makgato and Chirwa, 2020).

In the 15% coal medium, the presence of bacteria was not detected at the beginning of growth; it could be due to an adaptation to a higher coal concentration (Figure 3). Then the cell concentration increased from hour 3 to 6, and the growth was kept relatively constant until hour 168. Meanwhile, the pH tended to decrease steadily until the end of incubation. Fluctuations occurred in the concentrations of dibenzothiophene and sulfate with a tendency: the DBT concentration decreased, the sulfate concentration increased, and vice versa. The consortium remained dominated by *M. osloensis* COK1, then *E. aerosaccus* COK5 (Figure 4). *M. osloensis* COK1 just appeared at hour 6, followed by the emergence of other bacteria. The appearance of other bacteria after *M. osloensis* COK1 indicated the interdependence of the consortium members. When the consortium reached the highest diversity (hours 36-48), the dibenzothiophene concentration increased, and the sulfate concentration decreased. It indicated that there was cooperation between bacteria in releasing sulfur compounds from coal and using them. The consortium members generally appeared to maintain the desulfurization function in the 15% coal medium, a relatively constant cell concentration since hour 6, with organic sulfur available and used. Although at hour 360, the release of dibenzothiophene from coal and sulfate uptake still occurred (Figure 3), the cultured bacteria COK1-COK6 were no longer detected (Figure 4), possibly due to the activity of unculturable microorganisms, and this requires further study.

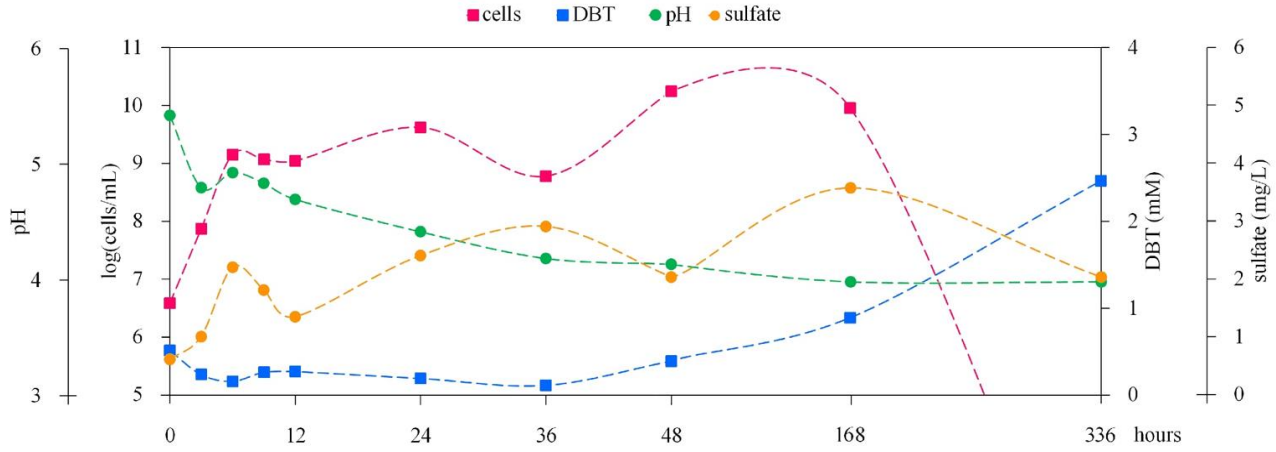

Figure 3. The activity of coal-origin bacteria consortium in 15% coal medium

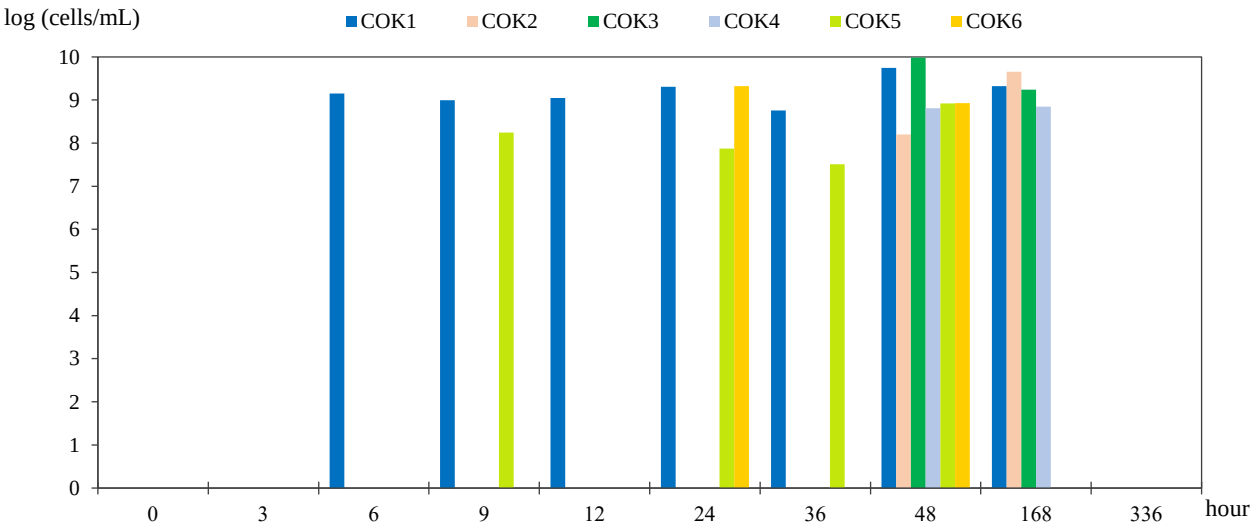

Figure 4. The concentrations of individual consortium members in 15% coal medium

In the 10% and 15% coal medium, *M. endophyticus* COK2 and *P. aeruginosa* COK3 always appeared concurrently and occurred after the appearance of *M. osloensis* COK1, *E. aerosaccus* COK5, and COK6. They were thought to be closely associated with each other and depended on the metabolic products of *M. osloensis* COK1, *E. aerosaccus* COK5, and COK6. *Pseudomonas* has been confirmed in degrading coal and dibenzothiophene (Li et al., 2019; Taiwo et al., 2020). Thus, *Pseudomonas aeruginosa* COK3 was assumed of using organic acids released from coal by the activities of the other members. In addition, *P. aeruginosa* COK3 was thought to facilitate the growth of *M. endophyticus* COK2. The rhamnolipid biosurfactant produced by *Pseudomonas* bacteria (Li et al., 2019) can facilitate the growth of other bacteria using hydrocarbon compounds in a consortium. The members that produce surfactants among coal-using bacteria can effectively lower the water surface pressure, indirectly assisting the absorption of nutrients into other cells. In an environment with complex hydrocarbons such as coal, microorganisms live in groups and complement each other through substrate exchanges to produce degradation products (Su et al., 2018).

Similar to the 15% coal medium, the growth in the 20% coal medium did not start immediately (Figure 5). The consortium members were adapting to a higher coal environment, and then the cell concentrations were relatively constant until the end of incubation. Dibenzothiophene and sulfate concentrations also fluctuated, showing a dynamic between the released and the used, as it did in the 10% and 15% coal medium (Figure 6). *M. endophyticus* COK2 and *P. aeruginosa* COK3, which appeared concurrently in the 10% and 15% coal medium, were not detected at the sampling points applied in the coal medium 20%. Presumably, these bacteria would appear slower, like the delay in their appearance in the 15% coal medium compared to the 10% coal medium. Higher coal concentrations mean a larger share of coal that microorganisms have to elaborate. They are limited in the face of challenges in the coal's porosity, cracks, and surface areas to further oxidation of sulfur forms, and intermediate products of the sulfur pathway can inhibit their growth (Makgato and Chirwa, 2020).

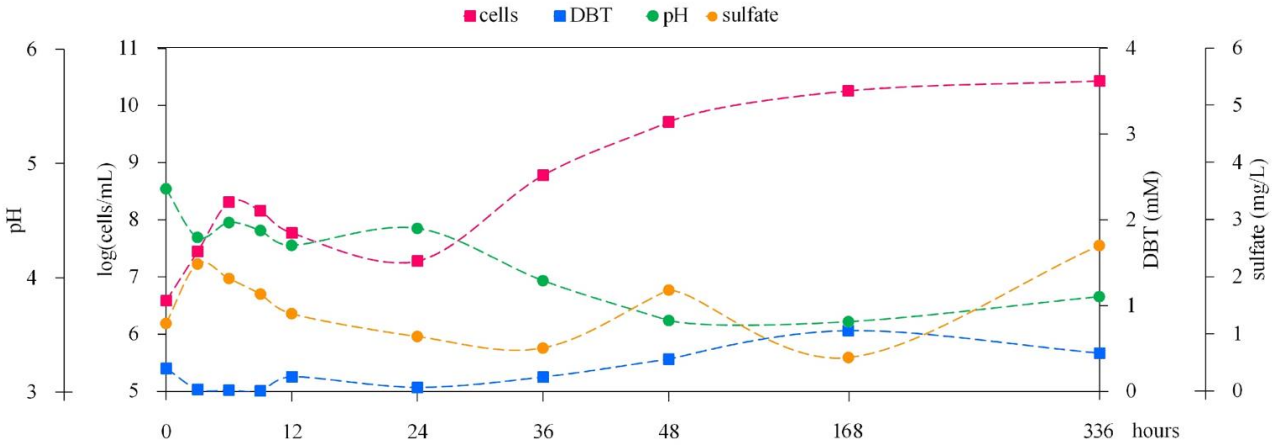

Figure 5. The activity of coal-origin bacteria consortium in 20% coal medium

In the three coal media (10%, 15%, and 20%), *M. osloensis* COK1 was the dominant bacteria in the coal consortium. Although the starter inoculum was made from a medium containing dibenzothiophene only, the bacteria increased their growth in the coal medium, which contained various organic sulfur. Likewise, *E. aerosaccus* COK5 has a role in providing sulfur in coal. These results add information about the bacterial species able to grow in coal as well as the desulfurization of organic compounds. Those bacteria that consume various organic sulfurs such as benzo- and dibenzothiophenes for their growth and metabolism are called sulfur-dependent bacteria, such as *Rhodococcus erythropolis, Lysinibacillus sphaericus*, and *Sphingomonas subarctica*, and were used to conduct biodesulfurization (Sousa et al., 2020).

The sequential appearance of consortium members in the coal media indicated a syntrophism interaction. For example, the growth of *P. psychrotolerans* COK4 depended on COK6, while the appearance of COK6 depended on *E. aerosaccus* COK5. Naturally, the bioconversion of complex materials often involves syntrophic interactions

among many microorganisms. The growth also occurred in bacterial communities during coal bioconversion in a coalfield, where the growth of *Methanosarcina* increased after consuming acetate produced by acetogenic *Propionibacterium* (Wang et al., 2019). This interaction caused partial degradation of the substrate while reducing the coal's complexity to be used by other bacteria that do not have the same ability.

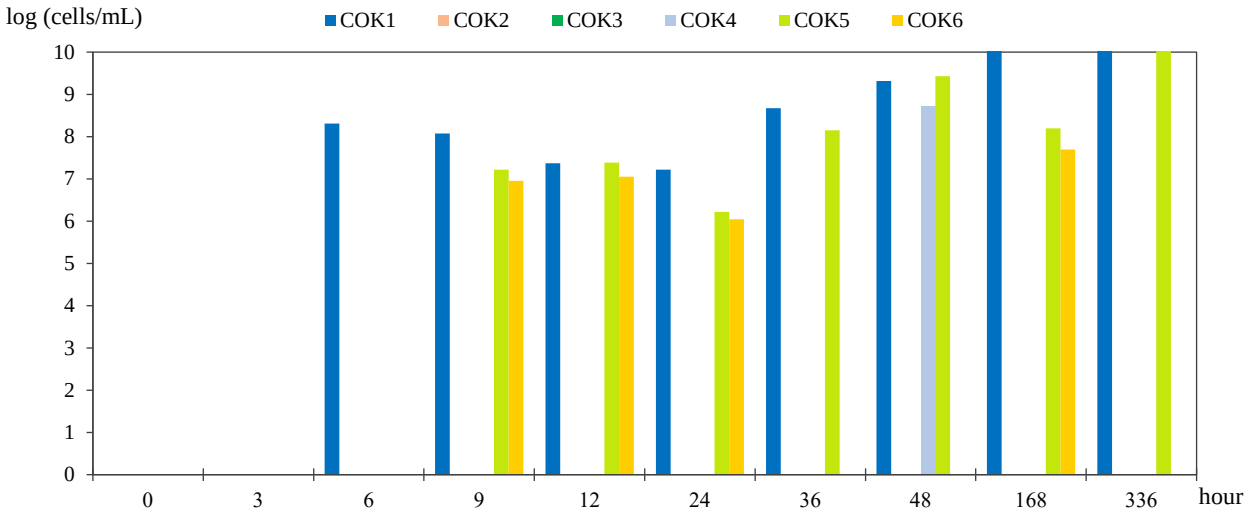

Figure 6. The concentrations of individual consortium members in 20% coal medium

By considering the occurrence and activity of consortium members, and their proximity to the published desulfurization bacteria, the potential role of each bacterium in the consortium can be predicted. The illustration in Figure 7 placed the bacteria members in the 4S pathway based on their activities and growth turnover in coal medium (Figures 1-6) and some references. The 4S is a well-known biodegradation pathway of dibenzothiophene (Jatoi et al., 2021; Li et al., 2019; Martín-Cabello et al., 2020; Mishra et al., 2016; Sousa et al., 2020). The most dominant role member in the coal consortium is *M. osloensis* COK1. Its activities at all stages and emergences in the three concentrations of coal medium made it thought to have a complete gene or enzyme system in processing organic sulfur in coal. In addition, it did not depend on the other members, especially in consuming the dibenzothiophene. Therefore, this bacterium plays in all steps in dibenzothiophene transformations until the release of sulfate in the 4S pathway.

Furthermore, according to several references, *P. aeruginosa* COK3 is an efficient user of hydrocarbon compounds related to its ability to produce biosurfactants (Ghosh and Mukherji, 2020; Li et al., 2019), but in this consortium, it seems to compete with *M. osloensis* COK1. Therefore, it is thought to play a secondary role in releasing dibenzothiophene from coal and some transformation steps, such as the further degradation of hydroxy biphenyl (HBP) *P. aeruginosa* is known to have an enzyme system to utilize biphenyl, a form of toxic persistent organic pollutants in the environment (Chakraborty and Das, 2016). Meanwhile, those that occasionally appear, such as *P. psychrotolerans* COK4, *E. enhydrobacter* COK5, and *M. endophyticus* COK2, required products of the primary members before playing the next steps of dibenzothiophene transformations; moreover, *M. endophyticus* COK2 played at a more downstream stage. Other consortium members who are challenging to detect in this experiment do not mean any role. The non-desulfurizing members make essential contributions to the desulfurization activity, including creating sulfur- deficient conditions by removing sulfur (sulphite/sulfate), thereby increasing the sulfur requirement for the desulfurized cells (Kilbane, 2016). In any case, the presumptions require further study of the role of each consortium member, including the participation of unculturable members.

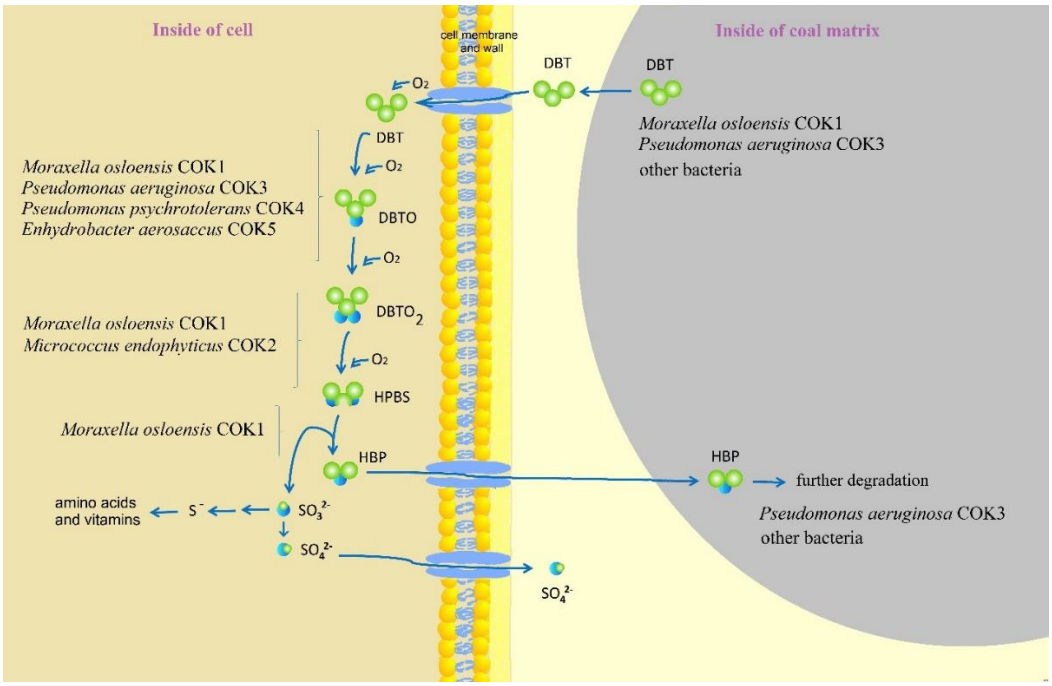

Figure 7. Hypothetical workflow regarding the potential role of consortium bacteria in the 4S pathway

4. CONCLUSION

This study revealed that bacteria work concurrently or sequentially in processing organic sulfur sources available in coal. They should be applied as a consortium culture because coal is a complex hydrocarbon interspersed by organic sulfur compounds that the degradation needs to be swarmed. Degradation and desulfurization of coal will be more extensive when a microbial consortium is applied because various bacteria cooperate to release the sulfur from the coal. The goal of producing clean coal is expected to be easily achieved by providing a diverse mixture of bacteria.

ACKNOWLEDGEMENTS

Authors are highly thankful to Pusat Laboratorium Terpadu Universitas Islam Negeri Syarif Hidayatullah Jakarta and School of Life Sciences and Technology Institut Teknologi Bandung for the research facilities, and Pusat Penelitian dan Penerbitan Universitas Islam Negeri Syarif Hidayatullah Jakarta for financial assistance. We also thank Ms. Valerie Calehr for proofreading this article.

REFERENCES

Altschul SF, Gish W, Miller W, Myers EW, Lipman DJ. Basic local alignment search tool. Journal of Molecular Biology 1990;215:403-10.

Burke V, Wiley AJ. Bacteria in coal. Journal of Bacteriology 1937;34:475-81.

Chakraborty J, Das S. Characterization of the metabolic pathway and catabolic gene expression in biphenyl degrading marine bacterium *Pseudomonas aeruginosa* JP-11. Chemosphere 2016;144:1706-14.

Chen S, Zhao C, Liu Q, Zhang X, Sun S, Zang M. Biodesulfurization of diesel oil in oil - water two phase reaction system by *Gordonia* sp SC-10. Biotechnology Letters 2019;41:547-54.

Colmer AR, Temple KL, Hinkle ME. An iron-oxidizing bacterium from the acid drainage of some bituminous coal mines. Journal of Bacteriology 1949;59:317-28.

Constanti M, Giralt J, Bordons A. Desulphurization of dibenzothiophe by bacteria. World Journal of Microbiology and Biotechnology 1994;10:510-16.

Etemadifar Z, Emtiazi G, Christofi N. Enhanced desulfurization activity in protoplast transformed *Rhodococcus erythropolis*. American-Eurasian Journal of Agriculture and Environmental Science 2008;3:795-801.

Ghosh P, Mukherji S. Degradation of carbazole, fluorene, dibenzothiophene and their mixture by *P. aeruginosa* RS1 in petroleum refinery wastewater. Journal of Water Process Engineering 2020;37:Article No. 101454.

Gunam IBW, Yaku Y, Hirano M, Yamamura K, Tomita F, Sone T, et al. Biodesulfurization of alkylated forms of dibenzothiophene and benzothiophene by *Sphingomonas subarctica* T7b. Journal of Bioscience and Bioengineering 2006;101:322-7.

Hamer U, Marschner B, Brodowski S, Amelung W. Interactive priming of black carbon and glucose mineralisation. Organic Geochemistry 2004;35:823-30.

Hirschler A, Carpito C, Maurer L, Zumsteg J, Villettte C, Heintz D, et al. Biodesulfurization induces reprogramming of sulfur metabolism in *Rhodococcus qingshengii* IGTS8: Proteomics and untargeted metabolomics. Microbiolgy Spectrum 2021; 9:e00692-21.

Jatoi AS, Aziz S, Soomro SA. Effect of native microorganism *Rhodococcus* spp SL-9 for dibenzothiophene degradation and its application towards clean coal approach. Cleaner Engineering and Technology 2021;3:Article No. 100126.

Kilbane JJ. Biodesulfurization: How to make it work ? Arabian Journal for Science and Engineering 2016;42:1-9.

Kotelnikov VI, Saryglar CA, Chysyma RB. Microorganisms in coal desulfurization (Review). Applied Biochemistry and Microbiology 2020;56:521-5.

Li L, Shen X, Zhao C, Liu Q, Liu X, Wu Y. Biodegradation of dibenzothiophene by efficient *Pseudomonas* sp. LKY-5 with the production of a biosurfactant. Ecotoxicology and Environmental Safety 2019;176:50-7.

Li M, Wang T, Simoneit BRT, Shi S, Zhang L, Yang F. Qualitative and quantitative analysis of dibenzothiophene, its methylated homologues, and benzonaphthothiophenes in crude oils, coal, and sediment extracts. Journal of Chromatography A 2012; 1233:126-36.

Makgato SS, Chirwa EMN. Recent developments in reduction of sulphur emissions from selected Waterberg coal samples used in South African power plants. Journal of Cleaner Production 2020;276:Article No. 123192.

Martín-Cabello G, Terrón-González L, Ferrer M, Santero E. Identification of a complete dibenzothiophene bio-desulfurization operon and its regulator by functional metagenomics. Environmental Microbiology 2020;22:91-106.

McLeish AG, Vick SHW, Grigore M, Pinetown KL, Midgley DJ, Paulsen IT. Adherent microbes in coal seam environments prefer mineral-rich and crack-associated microhabitats. International Journal of Coal Geology 2021;234:Article No. 103652.

Mishra S, Pradhan N, Panda S, Akcil A. Biodegradation of dibenzothiophene and its application in the production of clean coal. Fuel Processing Technology 2016;152:325-42.

Mohebali G, Ball AS. Biodesulfurization of diesel fuels - Past, present and future perspectives. International Biodeterioration and Biodegradation 2016;110:163-80.

Nassar HN, Amr SSA, El-gendy NS. Biodesulfurization of refractory sulfur compounds in petro-diesel by a novel hydrocarbon tolerable strain *Paenibacillus glucanolyticus* HN. Environmental Science and Pollution Research 2021;28:8102-16.

Sousa JPM, Ferreira P, Neves RPP, Ramos MJ, Fernandes PA. The bacterial 4S pathway - an economical alternative for crude oil desulphurization that reduces CO_2 emissions. Green Chemistry 2020;22:7604-21.

Strąpoć D, Picardal FW, Turich C, Schaperdoth I, Macalady JL, Lipp JS, et al. Methane-producing microbial community in a coal bed of the Illinois Basin. Applied and Environmental Microbiology 2008;74:2424-32.

Su X, Zhao W, Xia D. The diversity of hydrogen - producing bacteria and methanogens within an in situ coal seam. Biotechnology for Biofuels 2018;11:1-18.

Taiwo J, Oghenekume O, Edeki G, Keith A. Bacterial degradation of coal discard and geologically weathered coal. International Journal of Coal Science and Technology 2020;7:405-16.

Tamura K, Stecher G, Peterson D, Filipski A, Kumar S. MEGA6: Molecular evolutionary genetics analysis version 6.0. Molecular Biology and Evolution 2013;30:2725-9.

Vick SHW, Gong S, Sestak S, Vergara TJ, Pinetown KL, Li Z, et al. Who eats what? Unravelling microbial conversion of coal to methane. FEMS Microbiology Ecology 2019;95(7):Article Code. fiz093.

Wang B, Yu Z, Zhang Y, Zhang H. Microbial communities from the Huaibei Coalfield alter the physicochemical properties of coal in methanogenic bioconversion. International Journal of Coal Geology 2019;202:85-94.

Wasi S, Tabrez S, Ahmad M. Use of *Pseudomonas* spp. for the bioremediation of environmental pollutants: A review. Environmental Monitoring and Assessment 2013;185: 8147-55.

Yossifova MG, Valčeva SP, Nikolova SF. Exogenic microbial activity in coals. Fuel Processing Technology 2011;92:825-35.

Emissions of CH_4 and CO_2 from Wastewater of Palm Oil Mills: A Real Contribution to Increase the Greenhouse Gas and Its Potential as Renewable Energy Sources

Ledis Heru Saryono Putro

Department of Biology, Faculty of Science and Technology, Universitas Islam Negeri Raden Fatah Palembang, Palembang 30252, Indonesia

ARTICLE INFO

Received: 5 Aug 2021
Received in revised: 30 Sep 2021
Accepted: 3 Oct 2021
Published online: 28 Oct 2021
DOI:10.32526/ennrj/20/202100149

Keywords:
GHG emissions/ CH_4/ CO_2/ Renewable energy/ POME/ Conversion coefficients

*** Corresponding author:**
E-mail: lherusp@radenfatah.ac.id

ABSTRACT

Palm oil mill effluent (POME) treatment in Indonesia is still predominant using an open pond system. This system has the weakness of the unknown and uncontrollable value of greenhouse gas (GHG) emissions into the atmosphere. This study estimated GHG emissions (CH_4 and CO_2) from anaerobic ponds and their potential as a renewable energy source and obtain GHG emission conversion coefficients for each kg of COD POME and ton of crude palm oil (CPO). Gas samples were collected using a closed static chamber. GHG sample concentration testing was done using Gas Chromatography with a flame ionization detector (FID) and thermal conductivity detector (TCD). The results showed that the emission rate of CH_4 and CO_2 in the anaerobic pond POME treatment was relatively high, 261.93 and 595.99 g/m^2/day, respectively, equivalent to 48.572 t CO_2-eq/day or 14,571.5 t CO_2-eq/year. CO_2 emissions were greater than two times CH_4 emissions, both spatially and temporally. There was a process of facultative biodegradation, aerobic and or anaerobic process according to the biotic-abiotic environment and the levels of organic components in the substrate. In anaerobic ponds, the optimal requirements for the biodegradation process tended to be unfulfilled, so the emission rate of CH_4 was less than CO_2. The GHG conversion coefficient was obtained, namely each kg of COD from POME emitted 6.266 kg CO_2-eq of GHG; for each m^3 of POME emitted by 0.163 t CO_2-eq of GHG; and 0.556 t CO_2-eq/t CPO. The maximum potential for POME to energy conversion was 1.045 MWe with a power capacity of 8,603 MWh/year.

1. INTRODUCTION

Palm oil-based agroindustry is an essential pillar of community development in Indonesia because it is the largest provider of employment and foreign exchange-earners from the non-oil and gas sector. In 2016, Indonesia produced 33.23 million tons of crude palm oil (CPO) (57% of world production), with 25.1 million tons for exports which generated a foreign exchange of USD 17.8 billion, with a workforce of 5.9 million people (11%) (Ministry of Agriculture, 2016; IPOA, 2017). As a result of high CPO production, a large amount of waste will be generated, including solid waste, liquid waste, and gas. Solid waste such as empty fruit bunches (EFB), fiber, and shells have been used for manufacturing processes and organic fertilizers in plantations. However, palm oils mill effluent (POME) is relatively untapped. Still, in its processing, it produces methane gas (CH_4) as a greenhouse gas (GHG) which causes global warming and climate change (Rahayu et al., 2015; El-Fadel and Massoud, 2001; Wu et al., 2010).

Every processing of one ton of fresh fruit bunches (FFB) produced 0.5-0.7 tons of POME (palm oil mill effluent) (Hassan et al., 2004); 0.75-0.90 m^3 POME (Morad et al., 2008) or every one ton of CPO produced 2.5-3.0 tons of POME (Wu et al., 2010). Furthermore, each ton of FFB produces 20 m^3 of biogas (Alkusma et al., 2016), or every one ton of POME was equivalent to 28 m^3 of biogas (Yacob et al., 2006; Lam and Lee, 2011). The results of research

Citation: Putro LHS. Emissions of CH_4 and CO_2 from wastewater of palm oil mills: A real contribution to increase the greenhouse gas and its potential as renewable energy sources. Environ. Nat. Resour. J. 2022;20(1):61-72. (https://doi.org/10.32526/ennrj/20/202100149)

by Yacob et al. (2006), in Malaysia, found that one ton of POME would produce 12.36 kg of methane, similar to the report of 13.1 kg of methane by Pehnelt and Vietze (2013). In addition, one kg of chemical oxygen demand (COD) from POME, is equivalent to 0.238 kg of methane emissions. Other studies have found 6.54 kg of methane, equivalent to 137 kg of CO_2-eq (Schuchardt et al., 2008), and 6.67 kg of methane, equivalent to 163 kg of CO_2-eq (Suprihatin et al., 2012), emitted for each ton of fresh fruit bunches (FFB) processed.

The degradation of organic matter in POME in Indonesia is predominantly carried out conventionally with a ponding system and is still minimal in maintenance. This wastewater treatment system emits biogas as greenhouse gas (GHG), with the main composition of CH_4 and CO_2, into the atmosphere in unknown and uncontrolled quantities (Wu et al., 2010). Greenhouse gas (CH_4 and CO_2) accounts for more than 90% of all emissions from POME in palm oil mills (Rahayu et al., 2015; Hosseini and Wahid, 2015). The amount of biogas-methane emissions from wastewater treatment in palm oil mills is influenced by oil palm harvest season, the operational method of the palm oil mills (Yacob et al., 2006), POME organic matter content, type of wastewater treatment pond, work system for degradation of organic matter, the type and efficiency of the bioreactor (Ohimain and Izah, 2017), as well as the presence or absence of methane capture (Moriarty et al., 2014). Biogas-methane emissions would be proportional to the levels of organic matter in POME. Nutrient levels in organic matters are part of the nutrient cycle that occurs continuously in nature. Wastewater treatment through aerobic, facultative, and anaerobic processes would involve microorganisms and respiration-oxidation-reduction processes that produced CO_2 and or CH_4. Different compositions differed depending on the type and biodegradation process that occurs. Therefore, Indonesia, as the world's largest producer of CPO, reaching 40.5 million tons in 2018 (Ministry of Agriculture, 2018), with POME production of around 121.5 million cubic meters, will be a significant source of GHG emission contributors.

Globally, GHG from anthropogenic and natural sources includes CO_2 74%, CH_4 16%, N_2O 10%, and HFC, PFC, SF6, and CFC 1% (Tanaka, 2009). The dominant GHG emissions from POME processing are CH_4 and CO_2. In a study on GHG emissions, the value of GHG emissions was equated to CO_2 emissions based on their respective global warming potential (GWP) values. Apart from being a pollutant and GHG emitted into the atmosphere, biogas-methane is also a very potent renewable energy source. A palm oil mills (POM) with a capacity of 45 tons of FFB/hour could generate an electrical energy capacity of 1.25 MW (equivalent to 9,137 MWh/year) (Moriarty et al., 2014). However, few POM convert POME into energy (5%) (Lam et al., 2019; Taniwiryono et al., 2016).

In developing a strategy for reducing GHG emissions in palm oil mills, information on optimal performance and developing biogas-methane capture in POME processing is needed. For this reason, information on GHG emissions from anaerobic ponds in wastewater treatment plants (WWTP) is required. Especially in WWTP with multiple feeding systems based on direct measurements in the field, which has never been reported. Therefore, this research was conducted to estimate GHG emissions (CH_4 and CO_2) from anaerobic ponds based on direct measurements in the field and calculate their potential as a renewable energy source.

2. METHODOLOGY

2.1 Sriwijaya palm oil Indonesia mill

The palm oil mill of this study has a processing capacity of 30 tons of FFB/hour, located in Talang Kelapa District, Banyuasin Regency, South Sumatra Province (-2.826S, 104.732E). This factory belongs to the PT SPOI group of companies, processing FFB from the company itself and the plantations of the surrounding community. The writer conducted his research at the WWTP of the mill in an anaerobic pond (AP). The WWTP facility consists of seven ponds, namely three deoiling ponds, one cooling pond, and three anaerobic ponds (AP). The study was in anaerobic ponds I and II (AP2-AP1, which are functionally connected) with a depth of 6 meters and a total volume of 40,519 m^3. Wastewater flow path in AP2-AP1 combined pond: enters inlet AP2 to AP1 back to AP2 and finally at outlet AP2. Furthermore, the AP2 outlet to the AP3 inlet continues to the AP3 outlet (end of the WWTP) for land application.

2.2 Gas sampling and GHG concentration tests

The capture of biogas used closed static chambers, which were made of polypropylene (PP) material, was in the form of a cylinder with a size of 0.30 × 0.28 × 0.415 m (top diameter × bottom diameter × height), chamber's volume 0.02742 m^3 and a cross-sectional area of 0.07 m^2 (Figure 1). The containment volume became 25.44 liters when the application was

above the anaerobic pond, with 3 cm submerged under the surface of the pond (effective height of the containment 0.385 m). The chamber was positioned at three locations, one each in the inlet, middle, and outlet of the anaerobic ponds (combined AP2-AP1) (Figure 2). The distance between chamber S1 to chamber S2 and chamber S1 to chamber S3 was 118 meters. The chamber placement was carried out proportionally and took into account the performance of the anaerobic pond.

(a) (b) (c)

Figure 1. Closed static chamber for capturing biogas (CH_4 and CO_2) on site, (a) inlet, (b) midle, and (c) outlet

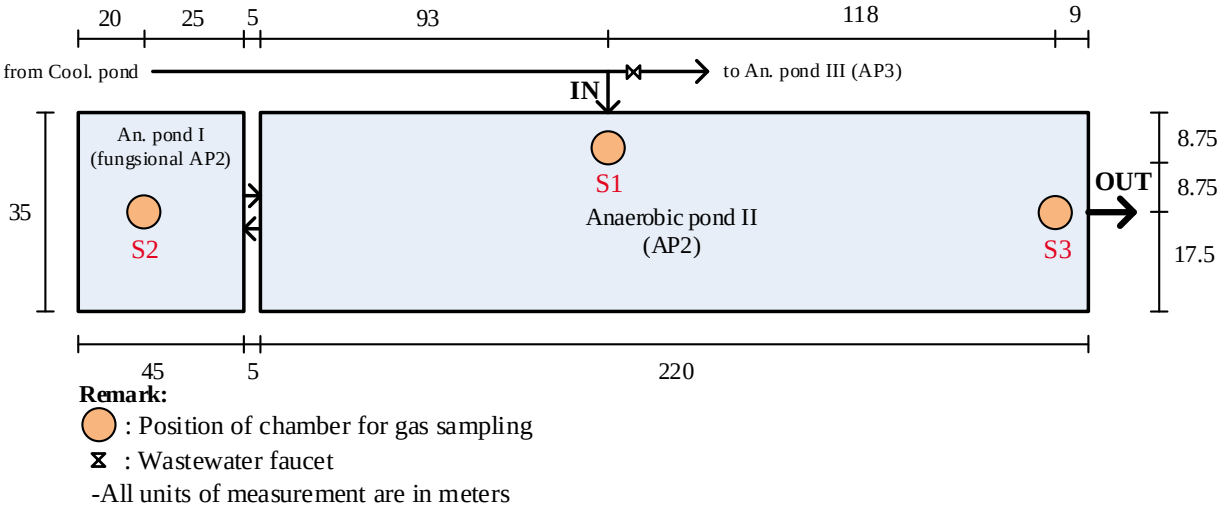

Figure 2. Placement of closed static chamber in an anaerobic pond

The chamber had a septum (rubber) and an air thermometer installed. For the homogeneity of the gas mixture in the chamber, it was equipped with a DC 6 Volt (1,500 rpm) electric fan with a size of 6×6 cm that was turned on when the sampling period was done. The septum was used to allow the insertion of syringes to take gas samples. The glass thermometer was used to measure the temperature of the chamber room air and was mounted tightly on the top of the chamber.

Biogas sampling with a syringe equipped with a faucet and a lever to pull it from the lid and push it into the 10 mL sample container (vial) bottle. Before using the vial, the tube had been made airtight (vacuum). Biogas sampling time intervals were 0, 10, 20, and 30 minutes (n=4). In the morning period (08.00), afternoon (12.00), and evening (18.00), as well as at three sampling locations in AP2-AP1 (inlet, middle, and pond outlet), 36 samples were obtained per day, carried out in three days (n=3) May 12 and 17, and June 23, 2019.

At each observation period, vials containing biogas samples were collected and stored in refrigerated containers and immediately sent to the laboratory for CH_4 and CO_2 gas concentration testing. Biogas samples were analyzed by using a Gas Chromatography (GC-Shimadzu 14A) equipped with a flame ionization detector (FID) for methane and thermal conductivity detector (TCD) for CO_2 gas

analysis (Setyanto et al., 2014). The gas sample test was carried out in the Agricultural Environment Research Institute, Pati Regency, Central Java.

2.3 Monitoring the characteristics of POME and anaerobic pond wastewater

Wastewater sampling was carried out at three points: WWTP inlet (deoiling pond), around the AP2 inlet, and outlet. Each was carried out in palm oil mills operations in the morning (09.00) and evening (16.00). The results of the wastewater test are averaged so that each sampling point obtained one data per day. The test variables for wastewater characteristics are volatile solid (VS), COD, pH, ORP, POME temperature, and AP2 wastewater temperature. VS was with the Standard Methods for the Examination of Water and Wastewater (APHA, 1998) and COD variable with the colorimetric method using COD-Vario Photometer-System, Lovibond. Variable pH, ORP, temperature with a potentiometric method using Adwa AD-111 portable pH meter. AP2 wastewater temperature at a depth of 15 cm below the pond water's surface, with hourly measurements for 24 h/day using the HOBO-MX2203 temperature logger.

2.4 Data analysis

Methane and carbon dioxide emissions as the dominant compounds from greenhouse gases in POME processing are calculated according to the formula from IAEA (1992), Lantin et al. (1995), and Setyanto et al. (2014):

$$E = \frac{dc}{dt} \times \frac{Vch}{Ach} \times \frac{Wm}{Vm} \times \frac{273.2}{273.2+T} \quad (1)$$

Where; E is CH_4 or CO_2 emissions/flux ($mg/m^2/min$); dc/dt difference in CH_4 or CO_2 concentration per unit time (ppm/min) (as linear slope regression of time and CH_4 or CO_2 concentration, with $R^2 \geq 85\%$) (Paredes et al., 2015); Vch is containment volume (m^3); Ach is an area of containment (m^2); Wm is CH_4 or CO_2 molecular weight, $16.04.10^3$ and $44.01.10^3$ mg, respectively; Vm is molecular volume CH_4 or CO_2 ($22.41.10^{-3}$ m^3); and T is average chamber air temperature during sampling (°C). CH_4 and CO_2 calculations are corrected with standard temperature and pressure (0°C and 1 atm).

The calculated value using equation (1) was used to obtain the value of methane emissions ($mg/m^2/hour$) according to the sampling period morning-afternoon-evening. To obtain all daytime data, periods of 8:00 to 18:00 and hourly intervals were carried out by interpolation (Chen et al., 2011; Khokhar dan Park, 2017). The "pchip" (cubic hermite) interpolation method was used. Calculation and data processing of the following interpolation process was with the Matlab R2017b program.

The total methane and carbon dioxide emission rates per sampling location per day were calculated by integrating the emission value per hour using the Simpson numerical method (Arif et al., 2015; Putro et al., 2019), as follows:

$$\int_a^b f(x)\,dx = \frac{b-a}{6}\left[f(a) + 4f\left(\frac{a+b}{2}\right) + f(b)\right] \quad (2)$$

Where; f(x) is the total emissions of CH_4 or CO_2 ($mg/m^2/day$); a is the initial hour of measurement of emissions and b is the final hour of measurement of emissions.

The potential energy generation capacity from POME conversion through anaerobic degradation was calculated using the following formula (IPCC, 2006; Rahayu et al., 2015):

$$\text{Power generation capacity} = CH_4 \text{ production} \times 35.7 \times 0.4 \times [1/(3.6 \times 24 \times 1000)] \quad (3)$$

$$\text{Power capacity} = \text{Power generation capacity} \times 8{,}760 \times 0.94 \quad (4)$$

$$CH_4 \text{ production} = \text{COD-loading} \times 0.2102 \quad (5)$$

$$\text{COD-loading} = \text{COD-removed} \times \text{POME production} \times 10^{-3} \quad (6)$$

Where; power generation capacity in MWe; CH_4 production in Nm^3/day; net calorific value (NCV) CH_4 35.7 MJ/Nm^3; engine efficiency 0.4 (Rahayu et al., 2015); conversion coefficient 1 kWh/3.6 MJ; power capacity in MWh/year; conversion coefficient hour/year 8,760; availability factor 0.94; COD-loading in kg/day; COD-removed in mg/L; POME production in m^3/day; CH_4 production in Nm^3/day; conversion coefficient Nm^3/kg COD-removed 0.2102 (Putro, 2021).

3. RESULTS AND DISCUSSION

3.1 Organic matter content and biodegradation of POME in the ponding system

Raw POME had an average COD level in the WWTP inlet, anaerobic pond II (AP2) inlet, and outlet, of 56,277, 32,608, and 6,541 mg/L, respectively (Table 1). It appeared that there had been a decrease in COD values since the WWTP inlet to the AP2 inlet and the inlet to the AP2 outlet; the mean values were

23,669 (42.06%), 26,067 mg/L (46.32%), respectively. The average COD removal in anaerobic ponds (AP2-AP1) was 26,067 mg/L (80.05%); this indicated the activity of the POME organic matter degradation by microorganisms and biogas (dominant composition CH_4 and CO_2) is produced in the WWTP system, especially in anaerobic ponds (Seadi et al., 2008; Lam and Lee, 2011; Choong et al., 2017).

The decrease in COD also occurred between the WWTP inlet (deoiling pond) to the AP2 inlet (23,669 mg/L). The value is almost the same as the COD removal from the AP2 inlet to an outlet (26,067 mg/L). The decrease in COD was due to the deoiling of the four initial WWTP ponds (deoiling ponds three and cooling pond one) to be returned to the fat-pit tank. In addition to oil-fat quoting, it is suspected that there has been aerobic degradation of POME in the four ponds. As a result of the above, there is a significant decrease in COD before POME reaches the AP2 inlet. At the beginning of the WWTP, this high organic matter degradation process is undoubtedly not expected if POME is processed to convert it into energy through an anaerobic bioreactor. The conversion of COD values is expected to occur in anaerobic bioreactors so that maximum biogas-methane is produced for its utilization as an energy source.

The mean value of VS inlet WWTP was 56,853±12,124 mg/L. The COD and VS value of fresh POME (influent) at the WWT inlet location was very high; this proved that the wastewater from processing oil palm fresh fruit bunches contained high organic matter levels. The high levels of organic components could also be indicated by other variables, namely: oil-fat, TS, and VS (Mahajoeno, 2008; Lam and Lee, 2011; Putro et al., 2019). The COD and VS variables in the previous anaerobic biodegradation study had a high enough correlation with the organic components of the substrate (solid and liquid waste), including POME, so that a conversion coefficient (factor) could be determined. The rapid detection of biogas-methane emissions from a substrate or waste was generally calculated using one or two of these variables in a conversion factor (Park and Craggs, 2007; Putro et al., 2019; Putro et al., 2020).

Table 1. AP2 inlet and outlet wastewater quality and organic loading (n=3)

Variable	Mean	Std. dev.	Interval
COD (raw effluent) (mg/L)	56,277	2,914	53,830-59,500
COD (inlet AP2) (mg/L)	32,608	1,882	30,900-34,625
COD (outlet AP2) (mg/L)	6,541	1,482	4,864-7,670
COD-removed (mg/L)[a]	26,067	873	25,210-26,955
COD-removed (%)[a]	80.05	3.65	77.85-84.26
POME inlet AP2 (m^3/day)	297.6	13.6	288.3-313.2
Organic loading rate (kg COD/m^3/day)	0.239	0.015	0.222-0.250
Organic loading (kg COD/day)	7,749.4	157.8	7581.9-7895.2

[a]POME degradation from the AP2-AP1 inlet to the AP2 outlet

An anaerobic process occurs at the bottom-middle of the pond, characterized by low redox potential (ORP) (negative; reduction) and DO close to zero to form biomethane. While in the middle-top (surface) of the pond, the aerobic process occurs with moderate ORP (zero to positive; oxidation) and a higher DO value (influenced by the interaction between POME and ambient air above the pond surface), resulting in a CO_2 emission rate>CH_4 (Putro et al., 2019; Nguyen et al., 2019; Deublein and Steinhauser, 2008; Yacob et al., 2006). Methane formation in anaerobic systems would go through a series of process steps: hydrolysis, acidogenesis, acetogenesis, and methanogenesis, which involved microbes, each of which required the terms and conditions of the substrate (organic components) at specific optimum values (Drapcho et al., 2008; Seadi et al., 2008; Deublein and Steinhauser, 2008; Korres et al., 2013). The biogas-methane resulting from the biodegradation of POME was emitted into the ambient air, increasing the concentration of greenhouse gases in the atmosphere. This biogas-methane emission was influenced by wastewater, biotic and abiotic environmental factors (Drapcho et al., 2008; Seadi et al., 2008; Putro et al., 2019).

Apart from COD, another variable that could indicate a change in organic matter in POME was volatile solid (VS). This variable was a volatile particle that correlated with organic matter, which is converted to biogas-methane. Like the research Putro et al. (2019), methane emission was influenced by COD-R, VS-R, COD-R/N tot-R ratio, and ML-R/N

tot-R ratio, with R^2 0.585 (R 0.765). So it means that together, these variables have 58.5% of the ability to determine methane emissions (R^2 or coefficient of determination), and other variables determine 42.5%. In the open pond system, POME treatment (lagoon/ponding system) with minimal maintenance, generally accumulating sludge at the pond's bottom would shorten the HRT and the organic matter biodegradation was not optimal. HRT correlated with the organic loading rate (OLR), had an inverse relationship, the higher the OLR, the shorter the HRT (Seadi et al., 2008; Choong et al., 2017; Ohimain and Izah, 2017). AP2 OLR value was 0.239 kg COD/m^3/day, or the average organic loading rate is 7,749.4 kg COD/day (Table 1). This OLR value was relatively small, characteristic of POME treatment in open pond systems (Choong et al., 2017). In the pond systems, generally high HRT (>100 days), low OLR (<1 kg COD/m^3/day), more waste ponds, high sludge accumulation, and require more land (Wu et al., 2010; Yacob et al., 2006). OLR that is too low causes the fermentation process (acidogenesis) to run slowly. On the other hand, if the OLR is too high, there will be an overload, and the substrate can inhibit the growth of microorganisms (Speece, 1996). HRT is related to the bioreactor (pond) volume, but HRT is inversely related to OLR. Therefore, it is necessary to optimize between these three variables to achieve maximum POME biodegradation performance.

The process of degradation of the organic matter in POME was strongly influenced by the characteristics of the organic matter and the type of bioreactor (ponding system) used. Open ponding systems had the lowest degradation performance compared to other types of bioreactors, but because they were easy and cheaper to operate, they were still widely used (>85%) (Wu et al., 2010; Ahmed et al., 2015). The use of the open ponding system WWTP has its disadvantages. In this system, biogas-methane is emitted directly into the atmosphere as GHG and is not environmentally friendly. Efforts to capture GHG can be carried out in this pond by building an airtight cover, including using a high-rate anaerobic lagoon system (HRAL) (Wall et al., 2000). HRAL and similar techniques can reduce GHG emissions in CPO production in palm oil mills by >70% (Prasetya et al., 2013; Rahayu et al., 2015) and obtain the benefits of biogas-methane as a renewable energy source from POME conversion.

3.2 Greenhouse gases emissions from POME processing

There had been GHG emissions into the atmosphere in POME processing with an open pond system (open lagoon with multiple feeding systems), in the form of gas methane and carbon dioxide. The mean CH_4 and CO_2 emissions from the combined anaerobic ponds AP2-AP1 were 261.93 and 595.99 g/m^2/day (10.91 and 24.83 g/m^2/hour), respectively, or 1,604.3 and 3,650.4 kg/day in the total effective area of the anaerobic pond 6,125 m^2 (degradation of wastewater by microorganisms was effective 5 m from anaerobic pond side) (Table 2; Figure 3). Methane emission in this study was lower than that of Yacob et al. (2006), in Malaysia, but higher than research of Mahajoeno (2008), in South Sumatra, that reported 759.7 and 179.2 g/m^2/day, respectively. The difference in methane emissions is caused by: the quality of oil palm fresh fruit bunches (FFB), differences in harvest seasons, plant operational systems and methods, wastewater treatment techniques, methane gas testing methods and equipment, and abiotic environmental factors (pond wastewater temperature, rainfall, air temperature) (Seadi et al., 2008; Drapcho et al., 2008; Putro et al., 2019).

Table 2. Emissions and GHG conversion coefficient values on biodegradation of POME

Variable	Unit	Mean
CH_4 emission rate	g/m^2/day	261.932±11.026
CH_4 emission[a]	kg/day	1,604.3±67.5
CO_2 emission rate	g/m^2/day	595.988±126.915
CO_2 emission[a]	kg/day	3,650.4±777.4
CH_4 emission (day) (equivalent)[b]	t CO_2-eq/day	44.921±1.891
CO_2 emission (day) (direct)[b]	t CO_2/day	3.650±0.777
GHG emission from POME (day)	t CO_2-eq/day	48.572±2.296
GHG emission from POME (year)[c]	t CO_2-eq/year	14,571.5
CH_4 emission proportion (GHG from POME)	%	92.48

Table 2. Emissions and GHG conversion coefficient values on biodegradation of POME (cont.)

Variable	Unit	Mean
Conversion coefficient of GHG:		
GHG vs. COD-POME	kg CO_2-eq/kg COD	6.266±0.193
GHG vs. POME volume	t CO_2-eq/m^3 POME	0.163±0.002
GHG vs. POME weight[d]	t CO_2-eq/t POME	0.184
GHG vs. FFB weight[e]	t CO_2-eq/t FFB	0.122
GHG vs. CPO weight[f]	t CO_2-eq/t CPO	0.556

[a]AP2 (220×35 m^2) and AP1 (45×35 m^2), effective area AP2-AP1 6,125 m^2 (effective ebullition process 66% AP2-AP1; factual activity in the field and according to Yacob et al., 2006)
[b]GWP CO_2 and CH_4 1 and 28, respectively (https://www.ipcc.ch/report/ar5/wg3/; Fifth Assessment Report; AR5, 2014)
[c]Assuming an average of 300 effective working days per year
[d]Density of POME 1,13 kg/L (Lam and Lee, 2011)
[e]0.75 m^3 POME/t FFB (Yuliasari et al., 2001; Morad et al., 2008)
[f]An average yield CPO 22% (field data)

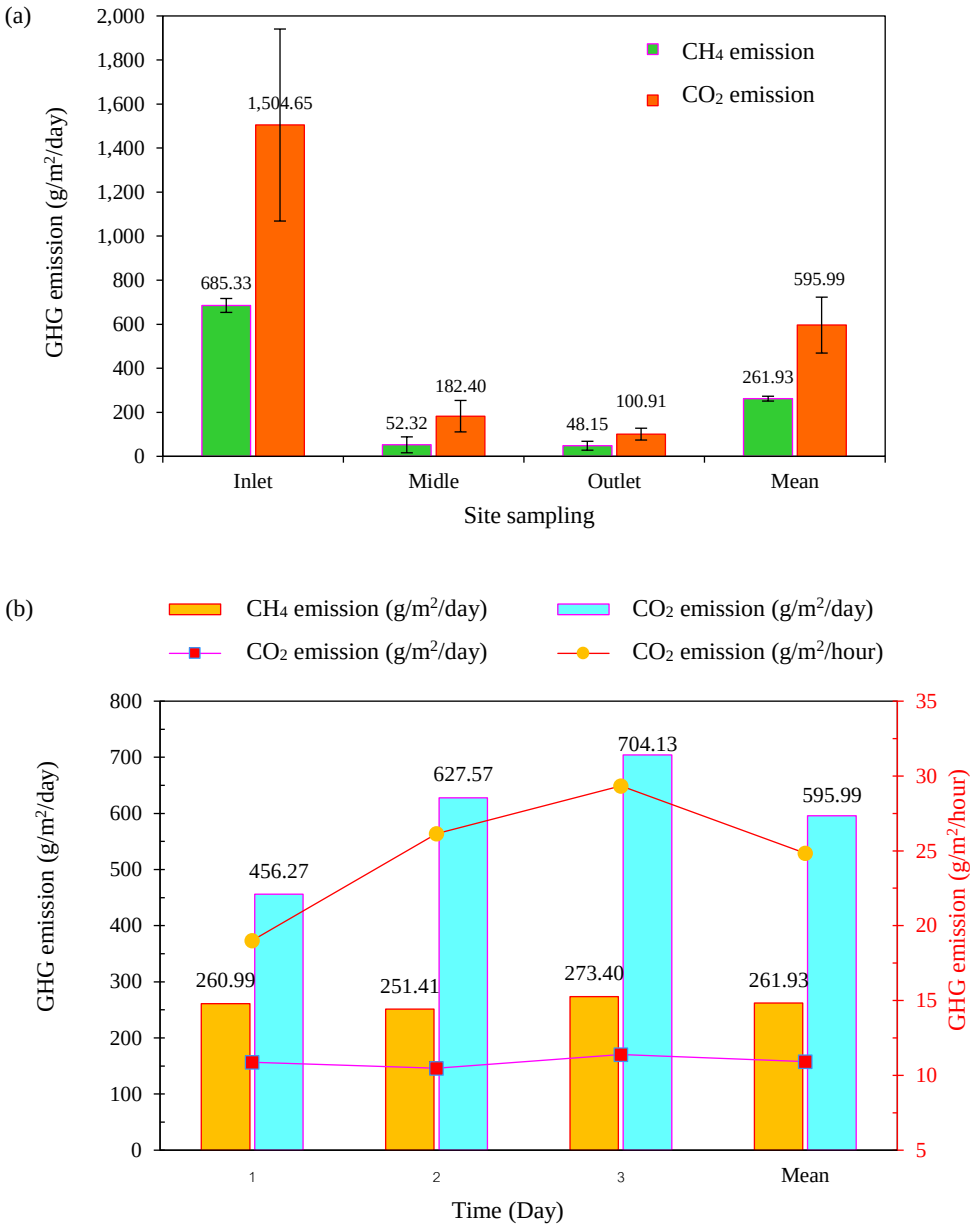

Figure 3. The dynamics of anaerobic pond GHG emissions based on, (a) sampling location and (b) sampling time

The highest CH_4 and CO_2 emissions occurred around the AP2 inlet, then around the middle AP2-AP1 location, and the lowest was around the AP2 outlet. The composition of CO_2 gas was more than two times the value of methane gas at each of these sampling locations (Figure 3(a)). It showed that the gradual and regular biodegradation of POME from inlet to outlet was proportionate to the gradual decrease in organic matter content from inlet to AP2-AP1 outlet. The dynamics of GHG emissions also occurred with an increasing trend from day 1 to day 3, which was caused by an increase in the amount of wastewater received by the anaerobic pond (288.3 to 313.2 m^3/day), although the level of COD degraded slightly decreased (26,955 to 25,210 mg/L). But the main thing is that CH_4 also follows the increase in CO_2 emission rates. This can be seen in various spatial (inlet-center-outlet locations) and temporal (days 1 to 3) conditions (Figure 3(a) and Figure 3(b)). This indicates that the biodegradation process occurs facultatively (aerobic and or anaerobic) under biotic-abiotic environments and substrate levels from various depths and locations in anaerobic ponds (AP2-AP1). In addition, the optimization requirements for anaerobic degradation processes tend not to be met, so that the emission rate of CH_4<CO_2 (Deublein and Steinhauser, 2008; Korres et al., 2013).

GHG emissions around the location of the highest AP2 inlet and influenced by the levels of COD variable. COD at the AP2 inlet was the highest compared to others (Table 1). The COD variable has a high correlation with GHG emissions, but this generally does not stand alone. The value of GHG emissions was also influenced by the role of other variables that have a moderate-high correlation with GHG emissions, such as volatile solids (VS), ORP, substrate temperature (waste pond water) (Putro et al., 2020; Putro, 2021). The decreasing value of GHG emissions from the inlet to outlet was in line with the reduction of the COD value. The decrease in GHG indicates that biodegradation of organic matter from POME has occurred in the anaerobic pond, resulting in the emission of biogas-methane into the atmosphere.

The optimum requirements for the hydrolysis and acidogenesis (fermentation) phases (temperature 25-35^{o}C and pH 4.0-6.3) and the methanogenesis phase have been met (mesophilic temperature 30-40^{o}C, pH 6.7-7.5, and Eh<-250 mV) at the AP2 inlet location (Table 3). These variables are the limiting variables for the rate of anaerobic biodegradation (Batstone, 2006; Putro, 2021). Several other conditions that explain this are: the optimum pH is achieved when the POME fed to the AP2 inlet mixes with the wastewater in the pond, the pH changes rapidly from 4.46 to 7.00 (optimum methanogenesis phase was achieved that is pH 6.7-7.5) (Putro, 2021; Deublein dan Steinhauser, 2008; Korres et al., 2013). Likewise, the optimum redox potential variable of the methanogenesis phase (Eh<-250 mV) was probably reached during the process from the bottom-center anaerobic pond. This was supported by the presence of gas bubbles during field observations, starting from the bottom-center of the pond zone without and or minimum oxygen (DO approaching 0 mg/L) towards the surface of the pond. Finally, biogas (CH_4 and CO_2) are released into the atmosphere (Nguyen, 2018). The phenomenon of active bubbles was very clearly visible around the inlet and was very active (high), especially in the morning to noon, compared to other locations (around the AP2 outlet and the middle of the AP1 pond), so this was an indicator that GHG emission rates occurred (CH_4 and CO_2) at that location (Mahajoeno, 2008; Yacob et al., 2006). The evidence above supports the arguments to that the location around the inlet had the highest GHG emissions compared to others.

Table 3. Value of pH, ORP, and temperature of anaerobic pond wastewater II (n=3)

Variable	Unit	Inlet		Outlet	
		Mean	Interval	Mean	Interval
pH	-	4.60±0.12	4.48-4.72	7.1±0.13	7.03-7.26
Eh	mV	147.2±6.5	141-154	(-18.2)±1.3	(-19.5)-(-17)
T_{POME}[a]	^{o}C	44.3±1.2	43.0-45.3	31.6±0.7	30.8-32.1
T_{WW}[b]	^{o}C	34.1±0.1	34.1-34.2	32.6±0.2	32.4-32.7

[a]Average POME temperature in the morning (09.00) and evening (16.00) sampling
[b]Average temperature of wastewater in AP2 for one day (24 hours)

The value obtained of GHG emissions, as CO_2 gas equivalents, from POME processing in palm oil mill was 48.572 t CO_2-eq/day, or 14,571.5 t CO_2-eq/year (Table 2). The value of GHG emissions (CH_4 and CO_2) in POME treatment in palm oil mills was different from previous studies, some are higher, and some are lower. However, from this study, the GHG emissions are almost the same as Suprihantin et al. (2012) (14,690.5 t CO_2-eq/year) (Table 4). The difference in GHG emissions is due to, among others: quality (variety and origin) of FFB, harvest season, FFB processing techniques, wastewater treatment systems, climatic factors (rainfall and air temperature), POME temperature, type of pond (bioreactor), levels of components organic matter of POME, and the amount of research data.

Table 4. GHG emission from palm oil mill effluent treatment

GHG emissions at 30 t FFB/hour (t CO_2-eq/year)	Reference
30,596[a]	Foong et al. (2021)
21,381.2[a]	Febijanto (2018)
26,091[b]	Moriarty et al. (2014)
10,670[a]	Sarono (2014)
14,690.5[a]	Suprihatin et al. (2012)
12,927	Febijanto (2010)
14,571.5	This study

[a]Calculated from POM 60 t FFB/hour
[b]Calculated from POM 45 t FFB/hour (GHG 39,136 t CO_2-eq/year)

From this research, it was also obtained that every kg of COD POME would emit 6.266 kg of CO_2-eq GHG, and every m^3 of POME would emit 0.163 t CO_2-eq of GHG; and 0.556 t CO_2-eq per ton of CPO produced, and 0.122 t CO_2-eq per ton of FFB processed, would be emitted (Table 2). These figures are new findings, and conversion factors (coefficients) helpful for a quick calculation of GHG emissions from POME in palm oil mills. This value was an initial estimate so that further and broader studies are needed at various mills with different operational conditions, climates, and sources (varieties and origins) of FFB. The conversion coefficient of 0.556 was almost the same as the results of the study of Rahayu et al. (2015) (0.51 t CO_2-eq/t CPO). This value was closely related to the yield of CPO, which was influenced by the efficiency of mill processing and the quality of processed FFB.

The methane emissions in the palm oil mill are the main part (92.48%) compared to CO_2 (7.5%) in GHG originating from POME processing in the WWTP (Table 2). Furthermore, GHG emissions resulting from POME processing constitute the largest share of GHG from palm oil mills (>90%) (Rahayu et al., 2015; Hosseini and Wahid, 2015). Therefore, controlling and reducing GHG emissions from POME must be essential for a palm oil mill. The utilization of methane from POME as a renewable energy source is an activity that needs to be done immediately for the palm oil industry, thus making the industry more environmentally friendly and sustainable. Several strategic efforts to control and reduce GHG from palm oil mills include the need for government regulations that encourage and require methane gas capture for conversion into energy and the active role of business actors in the palm oil sector. Another benefit obtained from the conversion of POME to energy is the certified emission reduction (CER) value in the clean development mechanism (CDM) scheme.

3.3 Potential for POME conversion to renewable energy

GHG emissions from POME biodegradation through anaerobic degradation would produce biogas as a renewable and sustainable energy source. Biogas has main contents of methane and carbon dioxide, respectively, of 45-80% and 20-55% (Coombs, 1991); 55-70% and 30-45% (Deublein and Steinhauser, 2008). With the optimum average POME production of 450 m^3/day, using a conversion coefficient of 0.2102 kg CH_4/kg COD (Putro, 2021), the efficiency of degradation of the organic components of WWTP is 85% (Rahayu et al., 2015), average COD of fresh POME was 56,277 mg/L (Table 1). The potential for maximum generating electricity from biogas power plants from palm oil mills with an installed capacity of 30 tons of FFB/hour was 1.045 MWe or 8,603 MWh/year (Table 5). This value was almost the same as the calculation in research by Rahayu et al. (2015) equal to 1.1 MWe.

The value of potential energy generation from POME conversion in palm oil mills varies. From the results of previous studies, POM installed capacities of 30, 45, 60, and 90 tons of FFB/hour, each of which has the potential to generate power of 0.53-1.10, 1.25-1.60, 0.74-2.10, 3.2 MWe (Rahayu et al., 2015; Febijanto, 2010; Moriarty et al., 2014; Taniwiryono et al., 2016). The optimum value for energy generation could be achieved through various efforts, including optimization of microbial performance for anaerobic biodegradation, high levels of substrate organic components, biogas purification (increasing methane

levels by removing water vapor, hydrogen sulfide, and CO_2), using high-efficiency gas engines (>42%), choose a bioreactor technology with high performance (high COD removal, equivalent to high conversion of COD to methane) (>80-95%). In addition, there is a need for operational-maintenance management capabilities in balancing: OLR (substrate), HRT, bioreactor volume, and optimal organic matter content for maximum biodegradation performance. Other efforts to achieve biodegradation performance with maximum biogas-methane yield through a biotechnology approach include (1) co-digestion; (2) pre-treatment (through oil extraction, precipitation, and pre-hydrolysis); (3) addition of inorganic supplements; (4) addition of biological supplements; and (5) modification of bioreactors (Choong et al., 2017; Aziz et al., 2019).

Table 5. Potential energy generation capacity maximum of POME conversion to renewable energy

Measurement (estimation)	Unit	Potential
POME fed to AP2-AP1	m^3 POME/day	450[a]
COD-removed	mg/L	47,835[b]
Conversion coefficient (COD to CH_4)	kg CH_4/kg COD	0.2102[c]
COD loading	kg COD/day	21,526
CH_4 production (unit weight)[d]	kg CH_4/day	4,524
CH_4 production (unit volume)	m^3 CH_4/day	6,321
Energy value CH_4[e]; (1 kWh = 3,6 MJ)	MJ/m^3 CH_4	35.7
Engine gas efficiency[e]	%	40
Energy generation capacity (electricity)	MWe	1.045
Availability factor[e]	%	94
Power capacity (electricity) per year	MWh/year	8,603

[a]Potential of POME production per day (30 tons of FFB/hour × 20 hours × 0.75 m^3 POME/ton FFB) (Morad et al., 2008)
[b]COD-removed potential (optimization of WWTP); raw POME COD 56,277 mg/L and 85% COD-efficiency (Rahayu et al., 2015; 80-95%)
[c]Convertion coefficient COD-removed to CH_4 according to Putro (2021)
[d]CH_4 density 0.7157 kg/m^3 (16.04 g/22.41 L; at STP 0ºC and 1 atm)
[e]According to Rahayu et al. (2015)

The development of POME conversion into bio-energy that could reduce its GHG through the various efforts above is an opportunity for future anaerobic digester technique research, with the application of effective-efficient and high-performance biotechnology. It is hoped that this can increase the value of energy output and achieve economic value. So that with an economical price, new and renewable energy (NRE) from POME conversion is competitive compared to other NRE sources (water, wind, solar, geothermal, ocean waves, and other biomass).

4. CONCLUSION

POME processing at the palm oil mill in anaerobic ponds emitted relatively high CH_4 (261.93 g/m^2/day) and CO_2 (595.99 g/m^2/day), equivalent to 48.572 t CO_2-eq/day or 14,571.5 t CO_2-eq/year. The average CO_2 emissions are greater than two times the average CH_4 emissions, both spatially (site) and temporally (time). There was a facultative, aerobic, and or anaerobic biodegradation process according to the interaction between the environment components of the biotic and abiotic and the organic content of the substrate. In the anaerobic pond, the optimum requirements for the anaerobic biodegradation process tended to be unfulfilled so that the emission rate of CO_2>CH_4. The GHG conversion coefficients were obtained for each kg of COD POME emitted 6.266 kg CO_2-eq, and each m^3 of POME emitted 0.163 t CO_2-eq and would be emitted 0.556 t CO_2-eq/t of CPO. The potential for conversion of POME into energy from a palm oil mill of 30 t FFB/hour was a maximum of 1,045 MWe and a power capacity of 8,603 MWh/year.

ACKNOWLEDGEMENTS

The author would like to thank PT SPOI, which was facilitated during the field research. The author also thanks the college students Adi Kurniadi and Ade Kusumah, and M. Syafriansyah. Each is from the Department of Biology, Universitas Islam Negeri Raden Fatah Palembang and the Department of Soil Science, Sriwijaya University, to take field data.

REFERENCES

Ahmed Y, Yaakob Z, Akhtar P, Sopian K. Production of biogas and performance evaluation of existing treatment processes in palm oil mill effluent (POME). Renewable and Sustainable Energy Reviews 2015;42:1260-78.

Alkusma YM, Hermawan, Hadiyanto. Development of alternative energy potential by utilizing palm oil liquid waste as a new renewable energy source in East Kotawaringin Regency. Jurnal Ilmu Lingkungan 2016;14(2):96-102.

American Public Health Association (APHA). Standard Methods for the Examination of Water and Wastewater. Washington DC, USA: American Public Health Association, American Water Works Association, and Water Environment Federation; 1998.

Arif C, Setiawan BI, Widodo S, Rudiyanto, Hasanah NAI, Mizoguchi M. Development of artificial neural network models to estimate greenhouse gas emissions from rice fields with various water regimes. Jurnal Irigasi 2015;10(1):1-10.

Aziz MMA, Kassim KA, Elsergany M, Anuar S, Jorat ME, Yaacob H, et al. Recent advances on palm oil mill effluent (POME) pretreatment and anaerobic reactor for sustainable biogas production. Renewable and Sustainable Energy Reviews 2019;119:1-14.

Batstone DJ. Mathematical modelling of anaerobic reactors treating domestic wastewater: Rational criteria for model use. Reviews in Environmental Science and Biotechnology 2006;5:57-71.

Chen W, Wolf B, Zheng X, Yao Z, Butterbach-Bahl K, Brüggemann N, et al. Annual methane uptake by temperate semiarid steppes as regulated by stocking rates, aboveground plant biomass and topsoil air permeability. Global Change Biology 2011;17:2803-16.

Choong YY, Chou KW, Norli I. Strategies for improving biogas production of palm oil mill effluent (POME) anaerobic digestion: A critical review. Renewable and Sustainable Energy Reviews 2017;82:2993-3006.

Coombs J. The Present and Future of Anaerobic Digestion. New York, USA: Elsevier Science Publishing Co.Inc.; 1991.

Deublein D, Steinhauser A. Biogas from Waste and Renewable Resources an Introduction. Weinheim, Germany: Wiley-VCH Verlag GmbH and Co. KGaA; 2008.

Drapcho CM, Nhuan NP, Walker TH. Biofuels Engineering Proces Technology. USA: McGraw-Hill Companies Inc.; 2008.

El-Fadel M, Massoud M. Methane emissions from wastewater management. Environmental Pollution 2001;114(2):177-85.

Febijanto I. Potential for catching methane gas and its use as fuel for power generation at PTPN VI Jambi. Jurnal Ilmiah Teknologi Energi 2010;1(10):30-47.

Febijanto I. Optimization of methane gas use as energy resource in palm oil mill as an anticipated selling price of electricity based on the existing average cost of generation. Jurnal Teknologi Lingkungan 2018;19(1):49-60.

Foong SZY, Chong MF, Ng DKS. Strategies to promote biogas generation and utilisation from palm oil mill effluent. Process Integration and Optimization for Sustainability 2021;5: 175-91.

Hassan MA, Yacob S, Shirai Y. Treatment of palm oil wastewaters. In: Wang LK, Hung Y, Lo HH, Yapijakis C, editors. Handbook of Industrial and Hazardous Wastes Treatment. New York, USA: Marcel Dekker, Inc.; 2004. p. 719-36.

Hosseini SE, Wahid MA. Pollutant in palm oil production process. Journal of the Air and Waste Management Association 2015;65(7):773-81.

Indonesian Palm Oil Association (IPOA). Palm Oil Industry Reflection 2016 and Prospects 2017. Jakarta, Indonesia: Indonesian Palm Oil Association; 2017.

Intergovernmental Panel on Climate Change (IPCC). IPCC Guidelines for National Greenhouse Gas Inventories: Volume 1-5. Hayama, Japan: Institute for Global Environmental Strategies; 2006.

International Atomic Energy Agency (IAEA). Manual on Measurement of Methane and Nitrous Oxide Emissions from Agriculture. Vienna, Austria: Food and Agriculture Organization of The United Nations and International Atomic Energy Agency; 1992.

Khokhar NH, Park J. A simplified sampling procedure for the estimation of methane emission in rice fields. Environmental Monitoring and Assessment 2017;189:1-10.

Korres NE, O'Kiely P, Benzie JAH, West JS. Bioenergy Production by Anaerob Digester, Using Agricultural Biomass and Organic Waste. Maryland, USA: Taylor and Francis; 2013.

Lam MK, Lee KT. Renewable and sustainable bioenergies production from palm oil mill effluent (POME): Win-win strategies toward better environmental protection. Biotechnology Advances 2011;29:124-41.

Lam WY, Kulak M, Sim S, King H, Huijbregts MAJ, Chaplin-Kramer R. Greenhouse gas footprints of palm oil production in Indonesia over space and time. Science of the Total Environment 2019;688:827-37.

Lantin RS, Aduna JB, Javeliana AM. Methane Measurements in Rice Fields. Manila, Philippines: International Rice Research Institute; 1995.

Mahajoeno E. Development of Renewable Energy from Palm Oil Mill Wastewater [dissertation]. Bogor, Indonesia: Bogor Agricultural Institute; 2008.

Ministry of Agriculture. Statistics of Indonesian Estates 2015-2017 Palm Oil. Jakarta, Indonesia: Ministry of Agriculture; 2016.

Ministry of Agriculture. Tree Crop Estate Statistics of Indonesia 2017-2019 Palm Oil. Jakarta, Indonesia: Ministry of Agriculture; 2018.

Morad N, Choo SS, Hoo YC. Simplified life cycle assessment of crude palm oil: A case study at a palm oil mill. Proceedings of the International Conference on Environmental Research and Technology 2008 (ICERT 08); 2008 May 28-30; Parkroyal Hotel, Pulau Pinang: Malaysia; 2008.

Moriarty K, Elchinger M, Hill G, Katz J, Barnett J. Methane for Power Generation in Muaro Jambi: A Green Prosperity Model Project. Colorado, USA: National Renewable Energy Laboratory (NREL); 2014.

Nguyen D, Wu Z, Shrestha S, Lee PH, Raskin L, Khanal SK. Intermittent micro-aeration: New strategy to control volatile fatty acid accumulation in high organic loading anaerobic digestion. Water Research 2019;166:1-10.

Nguyen DM. Oxidation-Reduction Potential-Based Micro-Aeration Control System for Anaerobic Digestion [dissertation]. Honolulu, USA: University of Hawaii at Mānoa; 2018.

Ohimain EI, Izah SC. A review of biogas production from palm oil mill effluents using different configurations of bioreactors. Renewable and Sustainable Energy Reviews 2017;70:242-53.

Paredes MG, Güerecaa LP, Molinab LT, Noyolaa A. Methane emissions from stabilization ponds for municipal wastewater treatment in Mexico. Journal of Integrative Environmental Sciences 2015;12(SI):139-53.

Park JBK, Craggs RJ. Biogas production from anaerobik waste stabilisation ponds treating dairy and piggery wastewater in New Zealand. Water Science and Technology 2007; 55(11):257-64.

Pehnelt G, Vietze C. Recalculating GHG emissions saving of palm oil biodiesel. Environmental Monitoring and Assessment 2013;15:429-79.

Prasetya H, Arkeman Y, Hambali E. Role of methane capture for sustainable biodiesel production from palm oil: A life cycle assessment approach. International Journal on Advanced Science, Engineering and Information Technology 2013;3(5):17-20.

Putro LHS, Budianta D, Rohendi D, Rejo A. Biomethane emissions: Measurement in wastewater pond at palm oil mill by using TGS2611 methane gas sensor. Journal of Ecological Engineering 2019;20(6):25-35.

Putro LHS, Budianta D, Rohendi D, Rejo A. Modeling methane emission of wastewater anaerobic pond at palm oil mill using radial basis function neural network. International Journal on Advanced Science, Engineering and Information Technology 2020;10(1):260-8.

Putro LHS. Biomethane from Palm Oil Mill Effluent: An Overlooked Renewable Energy Sources. Depok, Indonesia: Rajawali Pers; 2021.

Rahayu AS, Karsiwulan D, Yuwono H, Paramita V. Guide Book for Converting POME into Biogas: Project Development in Indonesia. Jakarta, Indonesia: Winrock International; 2015.

Sarono. The Greenhouse Gas Reduction Strategy through Conversion of Palm Oil Mill Liquid Waste into Electrical Energy (Case Study in Lampung Province) [dissertation]. Bogor, Indonesia: Bogor Agricultural Institute; 2014.

Schuchardt F, Wulfert K, Darnoko, Herawan T. Effect of new palm oil mill processes on the EFB and POME utilization. Journal Oil Palm Research 2008;Special Issue:115-26.

Seadi TA, Rutz D, Prassl H, Köttner D, Finsterwalder D, Volk S, et al. Biogas Handbook. Esbjerg, Denmark: University of Southern Denmark; 2008.

Setyanto P, Wihardjaka A, Yulianingsih E, Agus F. Greenhouse gas emissions from drainage channels in Jabiren peatlands, Central Kalimantan. In: Wihardjaka, A, Maftu'ah E, editors. Proceedings of the National Seminar: Sustainable Management of Degraded Peatlands for GHG Emission Mitigation and Economic Value Enhancement; 2014 Aug 18-19; Jakarta: Indonesia; 2014.

Speece RE. Anaerobic Biotechnology for Industrial Wastewaters. Tennessee, USA: Archae Press; 1996.

Suprihatin, Sa'id EG, Suparno O, Sarono. Palm oil mill wastewater potential as an alternative energy sources. Prosiding Seminar Nasional PERTETA; 2012 Nov 30 - Dec 2; Malang: Indonesia; 2012 (in Indonesian).

Tanaka N. Energy Sector Methane Recovery and Use: The Importance of Policy. Paris, France: International Energy Agency (IEA); 2009.

Taniwiryono D, Siswanto, Herman. Policy and Financial Analysis for Development of Biogas Power Plant in Palm Oil Mills "Towards Low Carbon Development in Oil Palm Sector". Jakarta, Indonesia: Coordinating Ministry for Economic Affairs; 2016.

Wall G, Hammond B, Donlon P, Johnson ND, Smith JC. Commissioning and operation of high rate anaerobic lagoon (HRAL) reactors. Proceedings of the 63rd Annual Water Industry Engineers and Operators Conference; 2000 Sep 6-7; Brauer College, Warrnambool: Australia; 2000.

Wu TY, Mohammad AW, Jahim JMd, Anuar N. Pollution control technologies for the treatment of palm oil mill effluent (POME) through end-of-pipe processes. Journal of Environment Management 2010;91:1467-90.

Yacob S, Hassan MA, Shirai Y, Wakisaka M, Subash S. Baseline study of methane emission from anaerobic ponds of palm oil mill effluent treatment. Science of the Total Environment 2006;366:187-96.

Yuliasari R, Darnoko, Wulfred K, Gindulis W. Oil palm wastewater treatment using fixed bed anaerobic reactor down-flow type. Warta Pusat Penelitian Kelapa Sawit 2001;9:75-81.

Evaluation of Ecosystem Service Changes due to Land Use and Land Cover Dynamics in Cham Chu Nature Reserve

Vo Thanh Son[1], Luu The Anh[1], Dao Minh Truong[1], Trong Dai Ly[1*], and Jing Sun[2]

[1]VNU-Central Institute for Natural Resources and Environmental Studies (VNU-CRES), Vietnam National University, Hanoi, Vietnam
[2]Tongling University, Tongling, Anhui, China

ARTICLE INFO

Received: 9 Jul 2021
Received in revised: 12 Oct 2021
Accepted: 15 Oct 2021
Published online: 9 Nov 2021
DOI: 10.32526/ennrj/20/202100131

Keywords:
Ecosystem service values/ Benefit transfer method/ Land use and land cover change/ Cham Chu nature reserve

*** Corresponding author:**
E-mail: dailt.cres@vnu.edu.vn

ABSTRACT

Assessment of ecosystem services is vital for successful natural resource allocation; however, these have been less studied within Vietnam. This study estimated the ecosystem services value (ESV) and its change in Cham Chu nature reserve, Vietnam using a benefit transfer method. Ecosystem service values estimation and trend analyses were carried out based on land use and land cover datasets from 1986, 1998, 2007, and 2017, with their corresponding global value coefficients. The results revealed that the total value of ecosystem services in Cham Chu was approximately 64.4, 63.9, 60.7, and 63.4 million USD in 1986, 1998, 2007, and 2017, respectively. Changes have also occurred in the values of individual ecosystem service functions. From 1986 to 2017, ecosystem service functions showed significant decreases in gas regulation, pollination, biological control, water regulation, water supply, and food production of 62.9%, 51.2%, 44.4%, 24.7%, 23.1%, and 13.0%, respectively. We conclude that the loss of ESV is a result of ecological deterioration in the studied landscape, and we propose further research to examine future solutions and establish action strategies. In summary, the research approach methodology developed can be used by land managers and planners in Vietnam as a guideline to estimate the importance of ecosystem services in Vietnam.

1. INTRODUCTION

Ecosystem services are material, resources, and knowledge flows from natural capital stocks combined with manufactured and human capital services to deliver human welfare (Reid et al., 2005). Ecosystem services are the conditions and uses of ecosystems for human benefit, as well as the ecological processes that humans rely on (Huang et al., 2019). They are also the greatest indicator of environmental effects, and thus monitoring the quantity or quality of ecosystem services is crucial (Zhou et al., 2017). Generally, changes in certain forms of ecosystem services will affect human welfare. Changing the composition of local forests, for example, can change terrestrial and marine habitats, impacting the benefits and costs of local human activities. Alcamo (2003) stated that land use and land cover (LULC) change is a direct factor that affects ecosystem service and therefore affects human welfare. The effect of LULC changes are an important part of the research on global climate change and global environmental change (Dubreuil et al., 2012), and can be characterized from ecosystem services value (Fei et al., 2018). As a result, evaluating improvements in ecosystem services values (ESV) in response to LULC transitions is critical for raising awareness and informing policy and decision-making on resource sharing that provides the best-valued services (Solomon et al., 2019).

The close relationships between LULC change and dynamics of ecosystem service values have been studied largely around the world, such as in mountainous areas in Africa (Gashaw et al., 2018; Kindu et al., 2016), in Asia (Huang et al., 2019; Rimal et al., 2019; Talukdar et al., 2020), for tropical forests in general (Bisui et al., 2021) and in protected areas (Chaudhary and Kastner, 2016), and in biosphere reserves (Abera et al., 2021). These studies show that all the changes in LULC, especially forest cover, will lead to the degradation of ecosystem services, and

Citation: Son VT, Anh LT, Truong DM, Ly TD, Sun J. Evaluation of ecosystem service changes due to land use and land cover dynamics in Cham Chu nature reserve. Environ. Nat. Resour. J. 2022;20(1):73-88. (https://doi.org/10.32526/ennrj/20/202100131)

ultimately impact local socio-economic development and living environment.

While forest ecosystem changes have been studied extensively in several ecological contexts in many countries in the world (Mamat et al., 2018a), in Vietnam, only a few studies have been carried out related to ecosystem services, such as modeling and mapping natural hazard regulating ecosystem services (Dang et al., 2018), provisioning services for food production (Son, 2003), non-timber forest products (Wetterwald et al., 2004), and planted forests (Paudyal et al., 2020). Other studies also assessed terrestrial ecosystem services in protected areas such as Bach Ma National Park (Hong and Saizen, 2019), Ba Be National Park (Dai and Ongsomwang, 2019), and Cat Tien National Park (GECD, 2014). However, these studies are often not systematic, or are time-consuming, costly, and usually evaluated for a short period so that they cannot assess the evolution of ecosystem services over time, especially compared with the past. This has led to the following research questions: What is the relationship between LULC and ecosystem services? Is it possible to retrospectively recall the value of ecosystem services in the past using easily accessible and systematically collected information such as remote sensing imagery for areas of high biodiversity value, such as protected areas? This study, therefore, is an attempt to answer these questions.

Cham Chu nature reserve (CCNR) was chosen as a case study to access ESV. The area is located inside Tuyen Quang Province, which has the highest biodiversity value in the northeastern part of Vietnam (Nguyen et al., 2018). The Tonkin Snub-nosed Monkey, one of the world's top 25 most endangered primates, listed as "Critically Endangered" on the IUCN's red list of threatened animals (Hoang and Covert, 2012), is found in the region. FFI (1999) estimates five groups of Tonkin Snub-nosed Monkeys in the Cham Chu region, totaling 75 to 89 primates. Furthermore, recent studies showed high species diversity of mammals (Hai et al., 2019; Tham et al., 2020), reptiles, and amphibians (Pham et al., 2019). This information makes the CCNR become one of the most important sites globally to conserve these species (Hughes, 2001). However, biodiversity conservation is facing some threats due to human activities, especially before 2014, when the CCNR was established. These threats have been intensified by the impact of macro socio-economic development policies, such as the reform policy (known as DOI MOI) in 1986 and WTO accession in 2007, which have contributed to making Vietnam a low-middle income country (2010), reaching 2,389 USD yearly income/per capita in 2017 (GSO, 2017). Vietnam's forestry policy has undergone significant changes, shifting from the economic sector of forest exploitation before 1986, to the policy of protection and limited exploitation of natural forests or "closure of the forest gates" from 1994-1995, and subsequent forest conservation and development policies since 2004 (MARD, 2004). In the period since Doi Moi (1986) to 2012, land use changes in the Northern mountainous region were characterized by the conversion of swidden land into arable land and afforestation land (Shivakoti et al., 2016). Nguyen et al. (2020) showed that forest governance regimes have a significant effect not only on forest LULC but also on the quantity and values of forest ecosystem service derived from forests. Thus, the evolution of forestry policy has affected LULC change and ultimately affects the value of biodiversity and ecosystem services. In addition, DARD (2014) found that illegal logging, woodland clearing for agriculture, forest fires, and hunting are the most severe threats to biodiversity in the CCNR and other mountainous areas in Viet Nam (Wood et al., 2013). The expansion of cropland changes the landscape pattern, as agricultural production is one of the underlying reasons for deforestation and forest degradation, causing a gradual increase in ecological deprivation (Khuc et al., 2018). Orange production on the sloping lands of local communes in the CCNR expanded from 1,473 ha (2008) to 3,595 ha (2017), and up to 3,614 ha (2020), which have contributed to a reduction of forest cover in the area (CCMB, 2020; Son et al., 2020). Therefore, it is necessary to quantify the effects of LULC change on ecosystem services values, which is a crucial tool to develop knowledge on management and to reorientate the attitudes of people towards maintaining biodiversity (Fritzsche et al., 2007). Thus, this study attempts to answer the question, how have LULC in the CCNR changed during development processes over the past 30 years, and how does this affect ecosystem services in the area.

The ultimate goal of this study was to estimate the ESV and its change in the CCNR after more than 30 years since 1986 using a benefit transfer method that applies estimated value from one location to a similar site in another area (Plummer, 2009). From 1986 to 2017, multi-temporal land use data sets were used to determine the ESV transition.

2. METHODOLOGY

2.1 Study area

The study area is the CCNR. It lies between 22°04'N-22°21'N and 104°53'E-105°14'E. It is located in the administrative boundaries of five communes: Trung Ha, Ha Lang, and Hoa Phu in Chiem Hoa District; Yen Thuan and Phu Luu in Ham Yen District, Tuyen Quang Province. The reserve area is 15,262.3 ha, with 6,168.4 ha in Ham Yen District and 9,093.9 ha in Chiem Hoa District. A mountainous topography characterizes the landscape of the CCNR, with the elevation varying from 30 m to 1,577 m.a.s.l. (Figure 1). The area is a large limestone mountain with many peaks such as Cao Duong peak (989 m), Pu Loan peak (1,154 m), Khau Vuong peak (1,218 m), and the highest peak Cham Chu (1,587 m) (Nguyen et al., 2018). Cham Chu region has a tropical monsoonal climate with two seasons: summer and winter. The summer is hot and has high humidity from May to October; the winter is cold and dry from November to April. The annual temperature is 23°C. The average annual rainfall of the area fluctuates in the range of 1,500 mm to 1,800 mm. While the rainfall in summer accounts for 85-94% of total annual rainfall, the value in winter only comprises 6-25% of the total yearly rainfall (Ranzi et al., 2012).

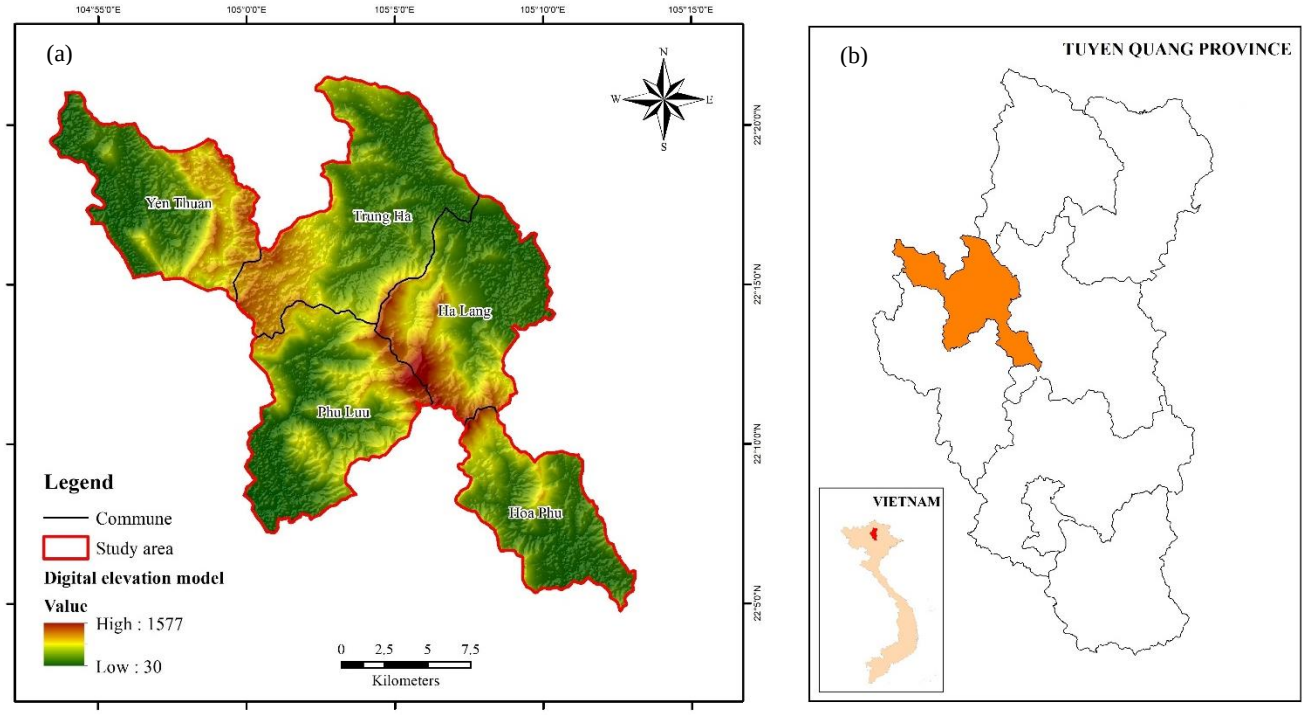

Figure 1. Location of the study area: (a) DEM of the CCNR and (b) the CCNR in Tuyen Quang Province, Vietnam

2.2 Research methodology

The research methodology workflow consisted of two components: (1) LULC classification and (2) ecosystem service evaluation (Figure 2). Details of each component are separately described in the following sections.

2.2.1 LULC classification

Data sources for LULC classification in this study are Landsat images taken over the area of Cham Chu. These images were collected from the United States Geological Survey (USGS) and were used as multi-temporal resolution remote sensing imagery over the study area. A set of four Landsat images from 1986, 1998, 2007, and 2017 was used for LULC classification and interpretation. They have similar acquisition seasons to ensure the image quality and avoid the effects of atmospheric conditions (haze, cloud cover) for compatible detection of LULC types (Table 1).

In this study, geometric corrections of the data were conducted using the image to map rectification based on topographic maps with a scale of 1:50,000 using the Erdas Imagine 2014 software. All data were re-projected to the Universal Transverse Mercator Projection System (UTM) Zone 48N with the World Geodetic System (WGS-1984) datum. After that, we classified LULC into five types, which are forest land,

bush, bareland, cropland, and water body. The description of the LULC category is shown in Table 2. The Landsat images were classified using a maximum likelihood classification, which is a method for calculating a known class of distributions as the maximum for a given statistic (Sun et al., 2013). Besides, visual interpretation of image features, e.g., shape, size, color, and texture for each class of LULC, was also performed to correct the misclassified LULC types (Mamat et al., 2018a; Ongsomwang et al., 2019; Thakkar et al., 2017).

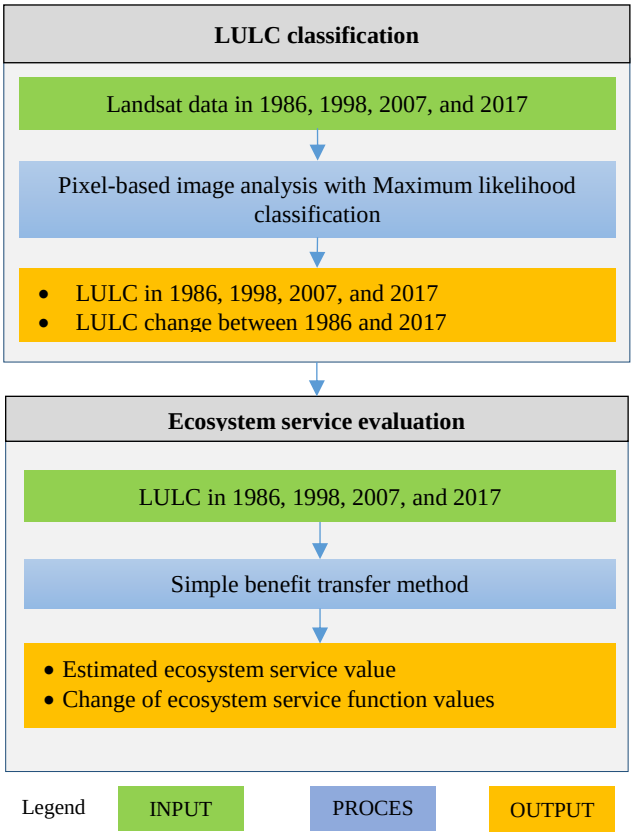

Figure 2. Workflow of research methodology

Table 1. The characteristic of Landsat images obtained for this study

No	Satellite	Path/Row	Date	Spatial resolution	No. of bands
1	Landsat 5-TM	127/045	01 July 1986	30 m	7
2	Landsat 5-TM	127/045	18 July 1998	30 m	7
3	Landsat 5-TM	127/045	24 May 2007	30 m	7
4	Landsat 8-OLI	127/045	04 June 2017	30 m	7

Table 2. LULC categories in the CCNR and their equivalent biome for ecosystem service evaluation

LULC type	Definition	Equivalent biome	Ecosystem Service Coefficient (USD/ha/year)
Forest land	Areas covered by trees both natural and planted, dense forest, and opened forest	Tropical forest	2,003
Bush	Bush mixed with the small woody tree, vines, and grass	Grass/rangelands	244
Bareland	Exposed soils, bare rocks, floodplain, quarries, and sparse vegetation	Desert	0
Cropland	Cropland, orchards, nurseries, horticultural land, fallow land, intensively, moderately, and sparsely cultivated land	Cropland	92
Water body	Rivers, lakes, and artificial water areas	Lakes/rivers	8,498

Note: Ecosystem Service Coefficients were computed from Van der Ploeg and de Groot (2010)

The corrected LULC maps were validated using overall accuracy and Kappa hat coefficient based on the reference maps in 1986, 1998, and 2007 from the Vietnam Ministry of Natural Resources and Environment and a field survey in 2017. Herein, 397 sample points with a confidence level of 95% and a precision of 5% for the LULC class and stratified random sampling were used in this study to assess the accuracy (Congalton and Green, 2008; Israel, 1992). Finally, the post-classification comparison technique (Jensen, 2005) was applied to detect LULC change between 1986 and 2017.

2.2.2 Ecosystem service evaluation

The derived LULC data in 1986, 1998, 2007, and 2017 were used to calculate the ESV based on the simple benefit transfer method, which refers to the process of transferring economic value figures from one place to a relative location (Kindu et al., 2016; Plummer, 2009). The ESV for a given LULC type is determined by multiplying the area of each LULC type by its value coefficients, and the cumulative ESV for each reference year is a total of the LULC types' values (Equation 1).

$$ESV = \sum(A_k \times VC_k) \quad (1)$$

Where; ESV is the total estimated ESV, A_k is the area (ha), and VC_k is the value coefficient (USD/ha/year) for LULC type k (Table 3).

In addition to estimating the total value of ecosystem services for LULC types, the values of services delivered by different ecosystem functions within the study area were also assessed using the following equation:

$$ESV_f = \sum(A_k \times VC_{fk}) \quad (2)$$

Where; ESV_f is the calculated ESV of function f, A_k is the area (ha), and VC_{fk} is the value coefficient of function f (USD/ha/year) for LULC type k (Talukdar et al., 2020) (Table 3).

Then, through comparing the values of one dataset to the equivalent value of the second dataset, the ESV change was determined as follows:

$$\text{ESV change} = \left(\frac{\text{ESV final year - ESV initial year}}{\text{ESV initial year}}\right) \times 100 \quad (3)$$

Where; ESV is the total estimated ESV, positive values of ESV indicate an increase, whereas negative values indicate a decrease in the amount of USD, and the ESV change is presented in percent (Kindu et al., 2016; Ongsomwang et al., 2019).

Table 3. Annual value coefficient for each ecosystem service function according to LULC type (Van der Ploeg and de Groot, 2010)

Ecosystem services	ESV (USD/ha/year) of each land cover type			
	Forest land	Bush	Cropland	Water body
Provisioning services				
Water supply	3			2,117
Food production	32	67	54	41
Raw material	315			
Genetic resources	41	0		
Regulating services				
Water regulation	6	3		5,445
Waste treatment	87	87		665
Erosion control	245	29		
Climate regulation	223	0		
Biological control		23	24	
Gas regulation		7		
Disturbance regulation	5			
Supporting services				
Nutrient cycling	922			
Pollination		25	14	
Soil formation	10	1		
Cultural services				
Recreation	112	2		230
Cultural	2			
Total	2,003	244	92	8,498

Finally, sensitivity analyses were performed to calculate the percentage change in ESV for a given percentage shift in the value coefficient. The sensitivity analysis was performed using the standard economic concept of elasticity, i.e., the percentage change in the output for a given percentage change in the input (Kreuter et al., 2001; Perloff, 2016), as shown in Equation (4). Consequently, the ecosystem modified value coefficients for the forest land, bush, cropland, and water body were individually adjusted by 50%, and the corresponding coefficient of sensitivity (CS) was calculated. If CS is higher than one, the estimated ecosystem value is elastic to the coefficient; but, if CS is less than one, the estimated ecosystem value is inelastic, and the outcome is reliable. The higher the proportional shift in the value of ecosystem services compared to the valuation coefficient, the more meaningful the use of a reliable ecosystem value coefficient (Mamat et al., 2018b; Solomon et al., 2019).

$$CS = \frac{(ESV_j - ESV_i)/ESV_i}{(VC_{jk} - VC_{ik})/VC_{ik}} \quad (4)$$

Where; ESV_i and ESV_j are primary and adjusted total estimated ESVs, respectively and VC_{ik} and VC_{jk} are primary and adjusted value coefficients for LULC type k.

3. RESULTS AND DISCUSSION

3.1 Land use and land cover classification

The results of the LULC classification in the CCNR between 1986 and 2017 are shown in Table 4 and Figures 3 and 4. Overall, forest land persists as the dominant cover type over 30 years. Forest land showed an initial decrease and then an increase, with a reduction from 76.41% of the total land in 1986 to 72.0% in 2007, and then an increase to 76.42% in 2017. The most significant land cover change occurred in bush and bareland. The bush experienced an initial increase then decrease, with an increase from 9.93% of the total land in 1986 to 11.31% in 2007, and then decrease to 3.68% in 2017. Bareland rapidly increased from 8.54% in 1986 to 10.30% in 2007 and then expanded to 15.23% in 2017. Likewise, cropland showed an increase from 4.71% in 1986 to 6.11% in 2007, then decreased to 4.39% in 2017. Water body initially experienced a slight increase from 0.40% in 1986 to 0.47% in 1998, then reduced to 0.28% in 2007 and 2017. The considerable increase in cropland and bareland, together with the decrease in forest land in 2007, is a result of the rapid development of illegal exploitation of forest products, clearance of forest for agriculture, and inadequate regulations for the protection of natural ecosystem in this period. However, after ten years, from 2007 to 2017, the forest land increased from 72.00% to 76.42%, and the cropland decreased from 6.11% to 4.39%. These findings imply the practical effort of nationwide reforestation programs of Vietnam's government (Clement and Amezaga, 2009; Huong et al., 2014).

Furthermore, the accuracy of LULC classification in 1986, 1998, 2007, and 2017 were 90%, 93%, 91%, and 89%, and the Kappa coefficients were 0.891, 0.918, 0.875, and 0.886, respectively. According to Fitzpatrick-Lins (1981), a Kappa hat coefficient of more than 80% represents strong agreement or accuracy between two maps. Turan and Günlü (2010) also stated that the overall accuracy is acceptable if it is greater than 80%. Both findings indicate that the LULC classification result in this study meets the accuracy requirement for land use classification.

Table 4. LULC pattern in the CCNR in 1986, 1998, 2007, and 2017

LULC types	1986		1998		2007		2017	
	Area (ha)	%	Area (ha)	%	Area (ha)	%	Area (ha)	%
Forest land	30,906	76.41	30,541	75.51	29,122	72.00	30,908	76.42
Bush	4,017	9.93	3,791	9.37	4,573	11.31	1,489	3.68
Bareland	3,456	8.54	4,070	10.06	4,165	10.30	6,161	15.23
Cropland	1,907	4.71	1,854	4.58	2,471	6.11	1,775	4.39
Water body	160	0.40	190	0.47	115	0.28	113	0.28
Total	40,446	100.00	40,446	100.00	40,446	100.00	40,446	100.00

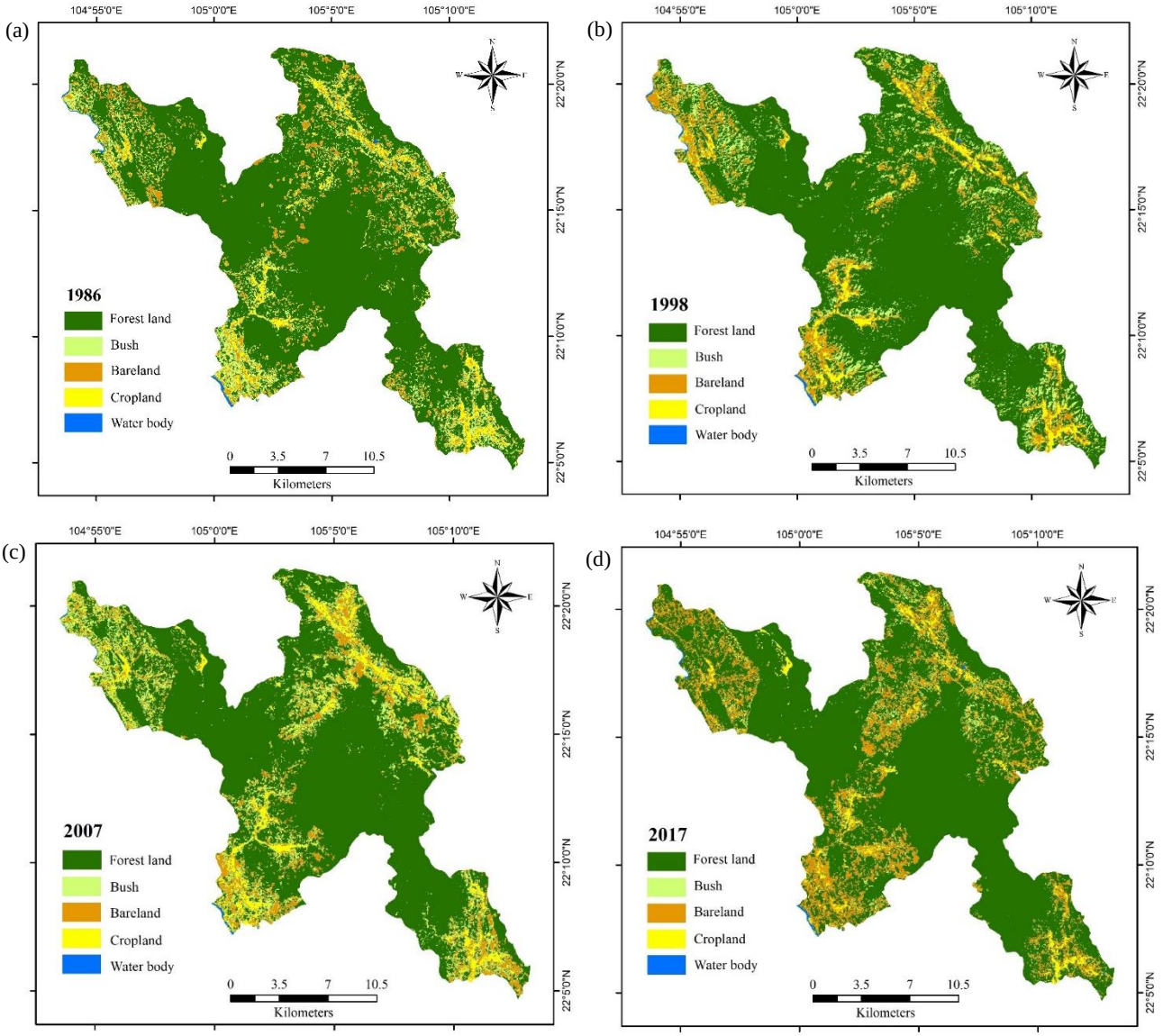

Figure 3. Spatial distribution map of LULC in the CCNR in (a) 1986, (b) 1998, (c) 2007, and (d) 2017

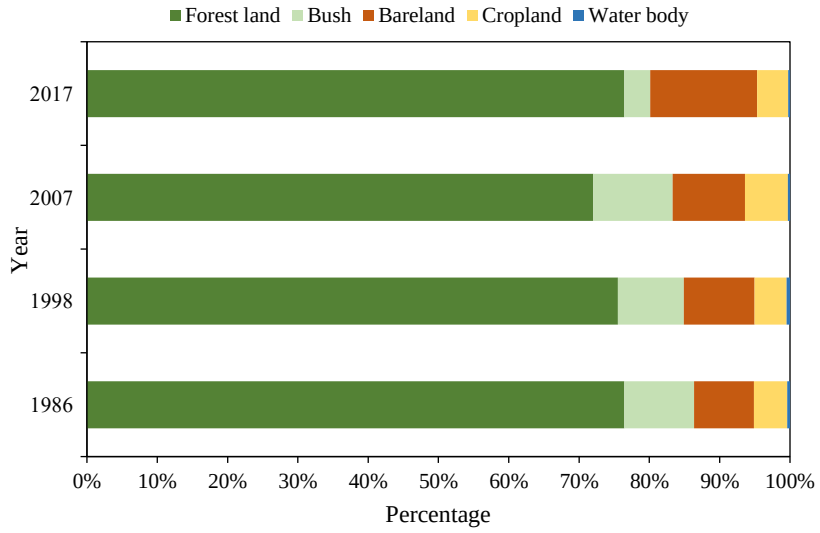

Figure 4. Multi-temporal LULC changes in the CCNR in 1986, 1998, 2007, and 2017

3.2 Land use and land cover change

Table 5 and Figure 5 revealed a complex transformation that occurred among each LULC type in the Cham Chu region from 1986 to 2017. Of about 30,907 ha of forest land in 1986, 26,282.61 ha were unchanged, while about 977.40 ha, 3,217.59 ha, 422.01 ha, and 6.93 ha were lost to bush, bareland, cropland, and water body, respectively. The total loss of forest land between 1986 and 2017 was about 4,624 ha. On the contrary, about 4,625 of forest land in 2017 was gained from the bush (about 2,220 ha), bareland (about 1,816 ha), cropland (about 574 ha), and water body (about 15 ha). Accordingly, the forest land increased over the study period by 1.17 ha, with an annual increased rate of 0.04 ha.

Table 5. LULC change matrix between 1986 and 2017

LULC type		LULC 1986 (ha)						
		Forest land	Bush	Bareland	Cropland	Water body	Class total	Gain
LULC 2017 (ha)	Forest land	**26,282.61**	2,220.03	1,816.02	574.02	15.03	30,907.71	4,625.10
	Bush	977.40	**259.56**	213.03	39.06	0.27	1,489.32	1,229.76
	Bareland	3,217.59	1,322.19	**1,081.89**	528.57	10.53	6,160.77	5,078.88
	Cropland	422.01	211.68	341.28	**752.85**	47.07	1,774.89	1,022.04
	Water body	6.93	3.96	3.96	10.17	**87.48**	112.50	25.02
	Class total	30,906.54	4,017.42	3,456.18	1,904.67	160.38		
	Loss	4,623.93	3,757.86	2,374.29	1,151.82	72.90		
Area change (ha)		1.17	-2,528.10	2,704.59	-129.78	-47.88		
Annual change rate (ha/year)		0.04	-81.55	87.24	-4.19	-1.54		

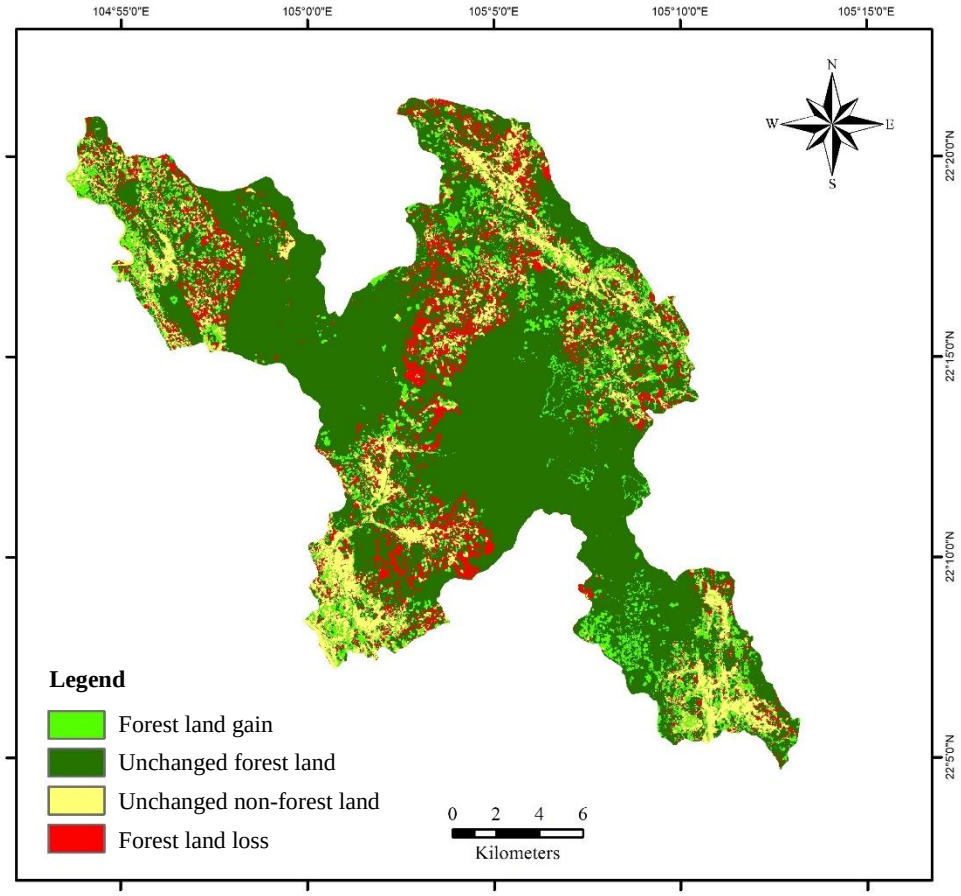

Figure 5. Forest land change map between 1986 and 2017 in the CCNR

About 260 ha of bush remained unchanged during the study period, while about 3,758 ha of bush in 1986 was converted into other LULC types in 2017, and about 1,230 ha of bush in 2017 was gained from different LULC types. The total area of bush decreased in the study period by 2,528.1 ha with an annual decrease of 81.55 ha/year. Meanwhile, about 1,082 ha of bareland was unchanged between 1986 and 2017, whereas about 2,374 ha was converted into other LULC types, and about 5,079 ha was gained from different LULC types. The annual increase of bareland was 87.24 ha/year. For cropland, about 752.85 ha remained unchanged, about 1,152 ha was converted into other LULC types, about 1,022 ha was gained from different LULC types, and the annual rate of decrease was 4.19 ha. About 87.48 ha was unchanged for the water body in the same period, about 723 ha was converted into other LULC types, and about 25 ha was gained from different LULC types. The total water body area decreased by 47.88 ha, with an annual rate of decrease of 1.54 ha.

3.3 Status of ecosystem service value

Table 6 shows the estimated ESV for each land cover type from 1986 to 2017. The total ESVs of the whole study area were about 64.4, 63.9, 60.7, and 63.4 million USD in 1986, 1998, 2007, and 2017, respectively. In 1986, forest land, bush, cropland, and water body accounted respectively for about 96.1%, 1.5%, 0.3%, and 2.1% of the total ESVs. In 1998, forest land contributed the most significant part (i.e., 95.8%), while bush, cropland, and water body accounted, respectively, for about 1.4%, 0.3%, and 2.5% of the total ESVs. Also, forest land, bush, cropland, and water body accounted for approximately 96.2%, 1.8%, 0.4%, and 1.6%, respectively, of the total ESVs in 2007. In 2017, forest land, bush, cropland, and water body accounted, respectively, for about 97.7%, 0.6%, 0.3%, and 1.5% of the total ESVs.

Table 7 and Figure 6 show changes in ecosystem services values between different periods. The total ESV during the first study period (1986-1998) decreased by about 0.5 million USD, which is about 0.8% of the value that existed in 1986. The total ESV was further reduced by approximately 3.2 million USD (5.1%) during the second period (1998-2007). Still, total ESV was increased by approximately 2.7 million USD (4.5%) during the third period (2007-2017). Nevertheless, the total ESV was reduced by roughly 1.0 million USD (1.6%) for the whole study period (1986-2017). During the whole study period, the change in ESVs for each land use type also showed a significant reduction of the values from bush, and water body, representing about 0.6 million USD (62.9%), and 0.4 million USD (29.4%) of the value that existed in 1986, respectively.

Table 6. Estimation of ESVs for each land use type of the different years in USD million per year of the study area

LULC types	1986		1998		2007		2017	
	ESV	%	ESV	%	ESV	%	ESV	%
Forest land	61.9	96.1	61.2	95.8	58.3	96.2	61.9	97.7
Bush	1.0	1.5	0.9	1.4	1.1	1.8	0.4	0.6
Bareland	0.0	0.0	0.0	0.0	0.0	0.0	0.0	0.0
Cropland	0.2	0.3	0.2	0.3	0.2	0.4	0.2	0.3
Water body	1.4	2.1	1.6	2.5	1.0	1.6	1.0	1.5
Total	64.4	100.0	63.9	100.0	60.7	100.0	63.4	100.0

Table 7. Changes in ESVs between different periods.

LULC types	1986-1998		1998-2007		2007-2017		1986-2017	
	Million USD	%	Million USD	%	Million USD	%	Million USD	%
Forest land	-0.7	-1.2	-2.8	-4.6	3.6	6.1	0.0	0.0
Bush	-0.1	-5.6	0.2	20.6	-0.8	-67.4	-0.6	-62.9
Bareland	0.0	0.0	0.0	0.0	0.0	0.0	0.0	0.0
Cropland	0.0	-2.8	0.1	33.3	-0.1	-28.2	0.0	-6.9
Water body	0.3	18.8	-0.6	-39.5	0.0	-1.7	-0.4	-29.4
Total	-0.5	-0.8	-3.2	-5.1	2.7	4.5	-1.0	-1.6

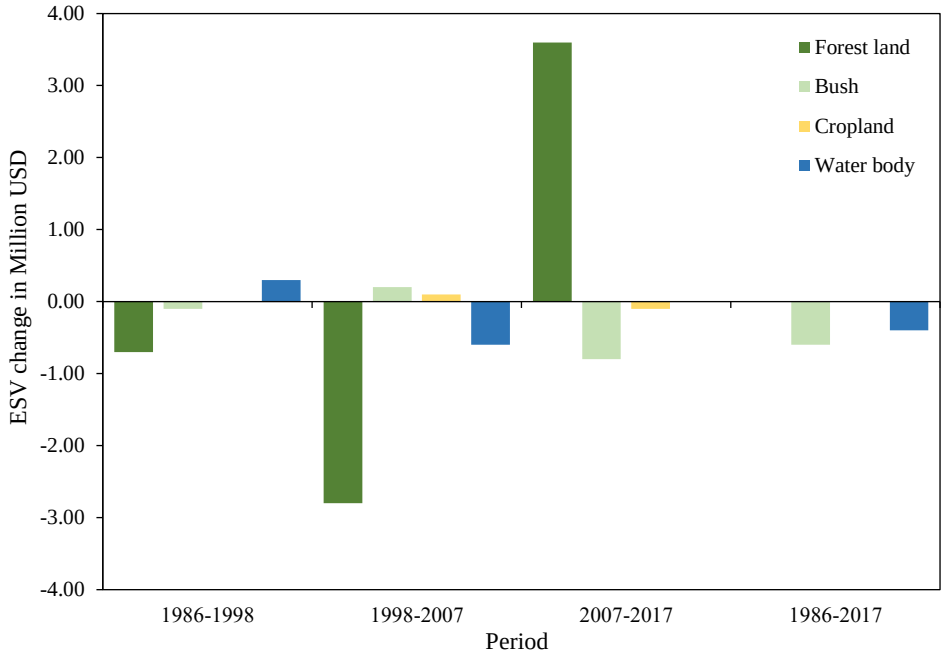

Figure 6. ESV change chart of the CCNR for 1986-1998, 1998-2007, 2007-2017, and 1986-2017

3.4 Estimated service value of individual ecosystem function and its change

The ecosystem function was determined using the value coefficients in Table 3 and areas of the land use categories (Table 4) to assess the impact of land use transition on each of the ecosystem functions and their contribution rate to the overall ESV within the CCNR over 30-year.

The estimated values of ecosystem service functions under each service category for different reference years and their changes are shown in Table 8. The values of ecosystem service functions ranged from 0.02 to 28.5 million USD, 0.02 to 28.2 million USD, 0.03 to 26.9 million USD, and 0.01 to 28.5 million USD in 1986, 1998, 2007, and 2017, respectively. The highest value was recorded for nutrient cycling for the whole study period, while the lowest was gas regulation. In this study, the value of the supporting services is the highest, indicating that supporting services are the main driver of the ecosystem services in the Cham Chu region ecosystem.

The changes in ecosystem service functions between periods are showed in Figure 7 and Table 8. From 1986 to 1998, most ecosystem function values decrease, except for water supply (14.5% increase) and water regulation (15.0% increase). From 1998 to 2007, the most significant change was observed for water regulation (33.7% decrease), followed by water supply (33.0% decrease), biological control (24.9% increase), pollination (23.3% increase), and gas regulation (20.6% increase). Between 2007 and 2017, the highest change was observed in gas regulation with a decrease of 67.4%, followed by pollination and biological control, which accounted for 58.3% and 53.3%, respectively.

For the whole study period (1986 to 2017), the change in ecosystem service functions showed significant decreases in gas regulation, pollination, biological control, water regulation, water supply, and food production of 62.9%, 51.2%, 44.4%, 24.7%, 23.1%, and 13.0%, respectively.

3.5 Ecosystem service sensitivity analysis

From 1986 to 2017, the coefficient of sensitivity (CS) was lower than one in all cases, indicating that the total ESVs estimated in the study area were relatively inelastic regarding the modified conservative ecosystem value coefficients (Table 9). In this study, the CS ranged from 0.00 to 0.97, and changes in the total value of the ecosystem services ranged from 0.16% to 48.74%. Adjusting the value coefficient by 50% for forest land affected the estimated 2017 ESV more (±48.74%) than the 1986 value (±48.14%). Adjustment to the modified value coefficient for bush affected the estimated 1986, 1998, 2007, and 2017 ESVs by ±0.78%, ±0.63%, ±0.82%, and ±0.32%, respectively. Adjusting the water body coefficient by 50% affected the estimated 1986, 1998, 2007, and 2017 ESVs by ±1.09%, ±1.25%, 1.65%, and

0.79%, respectively. Adjusting the cropland coefficient barely affected the estimated ESV by ±0.16% for the whole study period. Despite inconsistencies in the adjusted value coefficients used in the study, the sensitivity analysis indicated that the ESV prediction was robust. The value coefficients had a substantial impact on the precision of the predicted improvement in ESV from 1986 to 2017, implying that our findings are reliable and that the ESV index used in the study is a good match.

Table 8. Value of ecosystem service functions under each service category for different reference years and their changes in the CCNR

Ecosystem services	ESV million USD/year				ESV changes (%)			
	1986	1998	2007	2017	1986-1998	1998-2007	2007-2017	1986-2017
Provisioning services								
Water supply	0.4	0.5	0.3	0.3	14.5	-33.0	0.3	-23.1
Food production	1.4	1.3	1.4	1.2	-2.1	2.8	-13.6	-13.0
Raw material	9.7	9.6	9.2	9.7	-1.2	-4.6	6.1	0.0
Genetic resources	1.3	1.3	1.2	1.3	-1.2	-4.6	6.1	0.0
Regulating services								
Water regulation	1.1	1.2	0.8	0.8	15.0	-33.7	-1.2	-24.7
Waste treatment	3.1	3.1	3.0	2.9	-1.0	-3.4	-3.8	-8.0
Erosion control	7.7	7.6	7.3	7.6	-1.2	-4.3	4.8	-0.9
Climate regulation	6.9	6.8	6.5	6.9	-1.2	-4.6	6.1	0.0
Biological control	0.1	0.1	0.2	0.1	-4.7	24.9	-53.3	-44.4
Gas regulation	0.02	0.02	0.03	0.01	-5.60	20.60	-67.40	-62.90
Disturbance regulation	0.2	0.2	0.1	0.2	-1.2	-4.6	6.1	0.0
Supporting services								
Nutrient cycling	28.5	28.2	26.9	28.5	-1.2	-4.6	6.1	0.0
Pollination	0.13	0.12	0.15	0.06	-5.00	23.30	-58.30	-51.20
Soil formation	0.3	0.3	0.3	0.3	-1.2	-4.3	5.0	-0.8
Cultural services								
Recreation	3.5	3.5	3.3	3.5	-1.0	-5.0	5.9	-0.4
Cultural	0.1	0.1	0.1	0.1	-1.2	-4.6	6.1	0.0
Total	64.4	63.9	60.7	63.4	-0.8	-5.1	4.5	-1.6

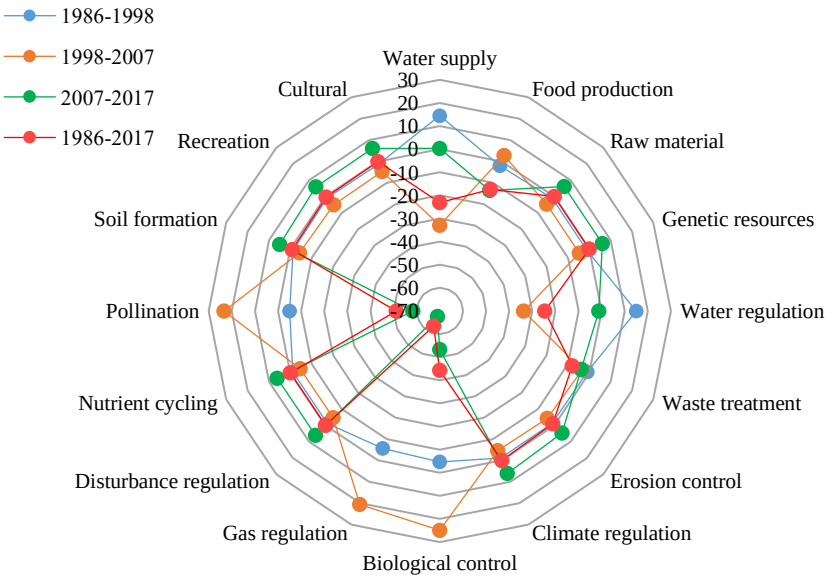

Figure 7. Changes in ecosystem service functions between the reference years in the percentage

Table 9. Changes in estimated total ESVs and CS

Change of ESV coefficient	1986		1998		2007		2017	
	%	CS	%	CS	%	CS	%	CS
Forest land ±50%	±48.14	0.96	±47.89	0.96	±47.94	0.96	±48.74	0.97
Bush ±50%	±0.78	0.02	±0.63	0.01	±0.82	0.02	±0.32	0.01
Cropland ±50%	±0.16	0.00	±0.16	0.00	±0.16	0.00	±0.16	0.00
Water body ±50%	±1.09	0.02	±1.25	0.03	±1.65	0.03	±0.79	0.02

3.6 The impact of LULC change on ecosystem service values

This research examined developments in ESVs over 30 years in the CCNR as a result of land cover dynamics. The total ecosystem service function value decreased in the first and second periods (1986-1998 and 1998-2007) then increased in the third period (2007-2017). The total ecosystem service function value in the entire study period still decreased. Among sixteen ecosystem services functions, gas regulation, pollination, biological control, water regulation, water supply, and food production functions experienced the most significant decline. These findings indicate the impact of LULC change on ecosystem function service in the area.

A significant change in the different land use types occurred between 1986 and 2007 in the Cham Chu region. Cropland and bareland increased, while forest land decreased. The changes in ESV of the land use types varied according to the changes in the area. The overall ecosystem service value declined during this period due to the degradation of forest land. The inefficiency of the State Forest Enterprises system for forest management during this period was the fundamental cause of the loss of forest land (MARD, 2001; Nguyen et al., 2001). USAID (2015) also stated that forest conversion to annual crops and commercial perennial plantations at household scale by local people and official forest conversion to infrastructure and commercial perennial plantations by both state-owned companies and private companies as a direct driving force for deforestation. Communities encroached on fields in order to obtain wood for fuel, building products, more arable land, and livestock feed, resulting in a slight decline in cover (Cochard et al., 2020). Between 2007 and 2017, the total estimated ESVs showed a slight increase resulting from the rise in forest land because the community and the government of Vietnam have implemented several interventions to modify the existing practices and reduce the effects of deforestation. Forest management in Vietnam is also moving towards greater participation of local citizens, especially indigenous communities, in managing forest resources, and reforestation policy also helps to explain the successes in increasing forest cover for the latter period in Vietnam (Tan, 2005).

3.7 Evaluation of ecosystem services and policy implication in Vietnam

Despite the fact that there are few studies in Vietnam on measuring total ESV, Table 10 shows a comparison of ecosystem services for forest ecosystems in protected areas in Vietnam in terms of total ESV per hectare. For comparison, a mangrove forest ecosystem in Thai Thuy Nature Reserve has a total ESV of 1,758 USD/ha (including provisioning, regulating, supporting, and cultural services) (ISPONRE, 2018), while forest ecosystems in Cat Tien Natural Park have a value of 726 USD/ha (including provisioning, regulating, and cultural services) (GECD, 2014). Meanwhile, Ca Mau mangrove forest ecosystem provisioning and regulating services are valued at up to 3,316 USD/ha (Vo et al., 2015). Although there are certain differences in the results of these studies because of different methods, the findings of this study using the value transfer method combined with the remote sensing gives a relative benefit that fits the particular context of Vietnam.

The overall assessment methodology in this study can be applied to the rapid assessment of ecosystem services for specific protected areas and regions, and be considered as the basis of land use planning and biodiversity conservation. While the value of global ecosystem services is estimated to be around 125-145 trillion USD for 2011 (in 2007 USD) (Costanza et al., 2014), the value of the ecosystems services in Vietnam is estimated at about 28.87 billion USD (WWF, 2013), equivalent to 16.8% of GDP in 2013. In fact, ecosystem services have not been appropriately considered in Vietnam in policymaking processes, while globally sustainable development policy is making more use of ecosystem services

valuation (Brondizio et al., 2019). Ecosystem services values are increasingly integrated into strategic environmental assessments and development policy for national and global conservation and resource management (Mukherjee et al., 2014).

Table 10. Comparison of total ESV for forest ecosystems in protected areas in Vietnam

Study sites/Area (Year of publication)	Total ESV (USD/ha)	Provisioning service (USD/ha)	Regulating service (USD/ha)	Supporting service (USD/ha)	Cultural service (USD/ha)	Main methods used and reference
CCNR/40,446 ha (2017)	1,569.2	309.1	457.6	713.5	89.0	Value transfer and GIS/RS
Cat Tien Natural Park/71,000 ha (2014)	726	39	668	-	11	Market price, cost-based, benefit transfer (GECD, 2014)
Ca Mau Mangrove Forest/187,533 ha (2015)	3,316	2,344	973	-	-	Market price, remote sensing (Vo et al., 2015)
Thai Thuy Mangrove Forest/13,100 ha (2016)	1,758	1,172	463	20	103	Market price, direct interview, value transfer (ISPONRE, 2018)

While the policy of payments for ecosystem services has strongly developed in North America and Europe, in Vietnam, this policy has only partly been demonstrated through payments for forest environmental services, mainly focusing on regulating services. Luong (2018) argued that the value of regulating services is about VND 1,700 billion for 2017 (74.1 million USD). This policy is also an important resource to support the conservation of forest ecosystems for local people. Although Vietnam has developed an essential legal basis related to the application of ecosystem services in policy, such as the Environment Law (No. 72/2020/QH14), which identifies the role of ecosystem services in development policy, or the Law on Forestry (No. 16/2017/QH14), which includes a policy on payment for forest environmental services, the lack of appropriate approaches and methodologies to quickly assess the value of ecosystem services limits the effects of these policies. Despite the limitations mentioned above, the results of this study also contribute to the implementation of biodiversity conservation policies through the assessment of ecosystem services in Vietnam.

4. CONCLUSION

The simple benefit transfer method was successfully applied to examine ecosystem service change due to land use and land cover change between 1986 and 2017 in Cham Chu nature reserve, Tuyen Quang Province, Vietnam. The study discovered that areas of forest land and water body were stable over time. Simultaneously, bare land, which did not provide any ecosystem service value, has continuously increased. This finding indicates the effects of land use and land cover change on ecosystem service values in the study area. Consequently, the total ecosystem service values decreased from 64.4 million USD in 1986 to 63.4 million USD in 2017. Also, ecosystem service functions under the provisioning, regulating, and supporting services of the Cham Chu nature reserve significantly decreased water supply, water regulation, biological control, gas regulation, and pollination. While the results of this study are quite consistent and comparable with the studies carried out so far in Vietnam, more importantly, this study is more systematic and assessed for a long period of time (1986-2017).

In conclusion, the current research framework can be used as a guideline to local governments for assessing ecosystem services values and functions in nature reserve areas. Additionally, the results of this study can provide essential information to support policymakers and decision-makers in managing and protecting the nature reserve area of the country. Furthermore, when ESVs are calculated using the simple benefit transfer method, the local coefficient value of ecosystem services should be investigated in more detail for each LULC type.

ACKNOWLEDGEMENTS

The authors would like to express their appreciation and gratitude to the anonymous reviewers and editors for their valuable comments, which helped

to improve the manuscript. This research was funded by the VNU Project of Science and Technology for the year of 2020, code QG.20.43 and the NAGAO Natural Environmental Foundation's Bio-ecological Nature Conservation Project in Mountainous Regions of Northern Vietnam.

REFERENCES

Abera W, Tamene L, Kassawmar T, Mulatu K, Kassa H, Verchot L, et al. Impacts of land use and land cover dynamics on ecosystem services in the Yayo coffee forest biosphere reserve, Southwestern Ethiopia. Ecosystem Services 2021;50:Article No.101338.

Alcamo J. Ecosystems and Human Well-being: A Framework for Assessment. Washington, USA: Island Press; 2003.

Bisui S, Roy S, Sengupta D, Bhunia GS, Shit PK. Assessment of ecosystem services values in response to land use/land cover change in tropical forest. In: Shit PK, Pourghasemi HR, Adhikary PP, Bhunia GS, Sati VP, editors. Forest Resources Resilience and Conflicts. Elsevier; 2021. p. 435-47.

Brondizio ES, Settele J, Díaz S, Ngo HT. Global Assessment Report on Biodiversity and Ecosystem Services of the Intergovernmental Science-Policy Platform on Biodiversity and Ecosystem Services. Bonn, Germany: IPBES secretariat; 2019.

Cham Chu Nature Reserve Management Board (CCMB). Forest and Production Statistics in Cham Chu Nature Reserve. Tuyen Quang, Vietnam: CCMB; 2020.

Chaudhary A, Kastner T. Land use biodiversity impacts embodied in international food trade. Global Environmental Change 2016;38:195-204.

Clement F, Amezaga JM. Afforestation and forestry land allocation in Northern Vietnam: Analysing the gap between policy intentions and outcomes. Land Use Policy 2009;26(2):458-70.

Cochard R, Nguyen VHT, Ngo DT, Kull CA. Vietnam's forest cover changes 2005-2016: Veering from transition to (yet more) transaction? World Development 2020;135:1-19.

Congalton RG, Green K. Assessing the Accuracy of Remotely Sensed Data: Principles and Practices. New York, USA: CRC Press; 2008.

Costanza R, de Groot R, Sutton P, van der Ploeg S, Anderson SJ, Kubiszewski I, et al. Changes in the global value of ecosystem services. Global Environmental Change 2014;26:152-8.

Dai LT, Ongsomwang S. Ecological suitability evaluation for conservation and development in Bac Kan Province, Vietnam. Applied Sciences 2019;9(24):531-60.

Dang KB, Burkhard B, Müller F, Dang VB. Modelling and mapping natural hazard regulating ecosystem services in Sapa, Lao Cai Province, Vietnam. Paddy and Water Environment 2018;16(4):767-81.

Tuyen Quang Provincial Department of Agriculture and Rural Development (DARD). Conservation and Development Planning for Cham Chu Nature Reserve. Tuyen Quang, Vietnam: Tuyen Quang People's Committee; 2014.

Dubreuil V, Debortoli N, Funatsu B, Nédélec V, Durieux L. Impact of land-cover change in the Southern Amazonia climate: A case study for the region of Alta Floresta, Mato Grosso, Brazil. Environmental Monitoring and Assessment 2012;184(2):877-91.

Fei L, Shuwen Z, Jiuchun Y, Liping C, Haijuan Y, Kun B. Effects of land use change on ecosystem services value in West Jilin since the reform and opening of China. Ecosystem Services 2018;31:12-20.

Fauna and Flora International (FFI). Field Report of Survey on Tonkin Snub-Nosed Monkey (*Rhinopithecus avunculus*) in Bac Kan, Thai Nguyen and Tuyen Quang Provinces. Hanoi, Vietnam: FFI Indochina Programme Office; 1999.

Fitzpatrick-Lins K. Comparison of sampling procedures and data analysis for a land-use and land-cover map. Photogrammetric Engineering and Remote Sensing 1981;47(3):343-51.

Fritzsche F, Zech W, Guggenberger G. Soils of the Main Ethiopian Rift Valley escarpment: A transect study. CATENA 2007;70(2):209-19.

Gashaw T, Tulu T, Argaw M, Worqlul AW, Tolessa T, Kindu M. Estimating the impacts of land use/land cover changes on ecosystem service values: The case of the Andassa watershed in the Upper Blue Nile Basin of Ethiopia. Ecosystem Services 2018;31:219-28.

German Federal Ministry for Economic Cooperation and Development (GECD). The Economic Value of Cat Tien National Park. Berlin, Germany: GECD; 2014.

General Statistics Office (GSO). General Statistical Yearbook of Vietnam. Hanoi, Vietnam: GSO; 2017.

Hai BT, Tu LN, Duong VT, Minh LD, Tham NT, Son NT. Supplementary data of insectivores (Mammalia, Eulipotyphla) in Vietnam. Journal of Biology 2019;41(2):393-407.

Hoang T, Covert H. New records of home range of Tonkin snub-nosed monkey (*Rhinopithecus avunculus* Dollman, 1912) in Khau Ca forest, Ha Giang Province. Academia Journal of Biology 2012;32(3):26-30.

Hong NT, Saizen I. Forest ecosystem services and local communities: Towards a possible solution to reduce forest dependence in Bach Ma National Park, Vietnam. Human Ecology 2019;47(3):465-76.

Huang A, Xu Y, Sun P, Zhou G, Liu C, Lu L, et al. Land use/ land cover changes and its impact on ecosystem services in ecologically fragile zone: A case study of Zhangjiakou City, Hebei Province, China. Ecological Indicators 2019; 104:604-14.

Hughes R. Sourcebook of Existing and Proposed Protected Areas in Vietnam. Hanoi, Vietnam: Vietnam Forestry Inventory and Planning Institute; 2001.

Huong TTT, Zeller M, Hoanh CT. The 'five million hectare reforestation program' in Vietnam: An analysis of its implementation and transaction costs: A case study in Hoa Binh Province. Quarterly Journal of International Agriculture 2014;53:341-75.

Institute of Strategy, Policy on Natural Resources and Environment (ISPONRE). Valuation of Ecosystem services in Pilot Wetland Protected Areas: A Case of Thai Thuy Coastal Wetland, Thai Binh Province. Hanoi, Vietnam: ISPONRE; 2018.

Israel GD. Determining Sample Size. Florida, USA: University of Florida Cooperative Extension Service, Institute of Food and Agriculture Sciences, EDIS; 1992.

Jensen JR. Introductory Digital Image Processing: A Remote Sensing Perspective. New Jersey, USA: Prentice Hall; 2005.

Khuc QV, Tran BQ, Meyfroidt P, Paschke MW. Drivers of deforestation and forest degradation in Vietnam: An exploratory analysis at the national level. Forest Policy and Economics 2018;90:128-41.

Kindu M, Schneider T, Teketay D, Knoke T. Changes of ecosystem service values in response to land use/land cover dynamics in Munessa-Shashemene landscape of the Ethiopian highlands. Science of the Total Environment 2016;547:137-47.

Kreuter UP, Harris HG, Matlock MD, Lacey RE. Change in ecosystem service values in the San Antonio area, Texas. Ecological Economics 2001;39(3):333-46.

Luong PH. Payment for forest environmental services: Current status and solutions. Journal of Science and Forestry 2018;1(2):5-12.

Mamat A, Halik Ü, Rouzi A. Variations of ecosystem service value in response to land-use change in the Kashgar Region, Northwest China. Sustainability 2018a;10(1):200-18.

Mamat Z, Halik Ü, Keyimu M, Keram A, Nurmamat K. Variation of the floodplain forest ecosystem service value in the lower reaches of Tarim River, China. Land Degradation and Development 2018b;29(1):47-57.

Ministry of Agriculture and Rural Development (MARD). State Forest Enterprises: Challenges and Development Opportunities. Hanoi, Vietnam: MARD; 2001.

Ministry of Agriculture and Rural Development (MARD). Handbook for Forestry: Orientation for Forestry Development. Hanoi, Vietnam: MARD; 2004.

Mukherjee N, Sutherland WJ, Dicks L, Hugé J, Koedam N, Dahdouh-Guebas F. Ecosystem service valuations of mangrove ecosystems to inform decision making and future valuation exercises. PloS One 2014;9(9):1-9.

Nguyen D, To M, Ha C, Trinh H, Nguyen K. Lam Nghiep Viet Nam 1945-2000 (Vietnamese Forestry 1945-2000). Hanoi, Viet Nam: Agricultural Publishing House; 2001.

Nguyen MD, Ancev T, Randall A. Forest governance and economic values of forest ecosystem services in Vietnam. Land Use Policy 2020;97:1-17.

Nguyen T, Oanh P, Phuong N, Xuyen D. Medicinal plant diversity at Cham Chu nature reserve area, Tuyên Quang Province. VNU Journal of Science: Natural Sciences and Technology 2018;34:41-5.

Ongsomwang S, Pattanakiat S, Srisuwan A. Impact of land use and land cover change on ecosystem service values: A case study of Khon Kaen City, Thailand. Environment and Natural Resources Journal 2019;17:43-58.

Paudyal K, Samsudin YB, Baral H, Okarda B, Phuong VT, Paudel S, et al. Spatial assessment of ecosystem services from planted forests in central Vietnam. Forests 2020;11(8):822-41.

Perloff J. Microeconomics: Theory and Applications with Calculus. London, United Kingdom: Pearson; 2016.

Pham C, Phan T, Do D, Nguyen T. New provincial records of genus Limnonectes (Amphibia: Anura: Dicroglossidae) from Vietnam. Journal of Biology 2019;41(1):169-76.

Plummer ML. Assessing benefit transfer for the valuation of ecosystem services. Frontiers in Ecology and the Environment 2009;7(1):38-45.

Ranzi R, Le TH, Rulli MC. A RUSLE approach to model suspended sediment load in the Lo River (Vietnam): Effects of reservoirs and land use changes. Journal of Hydrology 2012;422:17-29.

Reid WV, Mooney HA, Cropper A, Capistrano D, Carpenter SR, Chopra K, et al. Ecosystems and Human Well-Being-Synthesis: A Report of the Millennium Ecosystem Assessment. Washington, USA: Island Press; 2005.

Rimal B, Sharma R, Kunwar R, Keshtkar H, Stork NE, Rijal S, et al. Effects of land use and land cover change on ecosystem services in the Koshi River Basin, Eastern Nepal. Ecosystem Services 2019;38:Article No.100963.

Shivakoti G, Van Thanh M, Vien TD, Leisz SJ. Redefining Diversity and Dynamics of Natural Resources Management in Asia, Volume 2: Upland Natural Resources and Social Ecological Systems in Northern Vietnam. Elsevier; 2016.

Solomon N, Segnon AC, Birhane E. Ecosystem service values changes in response to land-use/land-cover dynamics in dry Afromontane forest in Northern Ethiopia. International Journal of Environmental Research and Public Health 2019;16(23):1-15.

Son VT. Food production and deforestation in the northern uplands: A cartographic approach. Geoinformatics 2003; 14(1):13-6.

Son VT, Truong DM, Phuong NTL. Relationship between forest cover changes, forestry conservation and development policies in Cham Chu species-habitat conservation reserve, Tuyen Quang Province. Scientific Workshop on Resource and Environmental Management and Sustainable Development of North-Western Region, Vietnam; 2020 Nov 5-7; Hanoi: Vietnam; 2020.

Sun J, Yang J, Zhang C, Yun W, Qu J. Automatic remotely sensed image classification in a grid environment based on the maximum likelihood method. Mathematical and Computer Modelling 2013;58(3):573-81.

Talukdar S, Singha P, Shahfahad, Mahato S, Praveen B, Rahman A. Dynamics of ecosystem services (ESs) in response to land use land cover (LU/LC) changes in the lower Gangetic plain of India. Ecological Indicators 2020;112:Article No.106121.

Tan NQ. Trends in forest ownership, forest resources tenure and institutional arrangements: are they contributing to better forest management and poverty reduction? The case of Vietnam [Internet]. 2005 [cited 2021 Jul 10]. Available from: https://www.fao.org/forestry/10582-08d5469cf92f69afa4aa73e8843aff998.pdf.

Thakkar AK, Desai VR, Patel A, Potdar MB. Post-classification corrections in improving the classification of land use/land cover of arid region using RS and GIS: The case of Arjuni watershed, Gujarat, India. The Egyptian Journal of Remote Sensing and Space Science 2017;20(1):79-89.

Tham NT, Tu LN, Duong VT, Hai BT, Duy ND, Abramov AV, et al. The first studies of small mammals of the Cham Chu and Bac Me nature reserves, North-Eastern Vietnam. Russian Journal of Theriology 2020;19(2):193-209.

Turan SÖ, Günlü A. Spatial and temporal dynamics of land use pattern response to urbanization in Kastamonu. African Journal of Biotechnology 2010;9(5):640-7.

United States Agency for International Development (USAID). Drivers of Deforestation in the Greater Mekong Sub-Region-Vietnam Country Report. Hanoi, Vietnam: Lowering Emissions in Asia's Forests (USAID LEAF); 2015.

Van der Ploeg S, de Groot RS. The TEEB Valuation Database-A Searchable Database of 1310 Estimates of Monetary Values of Ecosystem Service. Wageningen, Netherland: The Netherlands Foundation Sustainable Development; 2010.

Vo TQ, Künzer C, Oppelt N. How remote sensing supports mangrove ecosystem service valuation: A case study in Ca Mau Province, Vietnam. Ecosystem Services 2015;14:67-75.

Wetterwald O, Zingerli C, Sorg J-P. Non-timber forest products in Nam Dong District, Central Vietnam: Ecological and economic prospects. Schweizerische Zeitschrift Fur Forstwesen 2004;155:45-52.

Wood A, Stedman-Edwards P, Mang J. The Root Causes of Biodiversity Loss. London, United Kingdom: Routledge; 2013.

World Wide Fund for Nature (WWF). The Economic Value of Ecosystem Services in the Mekong Basin: What We Know, and What We Need to Know. Gland, Switzerland: WWF; 2013.

Zhou G, Zhou X, Zhang T, Du Z, He Y, Wang X, et al. Biochar increased soil respiration in temperate forests but had no effects in subtropical forests. Forest Ecology and Management 2017;405:339-49.

Alteration of Fractionation and Bioavailability of Arsenic (As) in Paddy Soil under Transition from Aerobic to Anaerobic Conditions

Apichaya Duangthong[1] and Seelawut Damrongsiri[1,2,3*]

[1]*Environmental Research Institute (ERIC), Chulalongkorn University, Bangkok 10330, Thailand*
[2]*Center of Excellence on Hazardous Substance Management (HSM), Chulalongkorn University, Bangkok 10330, Thailand*
[3]*Research Unit of Green Mining Management, Chulalongkorn University, Bangkok 10330, Thailand*

ARTICLE INFO

Received: 4 Aug 2021
Received in revised: 24 Oct 2021
Accepted: 9 Nov 2021
Published online: 16 Nov 2021
DOI: 10.32526/ennrj/20/202100150

Keywords:
Arsenic/ Paddy soil/ Fractionation/ Bioavailability/ Anaerobic

*** Corresponding author:**
E-mail: seelawut.da@chula.ac.th

ABSTRACT

The impact of the change from aerobic to anaerobic immersed soil conditions on arsenic (As) fractionation (Tessier's method) and its bioavailability (ethylene diamine tetraacetic acid extractable) were assessed. As-contaminated paddy soils were tested by laboratory simulation experiments. The samples were aerobic, with 35-49 mg/kg of As at low bioavailability (<2%). Most As was distributed in the stable fraction (77%), followed by As bound to ferric and manganese oxide (17%) and organic compounds (5%), while the mobile fraction (exchangeable and mildly acid-soluble) was limited (1%). After one month under anaerobic simulation, redox potential reduced to less than zero (-32 to -124 mV). The stable fraction of As decreased (-17%), while the mobile fraction increased (+16%) and As bioavailability also increased (+26% total As). Increase in the As mobile fraction was associated with freshly precipitated compounds. The As content in the soil altered from a stable fraction to an available fraction when confined in an anaerobic environment for a long period. Results indicated that agricultural methods which promoted anaerobic conditions in As-contaminated soil should be avoided.

1. INTRODUCTION

Arsenic (As) is a highly toxic and carcinogenic metalloid that occurs naturally as a component of several minerals in the Earth's crust. The geochemical map published by Thailand's Department of Mineral Resources shows that As is found at >0.5 mg/kg in rocks covering more than one-third of the land surface area. The background concentration (95th percentile) of As in soil in Thailand was determined at <26 mg/kg by the Department of Land Development (2015).

In Khao Luang, a sub-district of Loei Province in Northeastern Thailand, 70% of the land area is used for agriculture. The main crops are rice, corn, sugar cane, soybean and para rubber trees. The As background geochemical value in this province is higher than in the surrounding areas. Comprehensive measurements around Khao Luang determined As concentrations in the soil ranging between 2 and 95 mg/kg (Department of Primary Industries and Mines, 2012). Consumption of food contaminated with As via soil-plant transfer is considered to be the major pathway of human exposure to toxic elements (Foucault et al., 2013), suggesting that ingesting agricultural products from this area is risky. Arsenic that can be readily transported from soil to agricultural plants is known as bioavailable As. The bioavailability of As in soil depends on how its chemical speciation and fractionation are altered by several dynamic biogeological soil processes (Khalid et al., 2017). Hartley and Dickinson (2010) demonstrated that the mobility of As in sediments was higher when the redox potential (Eh) was less than 100 mV. Rice farming has the potential to turn soil conditions anaerobic due to waterlogging and microbial activity. The Eh of paddy soil can be as low as -200 mV (Yu et al., 2016), thereby promoting the mobility of As and increasing its bioavailability. Water management in paddy fields reduced the Eh of paddy soil, resulting in higher As uptake in the rice (Zia et al., 2017; Cao et al., 2020). Wang et al. (2015) and Liu et al. (2015) demonstrated that the bioavailable fraction of As was not associated

Citation: Duangthong A, Damrongsiri S. Alteration of fractionation and bioavailability of arsenic (As) in paddy soil under transition from aerobic to anaerobic conditions. Environ. Nat. Resour. J. 2022;20(1):89-95. (https://doi.org/10.32526/ennrj/20/202100150)

with ferric hydrous oxide or As-bearing minerals, while Yu et al. (2016) demonstrated that reductive release of As was related to the As fraction bound to iron compounds in the soil and linked to iron redox cycling induced by wet/dry paddy cycles.

Sequential extraction is a method that can be applied to indicate stability or mobility of As in the soil, and classifying the fractionation of As would help to understand the mechanisms of its behavior. Thus, our research interest involved investigating the changes when paddy soil ambient condition was changed from an aerobic to an anaerobic environment. Anaerobic conditions were induced in the laboratory using As-containing paddy soil as the sample. Soil properties, As fractionation and its bioavailability were quantified to assess the consequences of lowering soil Eh in the context of As paddy soil mobility. Our results will improve the current understanding of As movement in soil under strong anaerobic environmental conditions.

2. METHODOLOGY

2.1 Sample collection and preparation

The study area is located in Khao Luang sub-district, Loei Province, Thailand. The soil in this area is classified as Loei-soil series that are formed from residuum and local granite colluvium. The soil is clay or clay loam with a dark reddish-brown color. Field pH of the topsoil of this soil series was 6.0 (Malairotsiri et al., 2004). Four composite soil samples were collected from four paddies (A, B, C, and D) in the Nam-Huai Canal area during July 2017. In each paddy, four topsoil samples (0-20 cm) were collected using a shovel and kept in Ziplock bags in cool conditions before delivery to the laboratory. The soil samples were separated into two parts. One part was dried at 40°C and kept as a dry sample in a desiccator. Dry samples were used to analyze organic matter (OM) and total concentration of As and Fe. The other part of the composite sample was kept in a freezer as a field moist sample. Field moist samples were used to analyze soil pH, redox potential (Eh), acid volatile sulfide (AVS), fractionation and bioavailability of As to minimize the phase transition of metals in the sample (Qi et al., 2014).

2.2 Experiment

The soil samples were analyzed in a laboratory for pH, Eh, OM, AVS, total As, and Fe, fractionation of As and bioavailable As before undergoing a simulation experiment. Two simulation reactors were used for each paddy. The experiment was designed to observe changes in As fractionation and bioavailability, assuming that the paddy soil was in an immersed and strongly-reduced condition for one month. The goal of this simulation was to measure the negative Eh value and AVS that developed in a highly-reduced paddy soil environment (Yu et al., 2016).

The anaerobic simulation was conducted in batch mode. A 500-mL amber glass bottle was used as the reactor and filled with a 300 g dry soil sample from each paddy. Then, 350 mL of Nutrient Broth (MP Biomedicals) with solution strength equivalent to 5,000 mg/L of COD was applied to induce biogeochemical activity. An aliquot of 1.329 g of sodium sulfate (Na_2SO_4) (99%, Merck) was added as the seed for sulfide development, equivalent to 1,000 mg/kg of sulfide as the range of AVS in natural anaerobic soil (30-1,600 mg/kg, Essington, 2004; Kabata-Pendias, 2001). Each reactor bottle was tightly capped and kept in the dark for one month at room temperature.

2.3 Sample analysis

Total As and Fe, pH, Eh, AVS and OM were quantified. Tessier's sequential extraction method (Tessier et al., 1979) was applied to observe the fractionation of As in the soil. EDTA (ethylene diamine tetraacetic acid, 100%, Carlo Erba) extraction was used to determine the bioavailability of As in the soil as this expressed a good relationship to As in plants (Gregori et al., 2004). All analyses and measurements were performed in triplicate.

Details of the analytical methods are described in the Supplementary Material. Briefly, pH and Eh of the soil samples were determined by soaking a pH and ORP probe in the soil suspension (soil:water, 1:1 w/v) (U.S. EPA 9045D for pH and ASTM G200-09 for ORP). OM was quantified by the Walkley-Black modified acid-dichromate digestion-$FeSO_4$ titration method. The AVS in the sample was quantified by a method modified from van Griethuysen et al. (2002). Microwave digestion was applied to prepare the sample for total concentration measurement of As and Fe, while inductively coupled plasma optical emission spectroscopy was used to quantify As and Fe. The recovery of As was tested using European Reference Material (ERM-CC141), ranging from 91% to 103%.

The Tessier extraction procedure was applied for sequential extraction because this method interrelated well with the environmental conditions. Soil digestion using nitric acid and hydrochloric

acid was applied for the final extraction step, and extractant from each step was measured for As. Following this approach, the As in the soil was divided into five fractions as exchangeable fraction (F1), mild acid-soluble fraction (F2), reducible fraction (F3), oxidizable fraction (F4) and residual fraction (F5). Pseudo-total concentrations of As were evaluated as the sum of every fraction, with recovery checked against total concentration and ranging from 93% to 130%.

2.4 Data analysis

Statistical analyses were conducted using the SPSS program (ver. 22). The t-test was applied to examine differences between As fractionation before and after anaerobic simulation, and p-value 0.05 was used to determine significance.

3. RESULTS

3.1 Characteristics of paddy soil samples

The collected topsoil samples comprised brown clay loam with a natural soil smell. Soil characteristics are shown in Table 1. Sample pH values were similar to area background values and classified as fertile paddy soil (Rice Research Institute, 2004) by their OM content. Eh values of the soil samples were greater than +400 mV, indicating aerobic condition that oxygen was used as a terminal electron acceptor in biological transformation (Mitsch and Gosselink, 2015). AVS content was not detected (<100 mg/kg) consistent with the high Eh values.

Arsenic concentrations in the soil samples varied from 35 to 49 mg/kg, concurring with previous reports (Department of Primary Industries and Mines, 2012), while bioavailable As ranged 0.66-0.79 mg/kg (1.6-2.1% of total As) (Figure 1). The Tessier fractionation of As in soil samples is shown in Figure 2. Fractionation of As in all initial paddy soils was similar and mainly distributed in F5 (77±5%), followed by F3 (17±5%), F4 (5.0±1.3%), F1 (0.050±0.048%) and F2 (0.56±0.62%).

3.2 Characteristics of paddy soil samples after anaerobic simulation

After one month of simulation, soil conditions in each reactor changed as expected (Table 1). The Eh values of the systems decreased to less than zero and AVS developed as the goal of this simulation. The pH values changed from acid to neutral, concurring with other research studies (Sahrawat, 2015; Yamaguchi et al., 2011). The OM content did not change significantly (2.21-2.36%).

Table 1. Characteristics of paddy soil samples before and after anaerobic simulation

Initial paddy soil				
Characteristic	A	B	C	D
Total As (mg/kg)	40.95±0.61	36.59±2.75	48.65±0.47	35.14±1.46
Total Fe (g/kg)	33.13±1.56	27.20±2.07	29.56±1.32	22.94±1.95
Eh (mV)	614±9	560±2	676±9	595±13
pH	5.28±0.01	6.00±0.02	5.59±0.06	5.93±0.16
AVS (mg/kg)	nd	nd	nd	nd
OM (%)	2.60±0.16	2.07±0.12	2.18±0.08	2.31±0.18
Bioavailable As (mg/kg)	0.79±0.02	0.66±0.01	0.76±0.01	0.73±0.03
Paddy soil after anaerobic simulation				
Characteristic	A	B	C	D
Total As (mg/kg)	39.49±3.14	33.19±1.90	40.42±5.73	36.66±1.45
Total Fe (g/kg)	33.70±2.97	26.05±1.94	30.40±2.12	22.81±2.68
Eh (mV)	-124±9	-95±12	-32±14	-69±32
pH	7.28±0.01	7.37±0.05	7.55±0.02	7.34±0.02
AVS (mg/kg)	559±181	662±268	1,136±170	962±184
OM (%)	2.29±0.04	2.21±0.14	2.22±0.10	2.36±0.04
Bioavailable As (mg/kg)	11.83±2.85	9.90±1.55	11.24±1.38	11.47±1.34

Note: nd=not detected. Limit of quantification for AVS was 100 mg/kg.

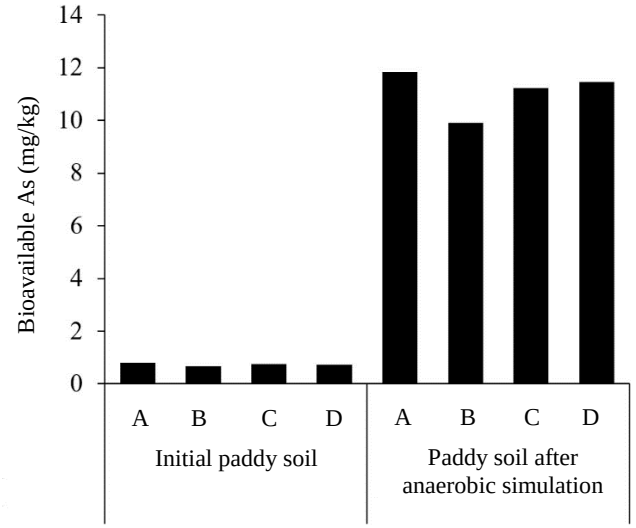

Figure 1. Bioavailability of Arsenic in paddy soil samples before and after anaerobic simulation

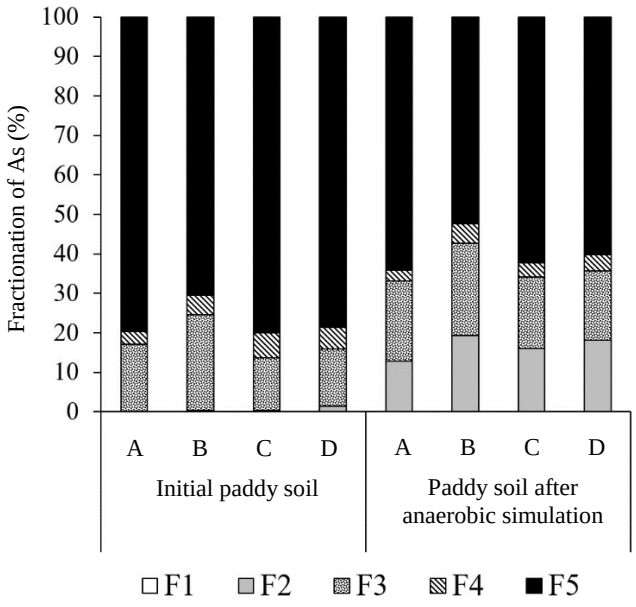

Figure 2. Fractionation of Arsenic in paddy soil samples before and after anaerobic simulation

Concentrations of As and Fe in the soil before and after the simulation were similar, while As in the supernatant was not measurable (<0.005 mg/L). Bioavailable As of the anaerobic paddy soil samples increased markedly from 0.66-0.79 mg/kg to 9.9-11.8 mg/kg (23-32% of total As) (Figure 1). The F2 and F5 values of As in paddy soil altered remarkably, while F1, F3, and F4 did not change significantly ($p>0.05$). The As content in F5 decreased from 77±5% to 60±5%, whereas As in F2 increased from 0.56±0.62% to 17±3% (Figure 2).

4. DISCUSSION

In the soil samples, As was mainly distributed in F5, indicating the geogenic origin of As in this area (Fu et al., 2011; Wang et al., 2015), which was considered stable**.** Due to the As in mobile forms, As bound to amorphous oxides and bound to organic matters were eliminated during the 1st to 4th extraction step. The As content in F5 of Tessier's fractionation likely comprised of As-sulfide minerals and well-crystallized forms of Fe and As. Drahota and Filippi (2009) and Kim et al. (2014) found that the major As-sulfide minerals in the mining area were arsenopyrite, orpiment and arsenic-bearing pyrite, while their main weathered minerals were well-crystalized Fe arsenates (scorodite) and As associated with well-crystalized Fe oxides generally found in naturally As-rich soil. In this study, based on the soil sample characteristics, we presumed that As in F5 was likely predominated by well-crystalized weathered minerals.

Similar to other studies, despite the stable form of As in the soil, As bound to amorphous ferric oxide formed the major fraction of As (Baig et al., 2009; Farooq et al., 2010; Devesa-Rey et al., 2008; Hsu et al., 2012; Kim et al., 2014; Wang et al., 2015). Natural soil generally contains high amounts of ferric oxide that can adsorb various trace elements by various mechanisms (Hooda, 2010). The distribution of As in our paddy soil samples conformed to trends that As in F3 was the second major fraction.

The As in F4 was released from oxidizable components in the soil as organic compounds and some sulfide compounds. However, the AVS in this soil sample was not detectable. As content in F4 was believed to be bound to organic compounds. Similar to other studies, the As content in F4 was a minor fraction (Baig et al., 2009; Farooq et al., 2010; Fu et al., 2011). The As in F1 was the exchangeable fraction, while F2 contained As that was readily releasable by mild acid conditions, such as As bound to carbonate compounds or fresh precipitates. Both these fractions contributed less than 1% of the total As in the soil samples.

After one month of anaerobic induction by microbial activity, only As in F5 (stable fraction) and F2 (mild acid-soluble fraction) changed. A 17% decrease of As in F5 was observed, responding to a 16% increase of As in F2. This change of As fractionation indicated the release and resorption of As among the soil materials. However, we did not anticipate any change of As in F5 but expected F3

(bound to amorphous Fe oxide) to decrease via the iron reduction process.

Some toxic heavy metals become non-mobile under anaerobic environmental conditions via sulfidation (Hartley and Dickinson, 2010), but As can be altered to mobile forms (Kumarathilaka et al., 2018) or released to an aqueous solution (Hartley and Dickinson, 2010; Xue et al., 2020; Zhang et al., 2019). The released As content correlated well with released iron as ferrous (Xue et al., 2020). The iron redox cycle is governed by wet/dry cycles in paddy fields. The general explanation is that the source of released As is associated with ferric hydrous oxides in the soil (Hashimoto and Kanke, 2018; Rinklebe et al., 2016; Xue et al., 2020; Yamaguchi et al., 2011). Amorphous ferric hydrous oxide plays a much larger role in this dynamic environment than well-crystallized forms, with greater sensitivity toward released/resorbed ions in soil-water systems due to greater surface area and surface activity (Yang et al., 2020). It is reductively dissolute during wet periods and oxidatively re-formed to be the amorphous ferric hydrous oxide state during dry periods (Winkler et al., 2018). Well-crystallized forms of ferric hydrous oxide are less sensitive to both redox reactions and release/resorption. Once dissolute, it cannot easily reform under general paddy conditions (Yang et al., 2020). Therefore, major As contents released and resorbed normally relate to amorphous ferric hydrous oxides. Nevertheless, only a small fraction of ferric hydrous oxide in the soil (e.g., surface of materials) contributes to this redox cycle, while most remains to resorb released ions. Fractionation of metals (and metalloids) associated with ferric hydrous oxide decreases, remains unchanged or increases when immersed in anaerobic conditions, depending on complex interactions between the many ions in the soil (Damrongsiri, 2018). This might explain why the F3 As content did not change significantly.

The stable form of As is less sensitive to environmental degradation. A recent study on the effects of farming on As-contaminated land by Yang et al. (2020) pointed out that scorodite can be reductively dissolved in the paddy environment. Arsenopyrites, which are stable, were can be significantly reduced and dissolved under anaerobic conditions (Kawa et al., 2019). Therefore, we presumed that both well-crystallized forms of As and Fe and arsenic sulfide minerals could be reductively dissolved, possibly explaining why the As content in F5 decreased during anaerobic incubation.

Once released, As is available for further reaction in anaerobic soil-water systems and re-associates with other soil materials. These resorbed materials and co-precipitates of As in soil initially appear as an early fraction, having loosely bound (Lu et al., 2019; Zhang et al., 2019). In our Eh-pH anaerobic system, dissolved As was near the theoretical transition line of $H_2AsO_4^-$, $HAsO_4^{2-}$, As_2O_3, and As_2S_3 in As-S-O-H systems (Brookins, 1988) and trending to become $HAsO_4^{2-}$ (As(V)); however, the speciation of As in soil is far more complex. In soil under anaerobic conditions, As(V) is released when As-bearing ferric hydrous oxide is dissolute. Some released As(V) is reduced to As(III) by microorganisms that can reduce both ferric materials and As(V) (Yu et al., 2016). Therefore, in an anaerobic paddy soil system, a large amount of As is in form of As(III) (Yamaguchi et al., 2011; Xu et al., 2016).

Under an anaerobic water-soil system, As(V) precipitates as ferric arsenate and ferrous arsenate (Fan et al., 2014). Beside, both As(V) and As(III) sorb to remaining ferric hydrous oxide and many freshly formed solids (Coker et al., 2006; Fan et al., 2014; Khalid et al., 2017). As could adsorbed to siderite (ferrous carbonate, $FeCO_3$) (Guo et al., 2013), troilite (ferrous sulfide, FeS) and pyrite (ferrous disulfide, FeS_2) (Bostick and Fendorf, 2003). In our anaerobic induction experiment, released As was reformed into F2 that was likely combination of these reviewed forms.

The very low bioavailability of As in our collected soil samples may relate to the very low distribution of As in F1 and F2. After one month of anaerobic induction, only As in F2 increased, responding directly to the increased bioavailability of As in the soil. In general, the bioavailability of elements relates to their mobile fraction (e.g., F1 and F2 of Tessier's fractionation). Liu et al. (2015) investigated the relationship between As in rice and the fractionation of As in soil. They found a positive correlation between As in rice and F1 and F2 of Wenzel's fractionation (non-specifically sorbed fraction and specifically sorbed fraction) of As in soil but a negative correlation with As bound to amorphous and crystallized iron oxide fraction and stable fraction. A similar result was shown by Wang et al. (2015). They used $NaHCO_3$ extractable As to indicate As bioavailability and investigated its relationship with the fractionation of As in soil, while Yu et al. (2017) demonstrated that the application of iron compounds in soil significantly decreased As accumulation in rice. These studies confirmed that, under anaerobic

condition, bioavailable As in soil was freshly precipitated As compounds, As re-adsorbed onto soil materials and As associated with freshly formed solids.

5. CONCLUSION

Samples of As-contaminated soil were collected and used in a simulation experiment. The soil samples exhibited aerobic conditions with 35-49 mg/kg As. The As was mainly distributed as a stable fraction, with a limited mobile fraction (<1%). The bioavailability of As was also very low (<2%). After one month of anaerobic incubation, the stable fraction of As (F5) in soil decreased significantly and reformed as As in the mobile fraction (F2), corresponding to an increase in bioavailability. Results indicated that the stable form of As in soil was released under an anaerobic environment. The released As then precipitated, bounded to soil materials or bounded to freshly-precipitated compounds. Results indicated that the bioavailability of As in paddy soil increased when the soil was subjected to anaerobic conditions for a long period. Therefore, agricultural activity that causes anaerobic induction in As-contaminated soil should be avoided. Cultivation of other crops without a waterlogging period or non-food plants should be considered.

ACKNOWLEDGEMENTS

The authors thank the S&T Postgraduate Education and Research Development Office (PERDO) for the financial support and the Ratchadaphiseksomphot Endowment Fund, Chulalongkorn University for the Research Unit of Green Mining Management.

REFERENCES

Baig JA, Kazi TG, Arain MB, Shah AQ, Sarfraz RA, Afridi HI, et al. Arsenic fractionation in sediments of different origins using BCR sequential and single extraction methods. Journal of Hazardous Materials 2009;167:745-51.

Bostick BC, Fendorf S. Arsenite sorption on troilite (FeS) and pyrite (FeS_2). Geochimica et Cosmochimica Acta 2003; 67(5):909-21.

Brookins D. Eh-pH Diagrams for Geochemistry. Berlin, Germany: Springer-Verlag; 1988.

Cao Z, Pan J, Yang Y, Cao Z, Xu P, Chen M, et al. Water management affects arsenic uptake and translocation by regulating arsenic bioavailability, transporter expression and thiol metabolism in rice (*Oryza sativa* L.). Ecotoxicology and Environmental Safety 2020;206:Article No. 111208.

Coker VS, Gault AG, Pearce CI, Van der Laan G, Telling ND, Charnock JM, et al. XAS and XMCD evidence for species-dependent partitioning of arsenic during microbial reduction of ferrihydrite to magnetite. Environmental Science and Technology 2006;40:7745-50.

Damrongsiri S. Transformation of heavy metal fractionation under changing environments: A case study of a drainage system in an e-waste dismantling community. Environmental Science and Pollution Research 2018;25:11800-11.

Department of Land Development. State of Soil and Land Resources of Thailand. Bangkok, Thailand: The Agricultural Cooperative Federation of Thailand; 2015 (in Thai).

Department of Primary Industries and Mines. The Survey on Spatial Distribution and Source of Heavy Metal Contamination in the Phu Thap Fah Gold Deposit, Khao Luang Subdistrict, Wang Saphung District, Loei Province. Bangkok, Thailand: Environmental Research Institute; 2012 (in Thai).

Devesa-Rey R, Paradelo R, Díaz-Fierros F, Barral MT. Fractionation and bioavailability of arsenic in the bed sediments of the Anllóns River (NW Spain). Water, Air, and Soil Pollution 2008;195(1-4):189-99.

Drahota P, Filippi M. Secondary arsenic minerals in the environment: A review. Environment International 2009; 35:1243-55.

Essington ME. Soil and Water Chemistry: An Integrative Approach. Florida, USA: CRC Press LLC; 2004.

Fan JX, Wang YJ, Liu C, Wang LH, Yang K, Zhou DM, et al. Effect of iron oxide reductive dissolution on the transformation and immobilization of arsenic in soils: New insights from X-ray photoelectron and X-ray absorption spectroscopy. Journal of Hazardous Materials 2014;279:212-9.

Farooq SH, Chandrasekharam D, Berner Z, Norra S, Stuben D. Influence of traditional agricultural practices on mobilization of arsenic from sediments to groundwater in Bengal delta. Water Research 2010;44:5575-88.

Foucault Y, Lévéque T, Xiong T, Schreck E, Austruy A, Shahid M, et al. Green manure plants for remediation of soils polluted by metals and metalloids: Ecotoxicity and human bioavailability assessment. Chemosphere 2013;93(7):1430-5.

Fu Y, Chen M, Bi X, He Y, Ren L, Xiang W, et al. Occurrence of arsenic in brown rice and its relationship to soil properties from Hainan Island, China. Environmental Pollution 2011; 159:1757-62.

Gregori I, Fuentes E, Olivares D, Pinochet H. Extractable copper, arsenic and antimony by EDTA solution from agricultural Chilean soils and its transfer to alfalfa plants (*Medicago sativa* L.). Journal of Environmental Monitoring 2004;6(1):38-47.

Guo H, Ren Y, Liu Q, Zhao K, Li Y. Enhancement of arsenic adsorption during mineral transformation from siderite to goethite: Mechanism and application. Environmental Science and Technology 2013;47:1009-16.

Hartley W, Dickinson NM. Exposure of an Anaerobic and contaminated canal sediment: Mobility of metal(loid)s. Environmental Pollution 2010;158(3):649-57.

Hashimoto Y, Kanke Y. Redox changes in speciation and solubility of arsenic in paddy soils as affected by sulfur concentrations. Environmental Pollution 2018;238:617-23.

Hooda PS. Trace Elements in Soils. United Kingdom: Blackwell Publishing Ltd; 2010.

Hsu WM, His HC, Huang YT, Liao CS, Hseu ZY. Partitioning of arsenic in soil-crop systems irrigated using groundwater: A case study of rice paddy soils in southwestern Taiwan. Chemosphere 2012;86:606-13.

Kabata-Pendias A. Trace Elements in Soils and Plants. Florida, USA: CRC Press LLC; 2001.

Kawa YK, Wang J, Chen X, Zhu X, Zeng XC, Wang Y. Reductive dissolution and release of arsenic from arsenopyrite by a novel arsenate-respiring bacterium from the arsenic-contaminated soils. International Biodeterioration and Biodegradation 2019;143:Article No. 104712.

Khalid S, Shahid M, Niazi NK, Rafiq M, Bakhat HF, Imran M, et al. Arsenic behaviour in soil-plant system: Biogeochemical reactions and chemical speciation influences. In: Anjum NA, Gill SS, Tuteja N, editors. Enhancing Cleanup of Environmental Pollutants Volume 2: Non-Biological Approaches. Switzerland: Springer International Publishing AG; 2017. p. 97-140.

Kim EJ, Yoo JC, Baek K. Arsenic speciation and bioaccessibility in arsenic-contaminated soils: Sequential extraction and mineralogical investigation. Environmental Pollution 2014;186:29-35.

Kumarathilaka P, Seneweera S, Meharg A, Bundschuh J. Arsenic speciation dynamics in paddy rice soil-water environment: sources, physico-chemical, and biological factors: A review. Water Research 2018;140:403-14.

Liu C, Yu HY, Liu C, Li F, Xu X, Wang Q. Arsenic availability in rice from a mining area: Is amorphous iron oxide-bound arsenic a source or sink? Environmental Pollution 2015; 199:95-101.

Lu G, Tian H, Wang Z, Li H, Mallavarapu M, He W. The distribution of arsenic fractions and alkaline phosphatase activities in different soil aggregates following four months As(V) ageing. Chemosphere 2019;236:Article No. 124355.

Malairotsiri K, Sujinai A, Huntrakun K. Characterization of Established Soil Series in the Northeast Region of Thailand Reclassified According to Soil Taxonomy 2003. Bangkok, Thailand: Department of Land Development; 2004 (in Thai).

Mitsch W, Gosselink J. Wetlands. 5th Ed. New York, USA: John Wiley and Sons; 2015.

Qi Y, Huang B, Darilek JL. Effect of drying on heavy metal fraction distribution in rice paddy soil. PLoS ONE 2014; 9(5):e97327.

Rice Research Institute. Guideline on the Application of Chemical Fertilizer Based on Soil Analytical Result. Bangkok, Thailand: Rice Department; 2004 (in Thai).

Rinklebe J, Shaheen SM, Yu K. Release of As, Ba, Cd, Cu, Pb, and Sr under pre-definite redox conditions in different rice paddy soils originating from the USA and Asia. Geoderma 2016;270:21-32.

Sahrawat KL. Redox potential and pH as major drivers of fertility in submerged rice soils: A conceptual framework for management. Communications in Soil Science and Plant Analysis 2015;46(13):1597-606.

Tessier A, Campbell PGC, Bisson M. Sequential extraction procedure for the speciation of particulate trace metals. Analytical Chemistry 1979;51(7):844-51.

Van Griethuysen C, Gillissen F, Koelmans AA. Measuring acid volatile sulphide in floodplain lake sediments: Effect of reaction time, sample size and aeration. Chemosphere 2002;47:395-400.

Wang Y, Zeng X, Lu Y, Su S, Bai L, Li L, et al. Effect of aging on the bioavailability and fractionation of arsenic in soils derived from five parent materials in a red soil region of Southern China. Environmental Pollution 2015;207:79-87.

Winkler P, Kaiser K, Thompson A, Kalbitz K, Fiedler S, Jahn R. Contrasting evolution of iron phase composition in soils exposed to redox fluctuations. Geochimica et Cosmochimica Acta 2018;235:89-102.

Xu L, Wu X, Wang S, Yuan Z, Xiao F, Ming Y, et al. Speciation change and redistribution of arsenic in soil under anaerobic microbial activities. Journal of Hazardous Materials 2016; 301:538-46.

Xue S, Jiang X, Wu C, Hartley W, Qian Z, Luo X, et al. Microbial driven iron reduction affects arsenic transformation and transportation in soil-rice system. Environmental Pollution 2020;260:Article No. 114010.

Yamaguchi N, Nakamura T, Dong D, Takahashi Y, Amachi S, Makino T. Arsenic release from flooded paddy soils is influenced by speciation, Eh, pH, and iron dissolution. Chemosphere 2011;83:925-32.

Yang PT, Hashimoto Y, Wu WJ, Huang JH, Chiang PN, Wang SL. Effects of long-term paddy rice cultivation on soil arsenic speciation. Journal of Environmental Management 2020;254: Article No. 109768.

Yu HY, Li FB, Liu CS, Huang W, Liu TX, Yu WM. Iron redox cycling coupled to transformation and immobilization of heavy metals: implications for paddy rice safety in the red soil of South China. Advances in Agronomy 2016;137:279-317.

Yu HY, Wang X, Li F, Li B, Liu C, Wang Q, et al. Arsenic mobility and bioavailability in paddy soil under iron compound amendments at different growth stages of rice. Environmental Pollution 2017;224:136-47.

Zhang T, Zeng X, Zhang H, Lin Q, Su S, Wang Y, et al. The effect of the ferrihydrite dissolution/transformation process on mobility of arsenic in soils: Investigated by coupling a two-step sequential extraction with the diffusive gradient in the thin films (DGT) technique. Geoderma 2019;352:22-32.

Zia Z, Bakhat HF, Saqib ZA, Shah GM, Fahad S, Ashraf MR, et al. Effect of water management and silicon on germination, growth, phosphorus and arsenic uptake in rice. Ecotoxicology and Environmental Safety 2017;144:11-8.

Maceral Association in Coal-bearing Formation of Mae Than Coal Mine in Lampang, Thailand - Implication for Depositional Environment

Thunyapat Sattraburut[1*] and Benjavun Ratanasthien[2]

[1]Faculty of Environment and Resource Studies, Mahidol University, Nakhon Pathom 73170, Thailand
[2]Department of Geological Sciences, Faculty of Science, Chiang Mai University, Chiang Mai 50200, Thailand

ARTICLE INFO

Received: 30 Aug 2021
Received in revised: 29 Oct 2021
Accepted: 9 Nov 2021
Published online: 23 Nov 2021
DOI: 10.32526/ennrj/20/202100166

Keywords:
Maceral/ Coal petrography/ Mae Than/ Miocene/ Lignite/ Paleoclimate

*** Corresponding author:**
E-mail: thunyapat.sat@mahidol.ac.th

ABSTRACT

The Mae Than Basin in Lampang Province contains low-ranked coal reserves of northern Thailand. Coal seams and ball clays were mined in the southern part of the basin. This study focuses on the coal petrography of coal samples collected from the upper coal seam in the Mae Than Coal Mine. Both the organic and inorganic constituents provide information on the nature and characteristics of the coal, reflecting the physical and chemical behaviors of coal. Petrological analysis reveals that the Mae Than coals contain more huminite than liptinite macerals, while inertinite is negligible. Huminite occurs mainly in the form of texto-ulminite, textinite, densinite, and gelinite. Liptinite consists of sporinite, cutinite, resinite, suberinite, liptodetrinite, and terpenite. The morphology of cutinite, sporinite, and the presence of terpenite indicate that the peat-forming vegetation may consist of conifers. In addition to the macerals, the coal samples contain a small to moderate amount of mineral matter. Silica and clay minerals are the main minerals found in the cavities and between the cracks of the coals. The assemblage of macerals and mineral matter indicates that the Mae Than coals were formed mainly from common peat-forming vegetation, possibly conifers, in a freshwater forest swamp or mire in a warm temperate climate. In addition, the high degree of preservation of the macerals indicates a high water table and suggests rheotrophic, anoxic, limnotelmatic to telmatic conditions during deposition.

1. INTRODUCTION

Coal is typically used to generate very high temperatures through combustion to provide electricity to small households, as well as large manufacturing facilities such as factories and transportation. The Mae Than coal mine in Lampang Province (Figure 1) was one of the most important coal resources in northern Thailand and had been operated by Siam Cement Public Company Limited (SCG) since 1993. It was economically exploited for sub-bituminous coals and ball clays. Open-pit coal mining (Figures 2(a) and 2(b)) was conducted in the near-surface deposits, particularly in the southern part of the basin.

Fossil fuels were deposited in intermontane basins during the Late Paleogene to Middle Miocene (commonly referred to as Tertiary) in Northern Thailand as a result of the movement of the Indian and Eurasian plates. These basins are generally composed of coal and oil shale. Coal deposits exist in many of the Tertiary Basins in Northern Thailand, such as Mae Moh Basin, Mae Than Basin, Li Basin, and Na Hong Basin. Series of faulted grabens were formed, which were later occupied by lakes during the Oligocene to early Miocene (Ratanasthien et al., 1999). This led to the deposition of fluvial and fluviolacustrine sediments and the accumulation of peat and oil shale. The quality of coal varied depending on the depositional environment. According to palynological studies, the climate during the Oligocene to late Miocene in Thailand was far from stable (Sepulchre et al., 2009; Songtham et al., 2005).

Citation: Sattraburut T, Ratanasthien B. Maceral association in coal-bearing formations of Mae Than Coal Mine in Lampang, Thailand - Implication for depositional environment. Environ. Nat. Resour. J. 2022;20(1):96-109. (https://doi.org/10.32526/ennrj/20/202100166)

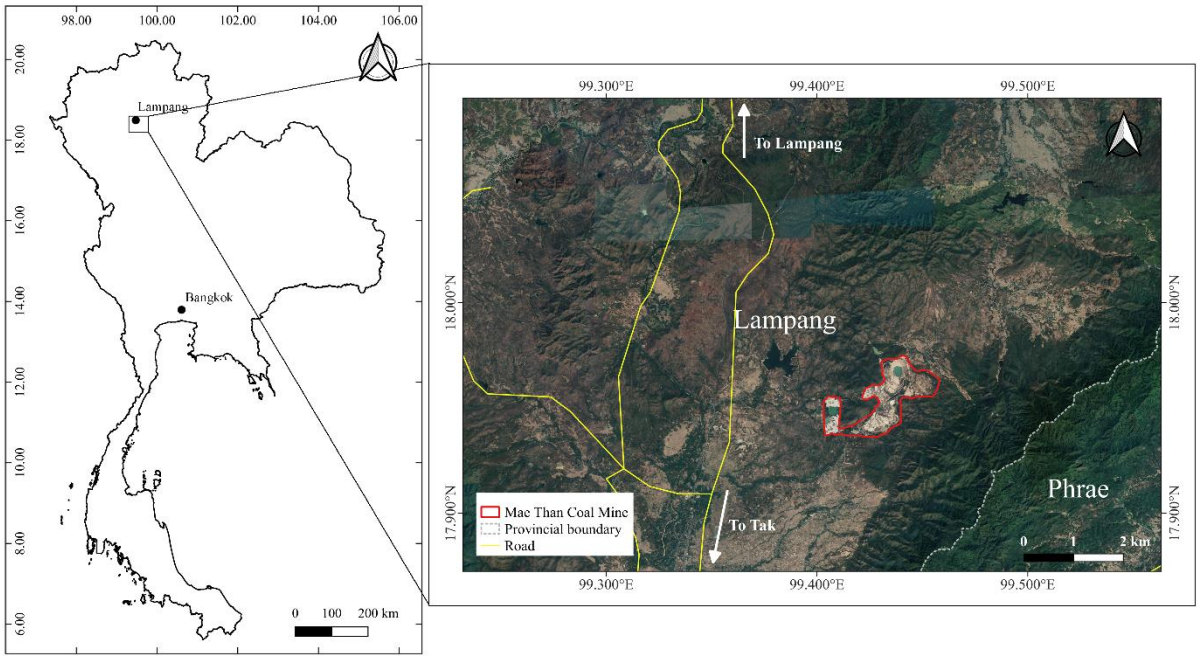

Figure 1. Location of the Mae Than Coal Mine, Mae Tha District, Lampang Province

Figure 2. (a) Mae Than open-pit coal mine (looking west), (b) coal seams and Inter Burden sediments (looking north), (c) woody texture coal, and (d) hard bright coal

Maceral, the organic component of coal and oil shale, can be observed under the petrographic microscope. The association of macerals with inorganic minerals is used to interpret the depositional environment of coal or oil shale based on the relationship of specific maceral compositions (Diessel, 1986; Sahay, 2011). The petrographic study of coal is important because maceral compositions reflect both the physical and chemical behaviors of coals, especially during their thermochemical reactions. However, limited number of studies have been conducted about coal in the Mae Than Basin and are outdated, whereas only one study (Kasetsomboon, 2012) dealt with coal petrography and the depositional

environment reconstruct of coals. Therefore, the main focus of this study is to examine the maceral association exposed in the Mae Than Coal Mine by the petrographic method and to discuss the depositional conditions during accumulation. A comparison with other nearby Tertiary basins is also made.

2. METHODOLOGY

2.1 Geological setting

As the influence of collision between the Indian and Eurasian plates, the Mae Than Basin was subjected to tectonic deformation during the Miocene to Quaternary (Muenlek, 1992), while Morley et al. (2011) proposed that small basins in northern Thailand may either had a very short history of the activity or were only episodically active. The approximate time of deposition in the Mae Than Basin is 17-7 Ma (Morley and Racey, 2011).

The Mae Than Basin is a small Tertiary Basin located between the Mae Tha and Sop Prap Districts and is about 58 km south-southeast of Lampang Province. The coal mine is situated in the southern part of the basin. The concession covers an area of approximately 9.4 km^2 and is bounded by latitudes 17°57´N and 17°59´N, and longitudes 99°26´E and 99°28´E. Coal qualities based on an air-dried basis in the Mae Than Coal Mine were reported that the volatile matter varied between 38.6 and 40.5%, ash content ranged from 10.5-12.0%, fixed-carbon content varied between 31.9 and 37.7%, heating value ranged from 4,700-5,022 Kcal/kg, and total sulfur content varied between 0.55-1.22% (Muenlek, 1992; Kasetsomboon, 2012). The coal from Mae Than coal mine was classified as sub-bituminous C.

The Mae Than Basin is an intermontane basin composed of Tertiary clastic sediments, particularly an economically important ball clay and coal seams of sub-bituminous rank. The basin has a half-graben geometry, generally dipping 10-15° to the east and thickening to the east (Morley and Racey, 2011). It is elongated towards NE-SW, 4-5 km wide and 10-12 km long (Muenlek, 1992). The basin is divided into two sub-basins: the southern and northern sub-basins. The Mae Than Coal Mine was operated in the southern sub-basin, which occupied an area of about 1.5-2.0 km^2. The southern sub-basin is controlled by the NNE-SSW and N-S trending faults. It is a flat terrain bounded by a high mountainous area with an elevation of 400-500 m. Permo-Triassic volcanic basement rocks bound the basin to the east and north (Figure 3).

The Tertiary succession can be divided into three units (Figure 4). The lower unit unconformably overlies the Permo-Triassic volcanic rocks. It is about 25-70 m thick and consists of gravelly sand, reddish-brown conglomeratic sandstone, clayey sandstone, siltstone, and conglomerate. The middle unit is about 70-200 m thick and consists of fluvial-lacustrine mudstone, sandstone, ball clay, and sub-bituminous coal. Two coal seams have been identified: the upper coal seam and the lower coal seam. The upper coal seam has a thickness of 3-16 m, while the lower coal seam with some associated oil shale has a thickness of 0.5-27.0 m. Fossils, including mastodon teeth, have been found in fluvial sediments in the upper part of this unit, indicating a Mid-Miocene age. The upper unit is about 30-80 m thick and consists of light-brown to reddish-brown sandstone, tuffaceous sandstone, siltstone, mudstone, and some conglomerates of alluvial deposits (Muenlek, 1992; Ratanasthien, 2011).

2.2 Material and methods

Twelve coal samples were collected from the upper coal seam of the Mae Than Coal Mine in Lampang, Northern Thailand. The sampling interval is approximately 0.5 m from the top to the bottom of the coal seam. The coals are black, dull to bright, hard, massive, and have a woody texture (Figures 2(c) and 2(d)). Firstly, the coal samples were air-dried for a day to remove surface moisture. Then, the samples were crushed into loose fragments and embedded in epoxy resin before polishing. The polished blocks were polished on a glass plate with aluminum oxide powder. They were then polished with chromium oxide followed by periclase powder on a high-speed polishing machine covered with chamois leather. Finally, the polished sections were examined with a coal petrographic microscope under white light, polarized light, and UV excitation in the Department of Geological Sciences, Faculty of Science, Chiang Mai University. The macerals were examined and identified. Macerals of coal are classified into three different groups based on their differences in reflectivity and chemical composition: the huminite or vitrinite group, the exinite or liptinite group, and the inertinite group. The methods for maceral identification are given in the works of Pickel et al. (2017), Sýkorová et al. (2005), International Committee for Coal and Organic Petrology (2001), Standard Association of Australia (1998), and Stach et al. (1982).

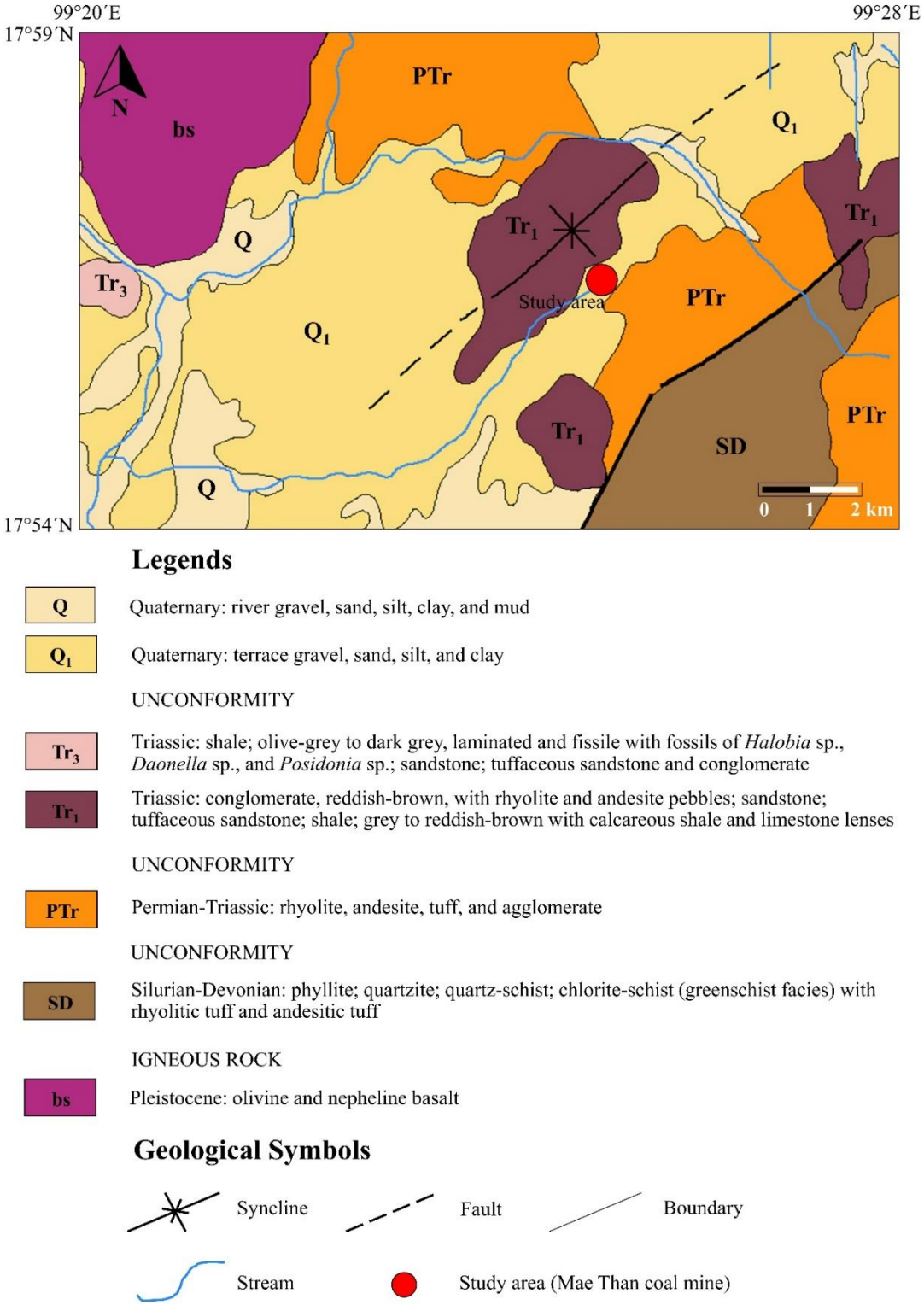

Figure 3. Geologic map of Mae Than Basin [modified from Geological Survey Division (1974)].

Coals always contain inorganic constituents. These minerals can occur as crystalline and/or non-crystalline particles. More than 150 types of minerals are present in coal. However, they are usually clays, pyrite, quartz, calcite, and lesser amounts of other minerals (Vorres, 1986). Mineral matter can be identified by petrographic examination of polished sections of coal in transmitted and reflected light. Several optical properties must be observed to identify minerals, such as color, morphology, reflectance, and anisotropy (Jenkins and Walker, 1978). Detailed methods for mineral matter identification are given in the works of Stach et al. (1982), Ward (2002), Xiuyi (2011), and Susilawati (2015).

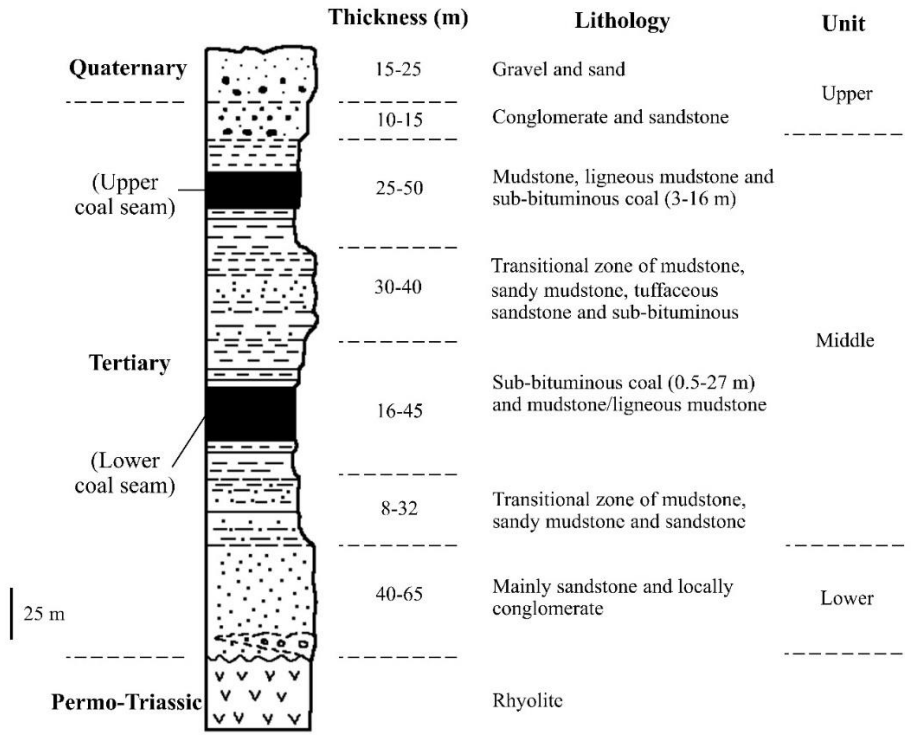

Figure 4. General stratigraphy of the Mae Than coal deposit [modified from Muenlek (1992)]

3. RESULTS

Coals from the Mae Than Coal Mine were examined. They show a variety of macerals in each maceral group. Overall, the dominant macerals are the huminite (vitrinite) groups (42-70%). The second prominent facies is dominated by the liptinite group (5-46%). A small amount of funginite from the inertinite group is also found (typically less than 3% of the total macerals). The maceral composition of the coals is shown in Table 1.

Table 1. The maceral composition (%) of the coals from the upper coal seam of the Mae Than Coal Mine

Sample	Tot Hum	Tot Lip	Tot Inert	Tot MM	Huminite			Liptinite					
					Tel	Gel	Det	Sp	Cu	Re	Lip	Su	Ter
MT01	56	5	0	39	37	16	3	2	0	2	1	0	0
MT02	69	21	0	10	26	32	11	3	14	1	2	0	1
MT03	61	34	0	5	34	27	0	6	0	3	1	0	24
MT04	55	28	1	16	14	12	29	9	5	10	4	0	0
MT05	63	11	1	25	41	14	8	3	4	2	2	0	0
MT06	70	22	0	8	4	54	12	7	1	9	5	0	0
MT07	67	13	1	19	46	21	0	3	2	0	4	0	4
MT08	42	14	0	44	8	11	23	2	2	5	4	0	1
MT09	69	11	3	17	45	16	8	3	3	3	0	0	2
MT10	48	46	0	6	1	43	4	9	13	6	16	2	0
MT11	56	13	1	30	45	11	0	1	8	1	3	0	0
MT12	54	36	0	10	15	31	8	12	2	6	2	0	14
Min	42	5	0	5	1	11	0	1	0	0	0	0	0
Max	70	46	3	44	46	54	29	12	14	10	16	2	24
Avg	59.2	21.2	0.6	19.1	26.3	24.0	8.8	5.0	4.5	4.0	3.7	0.2	3.8

Tot=total; Hum=huminite; Lip=liptinite; Inert=inertinite; MM=mineral matter; Tel=telohuminite; Gel=gelohuminite; Det=detrohuminite; Sp=sporinite; Cu=cutinite; Re=resinite; Lip=liptodetrinite; Su=suberinite; Ter=terpenite; Min=minimum; Max=maximum; Avg=average

3.1 Huminite

Two major maceral subgroups in the huminite group are telohumnite, in the form of textinite (Figures 5(e) and 5(f)) and texto-ulminite (Figures 5(a)-5(d), 5(g), and 5(h)), and gelohuminite, in the form of corpohuminite and a groundmass of gelinite (Figures 6(a), 6(b), and 6(f)). Detrohuminite is also found in the form of densinite (Figures 5(e) and 5(f)).

3.2 Liptinite

The liptinite macerals consist mainly of sporinite, cutinite, resinite, liptodetrinite, suberinite, and terpenite. The sporinite, which has the highest content and well-preserved forms, is usually bright yellow. Some of them have a circular body with an irregular rim, while the others have a saccate form of the pollen (Figures 6(a) and 6(b)). Sporinite is embedded in the groundmass of gelinite and densinite. Cutinite is found in moderate quantity with whole structures, and the margins are recognizable (Figure 6(a)). Resinite is roundish in shape and bright yellowish-orange under UV excitation (Figure 6(a)). Liptodetrinite (Figures 6(a) and 6(b)) is common in the groundmass. It occurs as small fragments derived from other liptinitic material, e.g., spores, pollen grains, cutin, algae, resin, and pigments. Suberinite shows layers of greenish-yellow cell walls under UV excitation. It associates with texto-ulminite. Terpenite (Figures 6(c) and 6(d)) generally occurs as a filling of woody cell structures and cavities. It is usually pale greenish-yellow under UV excitation.

3.3 Inertinite

Funginite (Figures 5(g) and 5(h)) is the only inertinite in this study. It accounts for less than 3% of the total macerals and is usually associated with huminite. It is characterized by a round to oval shape with varying sizes. Funginite is mainly composed of moderately to high reflecting multi-celled fungal spores or fungal remains. The cellular cavities are filled with mineral matter, especially silica.

3.4 Mineral matter

Mineral matter in coals (between 5 and 44%) consists mainly of silica (Figures 5(b) and 5(f)), and clay minerals (Figures 5(d) and 6(f)). It is dominated and commonly found in cracks, cavities, and fissures of the woody texture. Siderite, pyrite, goethite, and some carbonate minerals (Figure 6(e)) are present in low to moderate abundance.

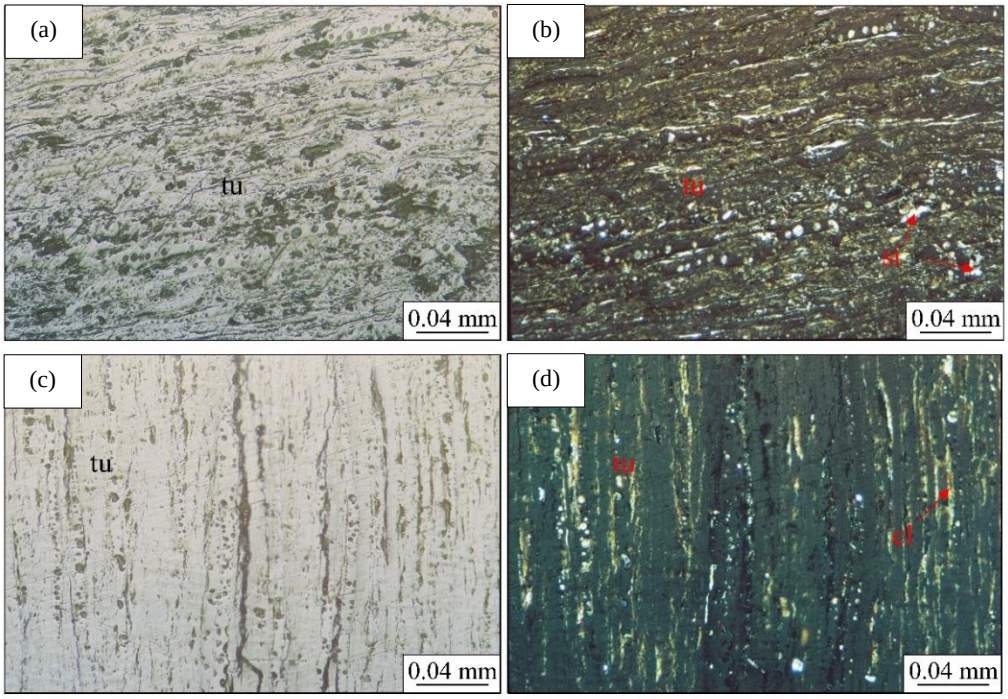

Figure 5. (a) and (b) texto-ulminite and silica in cavities and cracks; (c) and (d) texto-ulminite and clay minerals filled in cracks of wood structure; (e) and (f) textinite and densinite as groundmass. Weathering crack or desiccation crack is shown as a result of water loss. (g) and (h) funginite associated with texto-ulminite. tu=texto-ulminite; si=silica; cl=clay minerals; t=textinite; d=densinite; wc=weathering crack; fg=funginite. (a), (c), (e), and (g) are shown under white light; (b), (d), (f), and (h) are shown under polarized light.

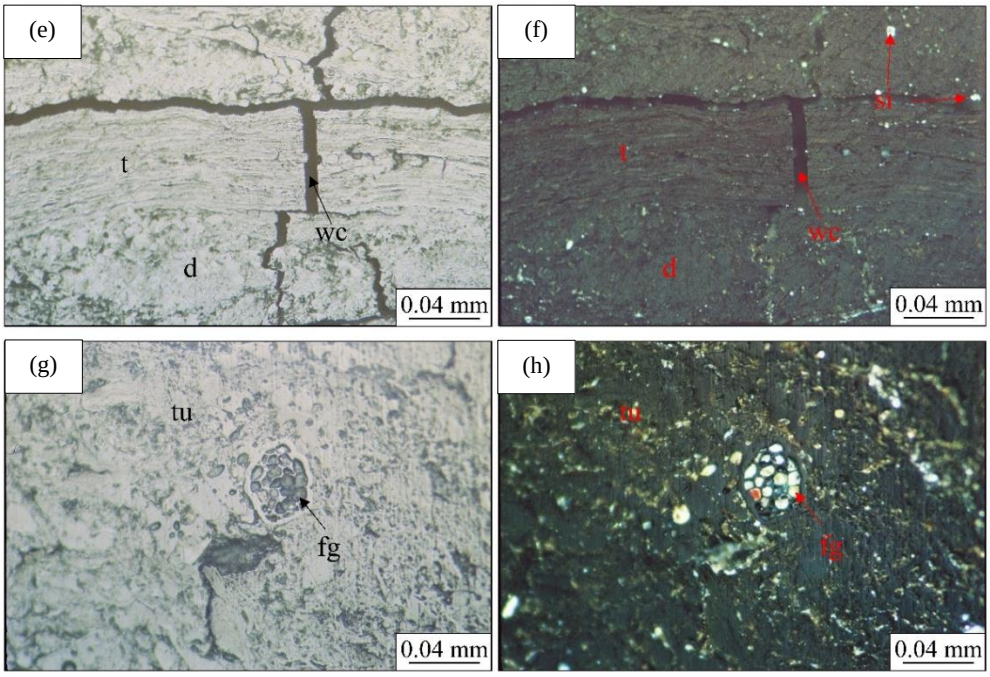

Figure 5. (a) and (b) texto-ulminite and silica in cavities and cracks; (c) and (d) texto-ulminite and clay minerals filled in cracks of wood structure; (e) and (f) textinite and densinite as groundmass. Weathering crack or desiccation crack is shown as a result of water loss. (g) and (h) funginite associated with texto-ulminite. tu=texto-ulminite; si=silica; cl=clay minerals; t=textinite; d=densinite; wc=weathering crack; fg=funginite. (a), (c), (e), and (g) are shown under white light; (b), (d), (f), and (h) are shown under polarized light (cont.).

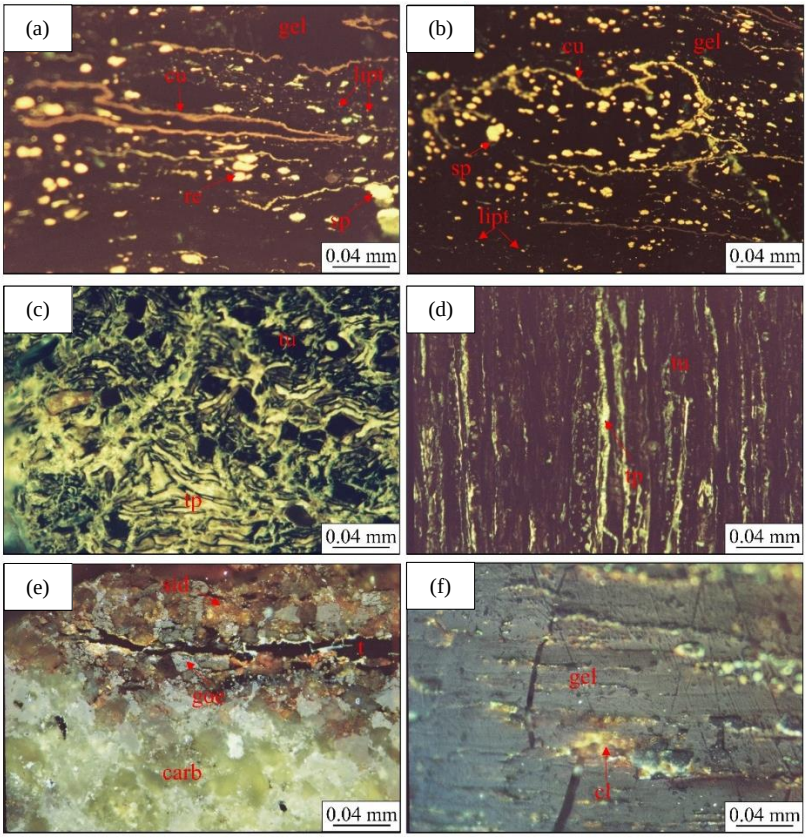

Figure 6. (a) long cutinite with needle-like morphology, with resinite, saccate sporinite, and small fragments of liptodetrinite embedded in a groundmass of densinite and gelinite; (b) bright yellow sporinite with convolute cutinite and liptodetrinite embedded in a groundmass of densinite and gelinite; (c-d) greenish yellow terpenite embedded between woody cell structures of texto-ulminite; (e) textinite and mineral matter in coals, including siderite, goethite, and carbonate minerals; (f) Gelinite with clay minerals filling the cavity. Cu=cutinite; re=resinite; sp=sporinite; lipt=liptodetrinite; gel=gelinite; tu=texto-ulminite; tp=terpenite; t=textinite; sid=siderite; goe=goethite; carb=carbonate minerals; cl=clay minerals. (a), (b), (c), and (d) are shown under UV excitation. (e) and (f) are shown under polarized light.

4. DISCUSSION

4.1 Petrographic compositions

The low-ranked Mae Than coal, classified as sub-bituminous, contains all three maceral groups in varying amounts. The most abundant maceral is huminite. Texto-ulminite and textinite of telohuminite are the most abundant macerals, followed by corpohuminite and gelinite of gelohuminite. Detrohuminite in the form of densinite is also found as a groundmass. The conspicuous telohuminite macerals are derived from the parenchymatous and woody tissues of roots, stems, barks, and leaves. In this study, large amounts of telohuminite and gelohuminite were found. This indicates preservation in a weakly oxidizing environment. This suggests the preservation of cell tissue under moist, possibly low pH conditions in forested peatlands (Ratanasthien, 2011). The presence of telohuminite in Tertiary coals usually indicates coniferous origin, as angiosperm wood and herbaceous plants are generally structurally decomposed (Diessel, 1992). However, in this study, gelohuminite is also present in significant amounts. It could be derived from intensely gelified plant tissues and other humic substances, which are enriched in limnotelmatic deposited peat. In addition, the assemblage of huminite and mineral matter in coals is commonly used as an indication of the depositional environment of ancient mires or peatlands (Wang et al., 2020; Wang et al., 2021).

Liptinite is considered the most important indicator for interpreting the depositional environment. In this study, cutinite exhibits clear cuticular ledges and shows well-preserved morphology. A needle-like cutinite (Figure 6 (a)) indicates a leaf of a conifer (Del Fueyo et al., 2019). These indicate a slightly reducing to strongly reducing condition of the deposit (Pophare et al., 2014; Stach et al., 1982). Leaf morphology is also useful in determining whether the climate in northern Thailand was seasonally tropical or temperate. In addition, sporinite as a saccate form of pollen in this study (Figures 6 (a) and 6 (b)) is restricted to members of Podocarpaceae and Pinaceae (Leslie, 2008), which are considered conifers. This suggests that the climate was temperate during the deposition of the Mae Than coal and conifers were the dominant vegetation (Wagner et al., 2019). Terpenite (Figures 6(c) and 6(d)) occurs only in low- to medium-rank coals where vitrinite reflectance was fixed at less than 1% Ro. This is consistent with the Mae Than sub-bituminous coal (0.40-0.44 %Ro). Terpenite is commonly represented as droplets or streaks derived from the essential oil of plants. Conifers are considered a source of highly aromatic hydrocarbons and *n*-alkanes (Qin et al., 2012; Schlanser et al., 2020), which generally yield a large amount of oil. This suggests that terpenite may be derived from conifer leaves. Evidence from the macroflora and palynology also supports a warm temperate climate during peat formation (Morley and Racey, 2011; Ratanasthien, 2011). The associations of sporinite, cutinite, resinite, liptodetrinite, and suberinite indicate deposition in a freshwater forest swamp or mire.

Funginite of the inertinite group is widespread in low-ranked Tertiary coals (Stach et al., 1982). It indicates the occurrence of recent weathering of peat under inhospitable conditions (International Committee for Coal and Organic Petrology, 2001). It also indicates aerobic conditions and microbial involvement during peat accumulation (Xie et al., 2019). In addition, inertinite could be formed by forest fires ignited by volcanic eruptions or lighting (Sun et al., 2017). The amount of inertinite in coal probably indicates how intense and/or widespread the wildfires may be (Xu et al., 2020). The absence of other inertinite macerals suggests that the Mae Than Basin has not experienced a particularly fire-prone period.

Mineral matter in coal is formed by various processes, such as detrital input from source rocks, diagenetic and epigenetic alteration, and precipitation from solutions. In this study, mineral matter consists mainly of silica and clay minerals. Silica is commonly found as pore or cell fillings in other coal macerals. This type of occurrence suggests an authigenic origin through epigenetic precipitation during the early stage of peat development (Sykes and Lindqvist, 1993; Dai et al., 2018). Quartz formed from solution and mostly of finely-crystalline structure. The dissolved silica could be originated from the leaching of the nearby silica-rich bedrock, which is volcanic rocks such as rhyolite, andesite, and tuff. Clay minerals dominate in cracks, cavities, and fissures between woody cell structures as finely distributed inclusions. This indicates that organic materials were impregnated with muddy water during deposition. Pyrite, along with siderite, is commonly found in woody cell cavities and fissures in coals. Siderite was initially formed by precipitation from solutions during syngenetic or diagenetic formation and then replaced by pyrite after coal consolidation (Smyth, 1966; Stach et al., 1982). Primary siderite can be converted to pyrite by descending or ascending H_2S-containing solutions

(Smyth, 1966). Siderite is usually found as an authigenic mineral in nonmarine, organic-rich environments under strongly reducing conditions (Passey, 2014). Other carbonate minerals were usually deposited during the second stage of the coalification process (Stach et al., 1982). They could be precipitated from leached carbonate solutions derived from Triassic limestone near the coal mine or they could be the result of organic matter degradation during coalification.

Several coal facies diagrams have been developed to reconstruct the paleoenvironment (Diessel, 1982; Mukhopadhyay, 1989; Calder et al., 1991; Diessel, 1992). The tissue preservation index (TPI) vs. gelification index (GI) diagram (Figure 7) and the vegetation index (VI) vs. groundwater index (GWI) diagram (Figure 8) are used to reconstruct conditions during organic matter accumulation. The TPI vs. GI diagram was originally proposed by Diessel (1992), while the VI vs. GWI diagram was first proposed by Calder et al. (1991). Later, these diagrams were modified by Kalaitzidis et al. (2004) for Tertiary low-rank coals. In this study, the TPI values vary between 0.02 and 4.09 (almost below 2.50), indicating moderate to strong organic matter preservation. The values of GI range from 11.00 to 57.63, indicating that the organic matter was gelified under very low oxygen content and wet conditions. The values of VI vary from 0.60 to 18.33. A high value of VI (>1) indicates that the preservation of plant tissues occurred under comparatively more reducing and acidic conditions (Oskay et al., 2019). The GWI values range from 0.87 to 53, indicating that the accumulation of organic matter developed under a rheotrophic hydrological regime (Oskay et al., 2019).

In addition, the TDF coal facies diagram along with the ABC coal facies diagram are applied to determine the paleoenvironment during peat accumulation based on coal composition. The TDF and ABC diagrams were originally proposed by Diessel (1982) and Mukhopadhyay (1989), respectively. In a TDF coal facies diagram, coals are on the left line of a triangle between limnotelmatic and telmatic conditions (Figure 9). This means the depositional environment developed in a flooded environment that is constantly covered with shallow water (Diessel, 1982). In the ABC coal facies diagram (Figure 10), all Mae Than coals fall within an area of anoxic conditions. It also shows that the water table is permanently above the depositional surface (Diessel, 1982).

All coal facies diagrams indicate that the swamp or mire was under anoxic conditions, which can be attributed to a permanently high water table under limnotelmatic to telmatic conditions (Oskay et al., 2019). Maceral compositions also suggest that peat was deposited in the mire to forest swamp.

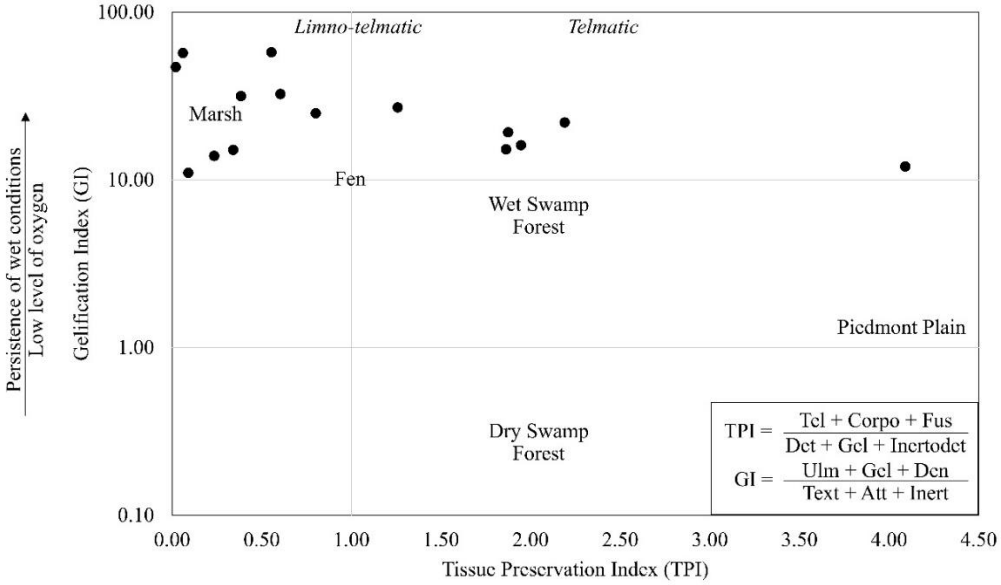

Figure 7. The tissue preservation index (TPI) vs. gelification index (GI) plot of coal samples from the Mae Than Coal Mine [after Diessel (1992), as modified from Kalaitzidis et al. (2004)]. Tel=telohuminite; Corpo=corpohuminite; Fus=fusinite; Det=detrohuminite; Gel=gelohuminite; Inertodet=inertodetrinite; Ulm=ulminite; Den=densinite; Text=textinite; Att=attrinite; Inert=inertinite

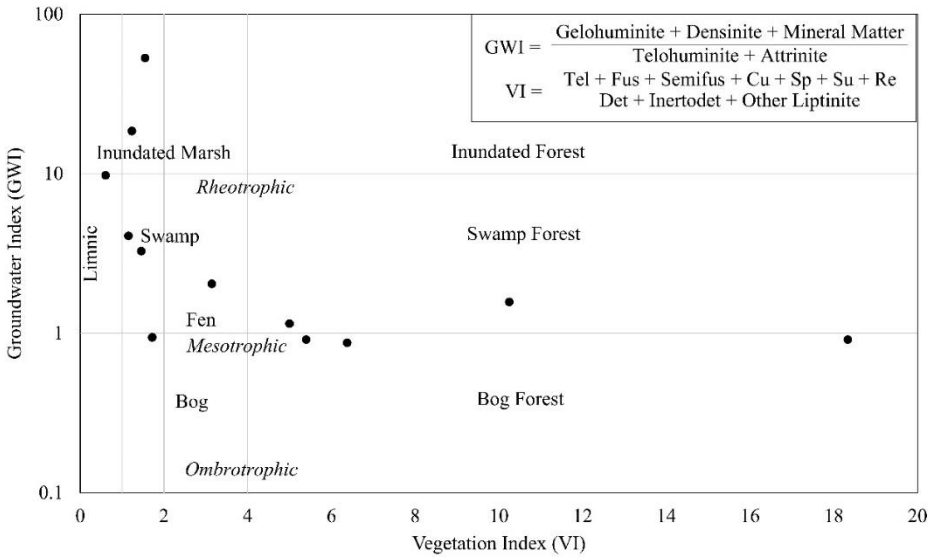

Figure 8. The vegetation index (VI) vs. ground water plot of coal samples from the Mae Than coal mine [after Calder et al. (1991), as modified from Kalaitzidis et al. (2004)]. Tel=telohuminite; Fus=fusinite; Semifus=semifusinite; Cu=cutinite; Sp=sporinite; Su=suberinite; Re=resinite; Det=detrohuminite; Inertodet=inertodetrinite

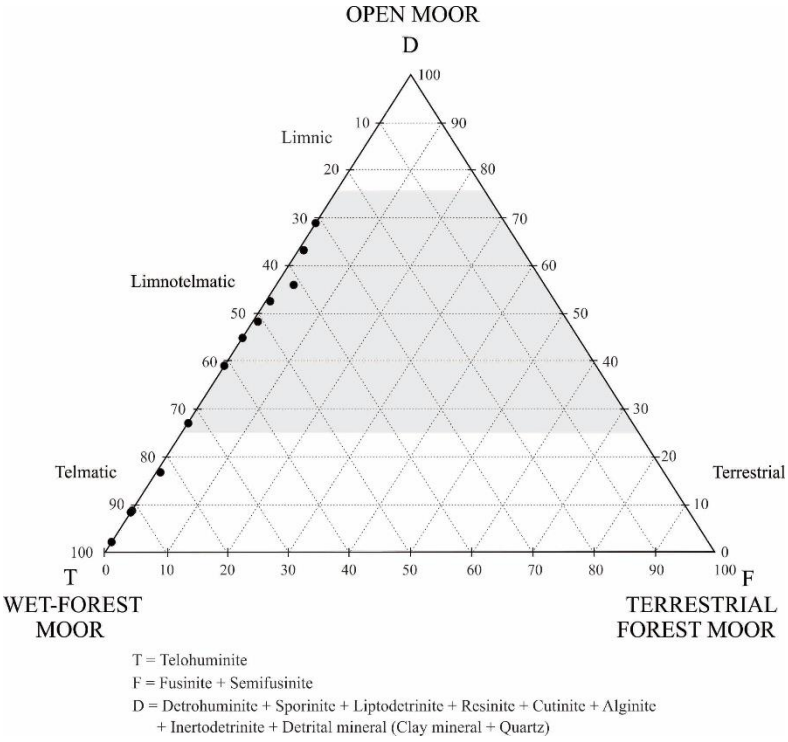

Figure 9. TDF coal facies diagram of the Mae Than coals based on maceral composition [after Diessel (1982), as modified from Edress et al. (2018)].

4.2 Comparison with other works

The petrography of the coal in this work is comparable to others. Kasetsomboon (2012) reported that the two major maceral groups found in the Mae Than Basin are huminite and liptinite. Humotelinite (or telohumnite) and humodetrinite (or detrohuminite) are two of the predominant huminites, commonly found in the form of texto-ulminite, humodetrinite, or densinite, and in a groundmass of gelinite and gelocollinite. Liptinite macerals consist mainly of alginate, cutinite, resinite, sporinite, liptodetrinite, suberinite, terpenite, exudatinite, and fluorinite. Alginite is commonly found as telaginite, including *Pila* sp. and *Botryococcus* sp. The inertinite group is

present in small amounts and consists of sclerotinite and fusinite. The maceral associations indicate that the Mae Than Basin was a forest or forest swamp with fluctuating water levels. The basin also yielded plants indicative of a temperate climate (Ratanasthien, 2011). Our results are consistent with other studies in which huminite and liptinite are the predominant maceral groups, suggesting a freshwater forest swamp or mire.

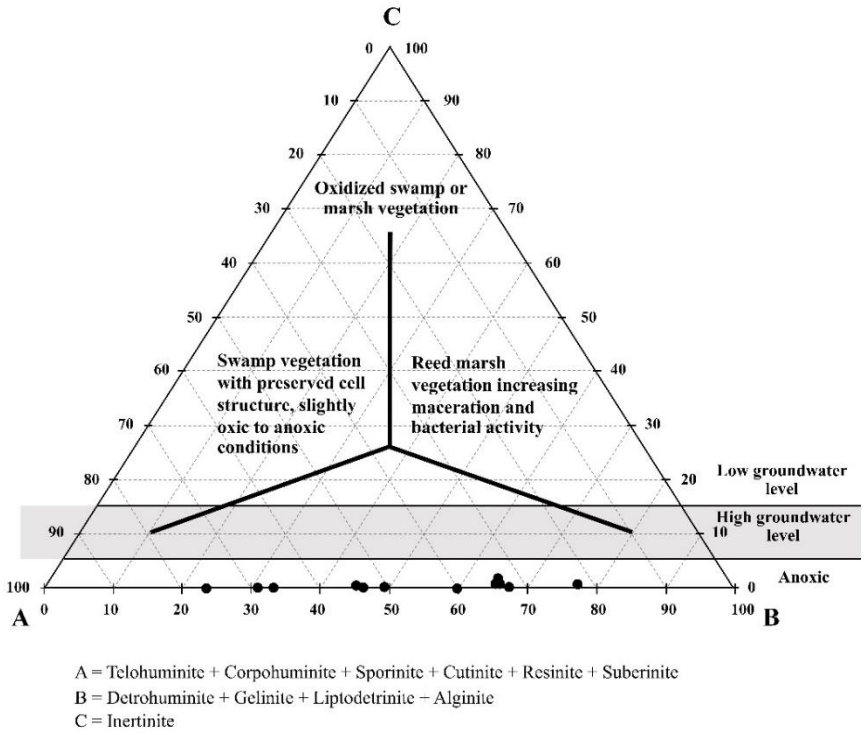

Figure 10. ABC coal facies diagram of the Mae Than coals based on maceral composition [after Mukhopadhyay et al. (1989), as modified from Edress et al. (2018)].

4.3 Comparison with nearby areas

Since there are not many detailed studies in the Mae Than Basin, we compare our work with the petrography of other coals and some macrofloral and palynological research studies from some nearby areas with Miocene coal-bearing basins in northern Thailand (Figure 11). Endo (1963) and Endo (1966) indicated from macrofossils that northern Thailand had a warm temperate climate during the Paleogene. Watanasak (1989) and Watanasak (1990) reported an extensive palynological assemblage from the Oligocene to Pliocene, consisting of various spore and pollen assemblages together with freshwater algae (*Pediastrum*) and some dinoflagellate cryst.

The Mae Moh Basin in Lampang is located to the Northeast of the Mae Than Basin and consists mainly of finely detritic humic components with small amounts of pollen grains and fungal spores, and rare sclerotinite and resinite. The coals have been identified as the decomposed product of leaves, stems, and roots of the herbaceous plant (Gibling and Ratanasthien, 1980). This is consistent with palynological studies showing that the Middle Miocene deposits of the Mae Moh Basin occurred in ponds surrounded by tropical vegetation at low to mid-elevations (Sepulchre et al., 2009).

The Mae Teep Basin in Lampang is a small Tertiary Basin Northeast of the Mae Than Basin. The petrography of the coal shows that the predominant macerals are the huminite group, mainly densitnite and texto-ulminite, while the liptinite group yields only minor amounts (Silaratana, 2005). The maceral associations suggest forest swamp and freshwater lacustrine during coal and oil shale deposition (Silaratana, 2005; Sangtong et al., 2021). Initially, it was a marsh or lake surrounded by saltwater covered by aquatic vegetation such as reeds and grass, followed by a forest swamp with forests and ferns (Sangtong, 2018).

The palynological study was conducted in the Tertiary Li Basin in Lamphun (Songtham et al., 2003). Assemblages of warm temperate and tropical vegetation were recognized. During the Oligocene to Miocene, the climate changed from warm temperate to tropical, probably due to the shift of the Southeast Asian landmass from temperate to tropical latitudes.

This may have led to a transition in vegetation types later on. The depositional environment of the Li Basin is interpreted as lacustrine and swamp deposits (Songtham, 2003). In addition, the relationship between coal quality and palynological assemblages was determined. It was found that coals from warm temperate zones are likely to be of better quality than those from the tropical zone. In addition, a seed wing of *Pinus* was recovered from the Li Basin (Grote and Srisuk, 2021). Based on the palynology and macrofossils, the climate of Northern Thailand was cooler than today in the late Oligocene and Miocene, while it became tropical in the middle Miocene (Grote and Srisuk, 2021; Songtham et al., 2003).

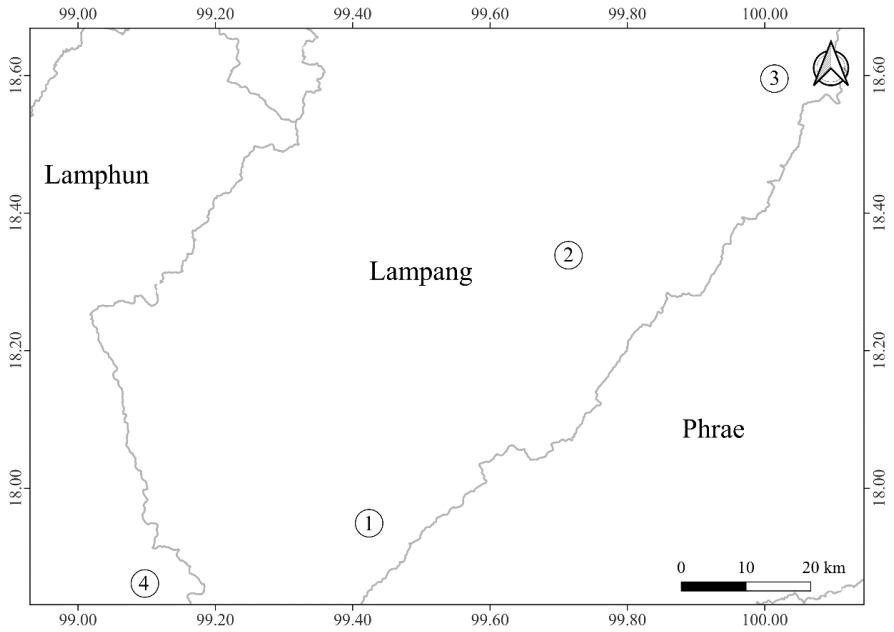

Figure 11. Regional map showing locations of some Tertiary Basins in Northern Thailand. 1=Mae Than Basin; 2=Mae Moh Basin; 3=Mae Teep Basin; 4=Li Basin

Most of the coals in the basins in northern Thailand are dominated by huminite and liptinite, indicating depositional conditions of forest swamps, mire, and lakes. They formed in intermontane pull-apart basins during extensional movements of the Himalayan orogeny in the Late Neogene. Of the other nearby basins, both the paleoclimate and depositional environment in the Mae Than Basin are comparable to those of the Li and Mae Teep Basins, probably due to similarity in topography, elevation, and tectonic evolution.

Overall, most of the intermontane basins in Northern Thailand, including the Mae Than Basin, consisted of coal seams of varying thickness deposited in peat swamps or lacustrine environments. The paleoclimate during deposition was warm temperate to tropical. Regarding the petrography of the coal, our work is consistent with other work. In addition, our study suggests that a dominant Mae Than coal probably originated from coniferous tree trunks.

5. CONCLUSION

The maceral assemblages in the Mae Than coal show an abundance of telohumnite, gelohuminite, and a small amount of detrohuminite. This suggests that the predominant maceral was derived from woody tissue of tree trunks, which was more or less gelified. Liptinite includes sporinite, cutinite, resinite, liptodetrinite, suberinite, and terpenite. The presence of needle-like cutinite, a saccate form of sporinite, and terpenite suggests that the source material of the coal may have come from coniferous trees, and also indicates a warm temperate climate. Dispersed mineral matter filled in cracks or cavities in the coals indicates that peat was impregnated with muddy water. The Mae Than coals were deposited in a freshwater forest swamp or mire and the water table was constantly above the depositional surface. Peat accumulated under rheotrophic, anoxic, limnotelmatic to telmatic conditions.

ACKNOWLEDGEMENTS

The authors would like to thank the Mae Than Coal Mine for permitting sampling and field study. Our thanks also go to the Department of Geological Sciences, Faculty of Science, Chiang Mai University for technical supports in the laboratory. We also acknowledge the critical comments and suggestions of anonymous reviewers, which significantly improved the manuscript.

REFERENCES

Calder J, Gibling M, Mukhopadhyay P. Peat formation in a Westphalian B piedmont setting, Cumberland Basin, Nova Scotia. Bulletin de la Société Géologique de France 1991;162:283-98.

Dai S, Guo W, Nechaev VP, French D, Ward CR, Spiro BF, et al. Modes of occurrence and origin of mineral matter in the Palaeogene coal (No. 19-2) from the Hunchun Coalfield, Jilin Province, China. International Journal of Coal Geology 2018;189:94-110.

Del Fueyo GM, Gnaedinger SC, Diaz MAL, Carrizo MA. Permineralized conifer-like leaves from the Jurassic of Patagonia (Argentina) and its paleoenvironmental implications. Earth Sciences 2019;91:e20180363.

Diessel CFK. An appraisal of coal facies based on maceral characteristics. Asurealian Coal Geology 1982;4(2):2-8.

Diessel CFK. The correlation between coal facies and depositional environment. Proceedings of the 20th Symposium of the Advances in the Study of the Sydney Basin. New South Wales: University of Newcastle; 1986. p. 19-22.

Diessel CFK. Coal-Bearing Depositional Systems. Berlin-Heidelberg, Germany: Springer-Verlag; 1992.

Edress NAA, Opluštil S, Sýkorová I. Depositional environments of the Jurassic Maghara main coal seam in north central Sinai, Egypt. Journal of Asian Earth Science 2018;140:241-55.

Endo S. Some older Tertiary plants from northern Thailand. Japanese Journal of Geology and Geography 1963;34(2-4):177-80.

Endo S. A supplementary note on the Paleogene Li flora in northern Thailand. In: Kobayashi T, Toriyama R, editors. Geology and Palaeontology of Southeast Asia. Tokyo, Japan: The University of Tokyo Press; 1966. p. 165-9.

Geological Survey Division. Geological Map of Thailand 1:250,000 Changwat Uttaradit NE47-11. Bangkok, Thailand: Geological Survey Division, Department of Mineral Resources; 1974.

Gibling M, Ratanasthien B. Cenozoic basins of Thailand and their coal deposits: A preliminary report. Geological Society of Malaysia, Bulletin 1980;13:27-42.

Grote PJ, Srisuk P. Fossil *Pinus* from the Cenozoic of Thailand. Review of Palaeobotany and Palynology 2021;295:Article No. 104501.

International Committee for Coal and Organic Petrology. The new inertinite classification (ICCP System 1994). Fuel 2001; 80:459-471.

Jenkins RG, Walker PL. Analysis of mineral matter in coal. In: Karr C, editor. Analytical Methods for Coal and Coal Products. New York: Academic Press; 1978. p. 265-92.

Kalaitzidis S, Bouzinos A, Papazisimou S, Christanis K. A short-term establishment of forest fen habitat during Pliocene lignite formation in the Ptolemis Basin, NW Macedonia, Greece. International Journal of Coal Geology 2004;57:243-63.

Kasetsomboon N. Petroleum Source Rock Potential in Mae Than Basin, Lampang Province [dissertation]. Chiang Mai, Thailand: Chiang Mai University; 2012.

Leslie AB. Interpreting the function of saccate pollen in ancient conifers and other seed plants. International Journal of Plant Sciences 2008;169(8):1038-45.

Morley C, Charusiri P, Watkinson IM. Structural geology of Thailand during the Cenozoic. In: Ridd MF, Barber AJ, Crow MJ, editors. The Geology of Thailand. London, United Kingdom: Geological Society; 2011. p. 273-334.

Morley C, Racey A. Tertiary stratigraphy. In: Ridd MF, Barber AJ, Crow MJ, editors. The Geology of Thailand. London, United Kingdom: Geological Society; 2011. p. 223-71.

Muenlek S. Coal geology of Mae Than Basin, Amphoe Mae Tha, Lampang. In: Piancharoen C, editor. A National Conference on Geologic Resources of Thailand: Potential for Future Development. Bangkok: Department of Mineral Resources; 1992. p. 112-21.

Mukhopadhyay P. Organic Petrography and Organic Geochemistry of Tertiary Coals from Texas in Relation to Depositional Environment and Hydrocarbon Generation. Taxas, USA: Bureau of Economic Geology; 1989.

Oskay RG, Christanis K, Salman M. Coal features and depositional environment of the Northern Karapinar-Ayranci coal deposit (Konya, Central Turkey). Turkish Journal of Earth Sciences 2019;28:1-15.

Passey SR. The habit and origin of siderite spherules in the Eocene coal-bearing Prestfjall Formation, Faroe Islands. International Journal of Coal Geology 2014;122:76-90.

Pickel W, Kus J, Flores D, Kalaitzidis S, Christanis K, Cardott BJ, et al. Classification of liptinite - ICCP System 1994. International Journal of Coal Geology 2017;169:40-61.

Pophare AM, Ramteke CP, Prasad ALV. Petrographic characteristics of coal seams of Kamptee Coalfield, Central India. In: Shrivastava KL, Kumar A, editors. Geo-Resources. Jodhpur, India: Scientific Publishers (India); 2014. p. 321-38.

Qin S, Sun Y, Tang Y, Jin K. Early diagenetic transformation of terpenoids from conifers in the aromatic hydrocarbon fraction: A long term, low temperature maturation experiment. Organic Geochemistry 2012;53:99-108.

Ratanasthien B, Kandharosa W, Chompusri S, Chartprasert S. Liptinite in coal and oil source rocks in Northern Thailand. Journal of Asian Earth Science 1999;17:301-6.

Ratanasthien B. Coal deposits. In: Ridd MF, Barber AJ, Crow MJ, editors. The Geology of Thailand. London, United Kingdom: Geological Society; 2011. p. 393-414.

Sahay VK. Limitation of petrographic indies in depositional environment interpretation of coal deposits. Central European Journal of Geosciences 2011;3(3):287-90.

Sangtong P, Wannakomol A, Terakulsatit B. Petroleum potential of Mae Teep organic sediments, northern Thailand. International Journal of GEOMATE 2021;20(80):128-34.

Sangtong P. Depositional Environment and Petroleum Source Rock Potential in Mae Teep Basin, Lampang Province [dissertation]. Nakhon Ratchasima, Thailand: Suranaree University of Technology; 2018.

Schlanser KM, Diefendorf AF, West CK, Greenwood DR, Basinger JF, Meyer HW, et al. Conifers are a major source of sedimentary leaf wax *n*-alkanes when dominant in the

landscape: Case studies from the Paleogene. Organic Geochemistry 2020;147:Article No. 104069.

Sepulchre P, Jolly D, Ducrocq S, Chaimanee Y, Jaeger JJ. Mid-Tertiary palaeoenvironment in Thailand: Pollen evidences. Climate of the Past Discussions 2009;5:709-34.

Silaratana T. Effects of Environmental Factors on Accumulation of Fossil Fuel Deposits in Northern Thailand [dissertation]. Chiang Mai, Thailand: Chiang Mai University; 2005.

Smyth, M. A siderite-pyrite association in Australian coals. Fuel 1966;45:221-31.

Songtham W, Ratanasthien B, Midenhall DC, Singharajwarapan S, Kandharosa W. Oligocene-miocene climatic changes in Northern Thailand resulting from extrusion tectonics of Southeast Asian Landmass. Science Asia 2003;29:221-33.

Songtham W, Ratanasthien B, Watanasak M, Midenhall DC, Singharajwarapan S, Kandharosa W. Tertiary basin evolution in Northern Thailand: A palynological point of view. Natural History Bulletin of the Siam Society 2005;53(1):17-32.

Songtham W. Stratigraphic Correlation of Tertiary Basins in Northern Thailand Using Algae Pollen and Spore [dissertation]. Chiang Mai, Thailand: Chiang Mai University; 2003.

Stach E, Mackowsky MT, Teichmüller M, Taylor GH, Chandra G, Teichmüller R. Stach's Textbook of Coal Petrography. Berlin, Germany: Gebrüder Bornstaeger; 1982.

Standard Association of Australia. Australian Standard AS2856.2 Coal petrography Part 2: Maceral analysis. New South Wales, Australia: Standards Australia; 1998.

Sun Y, Zhao C, Püttmann W, Kalkreuth W, Qin S. Evidence of widespread wildfires in a coal seam from the middle Permian of the North China Basin. Lithosphere 2017;9(4):595-608.

Susilawati R. Mineral matter in coal. Buletin Sumber Daya Geologi 2015;10(1):1-14.

Sykes R, Lindqvist JK. Diagenetic quartz and amorphous silica in New Zealand coals. Organic Geochemistry 1993;20:855-66.

Sýkorová I, Pickel W, Christanis K, Wolf M, Taylor GH, Flores D. Classification of huminite: ICCP System 1994. International Journal of Coal Geology 2005;62:85-106.

Vorres KS. Chemistry of Mineral Matter and Ash in Coal: An Overview. Washington, DC, USA: American Chemistry Society; 1986.

Wagner N, Eble C, Hower J, Falcon R. Petrology and palynology of select coal samples from the Permian Waterberg Coalfield, South Africa. International Journal of Coal Geology 2019;204:85-101.

Wang S, Shao L, Wang D, Hilton J, Guo B, Lu J. Controls on accumulation of anomalously thick coals: Implications for sequence stratigraphic analysis. Sedimentology 2020;67: 991-1013.

Wang S, Shao L, Li J, Li J, Jones T, Zhu M, et al. Coal petrology of the Yimin formation (Albian) in the Hailar Basin, NE China: Paleoenvironments and wildfires during peat formation. Cretaceous Research 2021;124:Article No. 104815.

Ward CR. Analysis and significance of mineral matter in coal seams. International Journal of Coal Geology 2002;50:135-68.

Watanasak M. Palynological zonation of Mid-Tertiary intermontane basins in Northern Thailand. Proceedings of the International Symposium on Intermontane Basins: Geology and Resources; 1989 Jan 30 - Feb 2; Chiang Mai: Thailand; 1989.

Watanasak M. Mid Tertiary palynostratigraphy of Thailand. Journal of Southeast Asian Earth Sciences 1990;4:203-18.

Xie P, Hower JC, Liu X. Petrographic characteristics of the brecciated coals from Panxian county, Guizhou, Southwestern China. Fuel 2019;243:1-9.

Xiuyi T. Mineral matter in coal. In: Gao J, editor. Coal, Oil Shale, Natural Bitumen, Heavy Oil, and Peat - Volume 1. Oxford, USA: EOLSS Publication; 2011.

Xu Y, Uhl D, Zhang N, Zhao C, Qin S, Liang H. Evidence of widespread wildfires in coal seams from the Middle Jurassic of Northwest China and its impact on paleoclimate. Palaeogeography, Palaeoclimatology, Palaeoecology 2020; 559:Article No. 109819.

INSTRUCTION FOR AUTHORS

Publication and Peer-reviewing processes of Environment and Natural Resources Journal

Environment and Natural Resources Journal is a peer reviewed and open access journal that is published twice a year (January-June and July-December). Manuscripts should be submitted online at https://ph02.tci-thaijo.org/index.php/ennrj/about/submissions by registering and logging into this website. Submitted manuscripts should not have been published previously, nor be under consideration for publication elsewhere (except conference proceedings papers). A guide for authors and relevant information for the submission of manuscripts are provided in this section and also online at: https://ph02.tci-thaijo.org/index.php/ennrj/author. All manuscripts are refereed through a **double-blind peer-review** process.

Submitted manuscripts are reviewed by outside experts or editorial board members of **Environment and Natural Resources Journal**. This journal uses double-blind review, which means that both the reviewer and author identities are concealed from the reviewers, and vice versa, throughout the review process. Steps in the process are as follows:

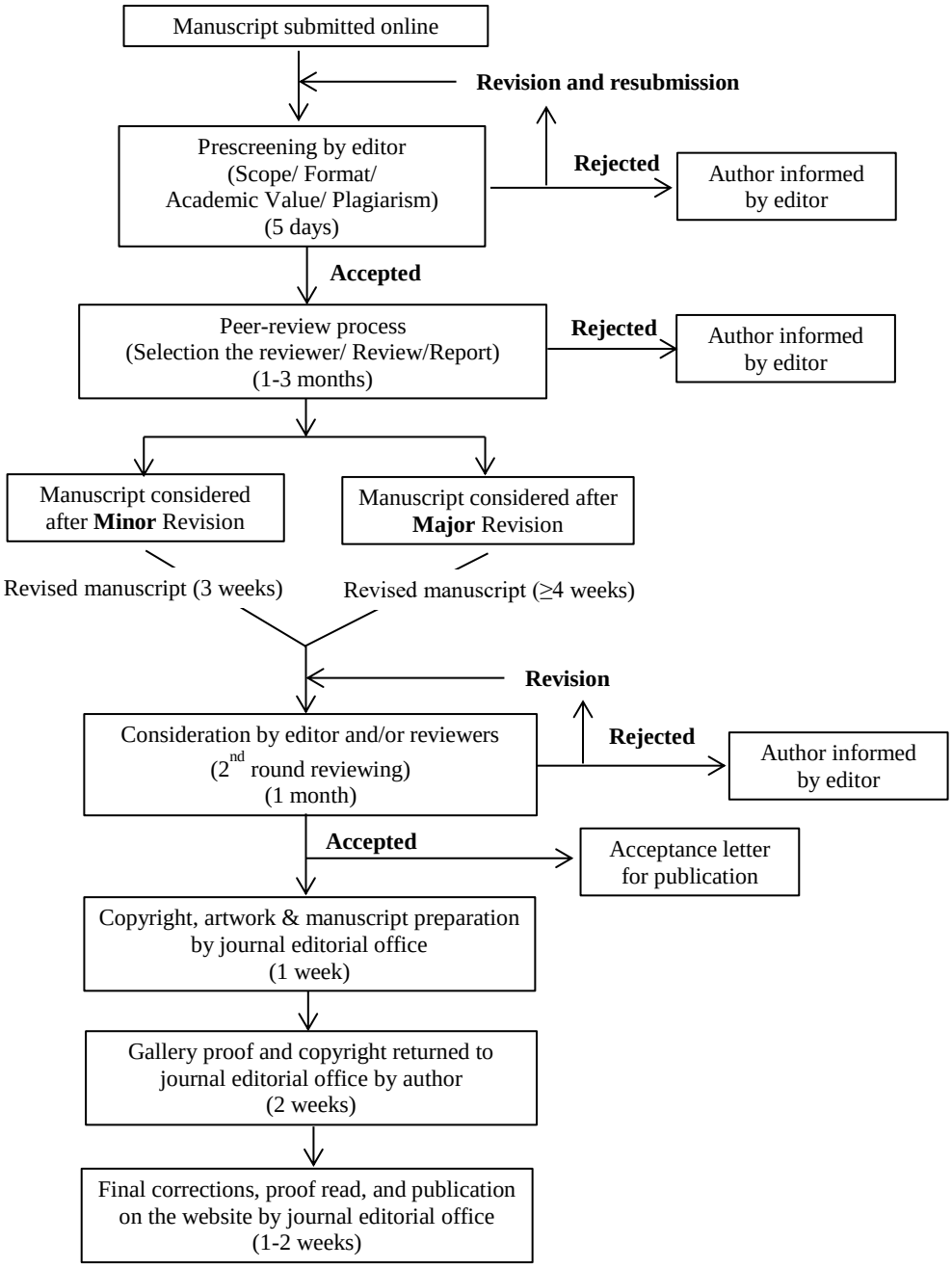

The Environment and Natural Resources Journal (EnNRJ) accepts 2 types of articles for consideration of publication as follows:

- *Original Research Article:* Manuscripts should not exceed 3,500 words (excluding references).
- *Review Article (by invitation):* This type of article focuses on the in-depth critical review of a special aspect in the environment and also provides a synthesis and critical evaluation of the state of the knowledge of the subject. Manuscripts should not exceed 6,000 words (excluding references).

Submission of Manuscript

Cover letter: Key points to include:

- Statement that your paper has not been previously published and is not currently under consideration by another journal
- Brief description of the research you are reporting in your paper, why it is important, and why you think the readers of the journal would be interested in it
- Contact information for you and any co-authors
- Confirmation that you have no competing interests to disclose

Manuscript-full: Manuscript (A4) must be submitted in Microsoft Word Files (.doc or .docx). Please make any identifying information of name(s) of the author(s), affiliation(s) of the author(s). Each affiliation should be indicated with superscripted Arabic numerals immediately after an author's name and before the appropriate address. Specify the Department/School/Faculty, University, Province/State, and Country of each affiliation.

Manuscript-anonymized: Manuscript (A4) must be submitted in Microsoft Word Files (.doc or .docx). Please remove any identifying information, such as authors' names or affiliations, from your manuscript before submission and give all information about authors at title page section.

Reviewers suggestion *(mandatory)*: Please provide the names of 3 potential reviewers with the information about their affiliations and email addresses. *The recommended reviewers should not have any conflict of interest with the authors. Each of the reviewers must come from a different affiliation and must not have the same nationality as the authors.* Please note that the editorial board retains the sole right to decide whether or not the recommended potential reviewers will be selected.

Preparation of Manuscript

Manuscript should be prepared strictly as per guidelines given below. The manuscript (A4 size page) must be submitted in Microsoft Word (.doc or .docx) with Times New Roman 12 point font and a line spacing of 1.5. *The manuscript that is not in the correct format will be returned and the corresponding author may have to resubmit*. The submitted manuscript must have the following parts:

Title should be concise and no longer than necessary. Capitalize first letters of all important words, in Times New Roman 12 point bold.

Author(s) name and affiliation must be given, especially the first and last names of all authors, in Times New Roman 11 point bold.

Affiliation of all author(s) must be given in Times New Roman 11 point italic.

Abstract should indicate the significant findings with data. A good abstract should have only one paragraph and be limited to 250 words. Do not include a table, figure or reference.

Keywords should adequately index the subject matter and up to six keywords are allowed.

Text body normally includes the following sections: 1. Introduction 2. Methodology 3. Results and Discussion 4. Conclusions 5. Acknowledgements 6. References

Reference style must be given in Vancouver style. Please follow the format of the sample references and citations as shown in this Guide below.

Unit: The use of abbreviation must be in accordance with the SI Unit.

Format and Style

Paper Margins must be 2.54 cm on the left and the right. The bottom and the top margin of each page must be 1.9 cm.

Introduction is critically important. It should include precisely the aims of the study. It should be as concise as possible with no sub headings. The significance of problem and the essential background should be given.

Methodology should be sufficiently detailed to enable the experiments to be reproduced. The techniques and methodology adopted should be supported with standard references.

Headings in Methodology section and Results and Discussion section, no more than three levels of headings should be used. Main headings should be typed (in bold letters) and secondary headings (in bold and italic letters). Third level headings should be typed in normal and no bold, for example;

2. Methodology
2.1 Sub-heading
2.1.1 Sub-sub-heading

Results and Discussion can be either combined or separated. This section is simply to present the key points of your findings in figures and tables, and explain additional findings in the text; no interpretation of findings is required. The results section is purely descriptive.
Tables Tables look best if all the cells are not bordered; place horizontal borders only under the legend, the column headings and the bottom.
Figures should be submitted in color; make sure that they are clear and understandable. Please adjust the font size to 9-10, no bold letters needed, and the border width of the graphs must be 0.75 pt. *(Do not directly cut and paste them from MS Excel.)* Regardless of the application used, when your electronic artwork is finalized, please 'save as' or convert the images to TIFF (or JPG) and separately send them to EnNRJ. The images require a resolution of at least 300 dpi (dots per inch). If a label needed in a figure, its font must be "Times New Roman" and its size needs to be adjusted to fit the figure without borderlines.

All Figure(s) and Table(s) should be embedded in the text file.

Conclusions should include the summary of the key findings, and key take-home message. This should not be too long or repetitive, but is worth having so that your argument is not left unfinished. Importantly, don't start any new thoughts in your conclusion.

Acknowledgements should include the names of those who contributed substantially to the work described in the manuscript but do not fulfill the requirements for authorship. It should also include any sponsor or funding agency that supported the work.

References should be cited in the text by the surname of the author(s), and the year. This journal uses the author-date method of citation: the last name of the author and date of publication are inserted in the text in the appropriate place. If there are more than two authors, "et al." after the first author' name must be added. Examples: (Frits, 1976; Pandey and Shukla, 2003; Kungsuwas et al., 1996). If the author's name is part of the sentence, only the date is placed in parentheses: "Frits (1976) argued that . . ."

Please be ensured that every reference cited in the text is also present in the reference list (and vice versa).

In the list of references at the end of the manuscript, full and complete references must be given in the following style and punctuation, arranged alphabetically by first author's surname. Examples of references as listed in the References section are given below.

Book
Tyree MT, Zimmermann MH. Xylem Structure and the Ascent of Sap. Heidelberg, Germany: Springer; 2002.

Chapter in a book
Kungsuwan A, Ittipong B, Chandrkrachang S. Preservative effect of chitosan on fish products. In: Steven WF, Rao MS, Chandrkachang S, editors. Chitin and Chitosan: Environmental and Friendly and Versatile Biomaterials. Bangkok: Asian Institute of Technology; 1996. p. 193-9.

Journal article
Muenmee S, Chiemchaisri W, Chiemchaisri C. Microbial consortium involving biological methane oxidation in relation to the biodegradation of waste plastics in a solid waste disposal open dump site. International Biodeterioration and Biodegradation 2015;102:172-81.

Published in conference proceedings
Wiwattanakantang P, To-im J. Tourist satisfaction on sustainable tourism development, amphawa floating marketSamut songkhram, Thailand. Proceedings of the 1st Environment and Natural Resources International Conference; 2014 Nov 6-7; The Sukosol hotel, Bangkok: Thailand; 2014.

Ph.D./Master thesis

Shrestha MK. Relative Ungulate Abundance in a Fragmented Landscape: Implications for Tiger Conservation [dissertation]. Saint Paul, University of Minnesota; 2004.

Website

Orzel C. Wind and temperature: why doesn't windy equal hot? [Internet]. 2010 [cited 2016 Jun 20]. Available from: http://scienceblogs.com/principles/2010/08/17/wind-and-temperature-why-doesn/.

Report organization:

Intergovernmental Panel on Climate Change (IPCC). IPCC Guidelines for National Greenhouse Gas Inventories: Volume 1-5. Hayama, Japan: Institute for Global Environmental Strategies; 2006.

Remark

** Please be note that manuscripts should usually contain at least 15 references and some of them must be up-to-date research articles.*

** Please strictly check all references cited in text, they should be added in the list of references. Our Journal does not publish papers with incomplete citations.*

Copyright transfer

The copyright to the published article is transferred to Environment and Natural Resources Journal (EnNRJ) which is organized by Faculty of Environment and Resource Studies, Mahidol University. The accepted article cannot be published until the Journal Editorial Officer has received the appropriate signed copyright transfer.

Online First Articles

The article will be published online after receipt of the corrected proofs. This is the official first publication citable with the Digital Object Identifier (DOI). After release of the printed version, the paper can also be cited by issue and page numbers. DOI may be used to cite and link to electronic documents. The DOI consists of a unique alpha-numeric character string which is assigned to a document by the publisher upon the initial electronic publication. The assigned DOI never changes.

Mahidol University

Wisdom of the Land

Research and Academic Service Section, Faculty of Environment and Resource Studies, Mahidol University
999 Phutthamonthon 4 Rd, Salaya, Nakhon Pathom 73170, Phone +662 441-5000 ext. 2108 Fax. +662 441 9509-10
E-mail: ennrjournal@gmail.com Website: https://www.tci-thaijo.org/index.php/ennrj